

TOPICS IN CURRENT CHEMISTRY

300

Volume Editors L. Prodi · M. Montalti · N. Zaccheroni

Luminescence Applied in Sensor Science

 Springer

300

Topics in Current Chemistry

Editorial Board:

**A. de Meijere • K.N. Houk • C.A. Hunter • J.-M. Lehn
S.V. Ley • M. Olivucci • J. Thiem • B.M. Trost • M. Venturi
P. Vogel • C.-H. Wong • H. Wong • H. Yamamoto**

Topics in Current Chemistry

Recently Published and Forthcoming Volumes

Luminescence Applied in Sensor Science

Volume Editors: Luca Prodi, Marco Montalti,
Nelsi Zaccheroni
Vol. 300, 2011

Chemistry of Opioids

Volume Editor: Hiroshi Nagase
Vol. 299, 2011

Electronic and Magnetic Properties of Chiral Molecules and Supramolecular Architectures

Volume Editors: Ron Naaman,
David N. Beratan, David H. Waldeck
Vol. 298, 2011

Natural Products via Enzymatic Reactions

Volume Editor: Jörn Piel
Vol. 297, 2010

Nucleic Acid Transfection

Volume Editors: Wolfgang Bielke,
Christoph Erbacher
Vol. 296, 2010

Carbohydrates in Sustainable Development II

Volume Editors: Amélia P. Rauter,
Pierre Vogel, Yves Queneau
Vol. 295, 2010

Carbohydrates in Sustainable Development I

Volume Editors: Amélia P. Rauter,
Pierre Vogel, Yves Queneau
Vol. 294, 2010

Functional Metal-Organic Frameworks: Gas Storage, Separation and Catalysis

Volume Editor: Martin Schröder
Vol. 293, 2010

C-H Activation

Volume Editors: Jin-Quan Yu, Zhangjie Shi
Vol. 292, 2010

Asymmetric Organocatalysis

Volume Editor: Benjamin List
Vol. 291, 2010

Ionic Liquids

Volume Editor: Barbara Kirchner
Vol. 290, 2010

Orbitals in Chemistry

Volume Editor: Satoshi Inagaki
Vol. 289, 2009

Glycoscience and Microbial Adhesion

Volume Editors: Thisbe K. Lindhorst,
Stefan Oscarson
Vol. 288, 2009

Templates in Chemistry III

Volume Editors: Broekmann, P., Dötz, K.-H.,
Schalley, C.A.
Vol. 287, 2009

Tubulin-Binding Agents: Synthetic, Structural and Mechanistic Insights

Volume Editor: Carlomagno, T.
Vol. 286, 2009

STM and AFM Studies on (Bio)molecular Systems: Unravelling the Nanoworld

Volume Editor: Samorì, P.
Vol. 285, 2008

Amplification of Chirality

Volume Editor: Soai, K.
Vol. 284, 2008

Anthracycline Chemistry and Biology II

Mode of Action, Clinical Aspects and
New Drugs
Volume Editor: Krohn, K.
Vol. 283, 2008

Anthracycline Chemistry and Biology I

Biological Occurrence and Biosynthesis,
Synthesis and Chemistry
Volume Editor: Krohn, K.
Vol. 282, 2008

Luminescence Applied in Sensor Science

Volume Editors:

Luca Prodi · Marco Montalti · Nelsi Zaccheroni

With Contributions by

A. Accetta · D.E. Achatz · R. Ali · S. Bonacchi · R. Corradini ·
A.B. Descalzo · A.P. de Silva · F. Dini · C. Di Natale · T. Fischer ·
D. Genovese · R. Juris · R. Marchelli · M. Montalti · D. Monti ·
R. Paolesse · L. Prodi · E. Rampazzo · K. Rurack · M. Sgarzi ·
S. Uchiyama · W. Wan · O.S. Wolfbeis · N. Zaccheroni · S. Zhu

 Springer

Editors

Dr. Luca Prodi
Dipartimento di Chimica "G. Ciamician"
Latemar Unit
Università degli Studi di Bologna
Via Selmi 2
40126 Bologna
Italy
luca.prodi@unibo.it

Dr. Marco Montalti
Università degli Studi di Bologna
Dipartimento di Chimica "G. Ciamician"
Via Selmi 2
40126 Bologna
Italy
marco.montalti2@unibo.it

Dr. Nelsi Zaccheroni
Università degli Studi di Bologna
Dipartimento di Chimica "G. Ciamician"
Via Selmi 2
40126 Bologna
Italy
nelsi.zaccheroni@unibo.it

ISSN 0340-1022 e-ISSN 1436-5049
ISBN 978-3-642-19419-1 e-ISBN 978-3-642-19420-7
DOI 10.1007/978-3-642-19420-7
Springer Heidelberg Dordrecht London New York

Library of Congress Control Number: 2011924780

© Springer-Verlag Berlin Heidelberg 2011

This work is subject to copyright. All rights are reserved, whether the whole or part of the material is concerned, specifically the rights of translation, reprinting, reuse of illustrations, recitation, broadcasting, reproduction on microfilm or in any other way, and storage in data banks. Duplication of this publication or parts thereof is permitted only under the provisions of the German Copyright Law of September 9, 1965, in its current version, and permission for use must always be obtained from Springer. Violations are liable to prosecution under the German Copyright Law.

The use of general descriptive names, registered names, trademarks, etc. in this publication does not imply, even in the absence of a specific statement, that such names are exempt from the relevant protective laws and regulations and therefore free for general use.

Cover design: WMXDesign GmbH, Heidelberg, Germany

Printed on acid-free paper

Springer is part of Springer Science+Business Media (www.springer.com)

Volume Editors

Dr. Luca Prodi

Dipartimento di Chimica "G. Ciamician"
Latemar Unit
Università degli Studi di Bologna
Via Selmi 2
40126 Bologna
Italy
luca.prodi@unibo.it

Dr. Marco Montalti

Università degli Studi di Bologna
Dipartimento di Chimica "G. Ciamician"
Via Selmi 2
40126 Bologna
Italy
marco.montalti2@unibo.it

Dr. Nelsi Zaccheroni

Università degli Studi di Bologna
Dipartimento di Chimica "G. Ciamician"
Via Selmi 2
40126 Bologna
Italy
nelsi.zaccheroni@unibo.it

Editorial Board

Prof. Dr. Armin de Meijere

Institut für Organische Chemie
der Georg-August-Universität
Tammanstr. 2
37077 Göttingen, Germany
ameijer1@uni-goettingen.de

Prof. Dr. Jean-Marie Lehn

ISIS
8, allée Gaspard Monge
BP 70028
67083 Strasbourg Cedex, France
lehn@isis.u-strasbg.fr

Prof. Dr. Kendall N. Houk

University of California
Department of Chemistry and Biochemistry
405 Hilgard Avenue
Los Angeles, CA 90024-1589, USA
houk@chem.ucla.edu

Prof. Dr. Steven V. Ley

University Chemical Laboratory
Lensfield Road
Cambridge CB2 1EW
Great Britain
Svl1000@cus.cam.ac.uk

Prof. Dr. Christopher A. Hunter

Department of Chemistry
University of Sheffield
Sheffield S3 7HF, United Kingdom
c.hunter@sheffield.ac.uk

Prof. Dr. Massimo Olivucci

Università di Siena
Dipartimento di Chimica
Via A De Gasperi 2
53100 Siena, Italy
olivucci@unisi.it

Prof. Dr. Joachim Thiem

Institut für Organische Chemie
Universität Hamburg
Martin-Luther-King-Platz 6
20146 Hamburg, Germany
thiem@chemie.uni-hamburg.de

Prof. Dr. Barry M. Trost

Department of Chemistry
Stanford University
Stanford, CA 94305-5080, USA
bmtrost@leland.stanford.edu

Prof. Dr. Margherita Venturi

Dipartimento di Chimica
Università di Bologna
via Selmi 2
40126 Bologna, Italy
margherita.venturi@unibo.it

Prof. Dr. Pierre Vogel

Laboratory of Glycochemistry
and Asymmetric Synthesis
EPFL – Ecole polytechnique fédérale
de Lausanne
EPFL SB ISIC LGSA
BCH 5307 (Bat.BCH)
1015 Lausanne, Switzerland
pierre.vogel@epfl.ch

Prof. Dr. Chi-Huey Wong

Scipps Research Institute
128 Academia Road, Section 2
Nankang, Taipei
Taiwan
chwong@gate.sinica.edu.tw

Prof. Dr. Henry Wong

The Chinese University of Hong Kong
University Science Centre
Department of Chemistry
Shatin, New Territories
hncwong@cuhk.edu.hk

Prof. Dr. Hisashi Yamamoto

Arthur Holly Compton Distinguished
Professor
Department of Chemistry
The University of Chicago
5735 South Ellis Avenue
Chicago, IL 60637
773-702-5059
USA
yamamoto@uchicago.edu

Topics in Current Chemistry Also Available Electronically

Topics in Current Chemistry is included in Springer's eBook package *Chemistry and Materials Science*. If a library does not opt for the whole package the book series may be bought on a subscription basis. Also, all back volumes are available electronically.

For all customers with a print standing order we offer free access to the electronic volumes of the series published in the current year.

If you do not have access, you can still view the table of contents of each volume and the abstract of each article by going to the SpringerLink homepage, clicking on "Chemistry and Materials Science," under Subject Collection, then "Book Series," under Content Type and finally by selecting *Topics in Current Chemistry*.

You will find information about the

- Editorial Board
- Aims and Scope
- Instructions for Authors
- Sample Contribution

at springer.com using the search function by typing in *Topics in Current Chemistry*.

Color figures are published in full color in the electronic version on SpringerLink.

Aims and Scope

The series *Topics in Current Chemistry* presents critical reviews of the present and future trends in modern chemical research. The scope includes all areas of chemical science, including the interfaces with related disciplines such as biology, medicine, and materials science.

The objective of each thematic volume is to give the non-specialist reader, whether at the university or in industry, a comprehensive overview of an area where new insights of interest to a larger scientific audience are emerging.

Thus each review within the volume critically surveys one aspect of that topic and places it within the context of the volume as a whole. The most significant developments of the last 5–10 years are presented, using selected examples to illustrate the principles discussed. A description of the laboratory procedures involved is often useful to the reader. The coverage is not exhaustive in data, but rather conceptual, concentrating on the methodological thinking that will allow the non-specialist reader to understand the information presented.

Discussion of possible future research directions in the area is welcome.

Review articles for the individual volumes are invited by the volume editors.

In references *Topics in Current Chemistry* is abbreviated *Top Curr Chem* and is cited as a journal.

Impact Factor 2009: 4.291; Section “Chemistry, Multidisciplinary”: Rank 20 of 138

Preface

We believe that the development of luminescent sensors will have a strong social and economical impact. As scientists actively working in this field since many years, we would like to start by thanking Prof. Vincenzo Balzani, who as a previous member of the editorial board of *Topics in Current Chemistry* was the one who proposed a volume on this subject.

In this volume, through a short but multisided overview, we try to provide the reader with an understanding of how deeply the merging of the three main scientific areas *sensing*, *luminescence* and *nanotechnology* can impact on our everyday life. In this preface, we will give a short introduction to the general fundamental principles of each, hoping that this will allow an easier and clearer understanding of the “result of their sum”.

We can say, from a very broad and generalized point of view, that sensing processes necessarily entail the exploitation of one or more chemical–physical phenomena to convey information about the external environment (the sensing domain). What follows this is the conversion of the stimulus of the sensed phenomenon/species into a signal or data stream that can be understood and manipulated.

In particular, *chemical sensing* involves the design of single molecules or of arrays of molecules that specifically recognize a chemical species in a reversible manner and in a given concentration range. The need for reversibility is an essential requirement for continuous or *in vivo* monitoring, but in the case of once-off measurements it is not always necessary. Moreover, in recent times, single analyte sensing has been flanked by new kinds of systems that are able to detect classes or mixtures of chemicals in a similar manner to which nature has developed human taste or smell.

As these requirements are rather complex, the advent of *luminescent signalling* systems and luminescent-based devices continues to bring about many advantages, since fluorescence measurements are usually very sensitive, low cost, easily performed and versatile, offering submicron visualisation and submillisecond temporal resolution. Consequently, luminescent chemical sensors play a major role in key fields such as industry, diagnostic and therapeutic medicine, and various kinds of environmental monitoring.

Likewise, since *molecular nanotechnology* is the most advanced frontier of research in many scientific areas, it is again not surprising how this is also the framework of the natural evolution and development of sensors. Nanotechnology is certainly still a science in its infancy, but it is already extensively affecting our daily lives with many different products that span the widest variety of applications. There are valid safety concerns about the production and use of nanomaterials, and increasingly research is still needed to separate speculative risks from real ones. This is particularly true for *nanoparticles*. In fact, nanoparticles, among all the nanostructured materials, not only have the highest number of industrial applications, but they are also the most extensively studied worldwide. These extremely versatile nanoobjects are usually described as small spheres with controlled dimensions and a radius in the range of nanometers, but their shape can vary significantly, as can their constituting material (metals, semiconductors, lipids, polymers, etc.), and their surface derivatization with different capping agents (receptors, reactive sites, electroactive or photoactive functionalities, DNA strains, etc.).

Merging nanotechnology and luminescent signalling can therefore lead to the creation of unique materials that can induce great improvements in the technical development of many areas. In this volume, leading scientists present comprehensive reviews on modern research trends that accompany the reader on a journey from optical and luminescent chemosensors and biosensors (cite the contributions of Prof. A.P. de Silva and Prof. O. Wolfbeis), also exploiting chiral sensing (Prof. Corradini), to their implementation in more complex structures to yield materials able to perform signal amplification (contributions of Prof. Rurack and Prof. Prodi) and to be included in detection devices (contributions of Prof. Rurack, Prof. Prodi, Prof. O. Wolfbeis and Prof. Paolesse).

We believe that the high impact on different fields and the variety of approaches to the topic will attract the attention of scientists from different communities such as chemistry, materials, technology, medicine and industry. We also hope that the writing style will enable readers from diverse areas of research to fully enjoy the presentations on this fascinating subject, and we hope to offer at least a taste of its huge potential.

February 2011

Marco Montalti
Luca Prodi
Nelsi Zaccheroni

Contents

Molecular Logic Gates and Luminescent Sensors Based on Photoinduced Electron Transfer	1
A. Prasanna de Silva and Seiichi Uchiyama	
Luminescent Chemical Sensing, Biosensing, and Screening Using Upconverting Nanoparticles	29
Daniela E. Achatz, Reham Ali, and Otto S. Wolfbeis	
Luminescence Amplification Strategies Integrated with Microparticle and Nanoparticle Platforms	51
Shengchao Zhu, Tobias Fischer, Wei Wan, Ana B. Descalzo, and Knut Rurack	
Luminescent Chemosensors Based on Silica Nanoparticles	93
Sara Bonacchi, Damiano Genovese, Riccardo Juris, Marco Montalti, Luca Prodi, Enrico Rampazzo, Massimo Sgarzi, and Nelsi Zaccheroni	
Fluorescence Based Sensor Arrays	139
Roberto Paolesse, Donato Monti, Francesca Dini, and Corrado Di Natale	
Enantioselective Sensing by Luminescence	175
Alessandro Accetta, Roberto Corradini, and Rosangela Marchelli	
Index	217

Molecular Logic Gates and Luminescent Sensors Based on Photoinduced Electron Transfer

A. Prasanna de Silva and Seiichi Uchiyama

Abstract The competition between Photoinduced electron transfer (PET) and other de-excitation pathways such as fluorescence and phosphorescence can be controlled within designed molecular structures. Depending on the particular design, the resulting optical output is thus a function of various inputs such as ion concentration and excitation light dose. Once digitized into binary code, these input-output patterns can be interpreted according to Boolean logic. The single-input logic types of YES and NOT cover simple sensors and the double- (or higher-) input logic types represent other gates such as AND and OR. The logic-based arithmetic processors such as half-adders and half-subtractors are also featured. Naturally, a principal application of the more complex gates is in multi-sensing contexts.

Keywords Fluorescent molecular sensors, Molecular logic, Logic gates, Molecular computation, Photoinduced electron transfer (PET)

Contents

1	Introduction	2
2	YES	2
	2.1 Cation Inputs	3
	2.2 Anion Inputs	6
3	NOT	6
	3.1 Cation Inputs	6

A.P. de Silva (✉)

School of Chemistry and Chemical Engineering, Queen's University, Belfast BT9 5AG, Northern Ireland

e-mail: a.desilva@qub.ac.uk

S. Uchiyama

Graduate School of Pharmaceutical Sciences, The University of Tokyo, 7-3-1 Hongo, Bunkyo-ku, Tokyo 113-0033, Japan

e-mail: seiichi@mol.f.u-tokyo.ac.jp

3.2	Anion Inputs	6
3.3	Photon Inputs	7
4	AND	8
4.1	Separate Inputs	8
4.2	Connected Inputs	12
4.3	All-Photonic Inputs	13
5	OR	15
6	NOR	16
7	NAND	17
8	INHIBIT	18
9	XOR	20
10	Half-Adder	20
11	Half-Subtractor	23
12	Conclusion	24
	References	25


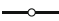
1 Introduction

In a previous contribution to this series [1], we reviewed the state of the art of fluorescent photoinduced electron transfer (PET) sensors as it stood in 1993. Much has happened since then. In particular, the field of luminescent sensors [2, 3] has given birth to the field of molecular logic gates [4–17] where computing concepts [18–20] are embedded in molecular structures. In spite of their apparent differences, the two fields share many ideas because of the historical parent-child relationship. The two fields of luminescent sensors and molecular logic gates are now too large to allow comprehensive reviewing in article in a chapter of this length. So we will adopt an illustrative approach in the present chapter and discuss some of the recent literature. Furthermore, we will consider conventional sensors as sub-sets of logic gates where the former are single-input devices with chemical species as an input and light emission as an output. The Boolean logic type [18–20] will be our main means of organization. Some Boolean logic types and their truth tables are shown in Figs. 1 and 2. When needed, the nature of the devices, inputs and outputs will be a secondary means of organization. We refer the reader to earlier reviews [1, 2] for foundational material.

2 YES

Fluorescent “off-on” sensors where an analyte causes a fluorescence enhancement (FE) can be understood as YES logic gates. A YES logic gate is a single-input device (Fig. 1) and is therefore one of the simplest logic gates.

Fig. 1 Boolean logic operations of 1-input logic gates. Input and output levels are represented in binary digit; 0 for low and 1 for high

Input	Output	
0	0	1
1	1	0
Name	YES	NOT
Symbol		


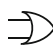
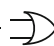
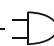
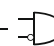
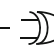
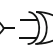


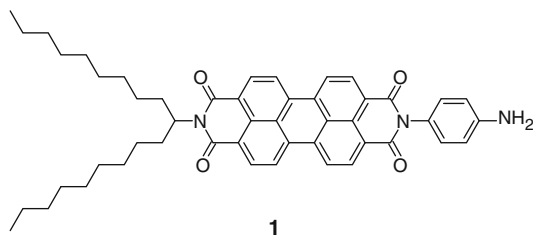
Inputs		Output									
(A)	(B)	(Carry)	(Sum)	(Borrow)	(Diff.)						
0	0	0	0	0	0	0	0	0	0	0	0
0	1	0	1	0	1	0	1	0	1	1	1
1	0	0	1	0	1	1	1	0	0	0	1
1	1	1	0	0	0	0	0	1	1	0	0
Name	AND	OR	NOR	NAND	INHIBIT	XOR	XNOR	Half-adder	Half-subtractor		
Symbol											

Fig. 2 Boolean logic operations of 2-input logic gates. The half-adder is composed of an AND gate for a carry digit and an XOR gate for a sum digit, whereas the half-subtractor consists of an INHIBIT gate for a borrow digit and an XOR gate for a difference digit

2.1 Cation Inputs

The earliest successes in fluorescent sensors were achieved with H^+ [21]. So we begin our discussion with simple cation inputs.

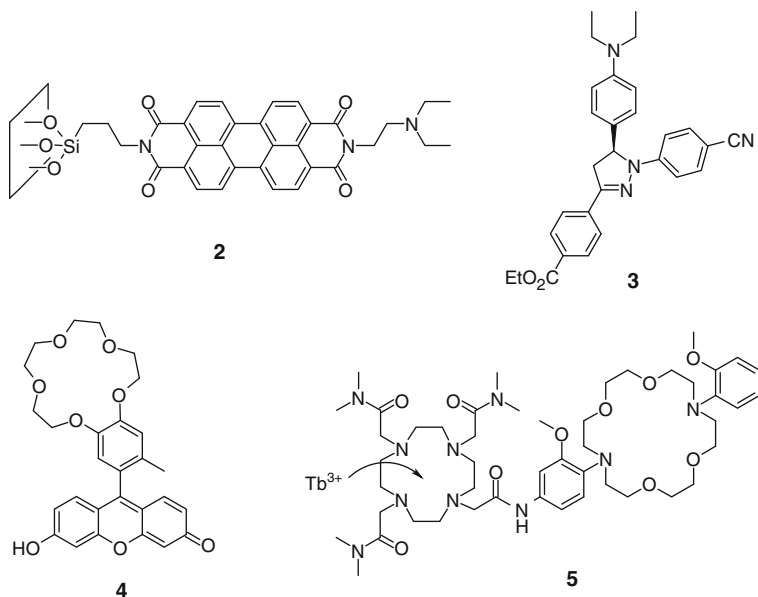
Adams' **1** [22] has a “fluorophore-spacer-receptor” format [1, 23–25] since the imide nitrogen forms a node in the molecular orbital system. Indeed, PET from the aniline unit to the perylenetetracarboxyl bisimide leads to negligible fluorescence. Protonation of the aniline unit stops this PET process to give strong fluorescence. The switching properties of **1** were observed at the single-molecule level by confocal scanning microscopy. The time trajectory of fluorescence intensity was similar to that previously seen in a non-PET pH sensor [26]. A newer example bearing a similar bisimide structure is **2** [27].



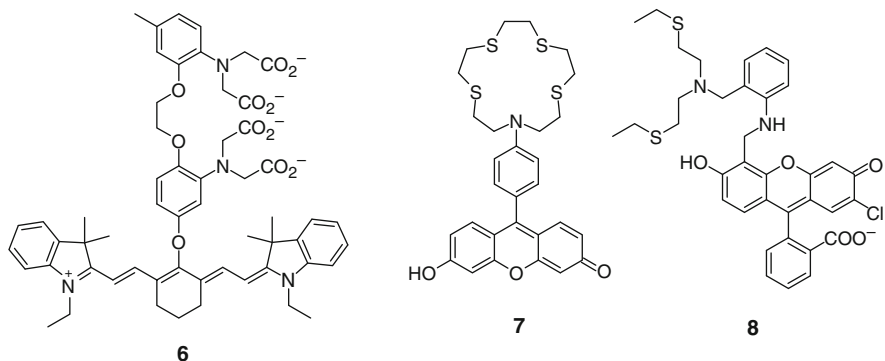
Fahmi's compound **3** [28, 29] switches “on” its emission when the aniline unit picks up H^+ . The structure and function of **3** has precedents [30, 31] which were designed to respond to Na^+ and Ca^{2+} , but were tested for their response to H^+ as well. PET from the aniline unit to the pyrazoline fluorophore carrying an electron-withdrawing group like a cyano group was first appreciated by Pragst and co-workers [32].

While noting that early cases [33–35] are available, we feature Nagano's **4** [36] which displays a Na^+ -induced FE factor of 5.3 in water. This is a virtually spaced PET system [37] aided by the steric effect of the strategically placed methyl group. Thermodynamic arguments and quantum calculations were offered to support PET in this case.

Though lanthanide-based PET systems are rare [38, 39], Gunnlaugsson and Leonard built an efficient “off-on” sensor **5** [40] for alkali cations in water. In this case, a spacer module is not evident. Similarly, an efficient fluorescence switching without a clear spacer can be seen in Akkaya's **6** [41], which targets Ca^{2+} with relatively long excitation and emission wavelengths (i.e. 760 nm and 782 nm, respectively).

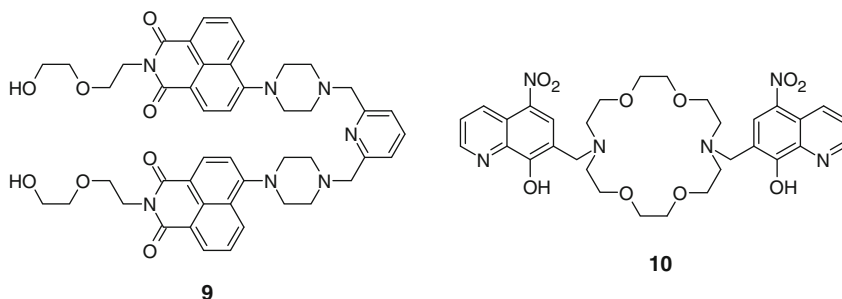


An environmentally important sensor is **7** [42] which switches “on” fluorescence in the presence of Hg^{2+} in pH neutral water. This compound successfully measured total Hg^{2+} levels as low as 0.1 ppm in acid-digested fish samples. The 1,4,7,10-tetrathia-13-azacyclopentadecane receptor nicely targets the soft cation, Hg^{2+} . The virtually spaced PET system [43] delivers the “off-on” action, as seen in a related case using a BODIPY (boron dipyrromethene) fluorophore [44] by Rurack et al. Sensor **8** [45] with a different receptor for Hg^{2+} bears favourable comparison.



Another excellent example is Qian's **9** [46] with high selectivity in Hg^{2+} sensing. This was from a 2,6-bis(aminomethyl)pyridine receptor and also functions in neutral aqueous solution. Two aminonaphthalimide fluorophores are incorporated within this classic PET system.

The origin of the excellent “off-on” Hg^{2+} -sensing ability of **10** [47] (though in mixed aqueous solution) is now analysed further [48]. X-ray crystallography of the complex, **10**/ Hg^{2+} clearly showed that the metal is only bound by the pair of hydroxyquinolines and not by the diazacrown. So the diazacrown structure serves two important roles: (1) as a scaffold for the ligating groups and (2) as an intramolecular base to pick up the protons from the phenols upon metal binding. PET from the amines would be inhibited by this protonation and strong fluorescence of the complex **10**/ Hg^{2+} would be tolerated.

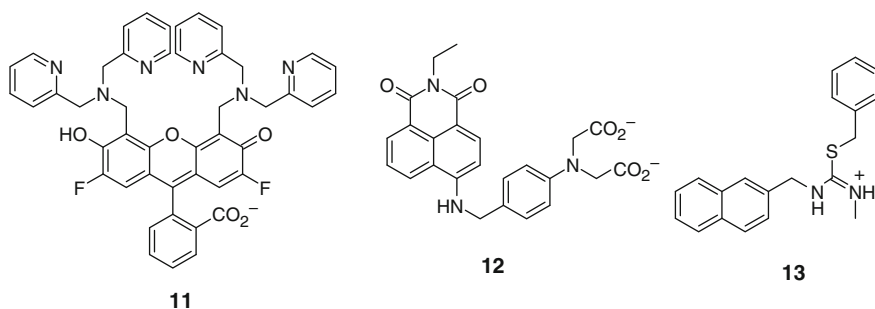


Lippard's **11** [49] targets Zn^{2+} and has halogen substituents on the fluorophore to move the inherent pH sensitivity of the sensor away from the physiological region [50]. Sensor **11** clearly has a “fluorophore-spacer-receptor” system operating PET from the tertiary amine to the fluorescein fluorophore until Zn^{2+} blocks it. This sensor permitted high level imaging of neuronal Zn^{2+} which has been associated with Alzheimer's disease and other neurological disorders.

Another PET sensor for Zn^{2+} in water, Gunnlaugsson et al.'s **12** [51], has the appeal of perhaps the simplest receptor. Nevertheless, an excellent Zn^{2+} - induced FE factor of 53 was found. This sensory function was pH-independent in the physiological range.

2.2 Anion Inputs

Kubo's **13** [52] is a fluorescent "off-on" sensor for AcO^- in acetonitrile. An FE factor of 4.1 was found because this anion decreases the electron accepting nature of the thiuronium unit and hence retards PET from the naphthalene.



3 NOT

Fluorescent "on-off" sensors where an analyte causes a fluorescence decrease can be understood as NOT logic gates. A NOT logic gate is clearly the inverse of a YES logic gate (Fig. 1).

3.1 Cation Inputs

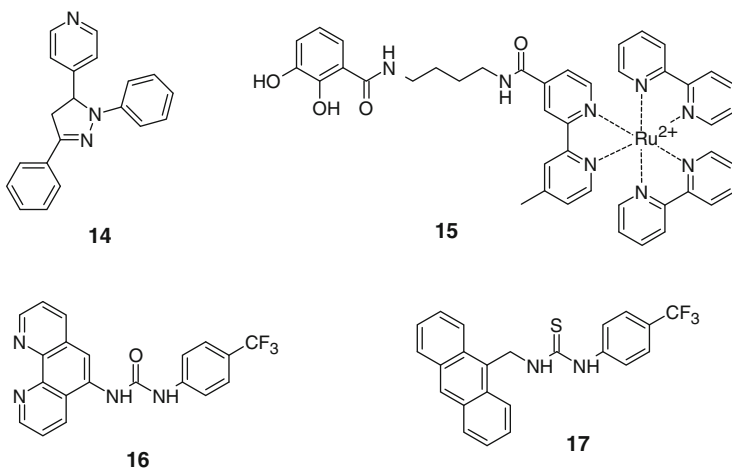
Sensor **14** [53] equips a fluorescent "fluorophore-spacer-receptor" system with a pyridine receptor for H^+ which becomes more reducible by protonation. So **14** galvanizes fluorescence-quenching PET from the pyrazoline fluorophore to the pyridine receptor only when H^+ arrives.

3.2 Anion Inputs

A tris(bipyridyl)Ru(II) lumophore is connected to the natural siderophore amino-chelin via a peptide link to produce **15** [54]. It shows clear PET behaviour upon pH

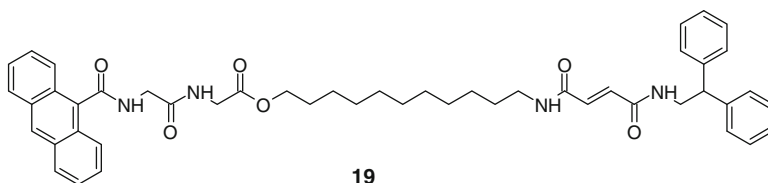
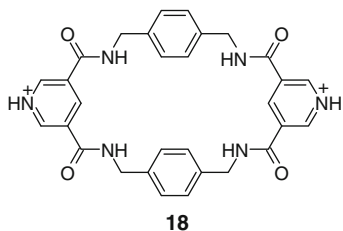
variation in that the production of the catecholates species at high pH produces smooth switching “off” of emission. Intramolecular phenolate-tris(bipyridyl)Ru(II) PET pairs are known in the literature [55]. The MoO_4^{2-} detection experiments were carried out at a suitably acidic pH value of 5.7 when effective emission quenching was seen. This was also due to PET as unequivocally shown by luminescence recovery in low temperature glasses (i.e. 77K). Careful pH control gave excellent selection of MoO_4^{2-} over Fe^{3+} and many other ionic species. The cationic lumophore also had a role in this pretty story because its charge repels the undesired Fe^{3+} and attracts the desired MoO_4^{2-} .

Sensor **16** [56] has a urea ligand which can bind to a number of anions in acetonitrile solution. For instance, AcO^- bound tightly (binding constant: $\log \beta = 5.2$) and caused almost complete quenching of fluorescence. This is AcO^- -driven NOT logic action. The binding of AcO^- to the urea receptor forms the hydrogen-bond array, resulting in an increase in electron density which enables PET from the binding site towards the phenanthroline fluorophore, even though a formal covalent spacer is not present in **16**. Sensor **17** [57, 58] uses a thiourea receptor for AcO^- . Acceleration of PET from the thiourea unit to the anthracene fluorophore by the anionic charge produced an AcO^- -driven NOT operation.



3.3 Photon Inputs

Pérez et al. [59] designed a “bead on a string” rotaxane consisting of **18** and **19**. The bead **18** sits on the *trans*-fumaric diamide station due to a hydrogen-bond array of high strength in dichloromethane solution. Then the anthracenamido fluorophore is remote from the electron-acceptor pyridinium units, so that PET is absent and the fluorescence is switched “on”. However, light irradiation at 312 nm isomerises the *trans*-fumaric diamide into the *cis*-maleic diamide. The hydrogen-bond array is disrupted in this new station geometry and so the bead moves across to the



glycylglycine station, which creates a hydrogen-bond array with intermediate strength. Now PET becomes strong at this small distance of separation between the anthracenamide and pyridinium units and the fluorescence is switched “off”. This is light dose-driven NOT logic operation with fluorescence output.

4 AND

An AND logic gate produces a high output (binary 1) only when both inputs are high (1) simultaneously. From chemical and biochemical viewpoints, the inputs may be separate species or they may be physically linked in a multifunctional molecule.

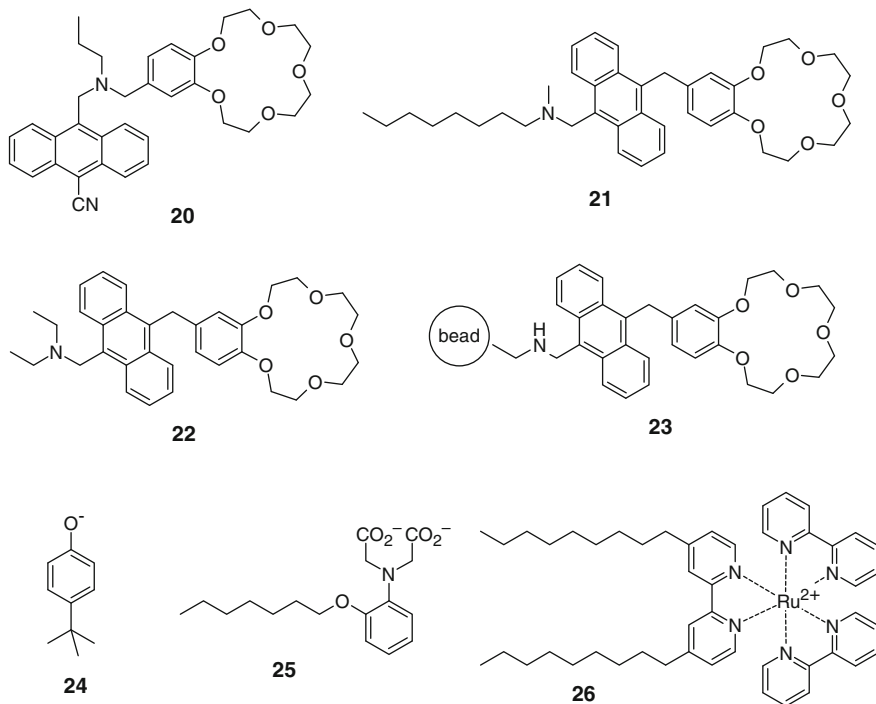
4.1 *Separate Inputs*

The first AND logic gate **20** was constructed using the PET-based “fluorophore-spacer₁-receptor₁-spacer₂-receptor₂” model [4]. A fluorescence signal was output by the anthracene unit only when both chemical inputs (H^+ and Na^+) were present in a sufficient concentration, thus satisfying the AND logic truth table (Fig. 2). The anthracene unit would normally fluoresce blue when it is exposed to ultraviolet light. In the system of **20**, however, the fluorescence was quenched because of a faster PET process, in which an electron was transferred to the anthracene unit from either the amine or benzo-15-crown-5 ether unit. The amine can act as a receptor for H^+ and the benzo-15-crown-5 ether can capture Na^+ . Even if one of these two receptor sites is occupied, PET still occurs from the other to the anthracene unit, and no fluorescence should be observed. If, however, both receptor sites are filled, i.e. H^+ and Na^+ ions are present, both PET paths are prevented and strong fluorescence should result.

Related examples are known [60–64], including a case [64] which operates in nanospaces 3 nm in diameter [65]. The latter were built up from simpler YES gates which operate in the same small milieu [66].

Just like compound **21** [64] was derived from the early AND gate **22** [60] by adding a micelle-anchoring unit, so was **23** [67] obtained by attaching a precursor of **22** to an amino-terminated polymer bead. Gate **23** can be distinguished by its fluorescence response to chemical stimuli as compared to YES and NOT gates. Such a molecular AND logic gate serves as an identification tag for small objects and can be applied to molecular computational identification (MCID) technique [67].

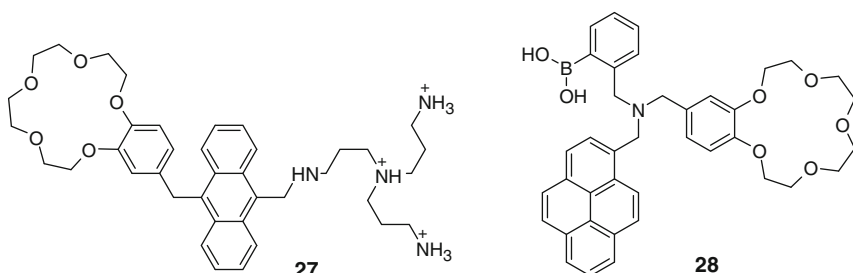
A way to exploit fluorophores for AND logic action is to use them as components of self-assembled systems, e.g. detergent micelles [68]. Aqueous micelles made from Triton X-100 contained the hydrophobic proton receptor **24** and the hydrophobic Ca^{2+} receptor **25**. The hydrophobic fluorophore **26**, which shows a long-lived excited state [69], was also included in the micelle so that it could be quenched quite efficiently by intermolecular PET from **24** and **25**. While it is true that intramolecular PET is faster, this pseudointramolecular system created within the micelle of about 5 nm radius [70] limited the separation distances between the components **24**, **25** and **26** to allow significant PET processes. Addition of H^+ and Ca^{2+} at sufficient concentration arrested both PET pathways to enhance fluorescence of **26** by a factor of 2.4. It has to be noted that this FE factor is quite modest,



but the avoidance of substantial synthesis is a clear advantage. Such self-assembled systems will help laboratories without synthesis capabilities to participate in new developments of molecular logic gates.

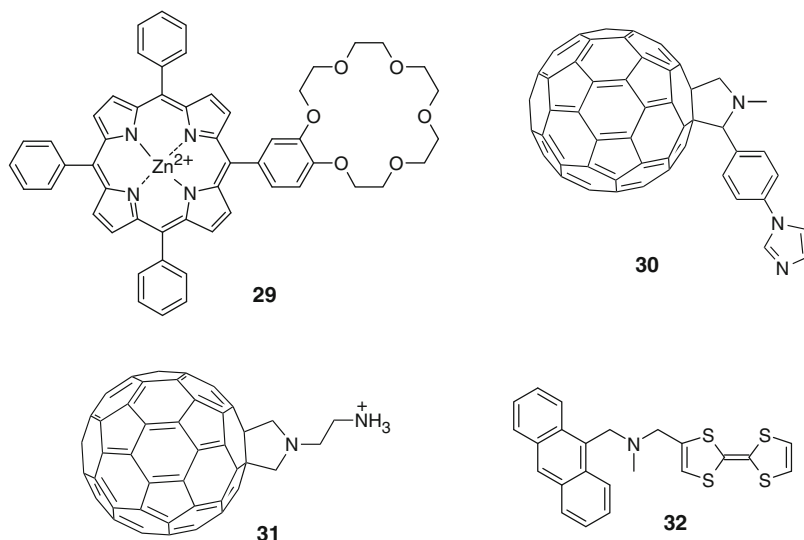
The PET-based “receptor₁-spacer₁-fluorophore-spacer₂-receptor₂” motif was also used in an AND logic gate working with ion pairs as chemical inputs. Incorporating a benzo-15-crown-5 ether to bind Na⁺ and a polyammonium site (developed by Czarnik [71]) to bind HPO₄²⁻, **27** [72] showed increased fluorescence only when both species were present to freeze two PET channels that quenched fluorescence of the anthracene unit (one from the benzo-15-crown-5 ether and the other from the tertiary amine). The polyamine receptor in **27** had poor selectivity in the aqueous methanol solvent and could bind other anions such as Cl⁻, F⁻ and BF₄⁻ prompting a fluorescence emission. However, there was a clear fluorescent enhancement of **27** at pH 8 when both Na⁺ and HPO₄²⁻ were present, i.e. Na⁺, HPO₄²⁻-driven AND action.

Gate **28** [73] by James neatly targets K⁺ and F⁻ together. **28** has a boronic acid moiety to capture F⁻ which facilitates the complexation of the benzocrown ether with K⁺ due to electrostatic attraction. The binding of each receptor to its target cuts off a PET process so that strong fluorescence is produced when the K⁺F⁻ ion pair is encountered.



Maligaspe and D’Souza used the crown-appended porphyrin-Zn(II) **29** complexed to C₆₀-appended imidazole **30** via the metal centre and bound to C₆₀-attached ammonium ion **31** via the crown as the starting state of the device [74]. The fluorescence of the porphyrin-Zn(II) unit was heavily quenched due to PET from it to the C₆₀ moieties. If this ternary complex **29/30/31** was treated with imidazole as input_A, **30** was displaced, thus ridding the one PET pathway which ruined its fluorescence. However, the PET pathway involving **31** was still around [75]. Similarly, treatment of **29/30/31** with K⁺ as input_B displaced **31** but fluorescence was not recovered owing to the continued presence of **30** [76]. It was only when imidazole and K⁺ were both simultaneously present that **29** was freed from the shackles to **30** and to **31**. Strong red fluorescence was the upshot.

Magri’s **32** [77] is an AND logic gate with a fluorescence output driven by redox and H⁺ inputs. Like the amine unit, the tetrathiafulvalene (TTF) unit serves as a



PET donor to the anthracene fluorophore. The PET process from the amine unit can be stopped by protonation as usual. Another PET process from the TTF unit stops after it is selectively oxidized to its dication form. Even then, the PET process from the anthracene to the dicationic TTF unit is apparently prevented only by the Marcus inverted region. The redox reactions of the TTF unit can also be induced by chemical oxidants like Fe(ClO₄)₃.

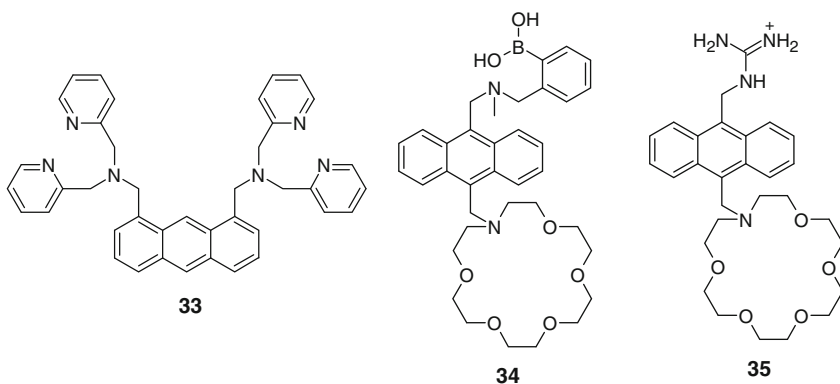
In the presence of Zn²⁺, the ability of **33** [78] to monitor biochemically vital phosphorylation reactions of peptides in water is quite rare and is likely to be very useful. Though the choice of dipicolylamine as a Zn²⁺ receptor is not surprising, the availability of the two receptors for the target phosphorylated peptides is crucial for its success. After the first Zn²⁺ has bound to one receptor, it is much harder to bind the second Zn²⁺ into the second receptor due to electrostatic repulsion. Binding of an anion to the first Zn²⁺ is a common behaviour of such dipicolylamine complexes with incomplete coordination shells. Importantly, Hamachi and colleagues chose a phosphorylated peptide sequence as this anion. Phosphates binding to the first Zn²⁺ facilitated the binding of the second Zn²⁺ to another dipicolylamine receptor by cutting down the aforementioned electrostatic repulsion. Then both PET channels from the benzylic nitrogens to the anthracene fluorophore were blocked, and a large FE was seen. The preliminary paper [79] did not carry this mechanism, however. As has been observed for a long time, blocking one PET channel out of two is not sufficient to obtain a good FE factor [80–82]. Crucially, the complex **33**/Zn²⁺ can discriminate between phosphorylated and non-phosphorylated peptide sequences since the former possess the all-important phosphate unit. At a simple level, we can view **33** as an AND logic gate with Zn²⁺ and phosphate species as inputs.

4.2 Connected Inputs

The idea of connected inputs would be less useful in a semiconductor device context but input chemical species for a molecular device can certainly be connected. These inputs are functional groups which could have existed on separated molecules but are now deliberately coupled within a new multifunctional compound. Such coupling produces a chelate effect where the advantages of higher effective concentration and reduced entropy loss upon binding are seen. A molecular device, with the appropriate geometric disposition of “ports”, can accept the input array presented by the multifunctional compound at lower concentrations than possible with separate input species. If the geometry is inappropriate, the input array at the low concentrations cannot be accepted by this type of molecular device and hence a low output (binary 0) is returned. Thus, the nature of a connector in the input array plays a critical role.

Imagine glucosammonium being split into glucose and ammonium units which can then be separately targeted by an aminomethylphenylboronic acid [83] and an azacrown ether [84] respectively. Indeed, PET has been arrested with these bindings to release fluorescence emission [33, 83]. For instance, sugar binding to aminomethylphenylboronic acid to produce boronate ester leads to a stronger B-N bond which stops the PET process. Then **34** [85, 86] with the two receptors at the appropriate distance of separation could target glucosamine. In this case, the pH value needs to be chosen so that glucosamine is protonated but not the nitrogen centre in the azacrown ether. Cooper and James obtained a fluorescence output signal with **34** in response to glucosamine at the physiological pH. On the other hand, simple ammonium ions and glucose at similar concentrations did not cause the fluorescence switching. The two PET processes present in **34** were arrested by the pair of functional groups binding to their correct receptors. Thus **34** with the heterobireceptor system can be regarded as a glucosammonium-driven AND logic gate.

A previous heterobireceptor system **35** [87] has only one PET process since the guanidinium unit is not sufficiently electroactive. Therefore, a proper AND action



could not be expected even though the bifunctional input γ -aminobutyric acid (GABA) was bound adequately. Indeed the selectivity of fluorescence detection of GABA as compared to related amino acids was not good. Wang's heterobireceptor system **36** [88] uses elements seen in **34** and **35** to target glucarate and again pays the price of the poor electroactivity of the guanidinium unit with a reduced selectivity of detection. Nevertheless, **34–36** are the vanguard of fluorescent sensors empowered with an AND logic operation to detect selectively small multifunctional molecules, many of which are found within cell signalling pathways.

4.3 All-Photonic Inputs

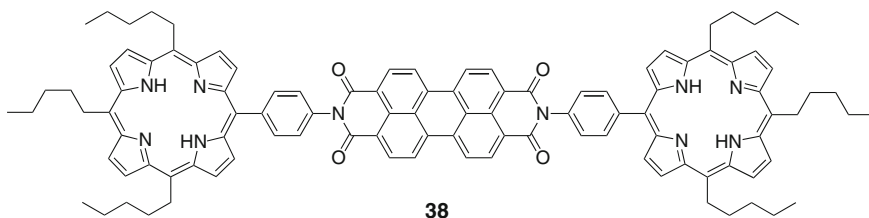
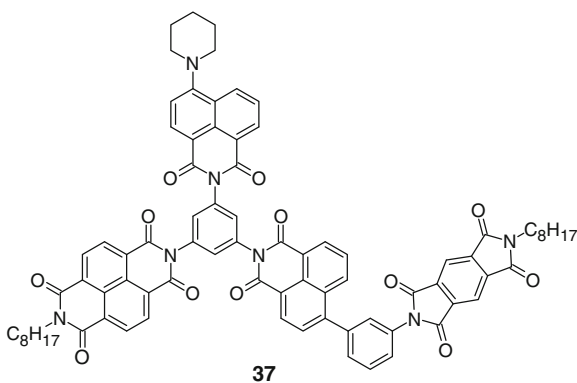
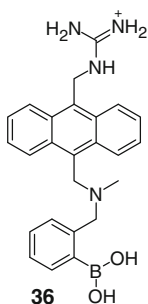
Chemical species are not essential to drive AND logic gates. We now feature cases where photons alone do the job. For instance, two nanosheet diodes built from polymer Langmuir-Blodgett films are operated at different wavelengths to produce an AND logic gate [89]. One nanosheet is constructed with a phenanthrene- and an electron-acceptor-based (dinitrobenzene) acrylate-acrylamide copolymer film and the other with an anthracene- and an electron-donor-based (dimethylamine) acrylate-acrylamide copolymer film. The input signals are light doses possessing excitation wavelengths for the two chromophores, phenanthrene and anthracene, each of which can be selectively excited. When the phenanthrene layer is excited at 300 nm, PET occurs to the dinitrobenzene-containing film, and a low photocurrent is observed. When the anthracene layer is excited at 380 nm, PET occurs from the dimethylamine layer to the anthracene film, giving a low current again. However, when both chromophore-containing polymers are excited simultaneously, charge transport occurs from the phenanthrene to the dinitrobenzene to the dimethylamine to the anthracene layer with a high photocurrent. Thus, an AND logic operation is demonstrated with two optical inputs and an electrical output.

Other examples of all-optical AND logic operations at the molecular-level have become available [90, 91] even though an old claim of this kind in conference proceedings seems not to have arrived in the refereed literature [92]. Gate **37** [90] due to the team of Wasielewski achieved his objective by a very different means. The tetra-chromophore system **37** is held together by *m*-substituted benzene rings. The 4-amino-1,8-naphthalimide was initially pumped at 420 nm to cause PET from it to the 1,4,5,8-naphthalenediimide. The other chromophores became involved only if the naphthalenediimide radical anion was pumped at 480 nm. Then the extra electron within the naphthalenediimide was passed to the 1,8-naphthalimide and then on to the 1,2,4,5-benzenediimide. So the absorption signature of the benzenediimide radical anion at 720 nm (the output) was only observed if the two femtosecond laser pulses at 420 nm (input_A) and at 480 nm (input_B) were applied sequentially (2-ns separation). It is notable, however, that conventional AND logic gates require simultaneous, not sequential, application of inputs and a

2-ns delay would matter in devices running near GHz rates. Nevertheless **37** is a rather fast gate since it resets in 25 ns.

Wasielowski's previous publication on **38** [93, 94] was the forerunner of the discussion concerning **37** [90]. The donor-acceptor molecule **38** was capable of a fast switch with potential logic capabilities. The two terminal porphyrin donor moieties could independently reduce the central perylene tetracarboxydiimide acceptor moiety via PET. When only one porphyrin was excited by a femtosecond laser pulse, the absorption due to the perylene tetracarboxydiimide radical anion was seen. If both porphyrins were excited simultaneously by a higher intensity laser pulse, two PET processes to the central acceptor could occur, giving a dianion with a different absorption band.

It was imagined that **38** could perform the AND logic operation if two light beams of different wavelengths were used as inputs, and if the dianion absorption was taken as the output. This would be possible for **38** since excitation of the perylene tetracarboxydiimide moiety would induce the first PET process, and the second input light dose should have a wavelength matching the porphyrin absorption. The speed of such light-driven molecular switches and gates would be testimony to the lightness of their only "moving part" – the electron. It can also be imagined how two laser pulses of sub-threshold intensity at the same wavelength can be combined to create the dianion absorption, i.e. AND logic operation.

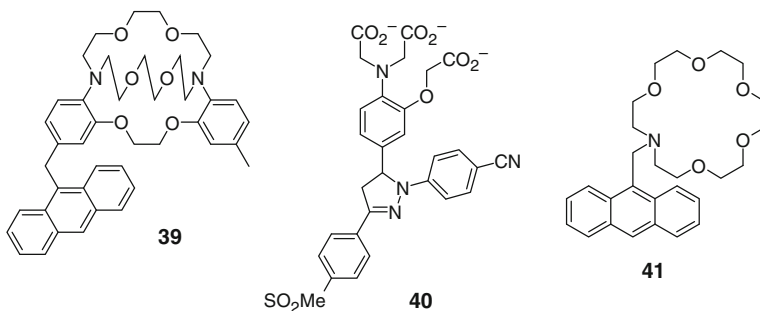


5 OR

Molecular OR logic gates might seem an antithesis since most chemical research aims for selective sensing. Nevertheless, unselective behaviour of a given receptor towards, say, two different guests enables us to approach an OR logic gate containing a single receptor alone, i.e. double-input logic gate with a single port.

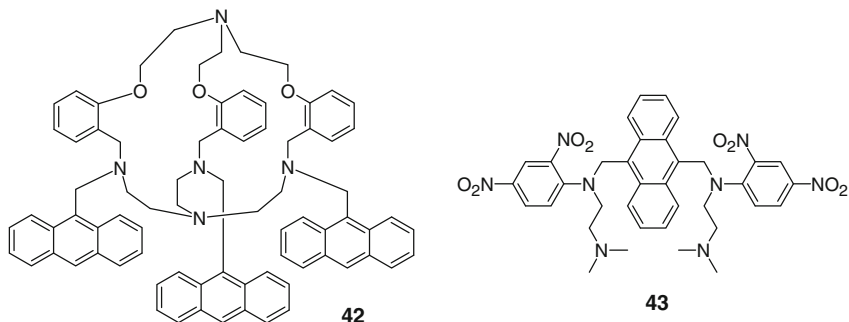
While an old example of molecular OR logic gates can be located in **39** [95], the first deliberately designed gate of this type was **40** [96]. Gate **40** with a “fluorophore-spacer-receptor” PET system has an aromatic amino acid receptor which acts as an electron donor towards the excited diarylpyrazoline fluorophore resulting in negligible emission. This receptor is sufficiently unselective to Ca^{2+} or Mg^{2+} so that binding of either ion, supplied at high enough concentration, blocks the electron rich sites of the receptor and prevents PET. Each ion produces essentially identical extents of switching “on”. This similarity is due to essentially identical conformational changes by the complexation. Each ion-bound state effectively decouples the amine substituent from the oxybenzene unit so that PET is similarly suppressed. This also means that the charge density difference between the two cations is of secondary importance in these conformationally switchable systems. It is also notable that a single-receptor system is sufficient in this case to achieve a two-input OR logic gate.

The gate **39** [95] mentioned above gave almost equal fluorescence enhancements when sufficient quantities of K^+ or Rb^+ were added, probably for a similar reason as for **40**. The relative rigidity of the cryptand moiety exacted a price. Only when neither input species was present, the fluorescence was seen to be switched “off” due to fast PET. Compound **41** [33] of the same PET design but without a conformational switch as in **40**, produced less unselective FE due to a charge density effect.



Gate **42** [97] is interesting because various transition metal ions serve to switch “on” fluorescence by more-or-less same amounts. The surprise in this system [97, 98] is that transition metal ions were acting contrary to their normal behaviour. Transition metal ions have a history of quenching fluorescence very efficiently by several mechanisms: heavy atom effects, PET, electronic energy transfers and

paramagnetic effects. The authors of **42** appear to have eliminated the possibility of artefacts arising from protonation due to hydration shells of highly charged transition metal ions. Other OR logic gates such as **43** [99, 100] have come from the same laboratory.

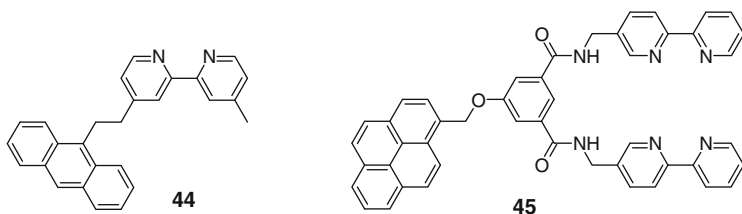


6 NOR

Although a NOR logic gate is as legitimate as any of the other 15 double-input, single-output logic gates, common computer literature represents it as a particular integration of NOT and OR gates (as its name and its symbol also suggest). A physical integration requires additional molecule-molecule linking that throws up obstacles towards molecular implementation. On the other hand, a functional integration of NOT and OR logic gates would be sufficient to achieve this goal without a physical connection of the two original gates. This idea can be extended to the design of new switches that integrate a number of logic functions within a single molecular structure [101] so that gates with more complex logic would emerge.

In a fluorescent photoionic context we can argue as follows. A NOT logic gate switches “off” fluorescence when an ionic species arrives. A two-input OR logic gate unselectively switches “on” fluorescence when either of two ionic species arrives. So a NOR logic gate switches “off” fluorescence when either of two ionic species arrives. For example, using a “fluorophore-spacer-receptor” motif consisting of an anthracene fluorophore, a methylene spacer and a 2,2'-bipyridyl receptor to bind either H^+ or Zn^{2+} , **44** [102] works as a NOR logic gate. When the 2,2'-bipyridyl unit complexes either H^+ or Zn^{2+} , it becomes more reducible due to its cationic nature and increased planarity [103]. This reducibility allows a PET process to occur from the anthracene fluorophore to the 2,2'-bipyridyl receptor to quench the fluorescence emission. The non-selectivity of the input-induced fluorescence response required for NOR logic gates is not as stringent as for OR logic gates provided that the quenching is efficient enough.

The pyrene-based fluorescence of Fages' **45** [104] was switched “off” by Zn^{2+} . H^+ should give a similar result, thereby recognizing **45** as a NOR logic gate.



Fluorescent crown-appended porphyrin-Zn(II) **29** [74], which was introduced in the former section of AND gates, becomes a representative NOR gate when **29** itself is viewed as a logic gate. Application of C₆₀-appended imidazole **30** (input_A) bound it to the Zn(II) centre of **29** and set off a PET process from the porphyrin-Zn(II) unit to the C₆₀ moiety which switches the emission “off” [76]. Similarly, treatment of **29** with C₆₀-attached ammonium ion **31** (input_B) bound the latter to the benzocrown ether of **29** and caused a PET process again [75]. The fluorescence was quenched as a result. Addition of both inputs formed a ternary complex **29/30/31** which was lumbered with two possible PET processes and no fluorescence was seen again.

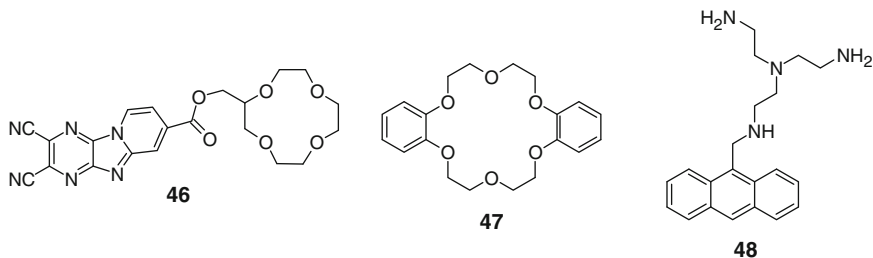
7 NAND

A NAND logic gate can be understood as an integration of NOT and AND gates where the output of the AND gate becomes the input to a NOT gate. Nice molecular examples are now available.

Iwata and Tanaka discussed **46** [105] in terms of an AND logic gate but now it is interpretable as the first molecular NAND logic gate. The fluorescence of the heteroaromatic unit was quenched only when Ba²⁺ and SCN⁻ ions were simultaneously present at suitably high concentrations. Since Ba²⁺ is large in comparison with the crown ether cavity, the ester carbonyl group probably co-ordinated as in the lariat ethers [84]. The large residual charge was counteracted by the binding of SCN⁻ to the captured Ba²⁺ in an apical fashion. Only when electron rich SCN⁻ was held near the fluorophore in this way did the fluorescence-quenching PET process kick in.

As far back as 1984, Wolfbeis described the fluorescence quenching of dibenzo-18-crown-6 ether **47** in the presence of K⁺ and I⁻ [106] which can now be understood to be NAND logic behaviour. It is likely that the oxidizable I⁻ is ion-paired to the crown-bound K⁺ in much the same way as in the system involving **46**, Ba²⁺ and SCN⁻.

Fabbrizzi's **48** [107] first receives Zn²⁺ into the tetraamine cavity and then an anionic nitrobenzoate guest can be held by coordination of the benzoate to the Zn²⁺'s free apical position. Provided Zn²⁺ is present in the binding site, the electron deficient nitrobenzoate engages in PET with the anthracene fluorophore of **48** to switch the fluorescence “off”.



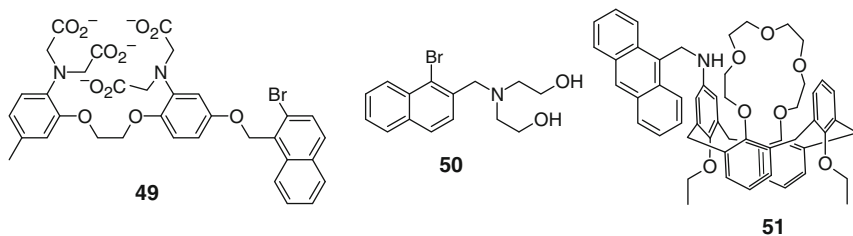
8 INHIBIT

An INHIBIT logic gate is another type which can be viewed as an integration of NOT and AND gates though in a different connectivity than seen with a NAND logic gate. The NOT operation is only applied to input_B (Fig. 2). So the input_B is really a disabling input that kills the output irrespective of the state of input_A.

A three-input version of INHIBIT logic gates can be demonstrated with **49** [102]. The gate **49** uses Ca^{2+} as input_A to the amino acid receptor [108] to block a PET process from this receptor to the triplet excited state of the bromonaphthalene phosphor [109]. **49** also uses β -cyclodextrin as input_B which actually encapsulates the phosphor [110, 111] to protect it from triplet-triplet annihilation which occurs between the triplet excited state of bromonaphthalene and another copy of itself to cause mutual de-excitation. It is important to note that β -cyclodextrin is transparent to the exciting light. The disabling third input is O_2 which, due to its paramagnetism, wrecks the phosphorescence emitted from the bromonaphthalene phosphor whether it is enveloped by β -cyclodextrin or not. Phosphorescence quenching is a general disabling process [112–115]. Functional rather than physical integration succeeds here too.

A newer gate **50** [116] replaces the Ca^{2+} receptor within **49** with an aliphatic amine unit which binds H^+ . The nitrogen atom in this amine unit serves as a PET donor to the triplet excited state of the bromonaphthalene phosphor. Therefore this is driven by H^+ , β -cyclodextrin and O_2 inputs where the last is the disabling input.

A two-input INHIBIT logic gate **51** [117] switches “on” fluorescence by H^+ but only as long as K^+ is absent. The 1,3-alternate calixcrown binds K^+ via

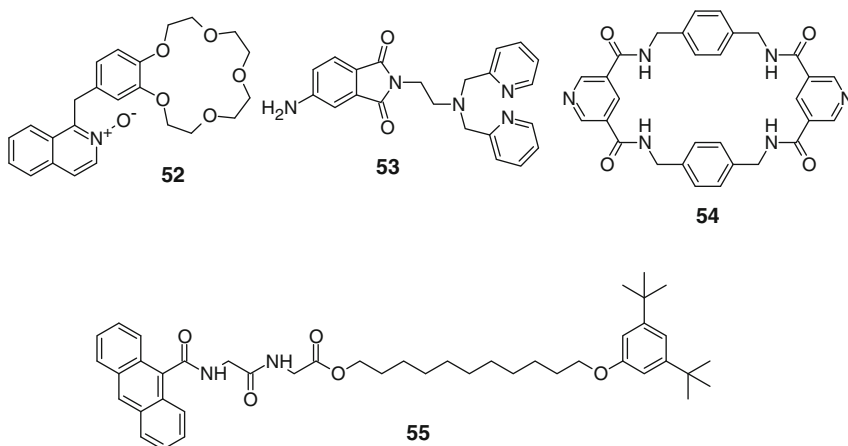


ion-dipole and cation- π interactions [118]. The bound K^+ electrostatically ejects H^+ from the anilinium moiety (if it had been previously protonated), but is apparently incapable of sufficient direct interaction with the lone pair of an anilino nitrogen and so PET is re-established from the aniline unit to the anthracene fluorophore.

Another gate is **52** [119] where PET unusually produces an observable charge transfer (CT) emission when the N-oxide attaches onto H^+ [120, 121]. In most cases, PET causes only the loss of the characteristic emission of the fluorophore in a locally excited (LE) state. However, in the present case, PET was arrested by attaching K^+ to the benzocrown ether and so the CT emission subsided as well. K^+ is therefore the disabling input of this INHIBIT gate. The fact that **52**'s emission could be observed from the CT or LE state, or even at intermediate wavelengths, is notable and that it could receive H^+ or Zn^{2+} at the N-oxide oxygen centre, besides receiving K^+ or Ba^{2+} at the crown ether, is an added distinction. From another viewpoint, **52** combines PET with an internal charge transfer (ICT) process since the N-oxide is integrated into the fluorophore. Such combined switching mechanisms are rare, too [122].

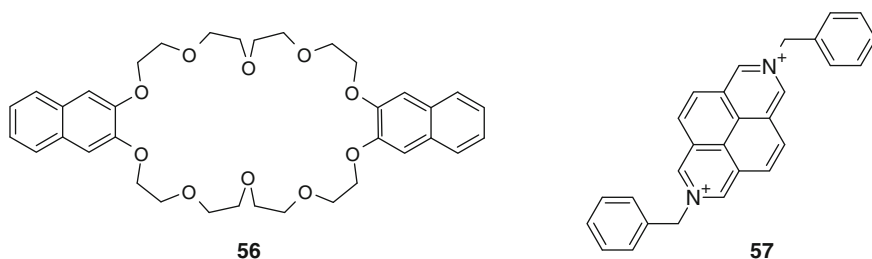
Fluorescence output from **53** [123] is observed in the presence of Zn^{2+} (or Cd^{2+} or Pd^{2+}) and in the absence of excess H^+ . Such high H^+ level displaces Zn^{2+} from the bis(2-picoly)amine receptor and the pyridinium groups so formed encourage PET from the aminophthalimide fluorophore. In the absence of this problem, Zn^{2+} blocks PET from the tertiary amine to the fluorophore, thus producing fluorescence emission. So this is a H^+ , Zn^{2+} -driven INHIBIT logic operation, with high levels of H^+ causing low output in all situations.

Rotaxane from **54** and **55** [124] and a related polymeric rotaxane have also been converted into INHIBIT gates driven by H^+ and polar solvents as inputs.



9 XOR

Though mathematicians give an XOR logic gate equal weight with another 15 two-input logic gates [125, 126], XOR logic gates have received more than the usual amount of attention since these are an essential part of semiconductor numeracy. The first XOR logic gate was produced by Balzani's and Stoddart's teams. Pseudorotaxane **56/57** [127] was non-emissive owing to PET-type CT processes. Either H^+ or Bu_3N can dissociate the pseudorotaxane components by binding with **56** or **57**, respectively. The protonation of the crown ether oxygens of **56** succeeded because of the poorly solvating organic medium. Overall, bright fluorescence was observed from free **56** or protonated **56**, both of which happen to emit in the same wavelength range. Clearly the addition of 1:1 H^+ and Bu_3N , a case of acid-base neutralization, gave no change from the original non-emissive situation. Thus the four rows of the XOR truth table (Fig. 2) were reproduced.

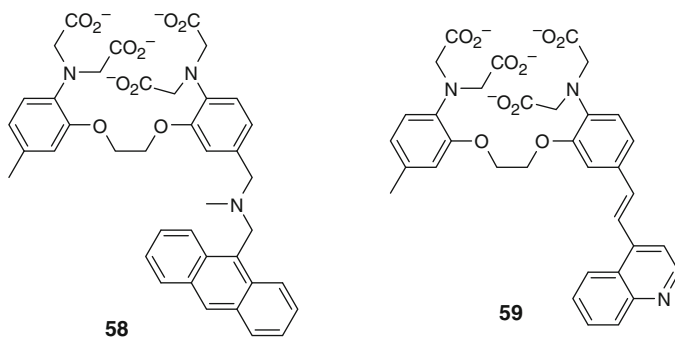


Matsui et al. have extended the nanosheet approach discussed in the section of AND logic gates [89] to a XOR logic gate as well [128].

10 Half-Adder

The first expression of molecular numeracy was special because people become (and remain) numerate via mysterious, but molecular, processes in their brains. An electronic half-adder circuit has two inputs and two output channels which is the basis of number processing in most electronic computers. Addition needs an AND logic gate for the carry digit and an XOR logic gate for the sum digit (Fig. 2) [129, 130].

In order to demonstrate a first molecular version, we selected the inputs to be Ca^{2+} and H^+ , while the outputs were fluorescence quantum yield for the carry digit and transmittance at 390 nm for the sum digit. **58** [60] is a PET-based AND logic gate very much in the mould of the very first example of this kind [4] but when combined in parallel with the compatible XOR logic gate **59** [60] we had molecular-scale arithmetic for the first time. Molecular arithmetic had been hampered



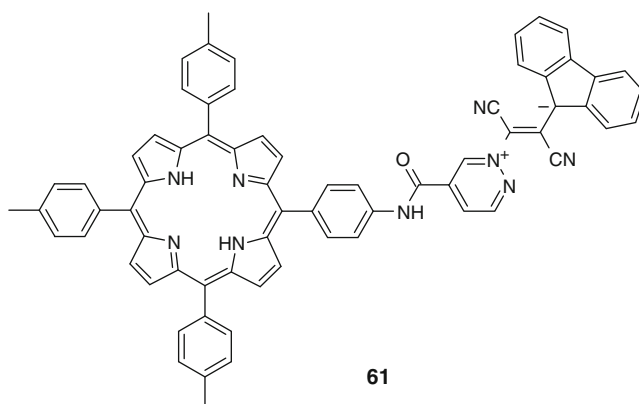
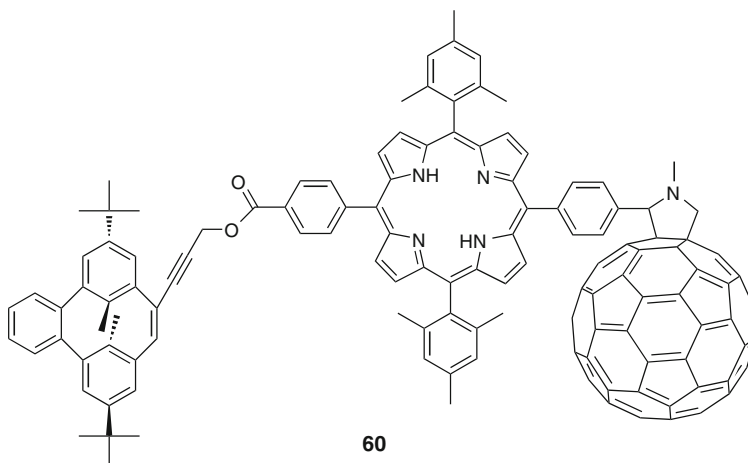
because the available AND and XOR gate molecules were not compatible with each other to permit their parallel operation. The truth table for the half-adder is indicated in Fig. 2.

The mechanism of action of the XOR gate **59** does not involve PET but concerns a push-pull system which has selective receptors at opposite terminals. The energy of the ICT excited state of **59** is perturbed in opposite directions when each receptor is blocked by its guest. So the absorption blue-shifts with Ca^{2+} and red-shifts with H^+ . When both guests are present, the shifts cancel and the status quo is regained. Observation of the transmittance of **59** at 390 nm now gives the XOR logic operation.

The system with **58** and **59** is notable because the parallelism is attained by deliberate mixing of gates. As shown in Fig. 2, the four rows for a half-adder show binary addition of 0 (input_A) and 0 (input_B) to give 00 (output), 0 and 1 to give 01, 1 and 0 to give 01, 1 and 1 to give 10. In the more common decimal numbering these operations become the kindergarten classics: $0 + 0 = 0$; $0 + 1 = 1$; $1 + 0 = 1$ and $1 + 1 = 2$. This also establishes the ascending hierarchy of numbers 0, 1 and 2 from a molecular perspective – something we learned on our mothers' knee.

An all-optical half-adder was demonstrated by Andreasson et al. [131]. They employed **60** and **61** that use light at 1,064 and 532 nm as inputs to show both logic types required for a half-adder. The absorption at 1,000 nm (AND logic) as well as the fluorescence at 720 nm (XOR logic) were the outputs, making this system a nice addition to molecular arithmetic. AND logic gate **60** is a triad consisting of a porphyrin linked to a C_{60} electron acceptor and a cyclophanediene photochrome. XOR logic gate **61** is a molecular dyad containing a porphyrin but coupled to a betaine photochrome instead.

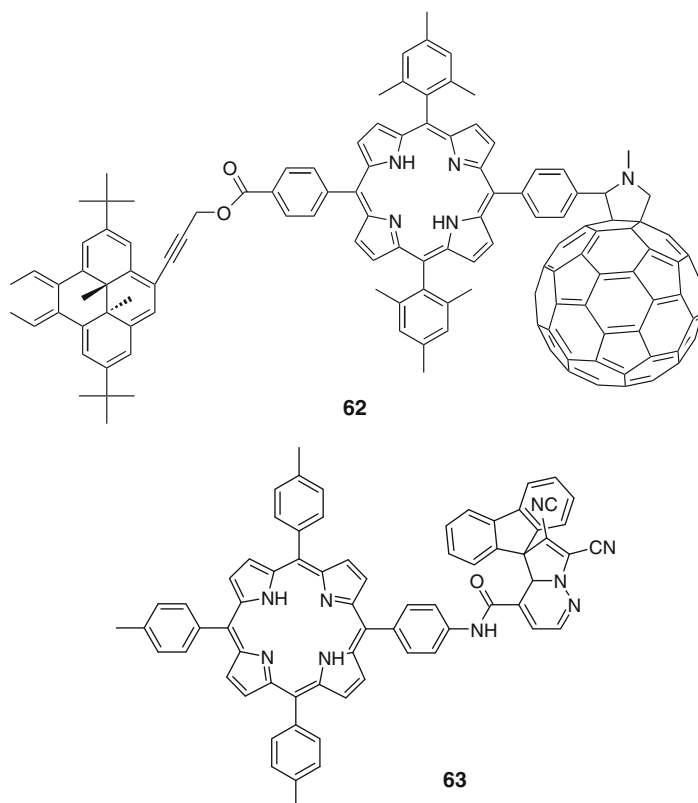
How did the AND action arise? Since the two inputs were 1,064 nm and 532 nm laser pulses, their simultaneous presence in an intervening third-harmonic generating crystal produced 355 nm light via frequency mixing. The light at 355 nm was absorbed by the cyclophanediene unit of **60** and it was converted to the dihydropyrene via an electrocyclic ring closure to produce **62**. When the central porphyrin unit in **62** was excited by a read laser at 650 nm, PET occurred from it to the C_{60} unit. Another thermal ET quickly followed from the dihydropyrene unit to the porphyrin



radical cation. The resulting dihydropyrene radical cation spaced by the porphyrin ground state from the C_{60} radical anion lasted for microseconds. This long-lived state's absorbance at 1,000 nm was the output of the AND gate. Clearly, the laser power was chosen so that the 1,064 nm pulse alone would not produce 355 nm light within the third-harmonic generating crystal. The 532 nm pulse could not do this.

The starting state **60** could be recovered by 532-nm irradiation for absorption by the dihydropyrene unit in **62** and electrocyclic ring opening. Of course, running photochromic reactions in the presence of photoactive units of lower excited state energy generally causes excitation energy transfer (EET) and efficiency losses should be expected.

The XOR gate **61**'s action arose as follows. The read laser elicited a low level of fluorescence from the porphyrin unit since the betaine unit is a PET acceptor. In addition, 1,064-nm illumination allowed thermal ring closure of the betaine unit to the dihydroindolizine unit and produced **63**. With the betaine unit gone, **63** has a high level of fluorescence. And 532-nm illumination also produced the same result,



but by photochemical ring closure. On the other hand, the two inputs of 1,032-nm and 532-nm pulses mixed together in the third-harmonic generating crystal to produce the 355 nm light caused photoisomerisation of the dihydroindolizine unit to the betaine unit to give **61** again.

It is clear that the essential third-harmonic generating crystal brings in a bulk material component to what is otherwise a molecular-scale experiment. However, the all-optical nature of inputs, outputs and power supplies are to be applauded even though quantitative input-output homogeneity was not achieved. A related case is by Guo et al. [132] which involves PET too.

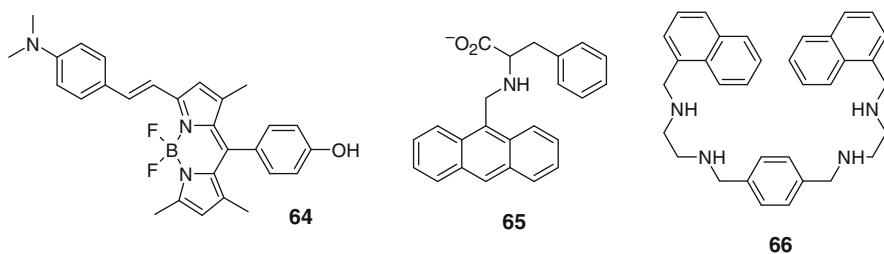
11 Half-Subtractor

Compound **64** [133] is an ICT fluorophore emitting at 660 nm in THF. The dimethylamino unit in **64** is an electron pushing component in this push-pull π -electron system. The addition of $t\text{-BuO}^-$ deprotonates the phenol group and the emission is switched “off” due to PET across the virtual spacer. Upon addition of H^+ , **64** gives a blue-shifted emission at 565 nm due to protonation of the

dimethylamino unit and the subsequent reduced ICT nature of the π -system. When equimolar $t\text{-BuO}^-$ and H^+ are added (both inputs “1”), nothing happens due to neutralization and the original fluorescence at 660 nm is preserved. If we choose emission at 565 nm as the output, **64** corresponds to an INHIBIT logic gate with $t\text{-BuO}^-$ as the disabling input.

If we reconfigure **64** by choosing emission at 660 nm as the output, this corresponds to an XNOR logic gate. The latter can be quickly converted to an XOR logic gate by using a negative logic convention for the output signals, i.e. by taking “high” output signals as logic state “0” and “low” signals as logic state “1”.

The $\text{H}^+\text{-OH}^-$ annihilation method introduced by Balzani and Stoddart for designing XOR logic gates [127] can also be applied to an equimolar mixture of Cu^{2+} and **65** [134] based on a “fluorophore-spacer-receptor” system. In this instance, the absorbance at 255 nm drops seriously at pH 7 (where **65** exists as the protonated form) but not when an equivalent of H^+ or OH^- is added. Naturally, when an equivalent each of H^+ and OH^- is added, the pH value remains at 7 and the absorbance at 255 nm remains low. This is the XOR gate component and suggests aggregation of electroneutral complex $(\text{65})_2/\text{Cu}^{2+}$ as an underlying mechanism in these phenomena. Since **65** has a PET system with an amine donor, it is clear that protonation prevents binding to Cu^{2+} besides stopping PET and releasing fluorescence. In the presence of OH^- , Cu^{2+} is precipitated as $\text{Cu}(\text{OH})_2$ and PET within the freed **65** switches fluorescence “off”. At pH 7, the complex $(\text{65})_2/\text{Cu}^{2+}$ is non-fluorescent because of EET from the fluorophore to the Cu^{2+} centre as well as PET. Here is the INHIBIT gate component. Operation of the two gate components in parallel results in the half-subtractor. Another example arises from a mixture of **66** [135] and Zn^{2+} driven by inputs of H^+ and OH^- .



12 Conclusion

We hope that the evidence gathered in this review, though nowhere near comprehensive, is sufficient to indicate how far the fields of molecular logic and luminescent sensing have come over the recent past. What will the near future bring? The answer lies in the hands and minds of the new generation of sensor and logic gate designers. If this review manages to attract a few bright people to swell the ranks of that new generation, we can rest happy.

References

1. Bissell RA, de Silva AP, Gunaratne HQN, Lynch PLM, Maguire GEM, McCoy CP, Sandanayake KRAS (1993) *Top Curr Chem* 168:223
2. de Silva AP, Gunaratne HQN, Gunnlaugsson T, Huxley AJM, McCoy CP, Rademacher JT, Rice TE (1997) *Chem Rev* 97:1515
3. Demchenko AP (2009) *Introduction to fluorescence sensing*. Springer, Netherlands
4. de Silva AP, Gunaratne HQN, McCoy CP (1993) *Nature* 364:42
5. de Silva AP, McClenaghan ND, McCoy CP (2001) In: Balzani V (ed) *Electron transfer in chemistry*, vol 5. Wiley VCH, Weinheim, p 156
6. de Silva AP, McClenaghan ND, McCoy CP (2001) In: Feringa BL (ed) *Molecular switches*. Wiley VCH, Weinheim, p 339
7. Raymo FM (2002) *Adv Mater* 14:401
8. de Silva AP, McClenaghan ND (2004) *Chem Eur J* 10:574
9. Gust D, Moore TA, Moore AL (2006) *Chem Commun* 1169
10. de Silva AP, Uchiyama S (2007) *Nat Nanotechnol* 2:399
11. Pischel U (2007) *Angew Chem Int Ed* 46:4026
12. Credi A (2007) *Angew Chem Int Ed* 46:5472
13. Szaciłowski K (2008) *Chem Rev* 108:3481
14. Balzani V, Credi A, Venturi M (2008) *Molecular devices and machines*, 2nd edn. Wiley-VCH, Weinheim
15. Benenson Y (2009) *Mol Biosyst* 5:675
16. Andréasson J, Pischel U (2010) *Chem Soc Rev* 39:174
17. Katz E, Privman V (2010) *Chem Soc Rev* 39:1835
18. Malvino AP, Brown JA (1993) *Digital computer electronics*, 3rd edn. Glencoe, New York
19. Boole G (1958) *An investigation of the laws of thought*. Dover, New York
20. Gregg JR (1998) *Ones and zeros*. IEEE Press, New York
21. Kirkbright GF (1972) In: Bishop E (ed) *Indicators*. Pergamon, Oxford, p 685
22. Zang L, Liu R, Holman MW, Nguyen KT, Adams DM (2002) *J Am Chem Soc* 124:10640
23. de Silva AP, Rupasinghe RADD (1985) *J Chem Soc Chem Commun* 1669
24. Harris RF, Nation AJ, Copeland GT, Miller SJ (2000) *J Am Chem Soc* 122:11270
25. Daffy LM, de Silva AP, Gunaratne HQN, Huber C, Lynch PLM, Werner T, Wolfbeis OS (1998) *Chem Eur J* 4:1810
26. Brasselet S, Moerner WE (2000) *Single Mol* 1:17
27. Ameloot R, Roeffaers M, Baruah M, De Cremer G, Sels B, De Vos D, Hofkens J (2009) *Photochem Photobiol Sci* 8:453
28. Fahrni CJ, Yang L, VanDerveer DG (2003) *J Am Chem Soc* 125:3799
29. Cody J, Mandal S, Yang L, Fahrni CJ (2008) *J Am Chem Soc* 130:13023
30. de Silva AP, Gunaratne HQN (1990) *J Chem Soc Chem Commun* 186
31. de Silva AP, Gunaratne HQN, Gunnlaugsson T, Nieuwenhuizen M (1996) *Chem Commun* 1967
32. Pragst F, Weber FG (1976) *J Prakt Chem* 318:51
33. de Silva AP, de Silva SA (1986) *J Chem Soc Chem Commun* 1709
34. Kollmannsberger M, Rurack K, Resch-Genger U, Rettig W, Daub J (2000) *Chem Phys Lett* 329:363
35. de Silva AP, Sandanayake KRAS (1989) *J Chem Soc Chem Commun* 1183
36. Kenmoku S, Urano Y, Kanda K, Kojima H, Kikuchi K, Nagano T (2004) *Tetrahedron* 60:11067
37. Bissell RA, de Silva AP, Gunaratne HQN, Lynch PLM, Maguire GEM, Sandanayake KRAS (1992) *Chem Soc Rev* 21:187
38. de Silva AP, Gunaratne HQN, Rice TE (1996) *Angew Chem Int Ed* 35:2116
39. de Silva AP, Gunaratne HQN, Rice TE, Stewart S (1997) *Chem Commun* 1891

40. Gunnlaugsson T, Leonard JP (2003) *Chem Commun* 2424
41. Ozmen B, Akkaya EU (2000) *Tetrahedron Lett* 41:9185
42. Yoon S, Albers AE, Wong AP, Chang CJ (2005) *J Am Chem Soc* 127:16030
43. de Silva AP, Gunaratne HQN, Kane ATM, Maguire GEM (1995) *Chem Lett* 125
44. Rurack K, Kollmannsberger M, Resch-Genger U, Daub J (2000) *J Am Chem Soc* 122:968
45. Nolan EM, Lippard SJ (2003) *J Am Chem Soc* 125:14270
46. Guo X, Qian X, Jia L (2004) *J Am Chem Soc* 126:2272
47. Prodi L, Bargossi C, Montalti M, Zaccheroni N, Su N, Bradshaw JS, Izatt RM, Savage PB (2000) *J Am Chem Soc* 122:6769
48. Bronson RT, Montalti M, Prodi L, Zaccheroni N, Lamb RD, Dalley NK, Izatt RM, Bradshaw JS, Savage PB (2004) *Tetrahedron* 60:11139
49. Chang CJ, Nolan EM, Jaworski J, Burdette SC, Sheng M, Lippard SJ (2004) *Chem Biol* 11:203
50. Tsien RY (1994) *Chem Eng News* 72(29):34
51. Gunnlaugsson T, Lee TC, Parkesh R (2003) *Org Biomol Chem* 1:3265
52. Kubo Y, Tsukahara M, Ishihara S, Tokita S (2000) *Chem Commun* 653
53. de Silva AP, Gunaratne HQN, Lynch PLM (1995) *J Chem Soc Perkin Trans 2* 685
54. Jedner SB, James R, Perutz RN, Duhme-Klair AK (2001) *J Chem Soc Dalton Trans* 2327
55. Grigg R, Holmes JM, Jones SK, Norbert WDJA (1994) *J Chem Soc Chem Commun* 185
56. dos Santos CMG, McCabe T, Gunnlaugsson T (2007) *Tetrahedron Lett* 48:3135
57. Gunnlaugsson T, Davis AP, Glynn M (2001) *Chem Commun* 2556
58. Gunnlaugsson T, Davis AP, Hussey GM, Tierney J, Glynn M (2004) *Org Biomol Chem* 2:1856
59. Pérez EM, Dryden DTF, Leigh DA, Teobaldi G, Zerbetto F (2004) *J Am Chem Soc* 126:12210
60. de Silva AP, McClenaghan ND (2000) *J Am Chem Soc* 122:3965
61. de Silva AP, Gunaratne HQN, McCoy CP (1997) *J Am Chem Soc* 119:7891
62. Magri DC, Coen GD, Boyd RL, de Silva AP (2006) *Anal Chim Acta* 568:156
63. Bag B, Bharadwaj PK (2005) *Chem Commun* 513
64. Uchiyama S, McClean GD, Iwai K, de Silva AP (2005) *J Am Chem Soc* 127:8920
65. Sumaru K, Matsuoka H, Yamaoka H, Wignall GD (1996) *Phys Rev E* 53:1744
66. Bissell RA, Bryan AJ, de Silva AP, McCoy CP (1994) *J Chem Soc Chem Commun* 405
67. de Silva AP, James MR, McKinney BOF, Pears DA, Weir SM (2006) *Nat Mater* 5:787
68. de Silva AP, Dobbin CM, Vance TP, Wannalerse B (2009) *Chem Commun* 1386
69. Domínguez-Gutiérrez D, De Paoli G, Guerrero-Martínez A, Ginocchietti G, Ebeling D, Eiser E, De Cola L, Elsevier CJ (2008) *J Mater Chem* 18:2762
70. Goyal PS, Menon SVG, Dasannacharya BA, Thiyagarajan P (1995) *Phys Rev E* 51:2308
71. Huston ME, Akkaya EU, Czarnik AW (1989) *J Am Chem Soc* 111:8735
72. de Silva AP, McClean GD, Pagliari S (2003) *Chem Commun* 2010
73. Koskela SJM, Fyles TM, James TD (2005) *Chem Commun* 945
74. Maligaspe E, D'Souza F (2010) *Org Lett* 12:624
75. D'Souza F, Chitta R, Gadde S, Zandler ME, McCarty AL, Sandanayaka ASD, Araki Y, Ito O (2005) *Chem Eur J* 11:4416
76. D'Souza F, Deviprasad GR, Zandler ME, Hoang VT, Klykov A, VanStipdonk M, Perera A, El-Khouly ME, Fujitsuka M, Ito O (2002) *J Phys Chem A* 106:3243
77. Magri DC (2009) *New J Chem* 33:457
78. Ojida A, Mito-oka Y, Sada K, Hamachi I (2004) *J Am Chem Soc* 126:2454
79. Ojida A, Mito-oka Y, Inoue M, Hamachi I (2002) *J Am Chem Soc* 124:6256
80. de Silva AP, Sandanayake KRAS (1990) *Angew Chem Int Ed Engl* 29:1173
81. Czarnik AW (1994) *ACS Symp Ser* 561:314
82. James TD, Sandanayake KRAS, Shinkai S (1994) *Angew Chem Int Ed Engl* 33:2207
83. James TD, Sandanayake KRAS, Shinkai S (1996) *Angew Chem Int Ed Engl* 35:1911.
84. Gokel GW (1991) *Crown ethers and cryptands*. Royal Society of Chemistry, Cambridge

85. Cooper CR, James TD (1997) *Chem Commun* 1419
86. Cooper CR, James TD (2000) *J Chem Soc Perkin Trans 1* 963
87. de Silva AP, Gunaratne HQN, McVeigh C, Maguire GEM, Maxwell PRS, O'Hanlon E (1996) *Chem Commun* 2191
88. Yang W, Yan J, Fang H, Wang B (2003) *Chem Commun* 792
89. Matsui J, Mitsuishi M, Aoki A, Miyashita T (2003) *Angew Chem Int Ed* 42:2272
90. Lukas AS, Bushard PJ, Wasielewski MR (2001) *J Am Chem Soc* 123:2440
91. Remacle F, Speiser S, Levine RD (2001) *J Phys Chem B* 105:5589
92. Birge R (1992) In: Crandall BC, Lewis J (eds) *Nanotechnology: research and perspectives*. MIT Press, Cambridge, p 149
93. Wasielewski MR, O'Neil MP, Gosztola D, Niemczyk MP, Svec WA (1992) *Pure Appl Chem* 64:1319
94. O'Neil MP, Niemczyk MP, Svec WA, Gosztola D, Gaines GL III, Wasielewski MR (1992) *Science* 257:63
95. de Silva AP, Gunaratne HQN, Sandanayake KRAS (1990) *Tetrahedron Lett* 31:5193
96. de Silva AP, Gunaratne HQN, Maguire GEM (1994) *J Chem Soc Chem Commun* 1213
97. Ghosh P, Bharadwaj PK, Mandal S, Ghosh S (1996) *J Am Chem Soc* 118:1553
98. Chand DK, Ghosh P, Shukla R, Sengupta S, Das G, Bandyopadhyay P, Bharadwaj PK (1996) *Proc Ind Acad Sci (Chem Sci)* 108:229
99. Bag B, Bharadwaj PK (2005) *J Phys Chem B* 109:4377
100. Bag B, Bharadwaj PK (2004) *J Lumin* 110:85
101. de Silva AP (2005) *Nat Mater* 4:15
102. de Silva AP, Dixon IM, Gunaratne HQN, Gunnlaugsson T, Maxwell PRS, Rice TE (1999) *J Am Chem Soc* 121:1393
103. Cesario M, Dietrich CO, Edel A, Guilhem J, Kintzinger JP, Pascard C, Sauvage JP (1986) *J Am Chem Soc* 108:6250
104. Sohna Sohna JE, Jaumier P, Fages F (1999) *J Chem Res (S)* 134
105. Iwata S, Tanaka K (1995) *J Chem Soc Chem Commun* 1491
106. Wolfbeis OS, Offenbacher H (1984) *Monatsh Chem* 115:647
107. De Santis G, Fabbrizzi L, Licchelli M, Poggi A, Taglietti A (1996) *Angew Chem Int Ed Engl* 35:202
108. Tsien RY (1980) *Biochemistry* 19:2396
109. Beecroft RA, Davidson RS, Goodwin D, Pratt JE, Luo XJ (1986) *J Chem Soc Faraday Trans 2* 82:2393
110. Bender ML, Komiyama M (1978) *Cyclodextrin chemistry*. Springer, Berlin
111. Bissell RA, de Silva AP (1991) *J Chem Soc Chem Commun* 1148
112. Gouterman M (1997) *J Chem Educ* 74:697
113. Mosharov V, Radchenko V, Fonov S (1998) *Luminescent pressure sensors in aerodynamic experiments*. Central Aerohydrodynamic Institute, Moscow
114. Lu X, Manners I, Winnik MA (2001) In: Valeur B, Brochon JC (eds) *New trends in fluorescence spectroscopy*. Springer, Berlin, p 229
115. Bolt JD, Turro NJ (1982) *Photochem Photobiol* 35:305
116. Mu LX, Wang Y, Zhang Z, Jin WJ (2004) *Chin Chem Lett* 15:1131
117. Bu JH, Zheng QY, Chen CF, Huang ZT (2004) *Org Lett* 6:3301
118. Casnati A, Pochini A, Ungaro R, Bocchi C, Ugozzoli F, Egberink RJM, Struijk H, Lugtenberg R, de Jong F, Reinhoudt DN (1996) *Chem Eur J* 2:436
119. Montenegro JM, Perez-Inestrosa E, Collado D, Vida Y, Suau R (2004) *Org Lett* 6:2353
120. Collado D, Perez-Inestrosa E, Suau R, Desvergne JP, Bouas-Laurent H (2002) *Org Lett* 4:855
121. Collado D, Perez-Inestrosa E, Suau R (2003) *J Org Chem* 68:3574
122. Callan JF, de Silva AP, Ferguson J, Huxley AJM, O'Brien AM (2004) *Tetrahedron* 60:11125
123. Banthia S, Samanta A (2005) *Eur J Org Chem* 4967

124. Leigh DA, Morales MÁF, Pérez EM, Wong JKY, Saiz CG, Slawin AMZ, Carmichael AJ, Haddleton DM, Brouwer AM, Buma WJ, Wurpel GWH, León S, Zerbetto F (2005) *Angew Chem Int Ed* 44:3062
125. Ben-Ari M (1993) *Mathematical logic for computer science*. Prentice-Hall, Hemel Hempstead
126. Sedra AL, Smith KC (2003) *Microelectronic circuits*, 5th edn. Oxford University Press, Oxford
127. Credi A, Balzani V, Langford SJ, Stoddart JF (1997) *J Am Chem Soc* 119:2679
128. Matsui J, Mitsuishi M, Aoki A, Miyashita T (2004) *J Am Chem Soc* 126:3708
129. Hughes E (1990) *Electrical technology*, 6th edn. Longman, Burnt Mill
130. Millman J, Grabel A (1998) *Microelectronics*. McGraw-Hill, London
131. Andréasson J, Kodis G, Terazono Y, Liddell PA, Bandyopadhyay S, Mitchell RH, Moore TA, Moore AL, Gust D (2004) *J Am Chem Soc* 126:15926
132. Guo X, Zhang D, Zhu D (2004) *Adv Mater* 16:125
133. Coskun A, Deniz E, Akkaya EU (2005) *Org Lett* 7:5187
134. Zong G, Lu G (2008) *Tetrahedron Lett* 49:5676
135. López MV, Vázquez ME, Gómez-Reino C, Pedrido R, Bermejo MR (2008) *New J Chem* 32:1473

Luminescent Chemical Sensing, Biosensing, and Screening Using Upconverting Nanoparticles

Daniela E. Achatz, Reham Ali, and Otto S. Wolfbeis

Abstract Upconverting nanoparticles (UCNPs) display the unique property of converting near-infrared light (with wavelengths of typically 800–1,000 nm) into visible luminescence. Following a short introduction into the mechanisms leading to the effect, the main classes of materials used are discussed. We then review the state of the art of using UCNPs: (1) to label biomolecules such as antibodies and (synthetic) oligomers for use in affinity assay and flow assays; (2) to act as nanolamps whose emission intensity is modulated by chemical indicators, thus leading to a novel kind of chemical sensors; and (3), to act as donors in luminescence resonance energy transfer in chemical sensors and biosensors.

Keywords Biosensor, Chemical sensor, Luminescence, Nanoparticles, Upconversion

Contents

1	Introduction	30
2	The Process of (Photonic) Upconversion	32
3	Upconverting Nanophosphors in Bioanalytical Assays	33
3.1	The Upconversion Phosphor Technology	33
3.2	Upconversion Phosphor Technology Reporters in DNA Microarrays	35
3.3	Upconversion Phosphor Technology in Lateral Flow Assays	36
3.4	Upconversion Phosphor Technology in Flow Cytometry	38
4	Upconverting Nanophosphors in Chemical Sensors	38
4.1	Sensors for pH, Carbon Dioxide, and Ammonia	38
4.2	Sensors for Oxygen	41

D.E. Achatz, R. Ali, and O.S. Wolfbeis (✉)

Institute of Analytical Chemistry, Chemo- and Biosensors, University of Regensburg, 93040 Regensburg, Germany
e-mail: otto.wolfbeis@chemie.uni-r.de

5	Biosensors	42
5.1	Biosensors for Oligonucleotides	42
5.2	Biosensors for Proteins, Ligand-Receptor Interactions, and Enzyme Activities	44
6	Conclusions	46
	References	47

1 Introduction

The term upconversion describes an effect [1] related to the emission of anti-Stokes fluorescence in the visible spectral range following excitation of certain (doped) luminophores in the near infrared (NIR). It mainly occurs with rare-earth doped solids, but also with doped transition-metal systems and combinations of both [2, 3], and relies on the sequential absorption of two or more NIR photons by the dopants. Following its discovery [1] it has been extensively studied for bulk materials both theoretically and in context with uses in solid-state lasers, infrared quantum counters, lighting or displays, and physical sensors, for example [4, 5]. Substantial efforts also have been made to prepare nanoscale materials that show more efficient upconversion emission. Meanwhile, numerous protocols are available for making nanoparticles, nanorods, nanoplates, and nanotubes. These include thermal decomposition, co-precipitation, solvothermal synthesis, combustion, and sol-gel processes [6], synthesis in liquid-solid-solutions [7, 8], and ionothermal synthesis [9]. Nanocrystal materials include oxides of zirconium and titanium, the fluorides, oxides, phosphates, oxysulfates, and oxyfluorides of the trivalent lanthanides (Ln^{3+}), and similar compounds that may additionally contain alkaline earth ions. Wang and Liu [6] have recently reviewed the theory of upconversion and the common materials and methods used.

The choice of the material is critical in terms of the color and intensity of the emission. For example, upconverting nanoparticles (UCNPs) doped with Er^{3+} emit mainly green light (510–570 nm) and red light (630–680 nm), but the peak maxima and relative intensities of the bands depend on the host lattice. The green emission is dominant in fluoride-based lattices, while in oxide-based lattices it is the red emission. Dopants such as Tm^{3+} result in mainly blue upconversion fluorescence (450–500 nm) that is accompanied by a weak red fluorescence in certain host crystals. Lattices doped with Ho^{3+} also show a green and red luminescence that is comparable to that of Er^{3+} .

NaYF_4 is the host lattice recognized to be one of the most efficient ones both for bulk phosphors and nanocrystals [2]. The upconversion efficiency of colloidal solutions of lanthanide-doped NaYF_4 is about eight orders of magnitude higher than for lanthanide-doped phosphate nanocrystals, for example [10]. In addition, the upconversion efficiency can be increased by a factor of up to 2.5 by coating UCNPs with gold nanoparticles [11]. Coatings with silica [12, 13] or an undoped shell of host lattice [14] were also found to be beneficial in terms of efficiency. One

general drawback of nanosized upconversion materials is their decreased upconversion efficiency when compared to the corresponding bulk (μm -sized) materials. This is due to the large surface-to-volume ratio of nanosized particles so that dopants located near the surface of the particles are more easily quenched by external perturbators [15, 16].

UCNPs (also termed upconversion nanophosphors; UNPs) have found applications in security and brand protection [17, 18], and in photodynamic therapy [19, 20]. It was soon recognized that their outstanding features also make them highly interesting for bioanalytical and biophysical studies. Since photoexcitation of UCNPs occurs in the NIR, the background fluorescence that often interferes in conventional fluorometry of biological samples is minimized, if not zero. This results in high sensitivity and high contrast imaging. Emission bands are narrow. This allows for a good signal separation and – conceivably – multicolor labeling and multiple sensing. UCNPs do not suffer at all from photobleaching. Their brightness usually is lower than that of quantum dots but, unlike those, they do not blink [10], nor are they toxic which is important with respect to *in vivo* applications. Finally, NIR light penetrates tissue much deeper than more shortwave light, and the laser intensities usually applied (0.1–1.0 W cw) do not substantially damage tissue.

Various kinds of surface chemistries for solubilization, functionalization, and bioconjugation of UCNPs have been reported [6]. However, routine instrumentation for this technology is not readily available. Most fluorometers still need to be adapted to NIR laser excitation, and respective microplate readers have not yet been commercialized. However, instrumentation for fluorescence microscopy of UCNPs has recently become available (www.leica.com).

Given these properties, it does not come as a surprise that UCNPs have also found interest in terms of chemical sensing, biosensing, and screening. Sensitivity is one important criterion in this context. Upconversion materials have the potential for enormous improvement of today's performance of optical sensors and assays for the reasons outlined before. Their photostability enables long operational lifetimes without fading. Readily available low-cost excitation sources will allow cost savings. Furthermore, there is a trend in sensing and screening towards multi-analyte detection without the need for further separation steps. Various types of UCNPs are known that have the same excitation wavelength (980 nm) but show well separated and narrow band emissions depending on the type of dopant. Therefore, simultaneous detection of more than one analyte in a complex sample will become possible using appropriate UCNPs.

This review focuses on methods of chemical sensing, biosensing, and screening of chemical and biological analytes and parameters using UCNPs. It covers sensors and assays based on upconversion nanomaterials with a size below 500 nm, but not on technologies using bulk (e.g., micro-sized) phosphors. We first give an introduction into the processes leading to upconversion emission in rare earth doped solids, then review affinity-based assays, and finally cover general sensing schemes of chemical sensors and biosensors based on UCNPs.

2 The Process of (Photonic) Upconversion

There are three main processes causing upconversion emission in rare earth doped materials, viz. excited state absorption (ESA), energy transfer upconversion (ETU), and photon avalanche (PA) processes. All are based on the sequential absorption of two or more photons. ESA occurs in one single ion that successively absorbs two photons (Fig. 1a). The first absorption process occurs at the energetic ground state (G) and is induced by a resonant photon (ground state absorption/GSA). It leads to the population of the metastable and long-lived level E1. The second resonant absorption promotes the ion from E1 to the higher level E2, from which the emission corresponding to the transition $E2 \rightarrow G$ occurs. The principle of ETU is similar, but energy transfer occurs between two adjacent ions (Fig. 1b). Each ion is excited via GSA to its E1 level. Thereafter, the excited state energy is transferred (by resonant energy transfer) to an adjacent one (also in the E1 state). The donor ion relaxes to its ground state G while the acceptor ion is promoted to the excited state E2. This is followed by an emissive transition $E2 \rightarrow G$ again. The third main process (PA) is based on an unconventional mechanism that only occurs at certain pump intensity. In the first step, weak non-resonant GSA occurs, followed by a resonant ESA at one ion which thus is promoted to energy level E2 (Fig. 1c). A cross-relaxation energy transfer to an adjacent ion in its ground state results in both ions occupying E1. Further resonant ESA and cross-relaxation energy transfers exponentially increase the population of E2 and therefore upconversion emission intensity.

The efficiency of upconversion of the three processes varies strongly. ESA generates the weakest emission. PA is the most efficient process but depends on the pump power and has a slow (up to several seconds) response to excitation due to the number of ESA and cross relaxation looping cycles. ETU is independent of pump power and occurs without delay after excitation.

Upconversion in single-doped host lattices is mainly accomplished by ESA (Fig. 1a). Co-doping with a second lanthanide, a so-called sensitizer, can significantly increase the upconversion efficiency by exploiting the more efficient ETU process (Fig. 1b). Yb^{3+} is a common sensitizer ion since it has a high absorption

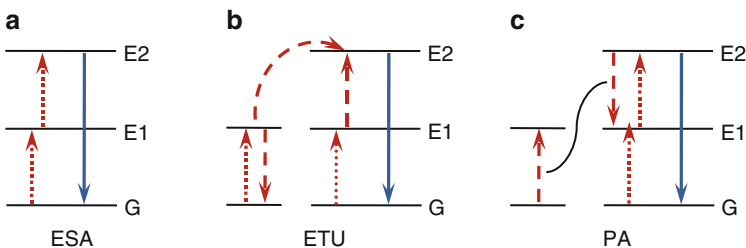


Fig. 1 Schematic representation of the three main types of processes causing upconversion in rare earth doped materials: (a) excited state absorption; (b) energy transfer upconversion; (c) photon avalanche. The *dotted lines* refer to photon excitation, *dashed lines* to non-radiative energy transfer, and *full arrows* to emissive processes, respectively

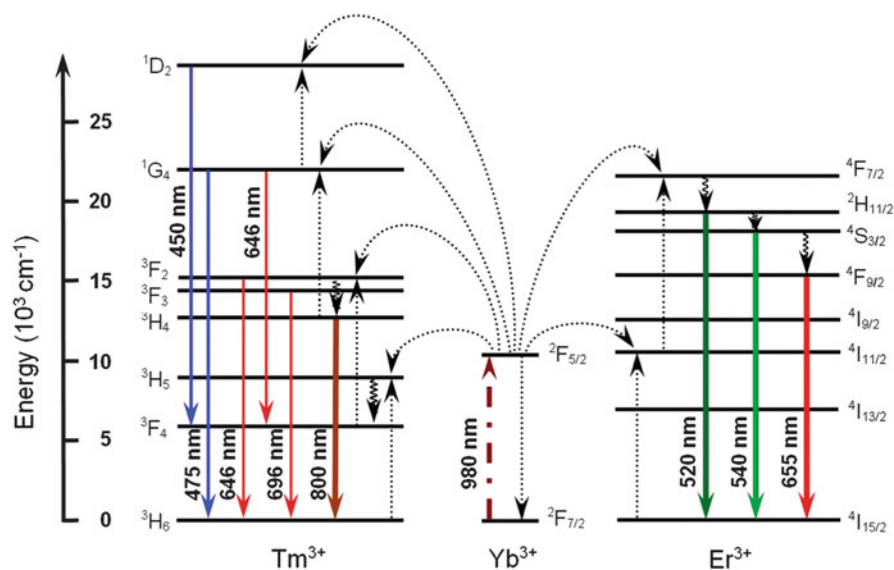


Fig. 2 Energy transfer and upconversion emission mechanisms in a NaYF₄ nanocrystal doped with Yb³⁺, Er³⁺, and Tm³⁺ doped under 980-nm excitation. The dashed-dotted, dotted, curly, and full arrows refer to photon excitation, energy transfer, multi-photon relaxation, and upconversion emission. The ^{2S+1}L_J notation applied to label the f energy states represent the spin (S), orbital (L), and angular (J) momentum quantum numbers according to the Russel–Saunders notation

cross-section and only one excited 4f state that is well resonant with the f–f transitions of Er³⁺, Tm³⁺, or Ho³⁺ (called activators). Hence, Yb³⁺ itself contributes no visible emission to the overall spectrum. Figure 2 gives an example for the transitions and energy transfers between Yb³⁺ acting as the sensitizer, and Er³⁺/Tm³⁺ as the activators.

Multiple luminescence emissions and varying intensity ratios of single peaks are obtained by varying the concentrations and combining more than two emissive lanthanide ions in one host material. The corresponding colloidal solutions cover the whole spectral range from the visible to the NIR as was demonstrated [21–23] for NaYF₄-based UCNPs (Fig. 3). Continuous efforts have been made to improve the shape, size, and upconversion efficiency of UCNPs by exploiting various kinds of host materials, dopant concentrations, dopant ratios, and coatings [13, 24, 25].

3 Upconverting Nanophosphors in Bioanalytical Assays

3.1 The Upconversion Phosphor Technology

The term upconversion phosphor technology (UPT) was introduced by Tanke et al. [26] back in 1999. They used luminescent reporters [27] for the sensitive detection

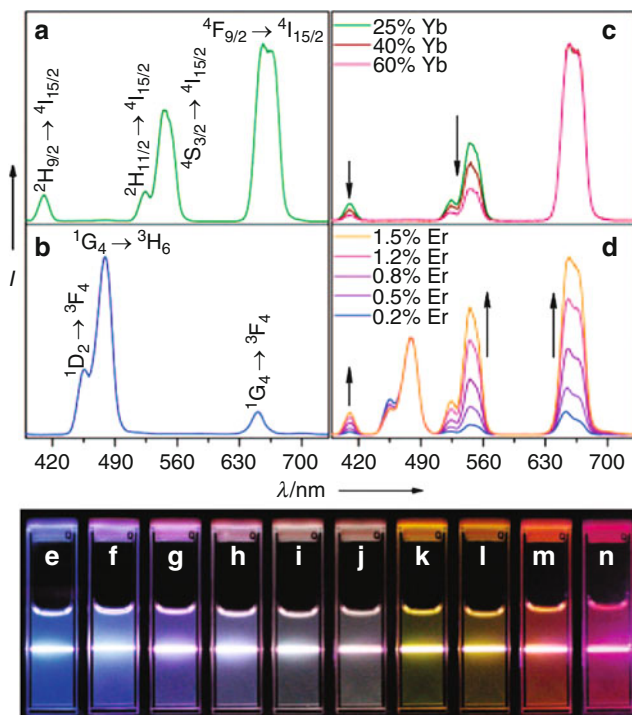


Fig. 3 Room temperature upconversion emission spectra of NaYF₄ nanocrystals doped with (a) Yb/Er (18/2 mol %), (b) Yb/Tm (20/0.2 mol %), (c) Yb/Er (25–60/2 mol %), and (d) Yb/Tm/Er (20/0.2/0.2–1.5 mol %) particles in ethanol solutions (10 mM). The spectra in (c) and (d) were normalized to Er³⁺ (650-nm) and Tm³⁺ (480-nm emissions), respectively. The photos on the bottom show corresponding colloidal solutions of NaYF₄ nanoparticles doped with (e) Yb/Tm (20/0.2 mol %), (f–j) Yb/Tm/Er (20/0.2/0.2–1.5 mol %), and (k–n) Yb/Er (18–60/2 mol %). The samples were excited at 980-nm with a 600-mW diode laser [21]

of antigens in tissue sections and on cell membranes. The reporters consisted of nanophosphors (lanthanide-doped yttrium oxysulfides, 200–400 nm in diameter) first coated with silica, then amino-functionalized, and then surface-labeled with avidin or antibodies. The resulting UCNPs have a core-shell structure and possess surface functional groups that make them suitable for bioconjugations. In being resistant to photobleaching and displaying unmatched contrast in biological specimens, they are representing a powerful tool in detection technologies. The UPT reporters were used in assays like in microarrays, lateral flow assays, and flow cytometry as will be described in the following. Unlike in the biosensing schemes described in Sect. 5, the UCNPs used in UPT act as labels only, but do not directly interact with the (otherwise labeled) biomolecule, for example via FRET, LRET, or the like.

3.2 Upconversion Phosphor Technology Reporters in DNA Microarrays

Nucleic acid microarrays are generally limited by low hybridization efficiency and the moderate sensitivity provided by conventional luminescent labels. Van de Rijke et al. [28] designed an experimental setup for the direct comparison of UPT and the conventional fluorophore Cy5 (Fig. 4a). Microarrays were hybridized with

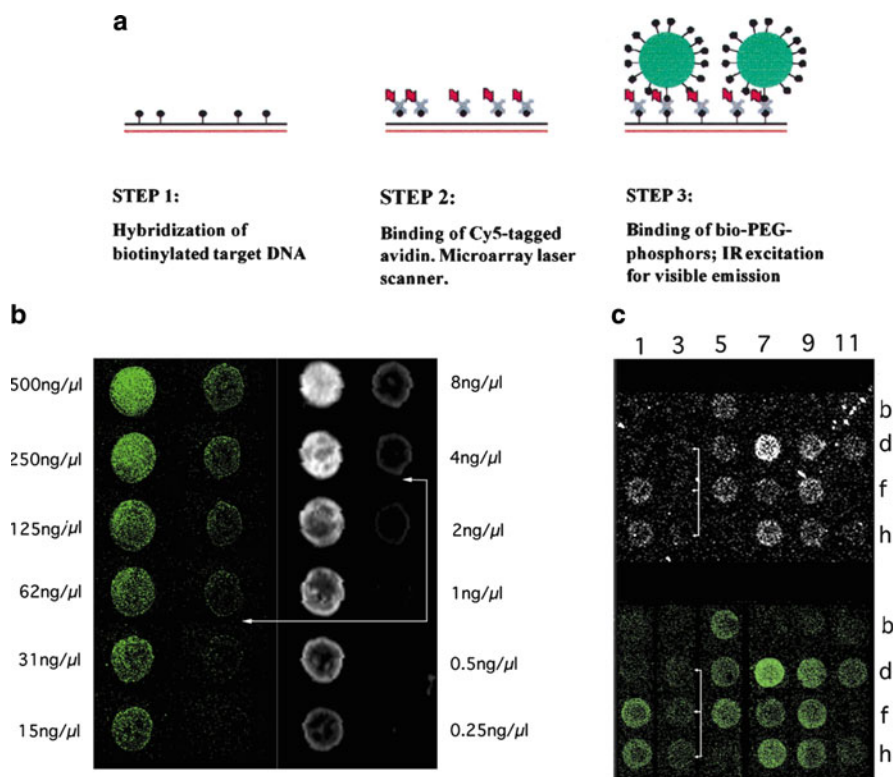


Fig. 4 (a) Schematic representation of the experiment designed to compare the detection sensitivity provided by conventional Cy5 fluorescence (microarray laser scanner) and upconverting phosphor particles (two-photon IR wide-field excitation for visible fluorescence). (b) Model low-complexity microarray hybridization with biotinylated DNA detected with avidin-Cy5 and laser scanning (*right panel*) and subsequent detection with bio-PEG UPT (*left panel*). Concentrations of DNA solutions used for spotting are given next to the spots (500 to 0.25 ng/ μ L). Concentrations along the *left side* refer to the first and third columns, whereas those on the *right* refer to the second and fourth columns. *Arrows* indicate detection sensitivity. (c) Complex cDNA microarray using avidin-Cy5 (*top*) and UPT (*bottom*) as reporter molecules, respectively; *white lines* indicate spots of very low expression not detected against the background of reporter Cy5 but visible with UPT [28]

biotinylated target-DNA (step 1), and the biotin afterwards was detected with Cy5-labeled avidin (step 2). Subsequently, the avidin was labeled with biotinylated UCNPs (bio-PEG-UPT; step 3). A microarray fluorescence scanner was used to detect the biotinylated target-DNA and avidin-Cy5 and a wide-field digital microscope to detect the biotinylated UCNPs. In this low-complexity model system, the UPT reporters showed a linear relationship between phosphor luminescence and target concentration over two orders of magnitude. A comparison between the UPT reporters and the label Cy5 resulted in an excellent correlation for variable target concentrations. UPT turned out to give a fourfold lower limit of detection (Fig. 4b). The same results were obtained with a complex microarray for hybridization of mixtures of various cDNAs (Fig. 4c).

3.3 *Upconversion Phosphor Technology in Lateral Flow Assays*

Given the costs of the health care system, there is a major interest in low-cost assays that are also rapid, highly sensitive, specific, reproducible, and based on affordable instrumentation. Point-of-care and on-site testing are extremely promising in that respect, not the least because it can be performed by rather unskilled personnel. Lateral flow (LF) assays (“test strips”) meet these requirements and UPT has the potential for enhanced sensitivity. Extensive research on UPT-LF bioassays was performed in the groups of Tanke, Corstjens, and Niedbala and has resulted in methods for the detection of several pathogenic microorganisms [29, 30], nucleic acids [31–33], drugs of abuse [34], cytokines [35], and antibodies [34, 36]. Screening is based on an UPT-LF assay either in a competitive format or as a sandwich-hybridization assay. The LF platform typically consists of a sample pad, a nitrocellulose membrane, and an absorbent pad. The nitrocellulose membrane provides one or more test lines for target capture, depending on whether one analyte is detected or a multiplex test is performed. These test lines contain antibodies specific to the target analyte of interest that is adsorbed onto the membrane. If the analyte is present in the sample it will be captured and subsequently labeled by UPT reporters (phosphor reagent) at this position. At least one additional control line captures any free UPT reporter in order to confirm correct performance. An exemplary format is schematically shown in Fig. 5.

These test strips were employed for the detection of human papilloma virus (amongst others) [32]. Haptenized DNA molecules (PCR amplicons from DNA samples of cervix carcinomas) were immuno-labeled with UCNPs. Subsequently, an LF assay was performed that resulted in a 100-fold improved sensitivity compared to established assays using gold nanoparticles. Improved sensitivity for amplified nucleic acid targets compared to immuno-gold and Cy5 detection-systems was also found in tests for *Vibrio cholerae* where attomole quantities of DNA could be detected [37].

The results indicate that UPT-based LF assays for nucleic acids are also possible without amplification. This is advantageous since amplification may lead to artifacts

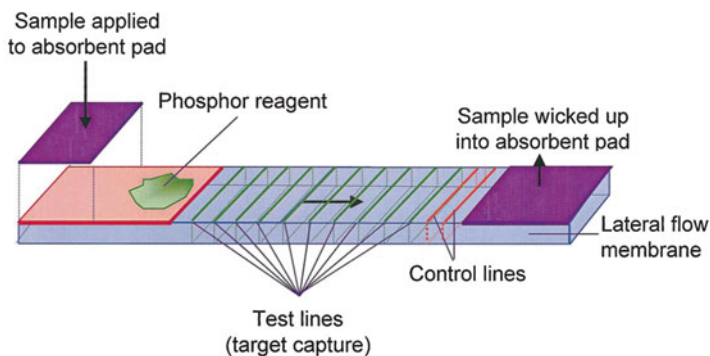


Fig. 5 Typical platform for an affinity-based UPT-LF assay consisting of a sample absorbent pad, a nitrocellulose membrane providing one or more test lines, and at least one control line, and an absorbent pad [34]

which in turn can lead to false positives. Moreover, complex equipment and expensive enzymes are needed. Zuiderwijk et al. [31] demonstrated this amplification-free method to be applicable to the detection of *Streptococcus pneumoniae* with less than 1 ng of genomic DNA. This is equivalent to the quantity of DNA extracted from 10^5 to 10^6 bacterial cells. Further work by Hampl et al. [38] demonstrated the potential of UPT for the detection of the pregnancy hormone human chorionic gonadotrophin (hCG). Li et al. [39] used UPT in an LF assay for the detection of hepatitis B surface antibody in standard positive sera and clinical sera. Again, distinctly higher sensitivities were obtained compared to conventional reporter systems.

Multiplex detection using UPT was performed by Corstjens et al. [36] for the simultaneous detection of human antibodies against human immunodeficiency virus, *Mycobacterium tuberculosis* and hepatitis C virus by using different antibodies adsorbed on adjacent test lines and one type of UCNPs. Hampl et al. [38] used two different types of particles (a thulium oxysulfide phosphor with blue emission and an erbium oxysulfide phosphor with green emission, both after being excited at 980 nm) for simultaneous detection of mouse IgG and ovalbumin.

An important step towards point-of-care and on-site monitoring using UPT-LF assays was accomplished [40] by the development of a portable UPT reader (called Uplink) for scanning LF strips. Originally developed for on-site testing of drugs of abuse in oral samples [41], the LF strip is integrated in a disposable plastic cassette, a self-contained immunoassay device that subsequently is inserted into the Uplink reader. A bar code scanner identifies the unique assay associated with each cassette. Cooper et al. [42] developed a similar (and battery-operated) handheld biosensor that reads LF assays primarily to detect biological warfare agents. Additionally, a rapid two-dimensional optical scanner for imaging and quantification of UPT reporters was presented [43] that was also used to perform a microfluidic chip immunoassay for the cytokine γ -interferon.

3.4 *Upconversion Phosphor Technology in Flow Cytometry*

Cooper et al. [42] also developed flow cytometric assays based on UPT for the detection of proteins (mouse IgG, ovalbumin), viruses (MS2 coliphage), bacterial cells (*Erwinia herbicola*), and spores (*Bacillus anthracis*). They used polystyrene or magnetic beads to capture the target of interest in a sandwich assay format and an antibody-functionalized UPT reporter for detection. Alternatively, detection was performed indirectly by first detecting the target with a biotinylated antibody followed by neutravidin-coated UCNP. Assay sensitivities of about 250 $\mu\text{g/mL}$ were demonstrated for mouse IgG, and multiplexing was shown to work by using latex beads labeled with different lanthanides and thus having different emission colors.

4 *Upconverting Nanophosphors in Chemical Sensors*

The assays described so far utilize UCNPs simply as labels but they can also be used for sensing chemical and biological parameters or analytes. According to [44], chemical sensors “are miniaturized analytical devices that can deliver real-time and on-line information on the presence of specific compounds or ions in complex samples.” Similar definitions do exist for biosensors [45]. There are additional definitions for sensors that also include more specific details like handiness, small size, operational and storage stability. One common criterion is the option of performing continuous and reversible measurements. However, this requirement is not always fulfilled, particular in the case of biosensors where binding constants are very high [46, 47].

The upconversion effect of lanthanide-doped materials is not directly related to any chemical property of a system that can be of (bio-)analytical interest except for temperature. Therefore, in order to be useful in a chemical recognition process (the fundamental process in chemical sensing), UCNPs have to be used in combination with suitable recognition elements. These can be crown ethers or indicator dyes, for example. The recognition element of a biosensor may consist of an enzyme, an antibody, a polynucleotide, or even living cells. Next, the process of (bio)chemical recognition has to be transduced into a signal given by the UCNPs. In the following, UCNP-based sensing schemes are presented along with examples to demonstrate their feasibility.

4.1 *Sensors for pH, Carbon Dioxide, and Ammonia*

One simple way to modulate the intensity of the emission(s) of UCNPs is to link them to classical indicator chemistry (such as for pH, ions) or chromogenic reactions.

One basic requirement is an overlap of the emission of the UCNPs and the absorbance of the indicator probe that need not be fluorescent. Its absorbance has to change with the concentration of the analyte of interest. A color change results in a stronger or weaker quenching (absorption) of the upconversion emission depending on the actual maximum of absorbance of the indicator.

The first sensor of that kind was presented by Sun et al. [48] who reported on a pH sensor based on the upconversion luminescence of NaYF₄:Yb,Er nanorods (see inset Fig. 6b) that were embedded in a matrix of hydrogel along with the longwave absorbing pH probe (bromothymol blue; BTB) that causes a pH dependent inner filter effect (Fig. 6a). The emission spectrum of the nanorods at NIR excitation and the pH dependent absorption spectrum of BTB for three pH values are shown in Fig. 6b.

The absorbance spectra partially overlap the visible emissions of the nanocrystals. BTB is not fluorescent by itself and its color changes from yellow at pH values of <5 via green (pH 6–7) to blue at pHs above 9. Depending on whether BTB is

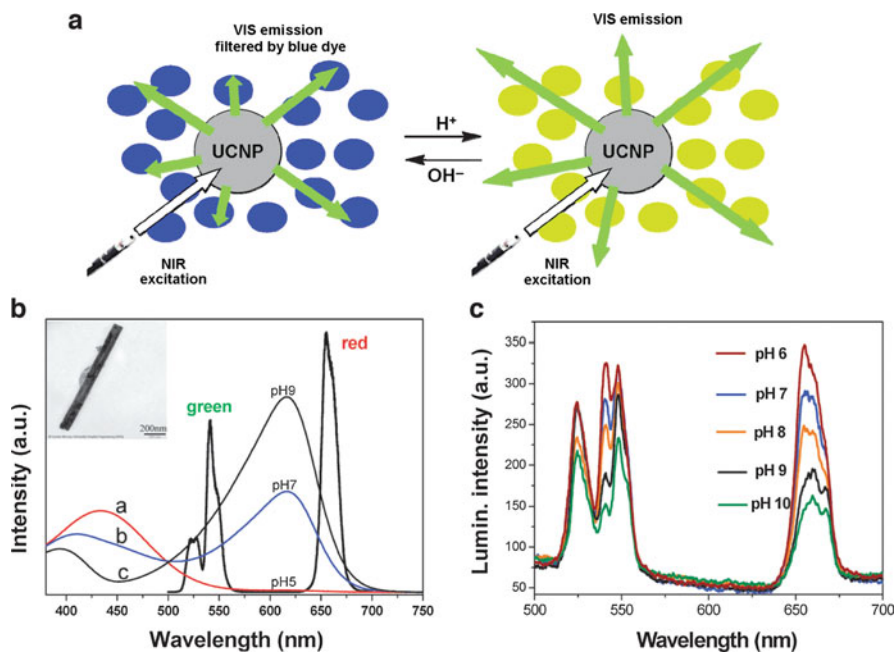


Fig. 6 (a) Schematic representation of the sensing scheme of the pH sensor using UCNPs based on an inner filter effect. The nanocrystals are excited in the NIR giving an emission in the visible spectral range. Dye molecules in the surrounding of the nanocrystal that are changing their characteristic absorbance in presence of an analyte have a filtering effect on the upconversion luminescence depending on the concentration of the analyte. (b) Absorption spectra of BTB in aqueous solutions of pH 5, 7, and 9, respectively (a, b, c); and luminescence emission (red and green) of the nanorods in cyclohexane solution following photo-excitation with a 980-nm laser. The inset shows a TEM image of the nanorods used. (c) Upconversion luminescence spectra of the sensor film as a function of pH upon diode laser excitation at 980-nm [48]

present in its blue base form or in its yellow acidic form, the dye either exerts a strong or an insignificant inner filter effect on both the red and green emission of the UCNP. The upconversion luminescence spectra of the sensor film at different pH values are shown in Fig. 6c, demonstrating the applicability of the system as pH sensor. The sensor membrane responds to pH values between 6 and 10 with a response time of less than 30 s and is fully reversibly. Sensors for pH and other species that operate in the longwave part of the visible spectrum [49] offer considerable advantages over sensors using shortwave wavelengths (i.e., below 450 nm) where the fluorescence of biological matter such as serum [50] is particularly strong.

The method for sensing pH can be extended to sense (dissolved) acidic gases such as carbon dioxide or (dissolved) ammonia. Usually, the sensor material in such sensors is composed of a gas-permeable but proton-impermeable polymer to make sensors insensitive to external pH values. Depending on whether acidic or basic gases are to be sensed, indicators of appropriate pK_a value need to be found. Ali et al. [51] have embedded $\text{NaYF}_4:\text{Yb,Er}$ nanoparticles along with the pH probe BTB in a matrix of polystyrene. Polystyrene was used as matrix since it is impermeable to protons but highly permeable to carbon dioxide. The organic base tetraoctylammonium hydroxide was added in order to convert BTB into its blue (anionic) form. Under pure argon atmosphere, the green and red emission of the UCNP is filtered off by the blue form of BTB (left part of Fig. 6a). If exposed to carbon dioxide, the pH value inside the film is lowered and the indicator dye turns yellow. As a result, the inner filter effect is strongly diminished (right part of Fig. 6a) which results in an increased emission of the UCNP. The film is capable of continuous sensing of carbon dioxide in the range of 0–3% (Fig. 7). Its limit of detection is small enough to detect carbon dioxide in air (Fig. 7).

Mader et al. [52] have developed a similar method to sense ammonia. UCNP of the type $\text{NaYF}_4:\text{Yb,Er}$ along with the pH probe Phenol Red (PR) were placed in a polystyrene film to obtain a sensor film responsive to dissolved and gaseous ammonia. It is also based on an inner filter effect on the luminescence of the UCNP. The pH probe used has a lower pK_a value (to better match the requirements of a sensor for ammonia). Its color changes from yellow at $\text{pH} \leq 5$ to pink at

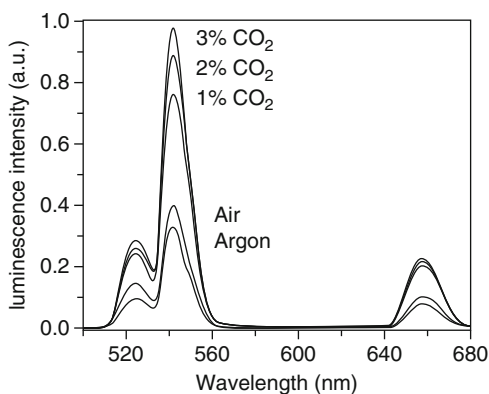


Fig. 7 Upconversion emission spectra of the sensor film after NIR excitation with a 980-nm diode laser under argon, air, and three concentrations of carbon dioxide [51]

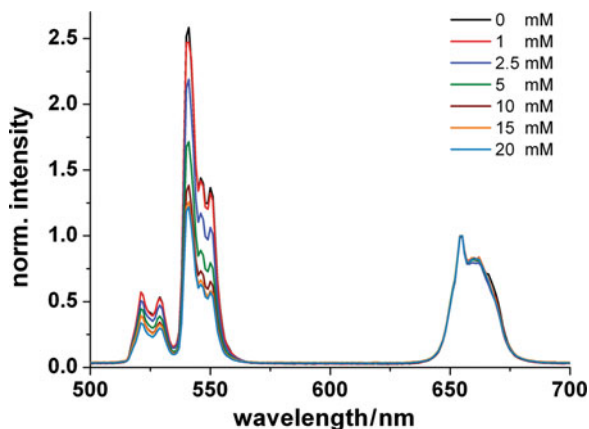


Fig. 8 Upconversion luminescence spectra of the ammonia sensor film at various concentrations of dissolved ammonia. Excitation wavelength 980 nm; spectra are normalized to the peak at 655 nm [52]

$\text{pH} \geq 8$. The pink (base) form strongly overlaps the green emission of the UCNPs and causes an inner filter effect and decreased green emission at $\text{pH} > 6$ (Fig. 8). Unlike the sensor for carbon dioxide (see above), the second band of this sensor (at around 660 nm) is not affected by the indicator dye so that it can serve as a reference band and thus enable referenced (i.e., more robust) sensing.

Dissolved ammonia (1–20 nM) can penetrate the polystyrene matrix and thus causes an increase of the local pH so that the color of the indicator changes from yellow to pink. Hence, the green emission decreases with increasing ammonia concentration which is shown in Fig. 8. The red emission of the UCNPs may serve as an internal reference signal for ratiometric measurements because it is not affected by ammonia. Ratiometric sensing makes measurements independent of inhomogeneities in the sensor membrane and fluctuations of the excitation source.

The sensing schemes described in this section may also be used for sensing other analytes that cause a change in pH. The preparation of nanosensors also is conceivable by coating single UCNPs with respective sensor chemistry.

4.2 Sensors for Oxygen

Sensing oxygen is extremely important given the significance of this species in physiology, clinical diagnosis, marine (and environmental) research, and clinical technology. Oxygen exerts a quenching effect on many fluorophores [44], and this forms the basis for numerous respective sensing schemes [53]. Oxygen sensors are also widely used in enzyme-based biosensors [54] and in biotechnology [55]. The emission of UCNPs is not affected by oxygen although the emission of certain transition metal complexes is known to be effectively quenched by oxygen. Recently

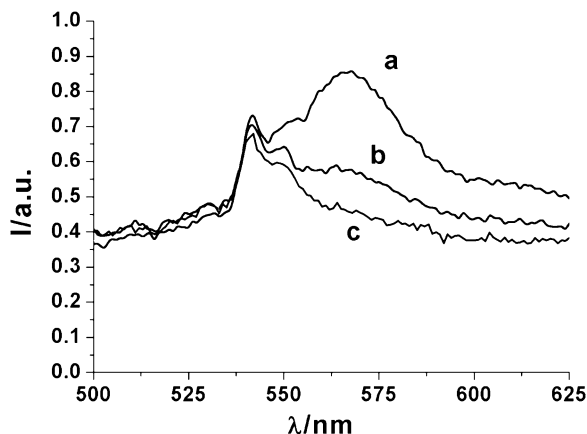


Fig. 9 Sensing oxygen via the quenching of the luminescence of a luminescent probe that is photoexcited by UCNPs. The spectra show the emission spectra of a sensor film (made from ethyl cellulose) containing the upconverting nanoparticles (UCNPs) of the type $\text{NaYF}_4:\text{Yb,Tm}$ and the oxygen probe $\text{Ir}(\text{C}_5)_2(\text{acac})$ following photoexcitation at 980 nm with a diode laser. (a) Spectrum under nitrogen; (b) spectrum under air; (c) spectrum under oxygen. The *green emission* of the oxygen probe peaks at 567 nm. erbium!

[65], a method was developed that makes use of UCNPs and an iridium(III) complex both embedded in a thin film of ethyl cellulose (a highly gas-permeable polymer). A sensor foil was prepared where the visible blue emission of $\text{NaYF}_4:\text{Yb,Tm}$ nanoparticles contained in the foil acts as the light source for photoexciting a quenchable iridium(III) complex that absorbs blue light [56].

Two mechanisms are conceivable. The first is a luminescence resonance energy transfer (LRET) from the UCNPs to nearby molecules of the iridium (or other) probe for oxygen. Alternatively (or in addition), the UCNPs may act as nanolamps whose blue emission leads to the photoexcitation of the iridium complex. The applicability and full reversibility was demonstrated on alternately exposing the sensor film to argon and oxygen, which resulted in a fully reversible increase and decrease of the emission of the iridium(III) complex, respectively, as shown in Fig. 9

5 Biosensors

5.1 Biosensors for Oligonucleotides

In the sensors described in this section, the UCNPs not only act as labels to render a system fluorescent (as in Sect. 3). Rather, their emission is modulated as a result of the biochemical recognition process, for example due to more or less efficient

LRET. Zhang et al. [57] have presented a simple and versatile design for a nucleotide sensor based on a sandwich-type hybridization format shown in Fig. 10a. Two short oligonucleotides with designed sequences were used to capture a longer target nucleotide. One of the short sequences was labeled with green emitting NaYF₄:Yb,Er nanoparticles, and the other one with the common fluorescent label TAMRA. The excitation spectrum of the latter overlaps the green emission of the UCNPs, and this led to efficient LRET between the UCNPs and the fluorophore. Conjugation of the UCNPs to the nucleic acid sequence was accomplished by coating the nanocrystals with a silica shell that was further functionalized with amino groups allowing for common conjugation chemistry. The viability of the detection scheme was proven by measuring the emission of the fluorophore in presence of a 26-base target oligonucleotide following NIR-excitation of the UCNPs. A detection limit of 1.3 nM was achieved for the perfectly matched target DNA, and also single-nucleotide mismatches could be discriminated.

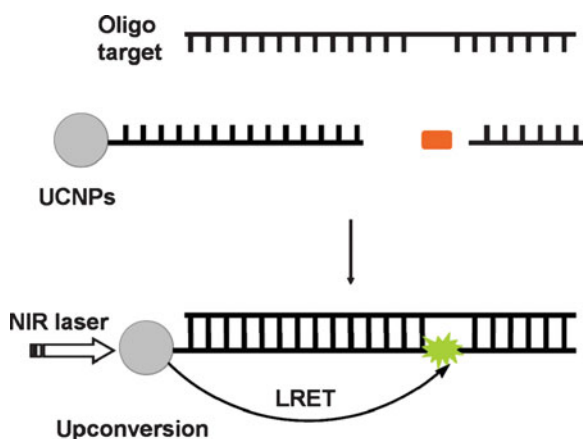


Fig. 10 Schematic of a oligonucleotide sensor design based on a sandwich-type-hybridization using an LRET between UCNPs and a second label [57]

This scheme was recently applied to the detection of point mutation associated with sickle cell disease [58]. The detection limit for the perfectly matched target was found to be 0.6 nM. The same group also demonstrated an even simpler detection scheme with a simpler capturing probe and making use of an intercalator [59] rather than of a labeled second capture probe. The method is schematically shown in Fig. 11. In essence, the capture probe is labeled with a UCNP. On addition of the target probe and an intercalator, a duplex will be formed where the intercalating dye comes into close (though varying) proximity to the UCNP. As a result, LRET (of varying efficiency due to its inverse sixth power dependence) can occur which serves as the analytical information. The detection limit for this sensor format is 0.1 nM, and single-mismatches are detectable.

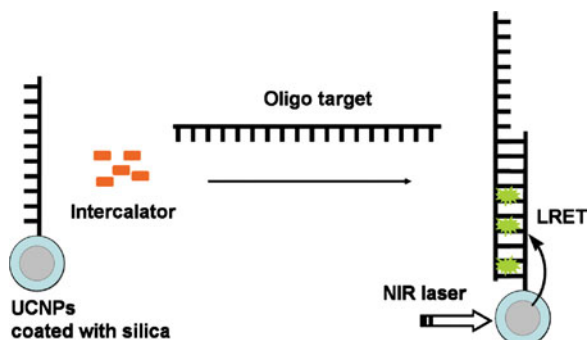


Fig. 11 Schematic of the oligonucleotide sensor design based on one UCNP-labeled capturing probe using an LRET between UCNPs and an intercalating dye

The group of Soukka et al. [60] utilized the dual (green and red) emission of $\text{NaYF}_4:\text{Yb,Er}$ in a sandwich-type hybridization for the simultaneous detection of two different target oligonucleotides, a β -actin sequence and an HLA-B27 sequence (both 32-mers). The corresponding capture sequences were immobilized on the red/green emitting UCNPs. Corresponding capture sequences were labeled with Alexa fluorophores overlapping the emission of the nanoparticles. This enables an LRET upon sandwich hybridization of the target with the capture and the probe sequence (Fig. 10). The multiplexed assay enabled a limit of detection of a quantity as small as 28 fmol (which is equal to a concentration of 0.35 nM) for both target sequences.

5.2 Biosensors for Proteins, Ligand-Receptor Interactions, and Enzyme Activities

The group of Wang et al. [61] exploited the LRET between UCNPs and gold nanoparticles to detect goat antihuman immunoglobulin (IgG). UCNPs of the type $\text{NaYF}_4:\text{Yb,Er}$ and gold nanoparticles were conjugated respectively to human IgG and rabbit antigoat IgG. This resulted in formation of an LRET system when goat antihuman IgG was added (Fig. 12a). The quenching (absorption) of the NIR-excited fluorescence of the UCNPs (Fig. 12b) by the gold nanoparticles was found to be linearly correlated to the concentration of the goat antihuman IgG. The detection limit is quite low (0.88 $\mu\text{g/mL}$), thus making the method applicable to trace detection of protein.

Previously, the same group developed another LRET system using gold and UCNPs on the basis of the binding of avidin and biotin [62]. Both UCNPs and gold nanoparticles were conjugated to biotin. This resulted in quenching of the green upconversion emission in the presence of avidin caused by the close proximity of the two biotinylated species.

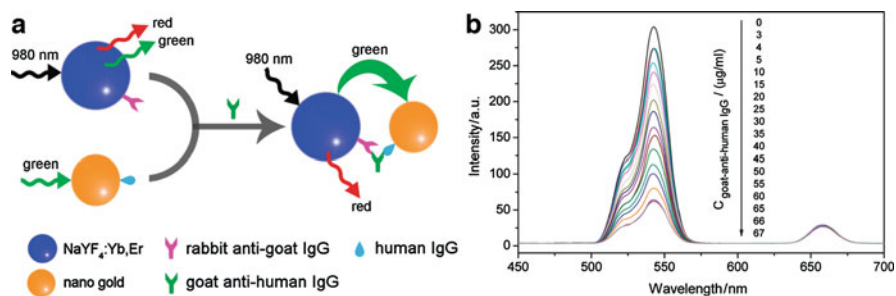


Fig. 12 (a) Schematic Illustration for the LRET process between $\text{NaYF}_4:\text{Yb,Er}$ UCNPs (donor) and gold nanoparticles (acceptor). (b) Upconversion fluorescence spectra of the LRET system at various concentrations of goat antihuman IgG and the relationship between the concentration of goat antihuman IgG and the upconversion fluorescence intensity at 542 nm [61]

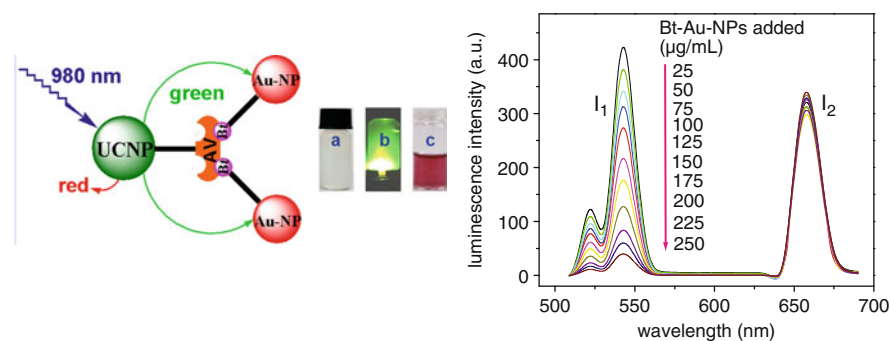


Fig. 13 *Left*: Schematic representation of the binding of biotinylated gold nanoparticles to avidinylated upconverting nanoparticles (UCNP-Av). On binding, the *green emission* of the UCNPs at 545 nm is absorbed by the pink biotinylated gold nanoparticles (Au-NPs-Bt). The *red emission* of the UCNPs at ~ 660 nm, in contrast, is not absorbed and may serve as a reference signal. Photographs: (a) colorless suspension of UCNP under visible light; (b) UCNPs with *green luminescence* following 980-nm laser excitation; (c) *red* Au-NPs under visible light. *Right*: Luminescence of the UCNPs (photo-excited at 980 nm) after addition of varying concentrations of biotinylated gold nanoparticles [62]

Saleh et al. [66] used a similar approach. Direct binding of avidin to biotin was optically detected by using (1) UCNPs that carry avidin on their surface and (2) biotinylated gold nanoparticles. The spectral overlap between the green upconversion emission and the absorption of the red gold nanoparticles results in a quenching of the UCNP fluorescence upon avidin–biotin interaction (Fig. 13b).

The group of Soukka et al. also demonstrated a UCNP-based method for the quantification of enzyme activities. The activity of benzonase endonuclease as model enzyme was determined in a quenching-based format employing UCNPs [63]. In common sensing formats without UCNPs, an oligonucleotide is labeled with both a fluorophore and a quencher, i.e., a donor and an acceptor that undergo

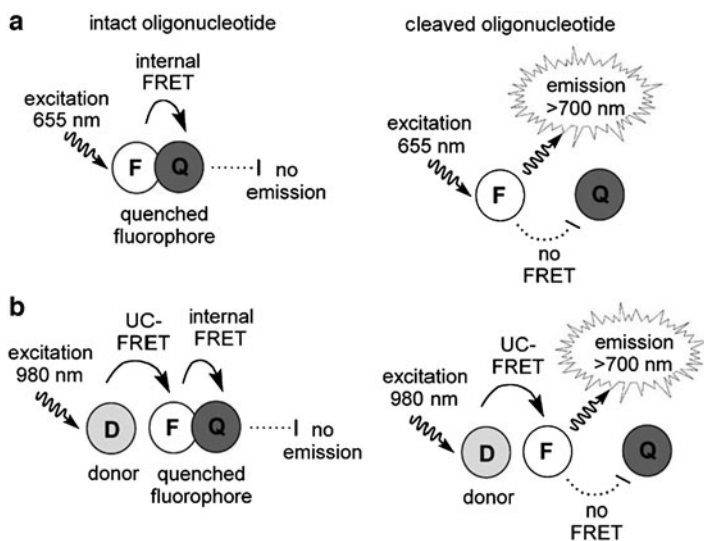


Fig. 14 Principle of the homogeneous enzyme-activity assay based on an internally quenched double-labeled substrate (a) without upconversion (conventional assay) or (b) with a UCNP donor. The hydrolytic enzyme reaction separates the fluorophore (F) and quencher (Q) located at the two ends of the substrate, and so the emission of the fluorophore is recovered. Intact substrates remain non-fluorescent [63]

LRET because they are in close proximity (Fig. 14a). The enzyme cleaves the substrate. LRET is interrupted as a result and leads to the recovery of the fluorescence of the donor fluorophore. The background luminescence from biomatter is one major drawback of this method and reduces sensitivity.

In order to overcome this, Soukka et al. employed UCNPs in a sensor format based on sequential LRET: UCNPs, excited in the NIR, transfer their visible upconversion luminescence to a fluorophore which acts as the donor in a conventional FRET with another acceptor fluorophore (Fig. 14b). In the system tested (benzonase endonuclease), an activity of 0.01 U was detectable, which is superior to the conventional fluorescence-based system.

6 Conclusions

This review shows that UCNPs have substantial merits and unique features in terms of chemical sensing, biosensing, and screening. The choice of the nanoparticles, the proper adjustment of spectra, size, and surface chemistry are critical. UCNPs can be used (1) as labels to render a (bio)molecule luminescent; (2) to report interactions over short distances (e.g., via resonance energy transfer between two labels), or (3) to convert indicator chemistry into a new kind of chemical sensing schemes as exemplified in sensors for pH and oxygen.

Current activities and needs include optimization of UCNPs and their surface, and a better control of their size. Large (>100 nm) particles can be disadvantageous in terms of sensitivity, kinetics, and dynamic range [37, 64]. Standardized protocols for reproducible preparation, coating, and functionalization of UCNPs are badly missing. Compromises will have to be made since upconversion efficiency decreases with the size of the nanophosphors. If current limitations can be overcome, techniques based on upconversion luminescence will represent a highly attractive alternative to existing optical methods and may set new standards not only in bioanalytical sensing but also in imaging, microscopy, and high-throughput-screening.

References

1. Auzel F (2004) Upconversion and anti-Stokes processes with f and d ions in solids. *Chem Rev* 104:139–173
2. Suyver JF, Aebischer A, Biner D, Gerner P, Grimm J, Heer S, Krämer KW, Reinhard C, Güdel HU (2005) Novel materials doped with trivalent lanthanides and transition metal ions showing near-infrared to visible photon upconversion. *Opt Mater* 27:1111–1130
3. Gamelin DR, Güdel HU (2001) Upconversion processes in transition metal and rare earth metal systems. In: *Topics in Current Chemistry*, vol 214. Springer, Berlin
4. Joubert MF (1999) Photon avalanche upconversion in rare earth laser materials. *Opt Mater* 11:181–203
5. Rapaport A, Milliez J, Bass M, Cassanho A, Jenssen H (2006) Review of the properties of upconversion phosphors for new emissive displays. *J Disp Technol* 2:68–79
6. Wang F, Liu X (2009) Recent advances in the chemistry of lanthanide-doped upconversion nanocrystals. *Chem Soc Rev* 38:976–989
7. Wang L, Li Y (2007) Controlled synthesis and luminescence of lanthanide doped NaYF₄ nanocrystals. *Chem Mater* 19:727–734
8. Wang X, Zhuang J, Peng Q, Li Y (2005) A general strategy for nanocrystal synthesis. *Nature* 437:121–124
9. Liu X, Zhao J, Sun Y, Song K, Yu Y, Du C, Kong X, Zhang H (2009) Ionothermal synthesis of hexagonal phase NaYF₄:Yb³⁺,Er³⁺/Tm³⁺ upconversion nanophosphors. *Chem Commun* 6628–6630
10. Heer S, Kömpe K, Güdel HU, Haase M (2004) Highly efficient multicolor upconversion emission in transparent colloids of lanthanide-doped NaYF₄ nanocrystals. *Adv Mater* 16:2102–2105
11. Zhang H, Li Y, Ivanov IA, Qu Y, Huang Y, Duan X (2010) Plasmonic modulation of the upconversion fluorescence in NaYF₄:Yb/Tm hexaplate nanocrystals using gold nanoparticles or nanoshells. *Angew Chem Int Ed* 49:2865–2868
12. Lü Q, Guo FY, Sun L, Li AH, Zhao LC (2008) Silica-/titania-coated Y₂O₃:Tm³⁺, Yb³⁺ nanoparticles with improvement in upconversion luminescence induced by different thickness shells. *J Appl Phys* 103:123533
13. Lü Q, Li A, Guo F, Sun L, Zhao L (2008) Experimental study on the surface modification of Y₂O₃:Tm³⁺/Yb³⁺ nanoparticles to enhance upconversion fluorescence and weaken aggregation. *Nanotechnology* 19:145701
14. Wang Y, Tu L, Zhao J, Sun Y, Kong X, Zhang H (2009) Upconversion luminescence of β-NaYF₄:Yb³⁺, Er³⁺@ β-NaYF₄ core/shell nanoparticles: excitation power density and surface dependence. *J Phys Chem C* 113:7164–7169

15. Vetrone F, Boyer JC, Capobianco JA, Speghini A, Bettinelli M (2003) Concentration-dependent near-infrared to visible upconversion in nanocrystalline and bulk $\text{Y}_2\text{O}_3:\text{Er}^{3+}$. *Chem Mater* 15:2737–2743
16. Yi G, Lu H, Zhao S, Ge Y, Yang W, Chen D, Guo LH (2004) Synthesis, characterization, and biological application of size-controlled nanocrystalline $\text{NaYF}_4:\text{Yb}$, Er infrared-to-visible upconversion phosphors. *Nano Lett* 4:2191–2196
17. Muth O, Brockmann H, Schmidt W, Bailieu A, Brauer G, Paeschke M, Ahlers B, Franz-Burgholz A, Zerbel H (2002) *Eur Pat* 1.241,021
18. Kim WJ, Nyk M, Prasad PN (2009) Color-coded multilayer photopatterned microstructures using lanthanide(III) ion co-doped NaYF_4 nanoparticles with upconversion luminescence for possible applications in security. *Nanotechnology* 20:85301–185307
19. Chatterjee DK, Fong LS, Zhang Y (2008) Nanoparticles in photodynamic therapy: an emerging paradigm. *Adv Drug Deliv Rev* 60:1627–1637
20. Bechet D, Couleaud P, Frochet C, Viriot ML, Guillemin F, Barberi-Heyob M (2008) Nanoparticles as vehicles for delivery of photodynamic therapy agents. *Trends Biotechnol* 26:612–621
21. Wang F, Liu X (2008) Upconversion multicolor fine-tuning: visible to near-infrared emission from lanthanide-doped NaYF_4 nanoparticles. *J Am Chem Soc* 130:5642–5643
22. Wang M, Mi C, Zhang Y, Liu J, Li F, Mao C, Xu S (2009) NIR-responsive silica-coated $\text{NaYF}_4:\text{Er}/\text{Tm}/\text{Ho}$ upconversion fluorescent nanoparticles with tunable emission colors and their applications in immunolabeling and fluorescent imaging of cancer cells. *J Phys Chem C* 113:19021–19027
23. Wang G, Peng Q, Li Y (2010) Luminescence tuning of upconversion nanocrystals. *Chem Eur J*. doi:10.1002/chem.200903099
24. Chen GY, Liu HC, Somesfalean G, Sheng YQ, Liang HJ, Zhang ZG, Sun Q, Wang FP (2008) Enhancement of the upconversion radiation in $\text{Y}_2\text{O}_3:\text{Er}^{3+}$ nanocrystals by codoping with Li^+ ions. *Appl Phys Lett* 92:113114
25. Yi GS, Chow GM (2007) Water-soluble $\text{NaYF}_4:\text{Yb}$, $\text{Er}(\text{Tm})/\text{NaYF}_4/\text{polymer}$ core/shell/shell nanoparticles with significant enhancement of upconversion fluorescence. *Chem Mater* 19:341–343
26. Zijlmans HJMAA, Bonnet J, Burton J, Kardos K, Vail T, Niedbala RS, Tanke HJ (1999) Detection of cell and tissue surface antigens using up-converting phosphors: a new reporter technology. *Anal Biochem* 267:30–36
27. Zarling DA, Rossi MJ, Peppers NA, Kane J, Faris GW, Dyer MJ (1998) Up-converting reporters for biological and other assays using laser excitation techniques. US Patent 5,736,410
28. van de Rijke F, Zijlmans H, Li S, Vail T, Raap AK, Niedbala RS, Tanke HJ (2001) Up-converting phosphor reporters for nucleic acid microarrays. *Nat Biotechnol* 19:273–276
29. Corstjens PLAM, van Lieshout L, Zuiderwijk M, Kornelis D, Tanke HJ, Deelder AM, van Dam GJ (2008) Up-converting phosphor technology-based lateral flow assay for detection of *Schistosoma* circulating anodic antigen in serum. *J Clin Microbiol* 46:171–176
30. Malamud D, Bau H, Niedbala S, Corstjens P (2005) Point detection of pathogens in oral samples. *Adv Dent Res* 18:12–16
31. Zuiderwijk M, Tanke HK, Niedbala RS, Corstjens PLMA (2003) An amplification-free hybridization-based DNA assay to detect *Streptococcus pneumoniae* utilizing the up-converting phosphor technology. *Clin Biochem* 36:401–403
32. Corstjens P, Zuiderwijk M, Brink A, Li S, Feindt H, Niedbala RS, Tanke H (2001) Use of up-converting phosphor reporters in lateral-flow assays to detect specific nucleic acid sequences: a rapid, sensitive DNA test to identify human papillomavirus type 16 infection. *Clin Chem* 47:1885–1893
33. Corstjens PLAM, Zuiderwijk M, Nilsson M, Feindt H, Niedbala RS, Tanke HJ (2003) Lateral-flow and up-converting phosphor reporters to detect single-stranded nucleic acids in a sandwich-hybridization assay. *Anal Biochem* 312:191–200

34. Niedbala RS, Feindt H, Kardos K, Vail T, Burton J, Bielska B, Li S, Milunic D, Bourdelle P, Vallejo R (2001) Detection of analytes by immunoassay using up-converting phosphor technology. *Anal Biochem* 293:22–30
35. Corstjens PLAM, Zuiderwijk M, Tanke HJ, van der Ploeg-van Schip JJ, Ottenhoff THM, Geluk A (2008) A user-friendly, highly sensitive assay to detect the IFN- γ secretion by T-cells. *Clin Biochem* 41:440–444
36. Corstjens PLAM, Chen Z, Zuiderwijk M, Bau HH, Abrams WR, Malamud D, Niedbala RS, Tanke HJ (2007) Rapid assay format for multiplex detection of humoral immune responses to infectious disease pathogens (HIV, HCV and TB). *Ann NY Acad Sci* 1098:437–445
37. Corstjens PLAM, Li S, Zuiderwijk M, Kardos K, Abrams WR, Niedbala RS, Tanke HJ (2005) Infrared up-converting phosphors for bioassays. *IEE Proc Nanobiotechnol* 152:64–72
38. Hampl J, Hall M, Mufti NA, Yao YMM, MacQueen DB, Wright WH, Cooper DE (2002) Upconverting phosphor reporters in immunochromatographic assays. *Anal Biochem* 288: 176–187
39. Li L, Zhou L, Yu Y, Zhu Z, Lin C, Lu C, Yang R (2009) Development of up-converting phosphor technology-based lateral-flow assay for rapidly quantitative detection of hepatitis B surface antibody. *Diagn Microbiol Infect Dis* 63:165–172
40. Mokkapati VK, Niedbala RS, Kardos K, Perez RJ, Guo M, Tanke HJ, Corstjens PLAM (2007) Evaluation of Uplink RSV: prototype rapid antigen test for detection of respiratory syncytial virus infection. *Ann NY Acad Sci* 1098:476–485
41. Steinmeyer S, Polzius R, Manns A (2005) Dräger drug test: test for illegal drugs in oral-fluid samples. In: Wong RC, Tse HY (eds) *Drugs of abuse*. Humana Press Inc, Totowa, New Jersey
42. Wright WH, Rundle G, Mufti NA, Yao YMM, Carlisle CB, Cooper DE (2007) Upconverting phosphors for detection and identification using antibodies. In: Van Emon JM (ed) *Immunoassays and other bioanalytical techniques*. CRC Press, Boca Raton
43. Li JJ, Ouellette AL, Giovangrandi L, Cooper DE, Ricco AJ, Kovacs GTA (2008) Optical scanner for immunoassays with up-converting phosphorescent labels. *IEEE Trans Biomed Eng* 55:1560–1571
44. McDonagh C, Burke CS, MacCraith BD (2008) Optical chemical sensors. *Chem Rev* 108:400–422
45. Borisov SM, Wolfbeis OS (2008) Optical biosensors. *Chem Rev* 108:423–461
46. Thevenot DR, Tóth K, Durst RA, Wilson GS (2001) Electrochemical biosensors: recommended definitions and classification. *Biosens Bioelectron* 16:121–131
47. Janata J (2009) *Principles of chemical sensors*, 2nd edn. Springer, Berlin
48. Sun L, Peng H, Stich MIJ, Achatz DE, Wolfbeis OS (2009) pH sensor based on upconverting luminescent lanthanide nanorods. *Chem Commun* 5000–5002
49. Wolfbeis OS, Werner T, Rodriguez NV, Kessler MA (1992) LED-compatible fluorosensor for measurement of near-neutral pH values. *Mikrochim Acta* 108:133–141
50. Wolfbeis OS, Leiner M (1985) Mapping of the total fluorescence of human blood serum as a new method for its characterization. *Anal Chim Acta* 167:203–215
51. Ali R, Saleh SM, Meier RJ, Azab HA, Elgawad I, Wolfbeis OS (2010) Upconverting Nanoparticle Based Optical Sensor for Carbon Dioxide. *Sens Actuators B Chem* 150:126–131
52. Mader HS, Wolfbeis OS (2010) Optical ammonia sensor based on upconverting luminescent nanoparticles. *Anal Chem* 82:5002–5004
53. Wang XD, Chen HX, Zhao Y, Chen X (2010) Optical oxygen sensors move towards colorimetric determination. *Trends Anal Chem* 29:319–338
54. Trettnak W, Wolfbeis OS (1990) Fiber optic cholesterol biosensor with an oxygen optrode as the transducer. *Anal Biochem* 184:124–127
55. Weigl BH, Holobar A, Trettnak W, Klimant I, Kraus H, O’Leary P, Wolfbeis OS (1994) Optical triple sensor for measuring pH oxygen and carbon dioxide. *J Biotechnol* 32:127–138
56. Borisov SM, Klimant I (2007) Ultrabright oxygen optodes based on cyclometalated iridium (III) coumarin complexes. *Anal Chem* 79:7501–7509

57. Zhang P, Rogelj S, Nguyen K, Wheeler D (2006) Design of a highly sensitive and specific nucleotide sensor based on photon upconverting particles. *J Am Chem Soc* 128:12410–12411
58. Kumar M, Guo Y, Zhang P (2009) Highly sensitive and selective oligonucleotide sensor for sickle cell disease gene using photon upconverting nanoparticles. *Biosens Bioelectron* 24:1522–1526
59. Kumar M, Zhang P (2009) Highly sensitive and selective label-free optical detection of DNA hybridization based on photon upconverting nanoparticles. *Langmuir* 25:6024–6027
60. Rantanen T, Järvenpää ML, Vuojola J, Arppe R, Kuningas K, Soukka T (2009) Upconverting phosphors in a dual-parameter LRET-based hybridization assay. *Analyst* 134:1713–1716
61. Wang M, Hou W, Mi CC, Wang WX, Xu ZR, Teng HH, Mao CB, Xu SK (2009) Immunoassay of goat antihuman immunoglobulin G antibody based on luminescence resonance energy transfer between near-infrared responsive NaYF₄:Yb, Er upconversion fluorescent nanoparticles and gold nanoparticles. *Anal Chem* 81:8783–8789
62. Wang L, Yan R, Huo Z, Wang L, Zeng J, Bao J, Wang X, Peng Q, Li Y (2005) Fluorescence resonance energy transfer biosensor based on upconversion-luminescent nanoparticles. *Angew Chem Int Ed Engl* 117:6208–6211
63. Rantanen T, Järvenpää ML, Vuojola J, Kuningas K, Soukka T (2008) Fluorescence-quenching-based enzyme-activity assay by using photon upconversion. *Angew Chem Int Ed* 47:3811–3813
64. Ouellette AL, Li JJ, Cooper DE, Ricco AJ, Kovacs GTA (2009) Evolving point-of-care diagnostics using up-converting phosphor bioanalytical systems. *Anal Chem* 81:3216–3221
65. Achatz DE, Meier RJ, Fischer LH, Wolfbeis OS (2010) Luminescent sensing of oxygen using a quenchable probe along with upconverting nanoparticles. *Angew Chem Intl Ed* 49 (in press). DOI: 10.1002/anie.201004902
66. Saleh SM, Ali R, Hirsch T, Wolfbeis OS (2010) Optical detection of biotin-avidin affinity binding by exploiting a self-referenced system composed of upconverting nanoparticles and gold nanoparticles. *Biosens Bioelectron* (Submitted)

Luminescence Amplification Strategies Integrated with Microparticle and Nanoparticle Platforms

**Shengchao Zhu, Tobias Fischer, Wei Wan, Ana B. Descalzo,
and Knut Rurack**

Abstract The amplification of luminescence signals is often the key to sensitive and powerful detection protocols. Besides optimized fluorescent probes and labels, functionalized nano- and microparticles have received strongly increasing attention in this context during the past decade. This contribution introduces the main signalling concepts for particle-based amplification strategies and stresses, especially the important role that metal and semiconductor nanoparticles play in this field. Besides resonance energy transfer, metal-enhanced emission and the catalytic generation of luminescence, the impact of multi-chromophoric objects such as dye nanocrystals, dendrimers, conjugated polymers or mesoporous hybrid materials is assessed. The representative examples discussed cover a broad range of analytes from metal ions and small organic molecules to oligonucleotides and enzyme activity.

Keywords Luminescence, Multi-Chromophore systems, Nanoparticles, Resonance energy transfer, Signal amplification

Contents

1	Introduction	52
2	Resonance Energy Transfer	53
2.1	Gold Nanoparticles	58
2.2	Quantum Dots	60
2.3	Up-Conversion Nanoparticles	64

S. Zhu, T. Fischer, W. Wan, and K. Rurack (✉)

Div I.5, BAM Bundesanstalt für Materialforschung und -prüfung, Richard-Willstätter-Str. 11,
12489, Berlin, Germany
e-mail: knut.rurack@bam.de

A.B. Descalzo

Div I.5, BAM Bundesanstalt für Materialforschung und -prüfung Richard-Willstätter-Str. 11,
12489, Berlin, Germany

Department of Organic Chemistry, Faculty of Chemistry, Complutense University of Madrid,
Avda. Complutense s/n, 28040, Madrid, Spain

3	Nanoscopic Objects with Inherent Signal Amplification	64
3.1	Conjugated Polymers	66
3.2	Dendrimers	67
3.3	Encapsulated Dye Nanocrystals	69
3.4	Functionalized Liposomes	70
3.5	Gated and Dye-Loaded Mesoporous Particles	70
4	Nanoparticles as Catalysts and Activity Enhancers	73
4.1	Gold Nanoparticles as Catalysts in Chemiluminescence Reactions	74
4.2	Gold Nanoparticles as Activity Enhancers of Enzymes	75
4.3	Particle-Mediated Enhancement of Electrochemiluminescence	76
5	Plasmonic Strategies to Luminescence Amplification	76
5.1	Surface Plasmon Resonance and Fluorescence	77
5.2	MEF-Based Signalling Applications	80
6	Conclusion	84
	References	85

1 Introduction

Fluorescence spectroscopy is becoming an ever more valuable and popular tool in analytical and bioanalytical chemistry [1–3]. Its outstanding sensitivity and versatility as well as the fact that fluorescence inherently allows the exploitation of several different parameters all contribute to this ongoing success. Luminescence measurements provide information on the spectral, intensity, lifetime and polarization features of the fluorescing species. It is a non-destructive and non-invasive technique and when adequate fluorophores and equipment are employed it allows the measurement against a zero-background. Today, under the influence of modern analytical trends for miniaturized detection protocols, whether in combination with laboratory-based and sophisticated instrumentation for high-throughput analysis and screening in clinical diagnostics or pharmaceutical screening or for implementation into mobile, handheld devices in point-of-care-testing or homeland security applications, fluorescent probe or sensor systems have to become more and more powerful [4–7]. The detection volume or the active area or spot sampled in such miniaturized protocols is often much smaller than in conventional fluorescence applications so that the amount of luminescence generated by a single probe should be as high as possible. To go beyond the signal provided by a single fluorescent tag such as for instance a single Cy3 or FITC (fluorescein isothiocyanate) molecule, the development of fluorescence amplification strategies has received increasing attention. However, the amplification features of single fluorophore molecules are intrinsically limited. Even if the fluorophore’s photoluminescence quantum yield (PLQY) amounts to 1, absorption of a single photon can only generate a single emitted photon. For fluorescent molecules as tags or labels, this limit cannot be surpassed. For fluorescent indicators or probes which indicate a certain target species by a specific change in fluorescence, strong signals are commonly only achieved when the PLQY of bound and unbound form differ as much as possible, i.e. when analyte-binding leads to a “switching on” of the fluorescence [8]. During

the last decade, several strategies have thus been proposed and realized to generate amplified fluorescence signals, many of them relying on nano- or micro-particulate or -structured objects, surfaces of interfaces. These concepts range from the improvement of the signal-to-noise ratio over the suppression of unspecific signals and the collective response of more than one fluorophore unit on the binding event to the catalytic production of fluorophores and the direct amplification of photophysical processes. The present contribution will give an overview of the most prominent approaches and will highlight representative examples in this exciting area of research. (Bio)molecular amplification techniques that are very powerful yet only lead to an increased signal by the catalytic amplification of an analyte, which is then conventionally treated, like the polymerase chain reaction (PCR), will not be covered here [9]. In addition, the discussion of enzymatic approaches like the rolling-circle amplification (RCA) would also go beyond the scope of the present chapter [9]. For a more general introduction of signal amplification involving molecular indicators and detection schemes, the reader is referred to [10].

2 Resonance Energy Transfer

The first section deals with a concept that is in most cases not a true amplification strategy in the sense that one analyte as input generates an output from a larger number of fluorophores, but the advantageous features here are based on the uniqueness of the signalling system. The latter involves two chromophores and a distance-dependent process and enables one to separate the excitation wavelength significantly from the emission spectrum, creating a system with a very large pseudo-Stokes shift. The concept is called *resonance energy transfer* or RET and the mechanism can be rationalized as follows. After photo-excitation, the energy absorbed by a molecule (the RET donor, D_{RET}) can be transferred over a certain distance to another molecule (the RET acceptor, A_{RET}) through resonance energy transfer. In the ideal case, exclusive donor excitation thus leads to exclusive acceptor emission. The pronounced pseudo-Stokes shift which is especially important for experimental reasons such as the suppression of scattering and background signals is based on the fact that the experimentally relevant spectra are the absorption spectrum of the donor and the emission spectrum of the acceptor (1), while the mechanically important spectra create the spectral overlap necessary for RET (Fig. 1) [11].

$$\Delta\tilde{\nu}_{\text{Stokes}}^{\text{pseudo}} = \tilde{\nu}_{\text{abs}}(D_{\text{RET}}) - \tilde{\nu}_{\text{em}}(A_{\text{RET}}) \approx \frac{1}{\lambda_{\text{abs}}(D_{\text{RET}})} - \frac{1}{\lambda_{\text{em}}(A_{\text{RET}})}. \quad (1)$$

Resonance energy transfer can occur when the emission spectrum of the donor overlaps to a sufficient degree with the absorption spectrum of the acceptor (Fig. 1) and when the distance between the excited donor and the acceptor in the ground

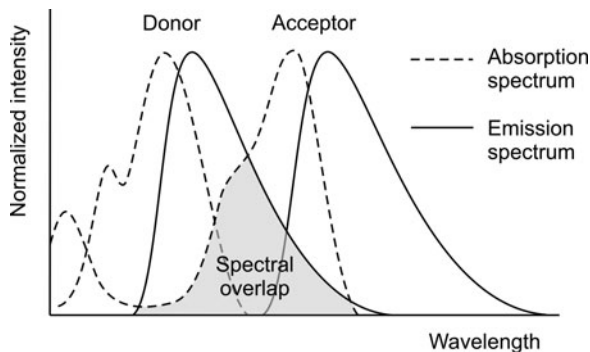


Fig. 1 Spectral characteristics of a RET system. The *highlighted area* corresponds to the mechanically important overlap between emission spectrum of the donor and absorption spectrum of the acceptor. (Reprinted with permission from [11]. Copyright 2009 Springer)

state lies between 1–10 nm. In addition, it is important to keep in mind that the energy is transferred through a non-radiative process and that no fluorescence (of the donor) is involved. Nowadays, RET is a widely used and popular approach in several areas of analytical, life and materials sciences [12].

According to Förster's theory [13], the efficiency of the resonance energy transfer (E_{RET}) is inversely proportional to the sixth-power of the distance (r) between donor and acceptor (2). In (2), R_0 is the so-called Förster distance at which the transfer efficiency is 50%. Förster RET is therefore a very sensitive process and can transduce small conformational changes into large intensity modulations. R_0 is characteristic for a particular donor–acceptor pair and depends on the overlap integral J between D_{RET} emission and A_{RET} absorption, the PLQY of D_{RET} in its unperturbed state Φ_{D} and the mutual orientation of the two partners expressed as geometry factor κ^2 which equals $2/3$ for random orientation of the partners (3). For a more detailed discussion of the mechanistic of RET, the reader is referred to the literature [12].

$$E_{\text{RET}} = \frac{R_0^6}{R_0^6 + r^6}. \quad (2)$$

$$R_0^6 = 8.875 \times 10^{-5} \frac{\kappa^2 \Phi_{\text{D}} J}{n^4} \quad \text{with} \quad J = \int F_{\text{D}}(\lambda) \varepsilon_{\text{A}}(\lambda) \lambda^4 d\lambda. \quad (3)$$

Depending on the donor chosen, RET systems can be divided into fluorescence resonance energy transfer (FRET) systems for which the donor is a fluorescent molecule, nanocrystal or an object such as a dye-doped particle, bioluminescence resonance energy transfer (BRET) systems for which the donor is a bioluminescent molecule and chemiluminescence RET (CRET) systems, the chemical equivalent

of BRET, for which the donor is a chemiluminescent molecule, respectively [14].¹ Whereas FRET is unique in generating a fluorescence signal after photo-excitation of the donor, BRET and CRET measurements do not require an external light source and do not have to account for autofluorescence background signals because excitation occurs through a chemical reaction. Besides a zero-background, the main importance of BRET and CRET is that photo-damaging, especially of biological samples, is avoided. A comparison of FRET and BRET is summarized in Fig. 2 and the different advantages and disadvantages of the two strategies are discussed for instance in [15, 16].

RET in conjunction with nano- or microparticles can be principally divided into three different categories. First, dye-doped particles can be used as RET partner, usually as D_{RET} , and mostly a dye attached to the target analyte serves as the RET acceptor. The particles employed here are mainly polymer and silica particles and their size commonly lies between 20 nm and 2 μm . Moreover, this approach can be further divided into three strategies.

In the prevalent case, the particles are doped with a high amount of one particular dye (Fig. 3a). The main advantage is that such particles are generally highly fluorescent and, because of the large number of dyes incorporated, possess a statistical advantage of yielding a FRET signal once an adequately labelled target is bound (or a labelled probe is displaced). In addition, the incorporation of many dyes into a single particle and the equipment of the particle's surface with many binding sites allow the detection of many analytes on a single particle [17]. The second strategy uses the favourable features of RET as a tuning element, i.e. for the tuning of the pseudo-Stokes shift. Several dyes with matched absorption and emission bands are integrated into a single particle, creating one or more "tandem" FRET pairs within the particle (Fig. 3b). If properly tailored, such a cascade of dyes allows for efficient excitation energy transfer – efficiencies of >90% can be reached – and can yield pseudo-Stokes shifts of >200 nm [18], potentially shifting the emission bands far into the "biological window", i.e. into the spectral range of 650–900 nm [19]. However, up to now, such particles have been mainly used for bar-coding and multiplexing applications, allowing the tracking and identification of certain particles or analytes [20, 21]. A combination of such FRET-tandem dye-doped particles, for instance as D_{RET} partner in a classical FRET assay with a conventional dye as A_{RET} , has not yet been realized (for one of the few examples of

¹ The IUPAC-approved term for FRET is Förster RET [14]. 'Fluorescence resonance energy transfer' is commented on as the: *Term frequently and inappropriately applied to resonance energy transfer in the sense of Förster-resonance energy transfer (FRET), which does not involve the emission of radiation.* In contrast, the literature uses both terms Förster RET and fluorescence RET with the latter even dominating in the biochemical and bioanalytical communities. Despite the correct classification by the IUPAC, the scientist is in a dilemma when trying to distinguish between FRET, BRET and CRET, all Förster-type processes which differ only in the properties of the donor. Interestingly, BRET and CRET are not included in the IUPAC Photochemistry Commission's recommendations. In the present case, it seems more appropriate for us to use FRET for a RET involving a potentially fluorescent donor and BRET (CRET) for a RET involving a potentially bioluminescent (chemiluminescent) donor here.

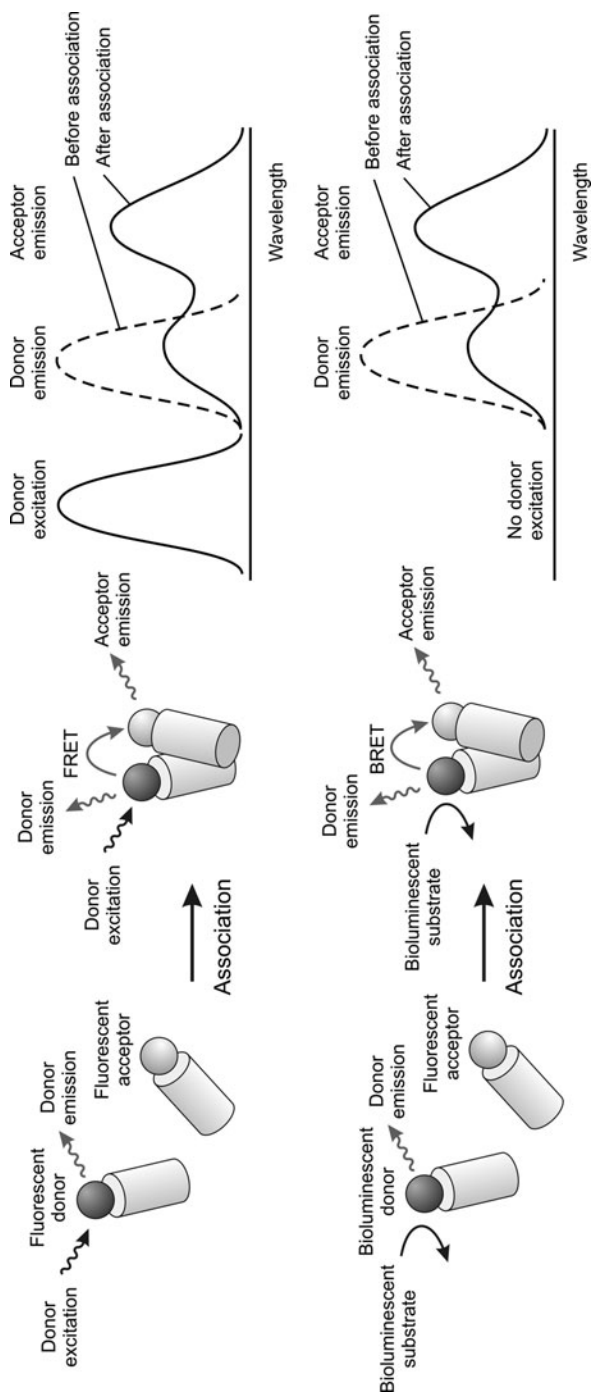


Fig. 2 Comparison of FRET (*top*) and BRET (*bottom*). (Reprinted with permission from [11]. Copyright 2009 Springer)

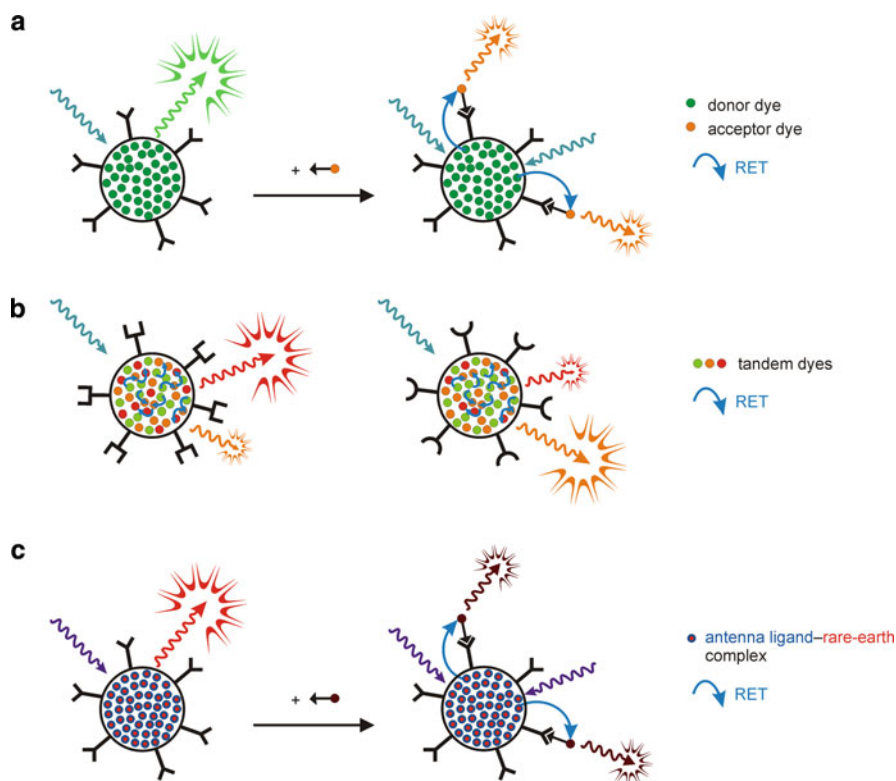


Fig. 3 Three different RET approaches involving polymer or silica particles as described in the text. (a) Particles doped with a large amount of a single dye for multiple FRET detection on a single particle; common case: excitation in the visible yields strong visible emission and *red-visible FRET signals*. (b) Particles with different receptors are doped with different ratios of FRET-tandem dyes yielding different emission colours for bar-coding or multiplexed detection; common case: excitation in the visible yields different emission colours in the *red-visible* and near infrared (NIR) range. (c) Particles doped with a rare earth-antenna ligand complex for multiple FRET detection on a single particle; common case: excitation in the UV yields strong red-visible emission through intra-complex energy transfer (not indicated in the sketch) and NIR FRET signals

FRET-tandems in a FRET assay, see Sect. 2.3 below). In a step further, the third strategy relies on rare earth emitters as D_{RET} . Because of the formally forbidden f-f transitions which are involved in rare earth luminescence and which possess only very low absorption coefficients, emitters such as Eu^{3+} or Tb^{3+} are usually complexed with an organic ligand which shows a sizeable absorption in the UV/vis region and is able to efficiently transfer its energy to the metal ion, i.e. to sensitize it. In the case of Eu^{3+} , for instance, such antenna ligands usually absorb in the 300–400 nm range while the strongest emission line of Eu^{3+} is found at 614 nm [22]. The ensemble antenna-rare earth cation thus intrinsically shows

the same features as the (multi-)tandem dye systems in the previous approach, i.e. pronounced pseudo-Stokes shifts, and can be doped into particles used as D_{RET} in a classical FRET approach (Fig. 3c). However, since the decay of the rare earth luminescence is quite slow, on the micro- to millisecond timescale again due to the f–f transitions involved, employment of particles doped with rare earth antenna chelates makes time-gated detection possible. Observation of the luminescence signal at a strongly pseudo-Stokes shifted wavelength with a time delay of several microseconds suppresses any background or autofluorescence signals most efficiently. Ultrasensitive assays can thus emerge [23].

The second category of particle-based RET systems utilizes inorganic particles such as gold nanoparticles (AuNPs), quantum dots (or semiconductor nanocrystals, QDs) or so-called up-conversion phosphor nanoparticles (or nanophosphors, UCPs) as one (or both) of the RET partners. These inorganic species are employed because of their unique and partly very favourable optical properties. AuNPs mainly function as efficient RET quenchers, QDs are basically employed as D_{RET} with high molar absorption coefficients and possible broad-band excitation and UCPs are particularly interesting because they can be excited with near infrared (NIR) light, show high PLQYs and very good chemical and photostability. Examples of these systems will be discussed in detail in the following sections.

The third category comprises metal NPs able to host surface plasmons that absorb in the visible spectral range and can therefore modulate intrinsic photophysical properties of organic dye molecules (and semiconductor nanocrystals), thus generating amplified signals. This last approach is discussed below in Sect. 5.2.3 together with other features of surface plasmon resonance (SPR) and metal-enhanced fluorescence (MEF). Due to this versatility in system design and the partly strong signal enhancement that can be achieved, micro- and nanoparticles are very popular building blocks in resonance energy transfer systems with improved performance in chemical and biochemical analytical applications.

2.1 Gold Nanoparticles

Gold nanoparticles (AuNPs) have several distinct advantages which qualify them as suitable RET partners in enhanced signalling applications. With respect to experimental issues, AuNPs are chemically and photochemically stable, do not show fluctuating signals and possess a very versatile functionalization chemistry. In addition, their synthesis in sizes that are still appropriate for RET applications, i.e. usually ca. 1–100 nm, is straightforward. Moreover, especially in this size range, they show intense (and size-dependent) SPR bands in the experimentally important visible wavelength range [24, 25].

AuNPs are almost exclusively used as potent quenchers in traditional RET applications. This is due to the fact that AuNPs of lower nanometric size efficiently quench the fluorescence of dyes because of a strong reduction of the radiative rate constant of the dye in close vicinity of the particle. In addition, the non-radiative

rate constant is increased when the fluorophore approaches the gold surface, however, with a much less dramatic effect. If the overall reduction in PLQY is considered, recent studies by Klar and Parak have shown that quenching is very efficient for AuNP–dye distances <4 nm but sizeable quenching is still found up to ca. 12 nm [26]. RET assays relying on AuNP are thus commonly designed in such a way that a non-luminescent FRET pair is formed between a potentially (highly) fluorescent D_{RET} dye and an AuNP as A_{RET} in the absence of the analyte. Binding of the target then liberates D_{RET} , reviving (strong) donor emission. For instance, an AuNP-based sensor for the detection of Hg^{2+} ions in aqueous solution has thus been developed, showing a strong modulation of the photoluminescence in the presence of the heavy metal ion. The assay is very potent and results in a 400-fold fluorescence enhancement in aqueous solution with analysis times of less than 10 min [27]. In a similar fashion, a FRET assay using a perylene bisimide (PBI) chromophore and AuNPs has been designed for Cu^{2+} [28]. The PBI chromophore carries two remote pyridine groups which coordinate to two AuNPs, invoking efficient quenching. Cu^{2+} complexation to the pyridine moieties unlocks the dye from the quenchers and revives emission. Because AuNP-mediated quenching is very efficient and considerably far reaching, the pyridine groups can be placed sufficiently far from the chromophore so that binding of the paramagnetic target does not result in fluorescence quenching in the liberated dye– Cu^{2+} complex. These examples show that FRET signalling can also elegantly accomplish the turn-on detection of notoriously quenching analytes such as Hg^{2+} and Cu^{2+} .

Besides metal ions, AuNPs are also popular quenchers in small-molecule and biomolecule RET assays. For example, a homogeneous sandwich immunoassay utilizing AuNPs as quenching acceptors has been reported for the detection of the protein cardiac troponin T (cTnT). As depicted in Fig. 4a, one of the antibodies (M11.7) is coupled to AuNPs and the other antibody (M7) is labelled with fluorescent Cy3B dyes [29]. In the absence of cTnT, the dyes emit their characteristic fluorescence. In the presence of cTnT, however, the two antibodies conjugate in sandwich arrangement and the fluorescence of the dyes is quenched by the AuNPs. Upon addition of analytes, the number of sandwich conjugates first increases, reaches a maximum, and then decreases again (Fig. 4a, bottom). The latter effect is measured above a certain threshold concentration of cTnT, when two antibodies do not bind in a sandwich fashion but individually to two analytes. Consequently, the fluorescence intensity decreases first, reaches a minimum, and increases again. For unambiguous quantification, careful system adjustment is thus necessary.

A popular field for AuNP-based FRET systems is DNA analysis. In an exemplary assay to monitor DNA cleavage, AuNPs have been functionalized with a Cy3-labelled oligonucleotide probe through a thiol–gold bond. Since the single-stranded probe wraps around the NP, the dye is close to the AuNP's surface and its fluorescence is strongly quenched. In the presence of the complementary target oligonucleotide, a double strand is formed, and the probe is moved away from the surface yet, in this design, is still within the quenching distance of the AuNP. Only after cleavage of the double strand from the particle by a single-strand specific nuclease is the Cy3 fluorescence revived. This assay is much faster and shows a

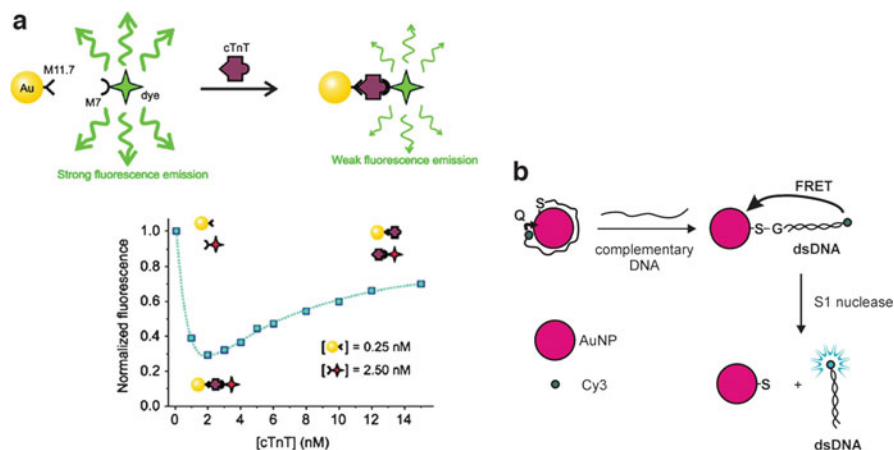


Fig. 4 (a) Schematic illustration of sandwich immunoassay for cTnT (*top*) and fluorescence intensity reading versus cTnT concentration (*bottom*). (b) Schematic illustration of the monitoring of DNA cleavage from AuNPs by a single-strand nuclease. (Reprinted and adapted with permission from [29, 30]. Copyright 2009, 2006 American Chemical Society)

sensitivity increase by several orders of magnitude compared to the traditional HPLC methods in assessing DNA cleavage (Fig. 4b) [30].

2.2 Quantum Dots

Quantum dots (QDs) or semiconductor nanocrystals have recently received strong attention in analytical chemistry because of their narrow emission bands, tuneable size-dependent emission spectra, spanning from the UV to the NIR, high PLQYs and high photostability [31, 32], including applications from fibre-optic sensing to multiplexed detection [33, 34]. Due to their broad excitation and narrow emission bands, QDs are ideal donors in FRET systems [35, 36]. Until recently, applications of QD-based RET probes have mainly used one of the following two approaches: (1) a QD as D_{RET} and a dye as A_{RET} , e.g. attached to a protein or DNA strand and (2) a QD as D_{RET} and a gold nanoparticle as A_{RET} quencher [37]. The scenario employing a QD as D_{RET} and a fluorescent protein as A_{RET} is less frequent [38] as is the case that uses a QD as D_{RET} and a conjugated polymer (CP) as A_{RET} (see below). Furthermore, approaches with two differently coloured QDs do not play a significant role yet in analytical chemistry [39], but are more important in the context of luminescent thin films and layer-by-layer architectures for various materials chemistry applications [40].

An elegant establishment of case (1) has been realized in conjunction with an aptamer-based recognition motif [41]. Here, a core-shell-type CdSe/ZnS QD is used as D_{RET} and an Atto 590 dye as A_{RET} , yielding enhanced red emission upon

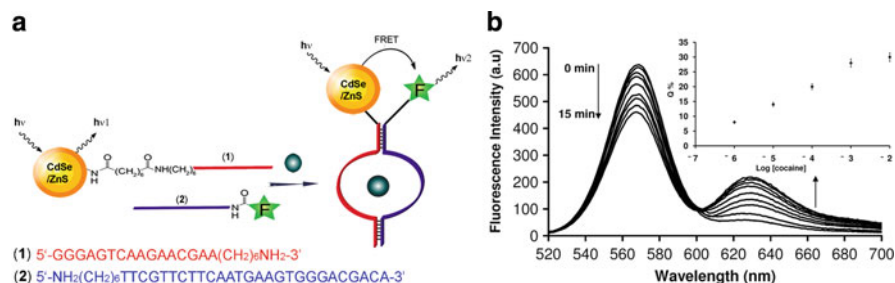


Fig. 5 (a) QD-based sensing of cocaine by the formation of a cocaine–aptamer supramolecular structure that triggers FRET. (b) Time-dependent luminescence spectra of the system in the presence of cocaine. The *inset* shows a calibration curve for variable concentrations of cocaine and a fixed observation time of 15 min. (Reprinted with permission from [41]. Copyright 2009 Royal Society of Chemistry)



Fig. 6 Schematic illustration of a QD-based FRET competition assay for TNT detection. (Reprinted with permission from [42]. Copyright 2005 American Chemical Society)

binding in the presence of the analyte cocaine (Fig. 5). Another example utilizing a FRET-quencher design has been realized for the detection of 2,4,6-trinitrotoluene (TNT). The system consists of a QD (CdSe/ZnS core-shell) and a quencher dye (Black Hole Quencher-10) as the FRET pair (Fig. 6). The QD is coupled with an anti-TNT antibody, and the quencher conjugated with the TNT analogue. The competition assay induces the inhibition of the FRET quenching process and thus enhances the fluorescence signal upon displacement of the quenching conjugate in the presence of a TNT molecule that can successfully compete for the binding site [42].

A representative example for case (2) introduced above consists of positively charged CdTe QDs capped with cysteamine (CA-CdTe QDs) and negatively charged AuNPs capped with 11-mercaptopundecanoic acid (MUA-AuNP) as FRET pair based on electrostatic attraction. In the absence of the target, the QD luminescence is effectively quenched in the FRET ensemble. The presence of Pb²⁺ then leads to a displacement of the CA-CdTe QDs and Pb²⁺-mediated aggregation of the MUA-AuNPs, thus inhibiting the FRET process. An interesting aspect of this approach is that indication of the analyte is transduced by an enhancement of the

QD luminescence and a shift in the plasmon absorption band because of AuNP aggregation [43]. An example for the detection of a small-molecule analyte has been realized in a similar fashion as a nanobiosensor for glucose in serum. The QDs are conjugated with concanavalin A (ConA) and the AuNPs are coupled with thiolated β -cyclodextrins (β -SH-CDs), respectively. In the presence of glucose, the AuNP- β -SH-CD segment is displaced by the sugar which competes with β -CD for the binding sites of ConA, resulting in luminescence recovery of the quenched QDs [44].

Electrostatic complex formation between a fluorescent CP and CdTe QDs is another promising way to generate strong FRET signals. The example shown in Fig. 7 has been developed for the detection of target DNA hybridization. In the complex, the cationic polymer poly[9,9-bis(3'-((*N,N*-dimethyl)-*N*-ethylammonium)propyl)-2,7-fluorene-*alt*-1,4-phenylene]dibromide (PDFD) is used for both light-harvesting and assembling of the negatively charged QDs and DNA molecules [45]. This is one of the few cases where QDs act at the same time as $A_{RET(1)}$ and $D_{RET(2)}$. (For selected examples of CP-based FRET assays, see Sect. 3.1.)

Owing to the broad absorption/excitation spectra of QDs, they can be excited by nearly all the bioluminescent proteins available and are thus suitable A_{RET} in BRET systems, taking advantage of the virtual absence of background fluorescence. For instance, a QD-based BRET assay has been developed by coupling carboxylate-functionalized QDs to a mutant of the bioluminescent protein *Renilla reniformis* luciferase (Fig. 8). Once stimulated, the ensemble emits long-wavelength bioluminescence light in cells and deep tissues. This advantage distinguishes bioluminescent QD probes as a very promising approach toward sensitive in vivo imaging, in vitro assays and multiplexing analysis [46].

Besides BRET, there is another less frequent RET method called chemiluminescence resonance energy transfer (CRET). CRET is closely related to BRET, utilizing a chemiluminescent (CL) instead of a bioluminescent D_{RET} , i.e. CRET commonly relies on the oxidation of a potentially luminescent substrate. Like BRET, CRET can dispense with an excitation source and thus shows excellent background suppression. A model CRET assay has been realized with bovine serum albumin- (BSA) coupled CdTe QDs and anti-BSA antibodies conjugated to horseradish peroxidase (HRP). Together with luminol as the substrate, HRP

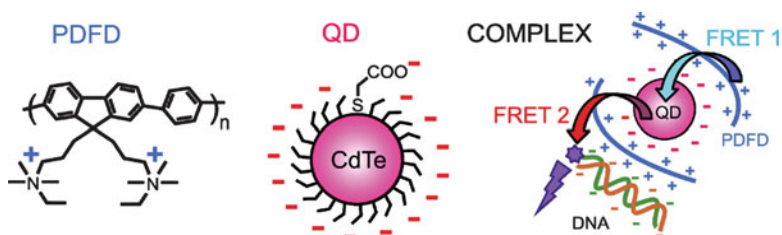


Fig. 7 Chemical structure of PDFD, schematics of a thiolglycolic acid (TGA)-capped CdTe QD and of the PDFD/QD/dye-labelled DNA complex for detecting DNA hybridization. (Reprinted with permission from [45]. Copyright 2009 American Chemical Society)

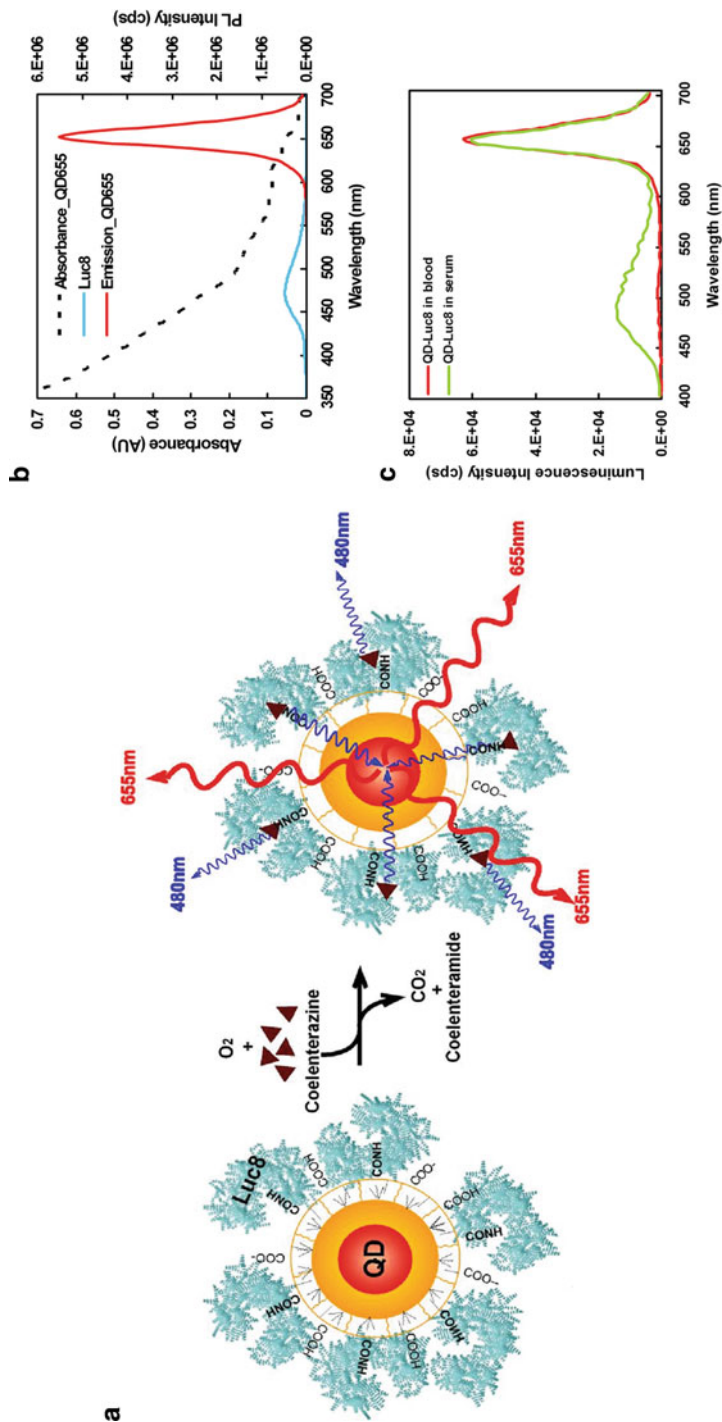


Fig. 8 (a) Schematic illustration of the QD-based BRET system and (b) spectral manifestation of the assay. (c) Two assays performed under identical conditions in mouse serum (*green*) and mouse whole blood (*red*). (Reprinted with permission from [46]. Copyright 2006 Macmillan Publishers Ltd)

constitutes a classical CL system and continuously catalyzes the production of chemiluminescence with, for instance (and like in this case), hydrogen peroxide as the oxidant. Once the QD-labelled BSA binds to the antibody, CL production occurs close enough in space to trigger red-shifted CRET emission from the QD as A_{RET} [47]. This method has significant potential for applications in immunoassays of various types. Recently, Zhao et al. also showed that CRET systems can be used in a rather unspecific manner as a very sensitive detection scheme in microfluidic separation techniques [48].

2.3 Up-Conversion Nanoparticles

As mentioned above, recent research has seen the introduction of another alternative RET partner, the so-called up-conversion (nano)particles (UCPs). UCPs are excited in the NIR region and emit in the visible range through the sequential absorption of two or more low-energy photons [49]. UCPs basically consist of a host material doped with lanthanide ions. Although they have only a short history in (bio)chemical signalling, they hold great potential for analytical applications because of their favourable characteristics such as high PLQYs, tuneable optical properties, high chemical stability and low toxicity [50, 51].

Until today, up-conversion particles have mainly been used as donors in RET assays. For instance, they have been employed in combination with AuNPs as A_{RET} for the detection of trace amounts of avidin [52]. In the sandwich-type assay, emission of biotinylated UCPs is recorded prior to conjugation of biotinylated AuNPs in the presence of avidin. The AuNP-mediated quenching of the UCP luminescence then shows a linear relationship with avidin concentration. An attractive homogeneous assay format based on up-conversion RET has been established in a competitive immunoassay for estradiol (E2). Whereas the UCPs coated with an anti-E2 antibody serve as D_{RET} , E2-conjugated Oyster-556 dyes are employed as A_{RET} (Fig. 9) [53]. Since here D_{RET} can be excited well in the NIR, autofluorescence and scattered light are successfully eliminated and do not perturb the A_{RET} signals in the visible range. Furthermore, the introduction of tandem dyes in conjunction with UCPs can dramatically enhance the acceptor emission [54].

3 Nanoscopic Objects with Inherent Signal Amplification

Whereas the implementation of specific photophysical processes to generate well-separated and strongly distance-dependent signals has been the focus of the previous section, the examples presented in the following will show how the encapsulation of chromophores in nanoscopic systems can lead to amplified signals when compared with the respective molecular systems. Signal enhancement can be a consequence of different factors. For example, in a similar manner as briefly

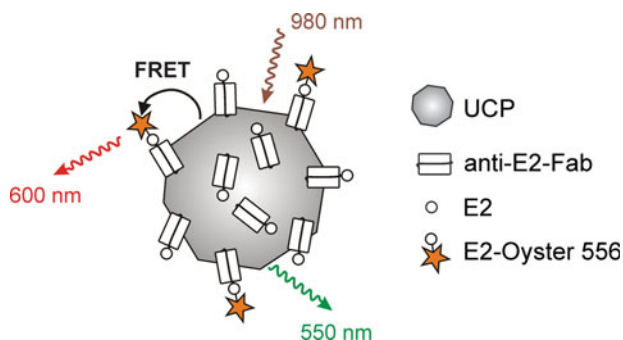


Fig. 9 Schematic illustration of UCP-based homogeneous FRET immunoassay for E2. (Adapted with permission from [53]. Copyright 2006 American Chemical Society)

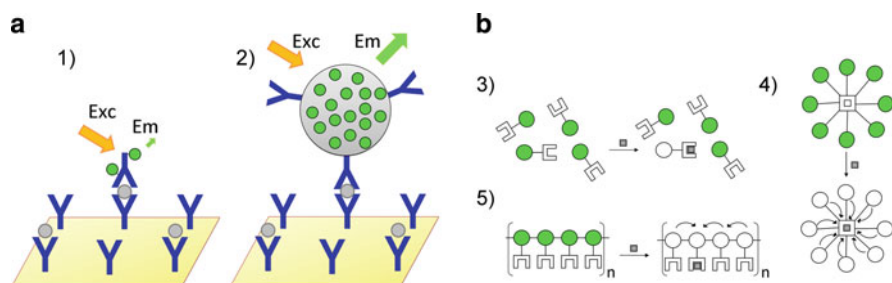


Fig. 10 (a) Representative scheme for the signal amplification concept by increasing the number of fluorophores per binding site in an antigen–antibody sandwich assay. Binding of a labelled antibody to the target yields an only moderate fluorescence signal because the antibody can be labelled with only a few fluorophores at maximum (1). Use of an antibody which is labelled with a nanoscopic object that contains a large number of fluorophores dramatically enhances the signal (2). (b) Effect of analyte coordination in (3) a traditional molecular indicator, (4) a fluorescent dendrimer and (5) receptors wired in series in a conjugated polymer. The curved arrows indicate the active processes, e.g. quenching

discussed in Sect. 2 (cf. Fig. 3a), the increase of the number of luminophores per binding site (i.e. the L/B ratio) can lead to an enhanced luminescence signal when dendrimers, fluorescent nanocrystals or liposomes are used as labels in binding assays, because every binding event is signalled by several tens, hundreds or thousands of fluorophores (Fig. 10). Collective energy migration or energy transfer processes, the latter closely related to the processes presented above, can also entail signal amplification, because, in contrast to conventional fluorescent indicator molecules, for which the recognition of the target by the receptor unit only affects the fluorescence properties of the single, covalently coupled fluorophore residue, in multi-fluorophore/multi- or single-binding site systems, more than one fluorophore unit can experience a modulation through a single binding event in its immediate neighbourhood. The underlying basis here is inter-fluorophore communication

which can occur in systems such as *fluorescently doped dendrimers* when the local concentration of fluorophores is comparatively high. Alternatively, analyte binding at a single receptor unit can influence multiple fluorescent repeat units of a CP because of the electronically delocalized structure of CPs which facilitates energy migration over large distances to the analyte–receptor complex as a “sink”. The net effect in all of these cases is the transduction of a single binding event by an amplified response of several fluorophores.

Representative examples of signal amplification in CPs, fluorescent dendrimers, encapsulated dye microcrystals as well as dye-loaded liposomes and mesoporous silica hybrids will be discussed below. For examples involving luminescently doped silica or polymer particles, which are very similar in nature, the reader is referred to [55].

3.1 Conjugated Polymers

The dominant attribute that has driven interest in fluorescent CP sensory materials is their ability to produce signal gain in response to interaction with analytes. The increased sensitivity (amplification) is derived from the ability of the CP's delocalized electronic structure (i.e. energy bands) to facilitate efficient energy migration over large distances. To rationalize how energy migration can amplify fluorescence-based sensory events, consider a CP with a receptor attached to every repeating unit. If energy migration is rapid with respect to the fluorescence lifetime, then the excited state can sample every receptor in the polymer, thereby allowing the occupation of a single binding site to change dramatically the entire emission of the system (Fig. 10b).

A first proof-of-principle for the signal amplification phenomenon in CPs has been reported by Zhou and Swager in 1995. By using poly(propylene ethynylene) as CP with 34-crown-10 groups attached to the CP as receptors for the recognition of the well-known quencher paraquat (PQ^{2+}), the authors could observe how PQ^{2+} binding produced a trapping site for excitons, which were effectively deactivated by electron transfer [56]. CPs have been employed in different formats like in homogeneous solution, as thin films or as molecularly imprinted polymers. A comprehensive overview of further examples and mechanistic descriptions of CP-based signalling systems can be found in [57].

CPs can also be prepared in nanoparticulate form [58–62]. The interesting aspect of such a formulation is that first reports have appeared which discuss how CP NPs can yield even stronger signal amplification. For example, silica NPs covered with layers of CPs have been employed for the detection of nitroaromatic quenchers with sensitivity enhancement factors of up to 200 with respect to the corresponding neat polymers in solution. Interestingly, in all cases, the microspheres coated with two layer pairs of CPs show larger Stern–Volmer quenching values than those coated with only one layer pair, which was ascribed to an energy migration effect [63].

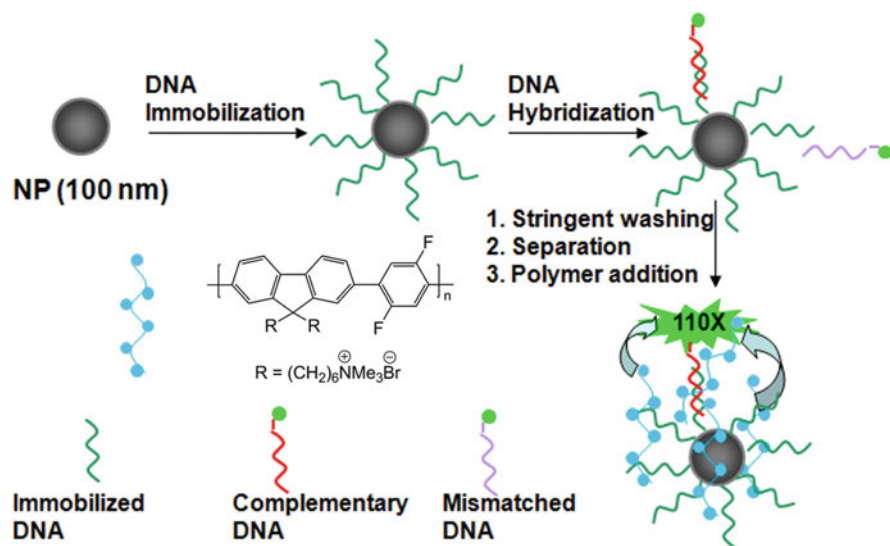


Fig. 11 Signal amplification with CPs via FRET in a DNA hybridization assay on silica NPs. First, the silica NPs are functionalized with the capture DNA. After DNA hybridization with a complementary dye-labelled DNA strand and subsequent washing and separation, CP is added, resulting in a 110-fold fluorescence increase. (Reprinted with permission from [67]. Copyright 2007 Royal Society of Chemistry)

CPs have also been successfully employed as energy harvesting systems in FRET based assays [64, 65] (for an introduction to resonance energy transfer, see Sect. 2). For instance, Liu et al. have used this property for amplifying fluorescence signals in silica NP-based FRET immunoassays [66] and DNA hybridization assays [67, 68], in a way resembling the enhanced excitation intensities at metal surfaces discussed in Sect. 5.1. The amplified emission by excitation of the CP relative to direct excitation of the dye label originates from the electron-delocalized backbone of the CP that allows rapid intrachain and interchain exciton migration via RET (Fig. 11) [67]. In a later work, the same authors have reported the surface functionalization of polyhedral oligomeric silsesquioxane (POSS) nanoparticles of 3.6 nm diameter with cationic oligofluorene for fluorescence amplification in cellular imaging. The cationic oligofluorene substituted POSS (OFP) possesses outstanding light harvesting properties for efficient RET. As a result, the fluorescence of intercalated ethidium bromide is amplified 52-fold upon excitation of OFP in buffer [69].

3.2 Dendrimers

A unique concept that can be employed when aiming to install energy funnelling processes and at the same time aspiring to increase the L/B ratio relies on *dendrimers*. Dendrimers are highly branched, tree-like polymers that possess a precise size and

shape and defined surface groups. They are multifunctional macromolecules which can bear multiple dyes and biomolecules. Fluorescent dendrimers have been used for instance for signal amplification in DNA assays using flow cytometry techniques. With the dendrimer assay, the minimum detectable amount of analyte DNA has been lowered from hundreds to tens of attomoles [70]. Dendrimers labelled with different families of organic dyes can also serve as strongly fluorescent probes for the detection of biomacromolecules [71].

Regarding *energy migration* in nanoscopic systems, dendrimers containing photoactive components can exhibit particularly interesting properties since cooperation among the photoactive units can allow the dendrimer to perform specific functions, e.g. light harvesting through antenna effects. Properly designed dendritic materials can show efficient migration of energy from the dendrons or peripheral groups to the more conjugated units or core, leading to dramatically enhanced fluorescence intensity changes (Fig. 10b). One of the first works realizing the application of dendrimers in optical sensing and signal amplification has been conducted by Vögtle, Balzani et al. [72]. They have used a fourth generation (4D) poly(propylene amine) dendrimer with 32 dansyl units at the periphery and containing 30 aliphatic amine units in the core for the detection of Co^{2+} . The fluorescence of all dansyl units is quenched when a single Co^{2+} ion coordinates to the aliphatic amine units. In a further work, another sensory dendrimer and a mono-dansylated reference compound have been investigated for comparison. Addition of Ni^{2+} or Co^{2+} to a basic solution of the mono-dansyl compound did not cause any effect in the absorption or emission properties of the molecule. However, in the case of the dendrimer – now a polylysine dendrimer branched at the 1,3,5-positions with eight fluorescent dansyl units in the periphery and six aliphatic amide units in the interior of each branch – a strong quenching of the dansyl emission at 514 nm has been observed [73]. At low metal ion concentration, each metal quenches ca. nine dansyl units. Interestingly, the authors have also observed an influence of the dendrimer size on the response, i.e. quenching of the signal is amplified with increasing dendrimer generation, n [74].

Optically active dendrimers have also been described for fluorescence detection of chiral compounds, like those based on chiral 1,1'-bi-2-naphthol (BINOL) [75]. The light harvesting antennas of the dendrimer funnel energy to the central BINOL unit, whose hydroxyl groups lead to fluorescence quenching upon interaction with a chiral amino alcohol. This mechanism renders the dendrimers' fluorescence responses much more sensitive than those of the corresponding small-molecule sensors. The enantioselective fluorescence recognition of mandelic acid, a chiral α -hydroxycarboxylic acid, has also been realized in such a way [76]. This last example is particularly interesting because, in contrast to the majority of systems, the light-harvesting effect in this case entails fluorescence enhancement instead of quenching.

Mechanistically, exciton migration phenomena seem to be responsible for the enhanced fluorescence quenching in dendrimers. Investigations of Guo et al. have shown that the quenching constant for a fluorescent dendrimer in the presence of TNT increases with the dendrimer generation number. They have also shown that

excitons can migrate over the dendrimer surface to the quenching site, the ability for exciton migration being the main contributor to the observed dynamic fluorescence quenching [77].

3.3 Encapsulated Dye Nanocrystals

Leaving specifically tailored photophysical processes aside, the simplest way to increase the number of emitters per binding site is perhaps to use *fluorescent nanocrystals* instead of a molecular label. Renneberg et al. have introduced this concept in 2002 and encapsulated crystalline fluorescein diacetate (FDA) with an average size of 500 nm in ultrathin polyelectrolyte layers of poly(allylamine hydrochloride) and poly(sodium 4-styrene sulphonate) via layer-by-layer (LbL) techniques [78]. The polyelectrolyte coating is subsequently used as an interface for the attachment of antibodies through adsorption. The L/B ratio, ranging from 5×10^4 to 2×10^5 , yields amplification rates of 70- to 2,000-fold for the nanocrystal label-based assay compared with the corresponding immunoassay performed with conventional, directly fluorophore-labelled antibodies. After the immunological reaction, the nanocrystals are dissolved by a release reagent and the dissolved molecules are released into the surrounding medium (Fig. 12). In subsequent works, the authors have optimized the performance of the assay by simplifying the preparation of the fluorescent conjugates. Assessing the analytical performance of the nanocrystal-based label system with a model sandwich

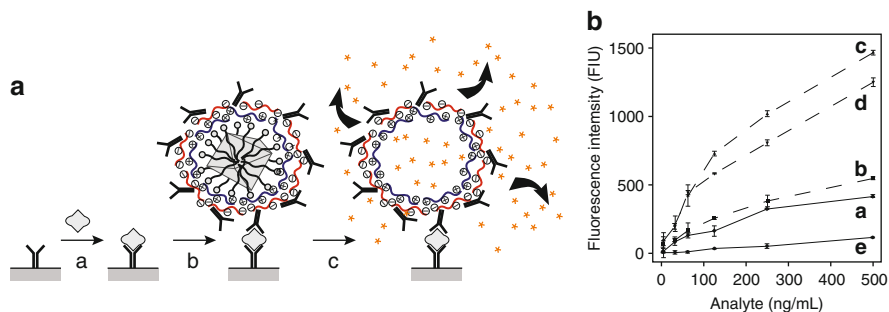


Fig. 12 (a) Principle of a sandwich immunoassay using FDA particulate labels. The analyte is first immobilized by the capture antibody pre-adsorbed on the solid phase (a) and then exposed to antibody-coated microparticle labels (b). Every microparticle contains $\sim 10^8$ FDA molecules. High signal amplification is achieved after dissolution, release and conversion of the precursor FDA into fluorescein molecules by the addition of DMSO and NaOH (c). (b) Calibration curves of IgG-FDA microcrystal labels with increasing surface coverage of detector antibody (a–d) compared with direct FITC-labelled detector antibody (e). The fluorescence signals increase with increasing IgG concentration. FDA microcrystals with a high IgG surface coverage (c,d) perform better than those with lower surface coverage (a,b). (Reprinted with permission from [78]. Copyright 2002 American Chemical Society)

immunoassay for the detection of mouse IgG, the authors could lower the LOD by a factor of 5–28 and increase the sensitivity 400- to 2,700-fold compared with conventional fluorescein isothiocyanate (FITC) conjugates [79]. The method has also been employed for avidin–biotin protocols [80] and for the quantitative detection of a PCR product [81].

3.4 Functionalized Liposomes

In a similar sense as discussed in the previous section, functionalized liposomes can be utilized as labels showing increased L/B ratios. Liposomes are synthetic spherical structures composed of one or more phospholipid bilayers in which soluble markers of interest can be encapsulated. This is commonly accomplished in two different ways. In the first approach, the dyes are embedded in the aqueous inner volume. For instance, Truneh et al. have included several hundreds of carboxy-fluorescein and sulforhodamine fluorophores in a single liposome, which is then used to label an antibody [82]. Alternatively, if the dyes possess a more hydrophobic character like, e.g. perylene dyes, they can also be incorporated into the bilayer membrane [83]. A 500-fold signal enhancement with dye-encapsulating liposomes over single fluorophore labels has been demonstrated by Edwards and Baeumner for the detection of specific DNA oligonucleotide sequences [84].

Liposomes can be detected either directly or through release of their cargo, e.g. after detergent-induced degradation once the analyte has been traced. The signal is then generated by the fluorophores which are liberated into the solution [85]. Although this approach is attractive, the preparation of microcapsules with liposomes is rather elaborate and the stability of the systems is often critical. Analogues of liposomes are nanosome systems which are prepared with amphiphilic block-copolymers. These vesicles can also encapsulate water-soluble fluorophores in the inner aqueous phase. Cross-linking of the vesicle membrane allows tuning of permeability, enhanced stability under physiological conditions and preservation of size and structure [86].

3.5 Gated and Dye-Loaded Mesoporous Particles

The liberation of a large number of indicator dyes by a distinctly smaller number of analytes can also be accomplished with another type of nanoscopic amplification system that utilizes mesoporous particles and various gating chemistries for locking and unlocking of the pore openings. The materials commonly employed here are organic-inorganic hybrid mesoporous silica nanoparticles. The basic concept includes the simple steric loading of a large number of dye molecules into the pores of the nanoparticle and the closing of the pore openings by attachment of a comparatively small number of sufficiently large molecules on the particle surface

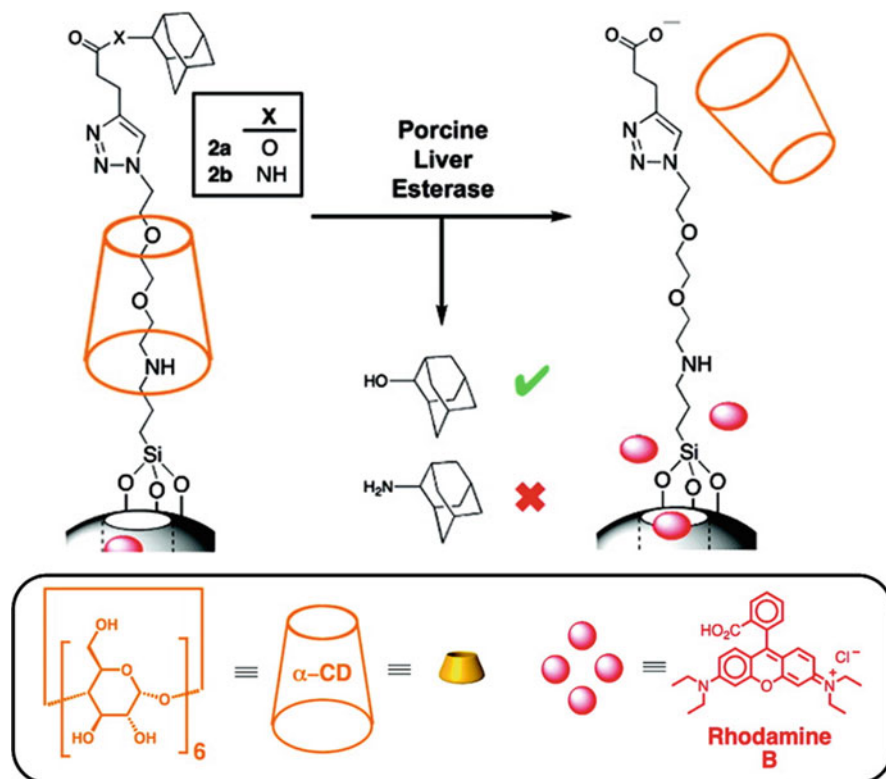


Fig. 13 Enzyme-mediated opening and dye release mechanism with selectivity for ester bond cleavage. (Reprinted and adapted with permission from [88]. Copyright 2008 American Chemical Society)

that block the pores. In contrast to drug delivery applications for which various gating mechanisms including redox and photo-switchable processes have been designed [87], the few systems developed for luminescence sensing rely on the oldest chemical technique for pore opening, a chemical reaction in the presence of the analyte that leads to the cleavage of the stopper. An inherent feature of this gating strategy is its nature as a truly amplifying process.

Although not yet established for analyte sensing, the enzyme-mediated release of dyes from porous silica particles as it has been recently developed to model nanocontainer-based, site-selective drug delivery can serve well as a representative example to illustrate the concept (Fig. 13) [88]. Rhodamine B which has been used as the model indicator dye is loaded into the mesopores of the silica material and entrapped by capping with a rotaxane, consisting of an ethylene glycol thread encircled by an α -cyclodextrin torus. The latter is fixed in the rotaxane state by a cleavable adamantane stopper at the terminal end of the ethylene glycol thread. If the stopper is connected through an ester bond, it will

be cleaved upon exposure to porcine liver esterase. Once the terminal stopper is dissociated, the torus of the rotaxane is free to be liberated, the pores can be opened and the dye can be released. The versatility of the approach and the promise it holds for sensing is evident from a look at an analogous system that has been realized a year later. Here, $\text{Ru}(\text{bpy})_3^{2+}$ (bpy = bipyridine) has been employed as the entrapped fluorescent indicator, lactose molecules have been used instead of the rotaxane as the caps and β -D-galactosidase as the uncapping enzyme [89].

A true sensing system for the detection of methylmercury has been designed in a similar fashion as follows [90]. Again, a mesoporous silica material with a homogeneous pore size distribution (2–3 nm) and large specific surface area ($>1,000 \text{ m}^2\text{g}^{-1}$) is used as the scaffold. This host is loaded with a large amount of the indicator dye safranin O by simple entrapment. The pores of the hybrid material are then coated with thiol groups and closed through a reaction with squaraine dyes which are sensitive to nucleophilic attack by the thiol groups, forming 2,4-bis(4-dialkylaminophenyl)-3-hydroxy-4-alkylsulfanylcyclobut-2-enone (APC) derivatives as pore blockers. This reaction converts the deep-blue coloured squaraine into its UV-absorbing leuko form (Fig. 14) [91]. Besides closing the pores, the sulfanyl-blocked APC leuko form of the squaraine is sensitive to thiophilic ionic mercury species, attack of which leads to a cleavage of the thiol–squaraine bond and restoration of the highly fluorescent squaraine fluorophore [92]. Since the aim of this study has been to target selectively methylmercury, an extraction step has been included in the protocol to discriminate against inorganic mercury species. In the final detection reaction, the presence of CH_3Hg^+ leads to the release of the squaraine dye, which entails the release of ca. 200 safranin O molecules per squaraine molecule from the uncapped pores [90]. Besides dramatic signal amplification, a unique feature of this system is that liberation of the safranin O molecules and restoration of the squaraine dyes, both absorbing and emitting in a different wavelength range, can be used for ratiometric signal assessment, a very useful aspect for self-calibrated analytical protocols.

Mechanistically, the gating reaction of this system involves the chemodosimetric production of a fluorophore. “Chemodosimetric” here means that the reaction of an analyte with a dye molecule precursor (or leuko dye) yields a fluorescent dye molecule and that these reaction events can be counted in a fashion that is similar to counting statistics in radiation measurements. An additional gain in signal enhancement is immanent to this increasingly popular technique: a non-fluorescent precursor, and thus a virtually zero-background, is converted into a fluorophore, the PLQY of which then determines the sensitivity of this reaction. Although this chemodosimetric approach gained rapidly in popularity for molecular indicators during the last decade [93], its implementation with nanoparticulate sensing systems has only been realized in a few examples so far. The reason for the latter is perhaps related to the fact that the reaction-based detection usually relies on a very selective reaction and thus does not require a supramolecularly

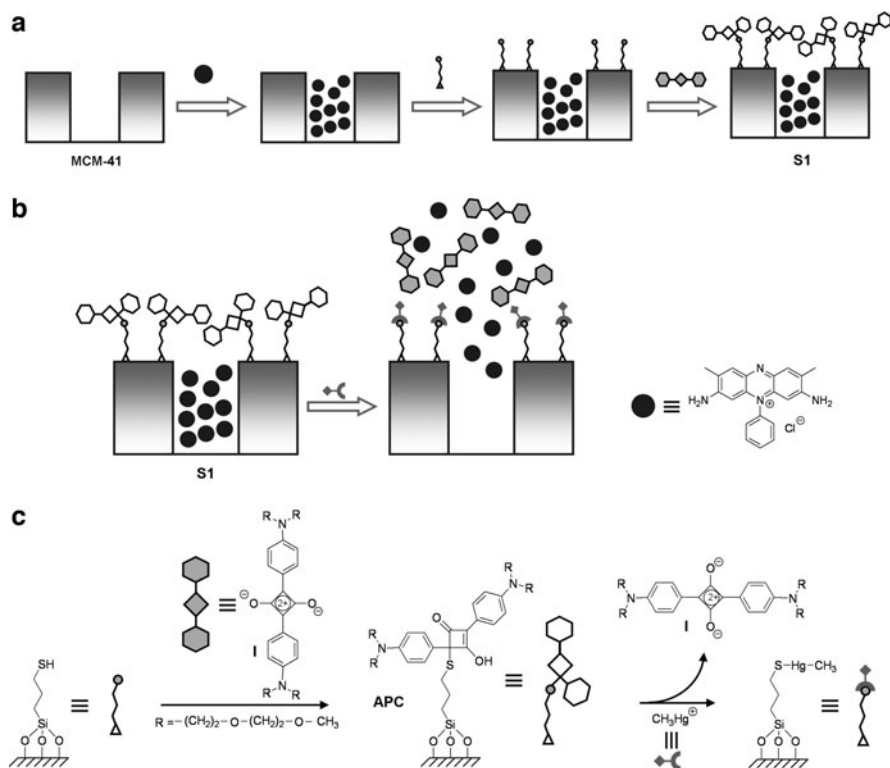


Fig. 14 (a) Synthetic scheme for the preparation of the safranine-entrapped and APC-capped material, (b) sensing mechanism and (c) molecular basis of the synthesis and sensing reaction. (Reprinted with permission from [90]. Copyright 2009 Wiley-VCH)

enhanced specificity. However, as the example above has shown, true massive signal amplification can arise from adequately designed systems.

4 Nanoparticles as Catalysts and Activity Enhancers

Chemical reactions in combination with nanoparticles can not only be used to unblock a large number of confined dyes and thus trigger the release of many more signalling units per binding event – they can also be used in a catalytic manner to produce directly light in a chemiluminescence (CL) reaction. CL detection in combination with particles has been realized in various ways. Whereas most of these approaches rely on a particle-based extraction step with subsequent CL detection, i.e. on a protocol in which no direct particle-mediated amplification

step is involved, only few strategies directly utilize nanoparticles in a catalytic fashion. Herein, we will focus on the latter cases; for a recent discussion of the others examples the reader is referred to [94].

4.1 Gold Nanoparticles as Catalysts in Chemiluminescence Reactions

Until today, systems that utilize metal nanoparticles as the catalysts in chemiluminescence reactions have been investigated mainly from a fundamental research point of view, most often employing gold nanoparticles (AuNPs) as the catalytic element [95–98]. AuNPs are known for their strongly size-dependent properties such as redox and photodynamic activity [24, 25]. For chemiluminescence systems involving luminol as the chemiluminescent reactant, various examples with different oxidants have been investigated and revealed a remarkable dependence on the particle size of AuNPs. If hydrogen peroxide is used as the oxidant, AuNPs with a diameter of 38 nm yield the highest chemiluminescence intensity [98]. In contrast, for ferrocyanide $[\text{Fe}(\text{CN})_6]^{3-}$ 25-nm AuNPs show optimum performance [96]. Mechanistically, the oxidation of luminol is catalyzed in these cases by AuNPs as shown in Fig. 15.

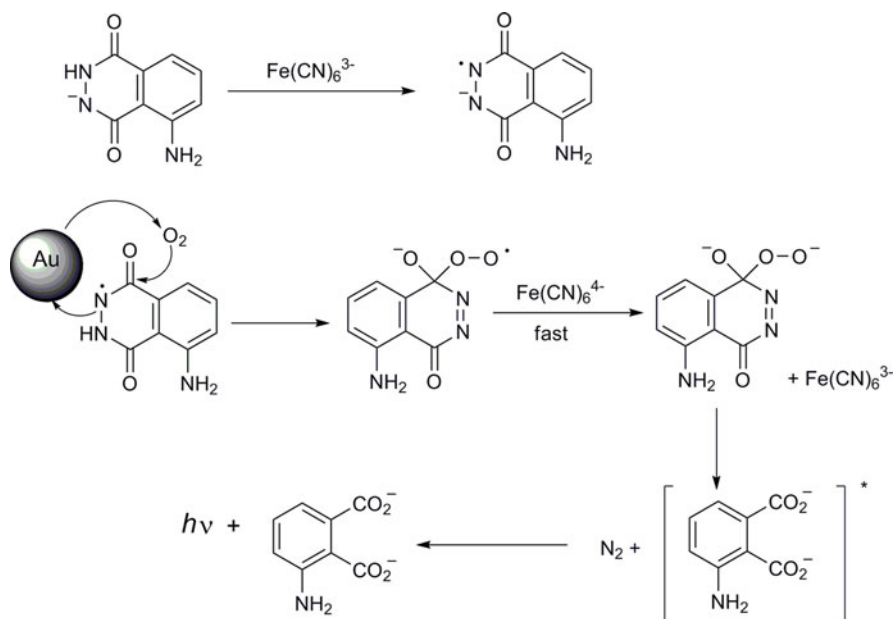


Fig. 15 AuNP-catalyzed oxidation of luminol with ferrocyanide (the AuNP-catalyzed step is more or less the same in the other systems mentioned). (Adapted from [96])

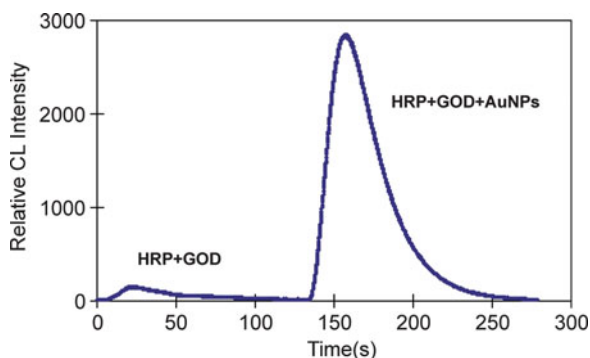


Fig. 16 Amplification effect of AuNPs on the HRP/GOD/luminol-based glucose detection. (Reprinted with permission from [100]. Copyright 2008 Elsevier)

In a recent example, Safavi et al. have shown that smaller AuNPs of 15 nm diameter yield the highest CL intensity in a AuNP-catalyzed luminol-hydrazine system. Here, the AuNPs play a double role as they first catalyze the formation of hydrogen peroxide and nitrogen from hydrazine and dissolved oxygen and secondly the subsequent oxidation of luminol by hydrogen peroxide [97].

4.2 Gold Nanoparticles as Activity Enhancers of Enzymes

It is well-known that gold nanoparticles can provide a suitable environment for redox active proteins to retain an activity like in their native environment [99]. Thus, the incorporation of AuNPs in enzyme-based chemiluminescence sensing systems is an obvious strategy and first examples have been recently published. For instance, Lan et al. could show that AuNPs greatly enhance the activity of a flow sensor for glucose based on glucose oxidase (GOD) and horseradish peroxidase (HRP) when the enzymes are co-immobilized on the gold particles via a sol-gel process [100]. The detection is based on the oxidation of glucose to D-gluconic acid and hydrogen peroxide by GOD and subsequent reaction of the peroxide with luminol under HRP-mediated catalysis, producing the well-known 2-amino-phthalic acid in its excited state (see Fig. 15). As Fig. 16 illustrates, the electron withdrawing effect of the gold nanoparticles amplifies the reaction about 20 times. Because the optimum size of the AuNPs for this reaction is 8 nm, it is unlikely that the AuNPs directly catalyze the oxidation of luminol with hydrogen peroxide; as mentioned above, the optimum size for this direct catalytic involvement has been determined to 38 nm.

4.3 *Particle-Mediated Enhancement of Electrochemiluminescence*

Because electrochemiluminescence (or electrogenerated chemiluminescence, ECL) is a valuable detection technique in analytical and especially bioanalytical chemistry [101], it is not surprising that nanoparticles have also been applied as enhancers in this context. Again, as for CL, the catalytic effect of AuNPs is also exploited in ECL applications. For instance, generation of ECL by luminol in an alkaline aqueous solution could be dramatically increased by up to three orders of magnitude when using a nanoparticle self-assembled electrode instead of a bulk electrode [102]. In this case, not only is the ECL signal directly assigned to the oxidation of luminol amplified, but the authors have found a new ECL signal at more negative potentials (vs SCE) which is not visible with the bulk electrode, indicating that AuNPs are necessary for the generation of this signal. The nanoparticle self-assembled electrode has also been shown to be stable for at least 1 month when stored in deionized water, even if it has been applied to cyclic voltammetric scans ranging from 1.52 to -1.49 V (vs SCE).

In a different approach not relying on AuNP–luminol redox chemistry, it has been shown that the incorporation of the well-known ECL-active dye $\text{Ru}(\text{bpy})_3^{2+}$ into silica nanoparticles can increase the ECL intensity about three orders of magnitude compared to the free dye by limiting self-quenching phenomena [103]. However, the mechanism of ECL in silica particles is rather complex and presumably depends on parameters such as the concentration and diffusion properties of a co-reactant (e.g. tripropylamine). For instance, the co-reactant is crucial to activate ECL if the $\text{Ru}(\text{bpy})_3^{2+}$ -containing core is completely passivated by the silica shell and resistant to direct oxidation or reduction, i.e. if the distance from the electrode is too large [104].

5 Plasmonic Strategies to Luminescence Amplification

Besides chemical amplification concepts and the quest for ultimately reducing background and autofluorescence signals or increasing the number of fluorophores that are affected by the binding event, a physical strategy to pronounced modulation of luminescence signals involving particles has received increasing attention in recent years, i.e. enhancement through coupling of luminescence with SPR phenomena [105, 106]. After early theoretical treatments [107, 108] and first experimental verifications [109, 110] of the changes in the fluorescence behaviour of dye molecules in closer vicinity to metal surfaces, especially Lakowicz and co-workers have developed a new technique they called radiative decay engineering (RDE) and have utilized it in the context relevant within this article [111]. In contrast to the classic strategy of tuning fluorescent indicator molecules toward “light-up”

applications, i.e. to install an efficient quenching (or RET) process which is revived (altered) after target binding and thus to modulate the non-radiative decay rate [10], RDE basically operates with a change of the radiative decay rate. This effect results in (often) dramatically reduced fluorescence lifetimes and increased radiative rate constants which both lead to a (greatly) enhanced fluorescence quantum yield of the fluorophore [112]. This unusual increase in PLQY is supposed to originate from the enhancement of the local electromagnetic field near the metal particles under SPR conditions. Today, the main analytical applications of RDE lie in the fields of DNA hybridization and immunoassay research.

5.1 Surface Plasmon Resonance and Fluorescence

Before discussing the implications of a metal particle environment on a chromophore or a RET pair in the context of sensing, a brief introduction to SPR and fluorescence is necessary. Surface plasmons can be considered as propagating electron density waves, i.e. collective charge-density oscillations, occurring at the interface between two materials, commonly a metal and a dielectric. If excited at a certain angle of incidence by an electromagnetic wave, electromagnetic coupling between the interfaces can occur and give rise to SPR [112]. When a dye molecule is present at an adequate distance from this plasmon source it can experience a strong enhancement of its fluorescence output as sketched in the following [113].

5.1.1 Fluorescence Enhancement at a Metal Surface

Amplified fluorescence near a metal surface depends first of all on the strength of the local electromagnetic field in close vicinity to the surface and is usually quantified for a fluorophore near a metal surface relative to the same fluorophore near an inert, metal-free surface under identical illumination conditions by the so-called apparent quantum yield Y according to (4) [114, 115].

$$Y = |L(\omega_{\text{exc}})|^2 Z(\omega_{\text{em}}) \quad \text{with} \quad Z(\omega_{\text{em}}) = \frac{\Phi^{\text{M}}}{\Phi^0}. \quad (4)$$

Here, $L(\omega_{\text{exc}})$ corresponds to the excitation intensity acting on the fluorophore. This quantity is enhanced by the presence of a local field, for instance, as a consequence of particle surface plasmon excitation. The possible enhancement features are determined by object and surface properties such as the particle size and shape or the roughness of a surface layer and the nature of the metallic material. For example, Kümmerlen et al. have reported that a sizeable enhancement of the local field of ca. 140 times can be found for spheroids or rods (of ca. 3:1 aspect ratio) at the tips of these objects [116]. Since the intensity is proportional to the

squared field strength, these effects can result in a 10^4 -fold or larger increase in the rate of excitation.

In (4), $Z(\omega_{em})$ is the relative radiation yield and corresponds to the PLQY of a dye in the presence of metal particles Φ^M relative to its unperturbed or intrinsic PLQY Φ^0 . Without going too far into theoretical details (see, e.g. [116]), two cases of fluorophores can be distinguished. For a fluorophore with a high intrinsic Φ^0 , the achievable enhancement is weak. However, for a dye with a low Φ^0 , high enhancement (with a limiting $Z(\omega_{em})$ factor of $[\Phi^0]^{-1}$) can result when the fluorophore can efficiently couple with the metal and the latter can act as an antenna to radiate a photon before the excitation is dissipated by non-radiative pathways within the dye molecule, corresponding to an enhancement of the radiative rate.

However, in contrast to surface enhanced Raman scattering (SERS), maximal enhancement of fluorescence is not observed from molecules that are directly adsorbed on the surface, but from those that are located at a short distance away from the metal surface. The reasons are two counterbalancing effects and can be deduced from Fig. 17a [117]. First, if positioned too close to the metal surface, Förster-type energy transfer can set in and $Z(\omega_{em})$ is rapidly reduced because of the onset of non-radiative quenching (Fig. 17a, dotted line; for the influence on the radiative rate constant, see Sect. 2.1) [118]. Second, if the dye is placed too far from the metal surface, coupling is inefficient because the induced field is an evanescent field and its intensity decays exponentially with the distance from the surface (Fig. 17a, solid line). For instance, considering a gold surface and water as the dielectric, the field has decayed to $1/e$ at ca. 150 nm. Thus, a maximum enhancement $Z(\omega_{em})$ exists only in a small zone at an optimum distance from the metal surface. For the Au/water system in

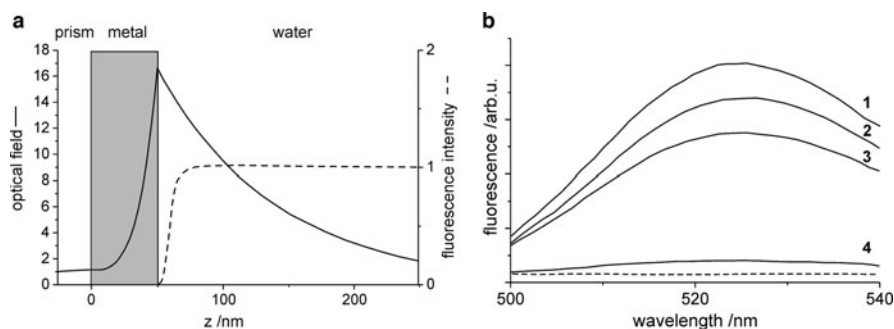


Fig. 17 (a) Schematic comparison of the distance dependence of the optical field of a surface plasmon mode, resonantly excited at a prism/50 nm Au/water interface (*solid line*) and the distance-dependent energy transfer-type quenching mechanism above the metal/water interface expressed as the relative fluorescence intensity (*dashed line*). (b) Emission spectra of biotin-FITC conjugates bound to the top avidin layer of six (1), four (2) and two (3) monolayers of an alternating BSA-biotin/avidin layer-by-layer (LbL) assembly on the surface of non-aggregated colloidal metal films. Trace (4) shows the characteristic emission spectrum obtained from a multi-LbL assembly adsorbed on bare glass slides (*dashed line*: background). (Adapted with permission from [113, 118]. Copyright 2000 Elsevier and 1998 American Chemical Society)

Fig. 17a, the surface electromagnetic field can be ca. 17 times as high as that in free space and the fluorescence intensity can be enhanced up to eightfold [119]. With regard to silver as the other metal substrate that plays a major role in SPR-based fluorescence applications and a bovine serum albumin-(BSA-) biotin/avidin multilayer system for distance adjustment, Cotton and co-workers could show that a monolayer yields only an 8-fold enhancement of the fluorescence while 6 layers increased the intensity gain to 15-fold (Fig. 17b) [118].

5.1.2 Radiative Decay Engineering

Taking a closer look at the photophysical processes that are active in an excited fluorophore, the concept of RDE becomes evident. The two parameters that are important here are the PLQY Φ and lifetime τ . The latter is a measure for the average time a fluorophore spends in the excited state before returning to the ground state by emitting a photon. It is an important criterion for the photostability of a fluorophore because photo-decomposition occurs during the lifetime of the excited state, i.e. a short lifetime or high decay rate commonly guarantees a low photo-bleaching rate.

In an inert environment, Φ^0 and τ^0 of a fluorophore are determined by the radiative (Γ) and non-radiative (k_{nr}) decay rates according to (5) and (6).

$$\Phi^0 = \frac{\Gamma}{\Gamma + k_{nr}}. \quad (5)$$

$$\tau^0 = (\Gamma + k_{nr})^{-1}. \quad (6)$$

Because Γ depends on the oscillator strength of an electronic transition and is largely independent of the dye's environment, for the classical case of a fluorophore as mentioned above in the introduction of Sect. 5, the only way to increase Φ^0 is to reduce k_{nr} . According to (6), however, this will also entail an increase in τ^0 . A gain in both intensity and photostability thus cannot be achieved at the same time by the conventional strategy.

The RDE concept of placing the fluorophore in the presence of a metal surface (either metal nanoparticles or a thin, roughened metal layer) now takes advantage of the fact that the interaction can be described by the introduction of a new decay path Γ^M . PLQY and lifetime are then given by (7) and (8). As Γ^M increases, Φ^M increases but τ^M decreases, i.e. both PLQY and photostability are gained. The RDE concept is often also referred to as the concept of metal-enhanced fluorescence (MEF).

$$\Phi^M = \frac{\Gamma + \Gamma^M}{\Gamma + \Gamma^M + k_{nr}}. \quad (7)$$

$$\tau^M = (\Gamma + \Gamma^M + k_{nr})^{-1}. \quad (8)$$

5.2 MEF-Based Signalling Applications

In an exemplary work, Lakowicz and co-workers have used the MEF strategy to increase the detectability of Cy3- and Cy5-labeled DNA on solid substrates covered with silver island films (SIFs) and have found a five- to tenfold increase in intensity from the silver particle-coated quartz substrate compared with uncoated quartz (Fig. 18) [120]. As one would expect from the aforementioned, these enhanced intensities have been accompanied by dramatically shortened fluorescence lifetimes, which in turn has led to a significantly higher photostability of Cy3 and Cy5 in the presence of the silver nanoparticles (AgNPs). In this study, the SIFs have been composed of silver nanoparticles with a diameter of 100–300 nm.

From the point of view of label-free luminescence detection, the MEF concept also harbours a certain potential. If small silver nanoparticles are produced in the SIF deposition process for which the surface plasmon absorption band is close to the short wavelength limit (ca. 420 nm; the practical limit in solution for AgNPs of ca. 10 nm diameter is ~ 400 nm [121]), direct amplification of the native DNA fluorescence is possible (Fig. 19) [122]. In this study, a remarkable 80-fold intensity enhancement has been observed. However, the authors have pointed out that only 1/25th of the DNA molecules dissolved in solution resides in the active MEF region, potentially making it possible to increase the enhancement to $>1,000$ when the localization of the target with respect to the SIF is better controlled. Again, as shown in Fig. 19, the increase in intensity is accompanied by a reduction of the fluorescence lifetime. Such strong amplification would render this method very interesting for DNA sequencing applications without extrinsic labelling.

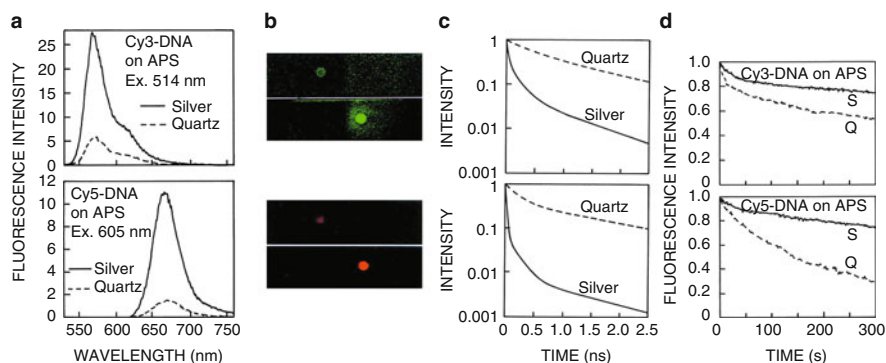


Fig. 18 (a) Emission spectra, (b) photographs and (c) fluorescence decays of the labelled DNA oligomers on neat quartz and SIF-coated quartz substrates. The quartz was treated with amino-propyltriethoxysilane (APS). (d) Photostability of Cy3-DNA and Cy5-DNA on APS-treated slides with and without SIFs. The excitation intensity was adjusted to yield the same emission intensities on neat and SIF-quartz. (Reprinted with permission from [120]. Copyright 2003 BioTechniques)

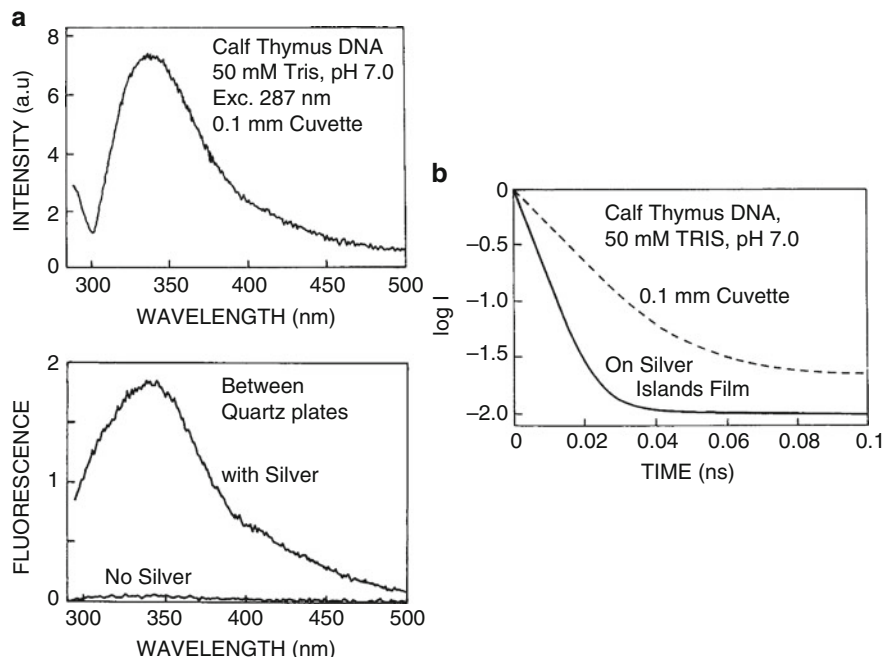


Fig. 19 (a) Emission spectrum of a buffered solution containing calf thymus DNA in a cuvette (*top*) and between quartz plates in the absence (labelled “No Silver”) and the presence of a SIF (labelled “with Silver”; *bottom*). (b) Decay of the fluorescence of calf thymus DNA in the absence (*dashed line*) and presence of a SIF (*solid line*). (Reprinted with permission from [122]. Copyright 2001 Academic Press/Elsevier)

5.2.1 MEF and Multiphoton Excitation

Two-photon or multi-photon excitation is a nonlinear absorption process in which fluorophores are excited with several photons of low energy. This technique offers the possibility to excite a fluorophore with rather long wavelengths, often in the NIR spectral region, which is especially attractive in bioimaging applications [123]; see also Sect. 2.3. At long wavelengths, scattering is significantly reduced, penetration of tissue enhanced and autofluorescence commonly negligible. However, the excitation rate is highly dependent on the excitation intensity and proportional to its square, i.e. usually comparatively strong laser excitation is required. Nonetheless, the employment of metal nanoparticles for which the above-mentioned field enhancement is operative can also lead to strong enhancement factors for multi-photon excitation processes of up to 10^8 [124].

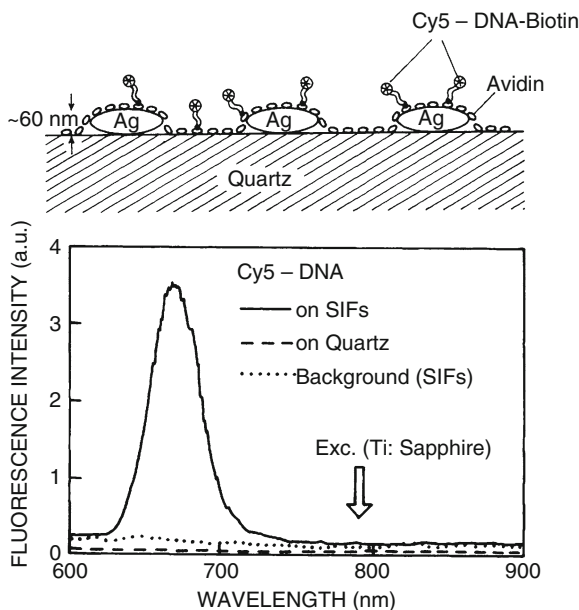


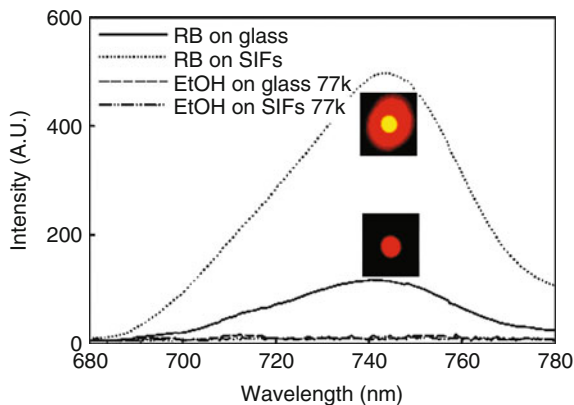
Fig. 20 Two-photon-excited emission spectra of Cy5-DNA on neat and SIF-coated quartz. The brightness of Cy5-DNA on SIFs is approximately 100-fold higher than on quartz. The *top panel* shows a sketch of the Cy5 deposited on SIFs. (Reprinted with permission from [125]. Copyright 2005 Academic Press/Elsevier)

As shown in Fig. 20, Lukomska et al. could realize a ca. 100-times amplified fluorescence signal with Cy5 by using a Ti-Sapphire laser and NIR excitation [125]. The authors have found that the average fluorescence lifetimes $\langle \tau \rangle$ of Cy5 on the SIF substrates are considerably reduced compared with the dye on a neat quartz support. In addition, they could show that $\langle \tau \rangle$ for one- and two-photon excitation were rather similar, $\langle \tau \rangle = 0.108$ and 0.117 ns, respectively, indicating that the intensity enhancement is mainly due to a stronger local field near the metal surface.

5.2.2 Metal Enhanced Phosphorescence

Besides fluorescence, another radiative decay path of an excited molecule is phosphorescence, which occurs from the lowest triplet state T_1 to the ground state S_0 . Such intersystem crossing is a highly forbidden process and therefore phosphorescence decay is significantly slower compared with fluorescence, commonly in the micro- to millisecond time regime. As mentioned above for the rare earth emitters as RET donors in Sect. 2, long lifetimes harbour the advantage of sensitive detection by time-resolved or time-gated spectroscopic methods. Provided that

Fig. 21 Phosphorescence spectra of Rose Bengal immobilized on an organic glass with and without SIFs at 77 K ($\lambda_{\text{exc}} = 532$ nm). (Reprinted with permission from [129]. Copyright 2006 American Chemical Society)



adequate probes are available, these features can also yield valuable information on rotational motions of proteins or particles on the micro- to millisecond time-scale through time-resolved phosphorescence anisotropy measurements [126–128].

To enhance the often weak phosphorescence signals, SPR-based coupling techniques can also be employed. For instance, Zhang et al. have reported a five times amplified phosphorescence emission for the dye Rose Bengal close to a SIF-covered glass surface compared with neat glass (Fig. 21) [129]. Detailed investigations as a function of temperature have revealed that the phosphorescence enhancement factor is temperature-dependent, increasing from 3.2 at room temperature to 5.7 at 77 K. The authors could further detect both, MEP and MEF, and explained this coexistence by enhanced absorption and reverse intersystem crossing involving a $S_1 \leftarrow T_1$ path.

5.2.3 Metal Nanoparticle-Enhanced RET

In the 1980s, first theoretical works have been published which described how the vicinity of metal particles could increase the RET efficiency in donor–acceptor systems [130, 131]. Instead of increased rates of radiative decay as found for fluorophores close to a metal surface, see above, the effect here is based on increased rates of resonance energy transfer. This enhancement of the RET rate has been predicted to increase by 100-fold at distances up to 700 Å, i.e. covering distances that are ca. tenfold larger than the Förster distances commonly achieved in bulk solution. Early studies on the calf thymus model DNA system (see Fig. 19) employing the minor groove-binding dye DAPI (4',6-diamidino-2-phenylindole) and the intercalating dye propidium iodide (PI) in the presence of SIFs have shown that the effective interaction distance R_0 of such non-covalently interacting systems can be increased fivefold [132]. For instance, for covalently labelled model systems FRET rates can increase by >20-fold for the Cy5/Cy5.5 pair conjugated to complementary oligonucleotides [133]. In a subsequent study employing silver particles

of 15, 40 and 80 nm diameter and varying the distances between the FRET dye pair and the particle surface (and not the distance between D_{RET} and A_{RET}), it has been found that the amplification of FRET increases with increasing nanoparticle size and that FRET is more efficient if the $D_{\text{RET}}/A_{\text{RET}}$ pair is located 10 nm above the surface instead of 2 nm [134].

Another interesting example of using modified AgNPs instead of SIFs to detect donor–acceptor proximity over a longer distance than the standard Förster range has been published recently. Lessard-Viger et al. have employed novel multilayer core-shell nanoparticles featuring a silver core surrounded by silica layers containing FRET donor and acceptor positioned at a precise distance from the core [135]. The presence of silver results in an increase in Förster efficiency by a factor of 4 and an increase in Förster range of ~30%.

Finally, we conclude this section with first approaches toward plasmonically enhanced RET systems using QDs. In 2007, Govorov et al. have investigated theoretically the possibilities of how RET between pairs of CdTe QDs, InGaN QDs and PbSe QDs can be enhanced by the presence of AgNPs and AuNPs [136]. A year later, Komarala et al. have experimentally investigated CdTe QD RET pairs, i.e. CdTe QDs of different size acting as D_{RET} and A_{RET} , and the enhancement of the energy transfer processes by AuNPs [137]. In contrast to the QD luminophore–AuNP quencher-type RET systems introduced in Sect. 2.2, the present approach shows true aspects of amplification yet requires more careful control.

In conclusion, all the examples discussed in this section require more attention with respect to architectural control when aiming at high (amplified) performance. At the same time, the nanoparticle chemistry used in most of these cases is quite simple, basically due to the physical nature of the processes responsible for amplification and a great variety of conventional chromophore systems can be employed in these MEF-based applications.

6 Conclusion

The present contribution has shown how versatile and manifold the application of luminescent nano- and microparticles in analytical and bioanalytical contexts that rely on signal amplification strategies is already today. The different applications range from utilizing mainly the particles' size, by doping particles with a large amount of emitters or by storing a large number of emitters in a porous particle network, over the catalytic (chemical) properties of NPs and physical enhancement effects to particular physical properties such as multi-photon excitation. The nature of the particles itself has been rather diverse and their combination with organic or bioorganic entities is almost limitless. The examples presented here have shown that today, amplification factors of more than three orders of magnitude can be readily accomplished.

In the last 10–15 years of research which showed the utmost activity in the field, so many different approaches have been realized that it is difficult to say where the

journey will lead to next. One approach that we believe will receive increasing interest is the combination of gold nanoparticles with QDs in applications where the AuNPs do not act as simple quenchers, but where the AuNPs amplify the luminescence of their semiconductor twins. First approaches have been realized recently, for instance, with CdSe QDs [138]. Alternatively, luminescence enhancement in 3D arrays of QDs in lamellar objects of micrometric size is possible by integrating small AuNPs [139]. Since these lamellae are also permeable for small molecules or ions, such structures are potentially suitable as sensory (micro)membranes.

With respect to efficiency and amplification, nature has created some of the best performing ensembles. Gated systems relying on the liberation of many indicators from a reservoir once the gate is unlocked resemble gated membrane channels in natural systems. Their development is also only at the beginning so far. For instance, if such gated systems are not only loaded with many indicators but are also equipped with a catalytic indication system on the outside, the arrival of one analyte can trigger the formation of many “catalytic keys”, unlocking many of the gates and liberating a very large number of the doped cargo. Truly massive amplification might thus arise. In the field of improving the optical properties of photosynthetic systems, a combination of coupling with QDs and invoking RET processes has already achieved promising results [140]. With respect to RET and metal nanoparticle-based enhancement, the introduction of electrochemiluminescent systems besides BRET and CRET offers another degree of flexibility and performance for “dark” excitation and first QD-based approaches have been realized lately [141].

Finally, when talking about amplifying nanoparticles, the applications are of course not only limited to spherical particles as mainly employed today and discussed here, but aspherical objects like cages, rods or wires offer a wealth of additional tuning modes and will presumably receive pronounced attention in the future [142].

References

1. Lakowicz JR (ed) (1992–2006) Topics in fluorescence spectroscopy series, vols 1–11. Plenum, New York and Springer, Berlin
2. Wolfbeis OS (ed) (2001–2008) Springer series on fluorescence, vols 1–6. Springer, Berlin
3. Demchenko A (2009) Introduction to fluorescence sensing. Springer, Berlin
4. Seidel M, Gauglitz G (2003) Miniaturization and parallelization of fluorescence immunoassays in nanotiter plates. *Trends Anal Chem* 22:385–394
5. LaFratta CN, Walt DR (2008) Very high density sensing arrays. *Chem Rev* 108:614–637
6. Hunt HC, Wilkinson JS (2008) Optofluidic integration for microanalysis. *Microfluid Nanofluid* 4:53–79
7. Myers FB, Lee LP (2008) Innovations in optical microfluidic technologies for point-of-care diagnostics. *Lab Chip* 8:2015–2031
8. Rurack K, Resch-Genger U (2002) Rigidization, preorientation and electronic decoupling – the ‘magic triangle’ for the design of highly efficient fluorescent sensors and switches. *Chem Soc Rev* 31:116–127

9. Gill P, Ghaemi A (2008) Nucleic acid isothermal amplification technologies – a review. *Nucleosides Nucleotides Nucleic Acids* 27:224–243
10. Descalzo AB, Zhu S, Fischer T et al (2010) Optimization of the coupling of target recognition and signal generation. In: Demchenko AP (ed) *Advanced fluorescence reporters in chemistry and biology. II. Molecular constructions, polymers and nanoparticles*. Springer, Berlin, pp 41–106
11. Roda A, Guardigli M, Michelini E et al (2009) Nanobioanalytical luminescence: Förster-type energy transfer methods. *Anal Bioanal Chem* 393:109–123
12. Sapsford KE, Berti L, Medintz IL (2006) Materials for fluorescence resonance energy transfer analysis: beyond traditional donor–acceptor combinations. *Angew Chem Int Ed* 45:4562–4588
13. Förster T (1948) Intermolecular energy migration and fluorescence. *Ann Phys* 2:55–75
14. Braslavsky SE (2007) Glossary of terms used in photochemistry. 3rd edition (IUPAC Recommendations 2006). *Pure Appl Chem* 79:293–465
15. Boute N, Jockers R, Issat T (2002) The use of resonance energy transfer in high-throughput screening: BRET versus FRET. *Trends Pharmacol Sci* 23:351–354
16. Eidne KA, Kroeger KM, Hanyaloglu AC (2002) Applications of novel resonance energy transfer techniques to study dynamic hormone receptor interactions in living cells. *Trends Endocrinol Metab* 13:415–421
17. Chen J, Zeng F, Wu S et al (2009) A facile approach for cupric ion detection in aqueous media using polyethyleneimine/PMMA core-shell fluorescent nanoparticles. *Nanotechnology* 20:365502
18. Roberts DV, Wittmershaus BP, Zhang YZ et al (1998) Efficient excitation energy transfer among multiple dyes in polystyrene microspheres. *J Lumin* 79:225–231
19. Weissleder R (2001) A clearer vision for in vivo imaging. *Nat Biotechnol* 19:316–317
20. Wang L, Tan W (2006) Multicolor FRET silica nanoparticles by single wavelength excitation. *Nano Lett* 6:84–88
21. Chen X, Estevez MC, Zhu Z et al (2009) Using aptamer-conjugated fluorescence resonance energy transfer nanoparticles for multiplexed cancer cell monitoring. *Anal Chem* 81:7009–7014
22. Bünzli JCG, Piguet C (2005) Taking advantage of luminescent lanthanide ions. *Chem Soc Rev* 34:1048–1077
23. Härmä H, Soukka T, Lövgren T (2001) Europium nanoparticles and time-resolved fluorescence for ultrasensitive detection of prostate-specific antigen. *Clin Chem* 47:561–568
24. Daniel MC, Astruc D (2004) Gold nanoparticles: assembly, supramolecular chemistry, quantum-size-related properties, and applications toward biology, catalysis, and nanotechnology. *Chem Rev* 104:293–346
25. Wei Q, Wei A (2010) Signal generation with gold nanoparticles: photophysical properties for sensor and imaging applications. In: Rurack K, Martínez-Máñez R (eds) *The supramolecular chemistry of organic-inorganic hybrid materials*. Wiley, Hoboken, NJ, pp 319–349
26. Dulkeith E, Ringler M, Klar TA et al (2005) Gold nanoparticles quench fluorescence by phase induced radiative rate suppression. *Nano Lett* 5:585–589
27. Huang CC, Chang HT (2006) Selective gold-nanoparticle-based “turn-on” fluorescent sensors for detection of mercury(II) in aqueous solution. *Anal Chem* 78:8332–8338
28. He X, Liu H, Li Y et al (2005) Gold nanoparticle-based fluorometric and colorimetric sensing of copper(II) ions. *Adv Mater* 17:2811–2815
29. Mayilo S, Kloster MA, Wunderlich M et al (2009) Long-range fluorescence quenching by gold nanoparticles in a sandwich immunoassay for cardiac troponin T. *Nano Lett* 9:4558–4563
30. Ray PC, Fortner A, Darbha GK (2006) Gold nanoparticle based FRET assay for the detection of DNA cleavage. *J Phys Chem B* 110:20745–20748
31. Gill R, Zayats M, Willner I (2008) Semiconductor quantum dots for bioanalysis. *Angew Chem Int Ed* 47:7602–7625

32. Frasco MF, Chaniotakis N (2010) Bioconjugated quantum dots as fluorescent probes for bioanalytical applications. *Anal Bioanal Chem* 396:229–240
33. Jorge PAS, Martins MA, Trindade T et al (2007) Optical fiber sensing using quantum dots. *Sensors* 7:3489–3534
34. Han M, Gao X, Su JZ et al (2001) Quantum-dot-tagged microbeads for multiplexed optical coding of biomolecules. *Nat Biotechnol* 19:631–635
35. Clapp AR, Medintz IL, Mattoussi H (2006) Förster resonance energy transfer investigations using quantum-dot fluorophores. *ChemPhysChem* 7:47–57
36. Algar WR, Krull UJ (2008) Quantum dots as donors in fluorescence resonance energy transfer for the bioanalysis of nucleic acids, proteins, and other biological molecules. *Anal Bioanal Chem* 391:1609–1618
37. Lee S, Park K, Kim K et al (2008) Activatable imaging probes with amplified fluorescent signals. *Chem Commun* 4250–4260
38. Hering VR, Gibson G, Schumacher RI et al (2007) Energy transfer between CdSe/ZnS core/shell quantum dots and fluorescent proteins. *Bioconjug Chem* 18:1705–1708
39. Willard DM, Mutschler T, Yu M et al (2006) Directing energy flow through quantum dots: towards nanoscale sensing. *Anal Bioanal Chem* 384:564–571
40. Tomczak N, Janczewski D, Han MY et al (2009) Designer polymer-quantum dot architectures. *Prog Polym Sci* 34:393–430
41. Freeman R, Li Y, Tel-Vered R et al (2009) Self-assembly of supramolecular aptamer structures for optical or electrochemical sensing. *Analyst* 134:653–656
42. Goldman ER, Medintz IL, Whitley JL et al (2005) A hybrid quantum dot-antibody fragment fluorescence resonance energy transfer-based TNT sensor. *J Am Chem Soc* 127:6744–6751
43. Wang X, Guo X (2009) Ultrasensitive Pb^{2+} detection based on fluorescence resonance energy transfer (FRET) between quantum dots and gold nanoparticles. *Analyst* 134:1348–1354
44. Tang B, Cao L, Xu K et al (2008) A new nanobiosensor for glucose with high sensitivity and selectivity in serum based on fluorescence resonance energy transfer (FRET) between CdTe quantum dots and Au nanoparticles. *Chem Eur J* 14:3637–3644
45. Jiang G, Susha AS, Lutich AA et al (2009) Cascaded FRET in conjugated polymer/quantum dot/dye-labeled DNA complexes for DNA hybridization detection. *ACS Nano* 12:4127–4131
46. So MK, Xu C, Loening AM et al (2006) Self-illuminating quantum dot conjugates for in vivo imaging. *Nat Biotechnol* 24:339–343
47. Huang X, Li L, Qian H et al (2006) A resonance energy transfer between chemiluminescent donors and luminescent quantum-dots as acceptors (CRET). *Angew Chem Int Ed* 45:5140–5143
48. Zhao S, Huang Y, Shi M et al (2010) Chemiluminescence resonance energy transfer-based detection for microchip electrophoresis. *Anal Chem* 82:2036–2041
49. Naruke H, Mori T, Yamase T (2009) Luminescence properties and excitation process of a near-infrared to visible up-conversion color-tunable phosphor. *Opt Mater* 31:1483–1487
50. Wang X, Li YD (2007) Monodisperse nanocrystals: general synthesis, assembly, and their applications. *Chem Commun* 2901–2910
51. Jalil RA, Zhang Y (2008) Biocompatibility of silica coated $NaYF_4$ upconversion fluorescent nanocrystals. *Biomaterials* 29:4122–4128
52. Wang L, Yan R, Huo Z et al (2005) Fluorescence resonant energy transfer biosensor based on upconversion-luminescent nanoparticles. *Angew Chem Int Ed* 44:6054–6057
53. Kuningas K, Ukonaho T, Pääkkilä H et al (2006) Upconversion fluorescence resonance energy transfer in a homogeneous immunoassay for estradiol. *Anal Chem* 78:4690–4696
54. Rantanen T, Pääkkilä H, Jämsen L et al (2007) Tandem dye acceptor used to enhance upconversion fluorescence resonance energy transfer in homogeneous assays. *Anal Chem* 79:6312–6318
55. Bonacchi S, Genovese D, Juris R et al (2010) Luminescent chemosensors based on silica nanoparticles. *Top Curr Chem* [this volume]

56. Zhou Q, Swager TM (1995) Fluorescent chemosensors based on energy migration in conjugated polymers: the molecular wire approach to increased sensitivity. *J Am Chem Soc* 117:12593–12602
57. Thomas SW III, Joly GD, Swager TM (2007) Chemical sensors based on amplifying fluorescent conjugated polymers. *Chem Rev* 107:1339–1386
58. Baier MC, Huber J, Mecking S (2009) Fluorescent conjugated polymer nanoparticles by polymerization in miniemulsion. *J Am Chem Soc* 131:14267–14273
59. Wu C, Szymanski C, Cain Z et al (2007) Conjugated polymer dots for multiphoton fluorescence imaging. *J Am Chem Soc* 129:12904–12905
60. Wu C, Bull B, Szymanski C et al (2008) Multicolor conjugated polymer dots for biological fluorescence imaging. *ACS Nano* 2:2415–2423
61. Moon JH, McDaniel W, MacLean P et al (2007) Live-cell-permeable poly(*p*-phenylene ethynylene). *Angew Chem Int Ed* 46:8223–8225
62. Howes P, Thorogate R, Green M et al (2009) Synthesis, characterisation and intracellular imaging of PEG capped BEHP-PPV nanospheres. *Chem Commun* 2490–2492
63. Wosnick JH, Liao JH, Swager TM (2005) Layer-by-layer poly(phenylene ethynylene) films on silica microspheres for enhanced sensory amplification. *Macromolecules* 38:9287–9290
64. McQuade DT, Hegedus AH, Swager TM (2000) Signal amplification of a “turn-on” sensor: harvesting the light captured by a conjugated polymer. *J Am Chem Soc* 122:12389–12390
65. Liu B, Bazan GC (2004) Homogeneous fluorescence-based DNA detection with water-soluble conjugated polymers. *Chem Mater* 16:4467–4476
66. Wang Y, Liu B (2009) Conjugated polymer as a signal amplifier for novel silica nanoparticle-based fluorimmunoassay. *Biosens Bioelectron* 24:3293–3298
67. Wang Y, Liu B (2007) Silica nanoparticle assisted DNA assays for optical signal amplification of conjugated polymer based fluorescent sensors. *Chem Commun* 3553–3555
68. Wang Y, Liu B (2009) Conjugated polyelectrolyte-sensitized fluorescent detection of thrombin in blood serum using aptamer-immobilized silica nanoparticles as the platform. *Langmuir* 25:12787–12793
69. Pu KY, Li K, Liu B (2010) Cationic oligofluorene-substituted polyhedral oligomeric silsesquioxane as light-harvesting unimolecular nanoparticle for fluorescence amplification in cellular imaging. *Adv Mater* 22:643–646
70. Lowe M, Spiro A, Zhang YZ et al (2004) Multiplexed, particle-based detection of DNA using flow cytometry with 3DNA dendrimers for signal amplification. *Cytometry A* 60A:135–144
71. Wängler C, Moldenhauer G, Saffrich R et al (2008) PAMAM structure-based multifunctional fluorescent conjugates for improved fluorescent labelling of biomacromolecules. *Chem Eur J* 14:8116–8130
72. Balzani V, Ceroni P, Gestermann S et al (2000) Dendrimers as fluorescent sensors with signal amplification. *Chem Commun* 853–854
73. Balzani V, Ceroni P, Gestermann S et al (2000) Effect of protons and metal ions on the fluorescence properties of a polylysine dendrimer containing twenty four dansyl units. *J Chem Soc Dalton Trans* 3765–3771
74. Vögtle F, Gestermann S, Kauffmann C et al (2000) Coordination of Co²⁺ ions in the interior of poly(propylene amine) dendrimers containing fluorescent dansyl units in the periphery. *J Am Chem Soc* 122:10389–10404
75. Pugh VJ, Hu QS, Zuo X et al (2001) Optically active BINOL core-based phenyleneethynylene dendrimers for the enantioselective fluorescent recognition of amino alcohols. *J Org Chem* 66:6136–6140
76. Xu MH, Lin J, Hu QS et al (2002) Fluorescent sensors for the enantioselective recognition of mandelic acid: signal amplification by dendritic branching. *J Am Chem Soc* 124:14239–14246
77. Guo M, Varnavski O, Narayanan A et al (2009) Investigations of energy migration in an organic dendrimer macromolecule for sensory signal amplification. *J Phys Chem A* 113:4763–4771

78. Trau D, Yang W, Seydack M et al (2002) Nanoencapsulated microcrystalline particles for superamplified biochemical assays. *Anal Chem* 74:5480–5486
79. Chan CP, Bruemmel Y, Seydack M et al (2004) Nanocrystal biolabels with releasable fluorophores for immunoassays. *Anal Chem* 76:3638–3645
80. Sin KK, Chan CPY, Pang TH et al (2006) A highly sensitive fluorescent immunoassay based on avidin-labeled nanocrystals. *Anal Bioanal Chem* 384:638–644
81. Chan CP, Tzang LC, Sin K et al (2007) Biofunctional organic nanocrystals for quantitative detection of pathogen deoxyribonucleic acid. *Anal Chim Acta* 584:7–11
82. Truneh A, Machy P, Horan PK (1987) Antibody-bearing liposomes as multicolor immunofluorescence markers for flow cytometry and imaging. *J Immunol Methods* 100:59–71
83. Schott H, Von Cunow D, Langhals H (1992) Labeling of liposomes with intercalating perylene fluorescent dyes. *Biochim Biophys Acta* 1110:151–157
84. Edwards KA, Baeumner AJ (2006) Optimization of DNA-tagged liposomes for use in microtiter plate analyses. *Anal Bioanal Chem* 386:1613–1623
85. Rongen HAH, Bult A, van Bennekom WP (1997) Liposomes and immunoassays. *J Immunol Methods* 204:105–133
86. Anraku Y, Kishimura A, Oba M et al (2010) Spontaneous formation of nanosized unilamellar polyion complex vesicles with tunable size and properties. *J Am Chem Soc* 132:1631–1636
87. Slowing II, Trewyn BG, Lin VSY (2010) Nanogated mesoporous silica materials. In: Rurack K, Martínez-Mañez R (eds) *The supramolecular chemistry of organic-inorganic hybrid materials*. Wiley, Hoboken, NJ, pp 479–502
88. Patel K, Angelos S, Dichtel WR et al (2008) Enzyme-responsive snap-top covered silica nanocontainers. *J Am Chem Soc* 130:2382–2383
89. Bernardos A, Aznar E, Marcos MD et al (2009) Enzyme-responsive controlled release using mesoporous silica supports capped with lactose. *Angew Chem Int Ed* 48:5884–5887
90. Climent E, Marcos M, Martínez-Mañez R et al (2009) The determination of methylmercury in real samples using organically capped mesoporous inorganic materials capable of signal amplification. *Angew Chem Int Ed* 48:8519–8522
91. Ros-Lis JV, García B, Jiménez D et al (2004) Squaraines as fluoro-chromogenic probes for thiol-containing compounds and their application to the detection of biorelevant thiols. *J Am Chem Soc* 126:4064–4065
92. Ros-Lis JV, Marcos MD, Martínez-Mañez R et al (2005) A regenerative chemodosimeter based on metal-induced dye formation for the highly selective and sensitive optical determination of Hg^{2+} ions. *Angew Chem Int Ed* 44:4405–4407
93. Cho DG, Sessler JL (2009) Modern reaction-based indicator systems. *Chem Soc Rev* 38:1647–1662
94. Zhao L, Sun L, Chu X (2009) Chemiluminescence immunoassay. *Trends Anal Chem* 28:404–415
95. Lin J, Liu M (2008) Chemiluminescence from the decomposition of peroxymonocarbonate catalyzed by gold nanoparticles. *J Phys Chem B* 112:7850–7855
96. Duan C, Cui H, Zhang Z et al (2007) Size-dependent inhibition and enhancement by gold nanoparticles of luminol-ferricyanide chemiluminescence. *J Phys Chem C* 111:4561–4566
97. Safavi A, Absalan G, Bamdad F (2008) Effect of gold nanoparticle as a novel nanocatalyst on luminol-hydrazine chemiluminescence system and its analytical application. *Anal Chim Acta* 610:243–248
98. Zhang Z, Cui H, Lai C et al (2005) Gold nanoparticle-catalyzed luminol chemiluminescence and its analytical applications. *Anal Chem* 77:3324–3329
99. Crumbliss AL, Perine SC, Stonehuerner J et al (1992) Colloidal gold as a biocompatible immobilization matrix suitable for the fabrication of enzyme electrodes by electrodeposition. *Biotechnol Bioeng* 40:483–490

100. Lan D, Li B, Zhang Z (2008) Chemiluminescence flow biosensor for glucose based on gold nanoparticle-enhanced activities of glucose oxidase and horseradish peroxidase. *Biosens Bioelectron* 24:934–938
101. Richter MM (2004) Electrochemiluminescence (ECL). *Chem Rev* 104:3003–3036
102. Cui H, Xu Y, Zhang Z (2004) Multichannel electrochemiluminescence of luminol in neutral and alkaline aqueous solutions on a gold nanoparticle self-assembled electrode. *Anal Chem* 76:4002–4010
103. Zanarini S, Rampazzo E, Della Ciana L et al (2009) Ru(bpy)₃ covalently doped silica nanoparticles as multicenter tunable structures for electrochemiluminescence amplification. *J Am Chem Soc* 131:2260–2267
104. Li M, Chen Z, Yam VWW et al (2008) Multi functional ruthenium(II) polypyridine complex-based core-shell magnetic silica nanocomposites: magnetism, luminescence, and electrochemiluminescence. *ACS Nano* 2:905–912
105. Das P, Metiu H (1985) Enhancement of molecular fluorescence and photochemistry by small metal particles. *J Phys Chem* 89:4680–4687
106. Lakowicz JR, Ray K, Chowdhury M et al (2008) Plasmon-controlled fluorescence: a new paradigm in fluorescence spectroscopy. *Analyst* 133:1308–1346
107. Morawitz H, Philpott MR (1974) Coupling of an excited molecule to surface plasmons. *Phys Rev B* 10:4863–4868
108. Philpott MR (1975) Effect of surface plasmons on transitions in molecules. *J Chem Phys* 62:1812–1817
109. Weber WH, Eagen CF (1979) Energy-transfer from an excited dye molecule to the surface-plasmons of an adjacent metal. *Opt Lett* 4:236–238
110. Benner RE, Dornhaus R, Chang RK (1979) Angular emission profiles of dye molecules excited by surface-plasmon waves at a metal-surface. *Opt Commun* 30:145–149
111. Lakowicz JR (2001) Radiative decay engineering: biophysical and biomedical application. *Anal Biochem* 298:1–24
112. Weitz DA, Garoff S, Hanson CD et al (1982) Fluorescent lifetimes of molecules on silver-island films. *Opt Lett* 7:89–91
113. Liebermann T, Knoll W (2000) Surface-plasmon field-enhanced fluorescence spectroscopy. *Colloids Surf* 171:115–130
114. Gersten J, Nitzan A (1981) Spectroscopic properties of molecules interacting with small dielectric particles. *J Chem Phys* 75:1139–1152
115. Wokaun A, Lutz HP, King AP et al (1983) Energy-transfer in surface enhanced luminescence. *J Chem Phys* 79:509–514
116. Kümmerlen J, Leitner A, Brunner H et al (1993) Enhanced dye fluorescence over silver island films: analysis of the distance dependence. *Mol Phys* 80:1031–1046
117. Ford GW, Weber WH (1984) Electromagnetic-interactions of molecules with metal-surfaces. *Phys Rep* 113:195–287
118. Sokolov K, Chumanov G, Cotton TM (1998) Enhancement of molecular fluorescence near the surface of colloidal metal films. *Anal Chem* 70:3898–3905
119. Knoll W (1998) Interfaces and thin films as seen by bound electromagnetic waves. *Annu Rev Phys Chem* 49:569–638
120. Lakowicz JR, Malicka J, Gryczynski I (2003) Silver particles enhance emission of fluorescent DNA oligomers. *Biotechniques* 34:62–68
121. Mafuné F, Kohno J, Takeda Y et al (2000) Formation and size control of silver nanoparticles by laser ablation in aqueous solution. *J Phys Chem B* 104:9111–9117
122. Lakowicz JR, Shen B, Gryczynski Z et al (2001) Intrinsic fluorescence from DNA can be enhanced by metallic particles. *Biochem Biophys Res Commun* 286:875–879
123. Diaspro A (1999) Introduction to two-photon microscopy. *Microsc Res Tech* 47:163–164
124. Gryczynski I, Malicka J, Shen Y et al (2002) Multiphoton excitation of fluorescence near metallic particles: enhanced and localized excitation. *J Phys Chem B* 106:2191–2195

125. Lukomska J, Gryczynski I, Malicka J et al (2005) Two-photon induced fluorescence of Cy5-DNA in buffer solution and on silver island films. *Biochem Biophys Res Commun* 328:78–84
126. De Beuckeleer K, Volckaert G, Engelborghs Y (1999) Time resolved fluorescence and phosphorescence properties of the individual tryptophan residues of barnase: evidence for protein-protein interactions. *Proteins* 36:42–53
127. Prochniewicz E, Janson N, Thomas DD et al (2005) Cofilin increases the torsional flexibility and dynamics of actin filaments. *J Mol Biol* 353:990–1000
128. Lettinga MP, van Kats CM, Philipse AP (2000) Rotational diffusion of tracer spheres in packings and dispersions of colloidal spheres studied with time-resolved phosphorescence anisotropy. *Langmuir* 16:6166–6172
129. Zhang Y, Aslan K, Previte MJR et al (2006) Metal-enhanced phosphorescence: interpretation in terms of triplet-coupled radiating plasmons. *J Phys Chem B* 110:25108–25114
130. Gersten J, Nitzan A (1984) Accelerated energy transfer between molecules near a solid particle. *Chem Phys Lett* 104:31–37
131. Hua XM, Gersten J, Nitzan A (1985) Theory of energy transfer between molecules near solid state particles. *J Chem Phys* 83:3650–3659
132. Lakowicz JR, Kuśba J, Shen Y et al (2003) Effects of metallic silver particles on resonance energy transfer between fluorophores bound to DNA. *J Fluoresc* 13:69–77
133. Zhang J, Fu Y, Lakowicz JR (2007) Enhanced Förster resonance energy transfer (FRET) on a single metal particle. *J Phys Chem C* 111:50–56
134. Zhang J, Fu Y, Chowdhury MH et al (2007) Enhanced Förster resonance energy transfer on single metal particle. 2. Dependence on donor-acceptor separation distance, particle size, and distance from metal surface. *J Phys Chem C* 111:11784–11792
135. Lessard-Viger M, Rioux M, Rainville L et al (2009) FRET enhancement in multilayer core-shell nanoparticles. *Nano Lett* 9:3066–3071
136. Govorov AO, Lee J, Kotov NA (2007) Theory of plasmon-enhanced Förster energy transfer in optically excited semiconductor and metal nanoparticles. *Phys Rev B* 76:125308
137. Komarala VK, Bradley AL, Rakovich YP et al (2008) Surface plasmon enhanced Förster resonance energy transfer between the CdTe quantum dots. *Appl Phys Lett* 93:123102
138. Chan YH, Chen J, Wark SE et al (2009) Using patterned arrays of metal nanoparticles to probe plasmon enhanced luminescence of CdSe quantum dots. *ACS Nano* 3:1735–1744
139. Lee A, Coombs NA, Gourevich I et al (2009) Lamellar envelopes of semiconductor nanocrystals. *J Am Chem Soc* 131:10182–10188
140. Govorov AO (2008) Enhanced optical properties of a photosynthetic system conjugated with semiconductor nanoparticles: the role of Förster transfer. *Adv Mater* 20:4330–4335
141. Shan Y, Xu JJ, Chen HY (2009) Distance-dependent quenching and enhancing of electrochemiluminescence from a CdS: Mn nanocrystal film by Au nanoparticles for highly sensitive detection of DNA. *Chem Commun* 905–907
142. Shegai T, Huang Y, Xu H et al (2010) Coloring fluorescence emission with silver nanowires. *Appl Phys Lett* 96:103114

Luminescent Chemosensors Based on Silica Nanoparticles

Sara Bonacchi, Damiano Genovese, Riccardo Juris, Marco Montalti,
Luca Prodi, Enrico Rampazzo, Massimo Sgarzi, and Nelsi Zaccheroni

Abstract The field of nanoparticles is amazingly many-sided and consequently their applications range between many different areas from industry to bio-analysis and catalysis. In particular, luminescent nanoparticles attract close attention in the areas of biology, medical diagnosis and therapy, where they already find many applications. In this so fascinating and wide framework we have focussed our attention on luminescent silica nanoparticles able to act as sensing materials. We highlight here the importance, especially with the aim of sensing, of gaining precise knowledge and control of their structures; the performance of a chemosensor is, in fact, totally dependent on its design. We then briefly present the state of the art and the progress both in the synthetic protocols and in the application of luminescent silica nanoparticles as chemosensors. We present many recent examples, organized into two main sections, the first dealing with systems presenting the signalling units on the surface (dye coated silica nanoparticles, DCSNs) and the second with systems entrapping the dyes inside the silica matrix (dye doped silica nanoparticles, DDSNs).

Keywords Chemical sensors, Fluorescence, Luminescence, Signal amplification, Silica nanoparticles

Contents

1	Introduction	95
1.1	Nanoparticles in Bioimaging and Sensing	97
2	Synthesis of Fluorescent Silica Nanoparticles	102
2.1	Stöber Method	102
2.2	Reverse Microemulsion Method	105
2.3	Direct Micelles as Template	106
3	Luminescent Silica Nanoparticles as Chemosensors	109

S. Bonacchi, D. Genovese, R. Juris, M. Montalti,
L. Prodi (✉), E. Rampazzo, M. Sgarzi, and N. Zaccheroni
Dipartimento di Chimica “G. Ciamician”, Latemar Unit, Università degli Studi di Bologna,
Via Selmi 2, 40126 Bologna, Italy
e-mail: luca.prodi@unibo.it

3.1 Introduction	109
4 Some General Remarks	130
References	131

Abbreviations

AOT	Bis(2-ethylhexyl) sulfosuccinate sodium salt
APTES	3-Aminopropyltriethoxysilane
AuNPs	Gold colloids
BODIPY	Dye class containing boron-dipyrromethene (4,4-difluoro-4-bora-3a, 4a-diaza- <i>s</i> -indacene) as core
CHEF	Chelation-enhanced fluorescence
CP	Conjugated polymers
DCSN	Dye coated silica nanoparticle
DDSN	Dye doped silica nanoparticle
DEDMS	Diethoxydimethylsilane
DETA	<i>N'</i> -[3-(Trimethoxysilyl)-propyl]diethylenetriamine
DMSO	Dimethyl sulfoxide
DNA	Deoxyribonucleic acid
DPA	Dipicolinic acid
EDTA	Ethylenediaminetetraacetic acid
EDTAD	Ethylenediaminetetraacetic dianhydride
FITC	Fluoresceine isothiocyanate
FIFFF	Flow field flow fractionation
FRET	Fluorescence resonance energy transfer
ICT	Internal charge transfer
MPS	Mercaptopropyltriethoxysilane
MRI	Magnetic resonance imaging
NBD	Nitrobenzoxadiazole
NIR	Near infrared spectral region
NP	Nanoparticle
ORMOSIL	Organic-modified silica
PBS	Phosphate buffered saline
PDT	Photodynamic therapy
PEG	Polyethylene glycol
PET	Photoinduced electron transfer
PPS	Diethynylbenzene and diiodo-dipropylloxysulphonate benzene units
PVP	Polyvinylpyrrolidone
QDs	Quantum dots
RES	Reticulo-endothelial system
RNA	Ribonucleic acid
SNP	Silica nanoparticle

SPB	Surface plasmon band
TEM	Transmission electron microscopy
TEOS	Tetraethoxysilane tetraethyl orthosilicate
TMSCl	Trimethylsilylchloride
TNT	Trinitrotoluene
TSQ	6-Methoxy-8- <i>p</i> -toluensulfonamide
VTES	Triethoxyvinylsilane
ϵ	Molar extinction coefficient
Φ	Fluorescence quantum yield

1 Introduction

Photochemistry, which deals with the fundamental interactions of light with matter, is attracting the interest of researchers from many different fields, both in fundamental and applied studies, spanning from investigations on processes involved in the origin of life on earth to design and engineering of new solutions useful for everyday life such as energy production, medical diagnosis and therapeutics, data storage, material and environmental sciences [1]. It is therefore not surprising that photochemistry is still undergoing tremendous development. In particular, interest is shifting from purely molecular systems to supramolecular architectures [1] and, more recently, nanostructures [2–5], where intermolecular interactions can result in novel photochemical and photophysical properties. Such architectures are in fact an ideal platform to couple elementary processes (light absorption and emission, energy and electron transfer) to give rise to more complex ones (directional excitation energy migration or multi electron photo injection) in order to design nanosized functional photochemical devices [1].

An extensive description of the theoretical bases of all the principles and processes typical of photochemistry is beyond the scope of this introduction, but can be found in the literature [6]. However, it is worth noting that all fluorescence parameters such as Stokes shift, fluorescence intensity and anisotropy, emission and excitation spectra, and fluorescence lifetime can be used to encode what is happening in the close neighbourhood of the monitored species. The versatility of fluorescence-based methods of analysis derives indeed from the wide number of variables that can be tuned and coupled to get the required information, allowing one to overcome even very complex analytical problems.

Fluorescent chemosensors in particular [7, 8] have already found wide applications in many fields, such as environmental monitoring, process control, food and beverage analysis, and also represent one of the most rapidly developing fields in biology and medicine [9]. The design of fluorescent chemosensors has been continuously evolving in the last decades and numerous are the reviews on this topic [10] and see, for example, [11, 12]. The classical design of a fluorescent probe includes two fundamental moieties, a receptor responsible for the molecular recognition of the analyte and a fluorophore responsible to signal the recognition event. There are three main strategies to approach the design of fluorescent molecular indicators for

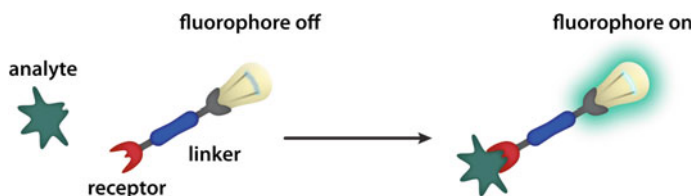


Fig. 1 Schematic representation of a chemosensor

chemical sensing in solution. The first is based on intrinsic fluorescent probes [7], which are fluorescent molecules where the signal transduction mechanism involves the interaction of the analyte with a ligand site that is part of the π -system of the dye. The second involves extrinsic fluorescent probes, in which the receptor moiety and the fluorophore are covalently linked but are electronically independent [13–15] (Fig. 1). The third strategy is called chemosensing ensemble, based on a competitive assay in which a receptor-fluorophore ensemble is selectively dissociated by the addition of an appropriate competitive analyte for the ligand, resulting in a detectable response of the fluorophore [16–18].

Very recently, the use of more complex architectures has allowed one to overcome many of the typical limitations of conventional fluorophores (organic dyes) such as poor photostability, low quantum yield, unsuitability for physiological conditions and therefore for *in vitro* and *in vivo* applications. These systems include, for example, conjugated polymers (CP), QDs, gold nanoparticles and silica nanoparticles doped with luminescent species [19–21].

The performances of such photophysical multi-component devices are essentially dependent on the possibility of controlling the mutual interactions between the molecular components in the assembly, and hence their spatial organization. This condition is fundamental to optimize the efficiency by minimizing the occurrence of undesired processes leading to energy loss and photo-degradation. A rigorous traditional synthetic approach surely allows very good control of the geometry, yielding fascinating, outstandingly efficient devices. However, in many cases, the performance is also related to the number of molecular units and the covalent interconnection of hundreds or thousands of molecules would require a tremendous effort. Self-assembling and self-organization [10] provide a lower degree of control of the electronic interactions between active moieties compared to traditional synthesis. Nonetheless, a much longer-range spatial control and organization is achievable with these methods, allowing a much higher level of complexity to be reached. However, such methods provide non-covalent systems, which are not always appropriate for applications in complex matrices such as cells and tissues, since they do not guarantee the necessary robustness to ensure long-run lifetimes. In these cases a bottom-up approach, which allows the design of nanometric systems based on molecular units held together by covalent bonds, is one of the possible solutions.

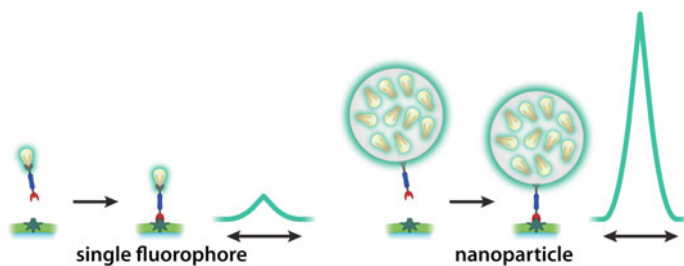


Fig. 2 Comparison between the signals arising from a molecular chemosensor and a nanoparticle-based one

Nanotechnology is an emerging science that exploits the characteristic and unique properties of these materials at the nanoscale level. An inventory of the nanotechnology-based consumer products currently on the market can be found in some specialized websites and, though not comprehensive, it includes more than 1,000 items, which are the fruit of more than 20 years of basic and applied research. In this context nanoparticles represent one of the main subjects of interest [22]. These systems have, in fact, rapidly found many industrial uses in a wide range of fields such as electronic, optoelectronic, biomedical, pharmaceutical, cosmetic, catalytic and materials areas. Among all these applications, one of the cut-edge research topics in the field of photoactive nanoparticles is the development of innovative nanosystems for biological imaging, medical diagnostics and therapeutics (Fig. 2).

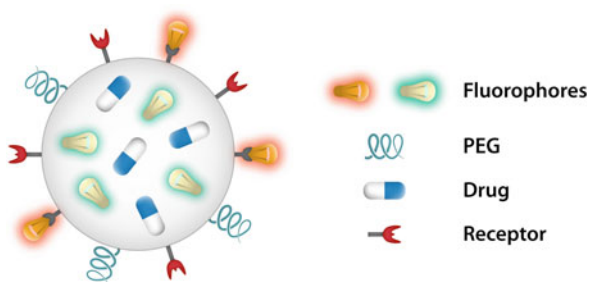
In this chapter we will focus our attention on properly modified silica nanoparticles that are able to conjugate unique photophysical and photochemical properties to simple and low-cost preparation. Moreover, the versatility of the chemistry of silica offers the possibility to obtain easily sophisticated, but robust, multifunctional systems [23, 24].

In the following sections different families of nanoparticles will be compared to emphasize the unique features of doped luminescent silica nanostructures, and to underline the challenges that these systems are expected to face, mainly in the field of sensing.

1.1 Nanoparticles in Bioimaging and Sensing

Luminescent organic or metallorganic species, polymers and proteins are the most commonly used moieties for imaging and sensing. It has to be noted, however, that in these applications dye molecules are exposed to a variety of harsh environments and often suffer from photobleaching and quenching due to interactions with solvent molecules and reactive species, such as oxygen or ions, dissolved in solution. Furthermore, π - π stacking can occur at high local concentrations, e.g. when the dyes are deposited on surfaces or interfaces, leading to energy transfer and

Fig. 3 Multifunctional nanoparticle: receptor units recognize the proper target; polyethylene glycol (PEG) chains improve the particle stability; fluorophores provide a means for detection; drug can be hosted inside



self-quenching. All this has greatly limited the use of fluorophores for in vitro assays and in vivo cellular imaging and sensing, and much effort is devoted to improve their stability and sensitivity.

Nanoparticles often provide a protected environment where active species are not affected by external and unforeseeable triggers (such as the case of silica, titania, latex nanoparticles) [25], or are intrinsically less sensitive to the environment than molecular dyes (QDs, metal nanoparticles) [26, 27]. Moreover, unique features arise from their particular size-dependent opto-electronic properties, their size – similar to biomolecules such as proteins and polynucleic acids – and their high surface-to-volume ratio. With proper engineering and surface modification, nanoparticle probes can also be obtained featuring enhanced fluorescence signals, increased sensitivities, a prolonged detection time and a better reproducibility. Figure 3 schematizes the versatility of these systems, summarizing a few important desirable properties of multifunctional nanoparticles [28].

There are several classes of nanoparticles such as organic, inorganic and metallic, all of them currently employed as fluorescent emitters, present pros and cons, and are more or less suitable for each particular application. Hereafter we present a brief overview of each of these classes to introduce this fascinating field, while in Sect. 3 we will discuss in much more in detail silica nanoparticles that are the focus of this contribution.

1.1.1 Quantum Dots

Quantum dots (QDs) were developed in the early 1970s. These atomic clusters are luminescent nanometer-scale (1.5–12 nm) heterostructures, containing from a few hundred to a few thousand atoms of a semiconductor material (CdSe, CdS or InP and InAs). They can be coated with an additional semiconductor shell (e.g. zinc sulphide) to improve their optical properties such as their brightness, and the photostability of the material since, in the core-shell QDs, photobleaching effects are strongly reduced [29].

The optical properties of QDs are very characteristic [30]. The energy of their excited states depends not only on the constituent material but also upon the particle

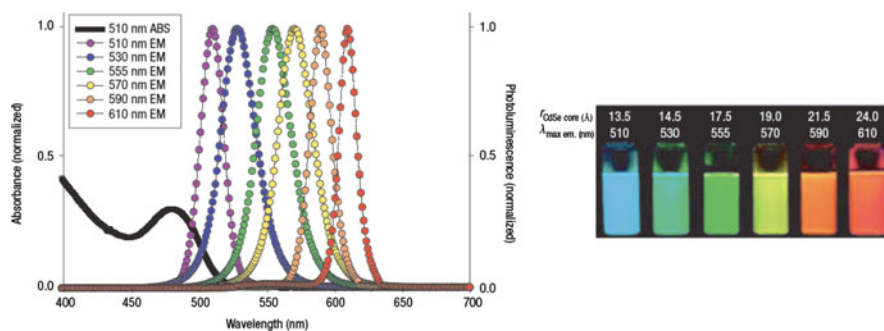


Fig. 4 *Right*: absorption and emission of six different QD dispersions. *Left*: photo demonstrating the size-tunable fluorescence properties and spectral range of the dispersions plotted on the right vs CdSe core size (excited with a 365 nm UV lamp). Adapted with permission from [29]

size (Fig. 4) and this *tunability* has been widely exploited for designing multicolour assays, thanks also to the narrow emission spectra of homogeneously sized QDs solutions. They also present a broad absorption spectrum, large molar extinction coefficients (ϵ), high fluorescence quantum yields (Φ), very long emission lifetimes (up to the range of μs) and a much higher photostability than traditional fluorescent molecules.

QDs do not disperse well in water, but by modifying their coating it is possible to make them water soluble, facilitating their conjugation to biomolecules and making them useful for biological imaging [31]. Several different methods are used to make them biocompatible and to introduce binding specificity [32, 33]. Many reports have appeared regarding applications of QDs as *in vitro* or *in vivo* diagnostic tools. However, they present many drawbacks, the most significant being cytotoxicity: the toxicity of elements such as cadmium, which is present in many of these nanocrystals, is well known, and thus it is critical to know whether these cytotoxic substances can leak out of the QD particles over time, upon illumination or oxidation. It has to be said that this is still a controversial point since there are reports in the literature that provide evidence of cytotoxicity of QDs [34], and others in which no cytotoxicity is observed [35]. Recently much progress has been reported toward overcoming their limitations [36–39] and several appealing examples of QDs bio-sensors based on FRET [40] have appeared.

1.1.2 Gold Nanoparticles

In the twentieth century, various methods for the preparation of gold colloids (AuNPs) were reported and reviewed [41]; among them, the Brust–Schiffrin method for AuNPs synthesis [42], published in 1994, has had considerable impact on the field since it allowed, for the first time, the facile synthesis of thermally stable and air-stable AuNPs of reduced dispersity and controlled size.

As far as physical properties are concerned, the deep red colour of AuNPs solutions or glasses is due to the so-called surface plasmon band (SPB), a broad absorption band in the visible region. The SPB arises from the collective oscillations of the mobile electrons at the surface of the nanoparticles induced by the electromagnetic field of the incoming light, and has been theoretically described by the Mie theory [43] and studied by many authors. This band is negligible in AuNPs with a diameter of less than 2 nm, as well as bulk gold, while for AuNPs of a diameter below 100 nm, the SPB maximum λ_{\max} was observed in aqueous media in the 510–580 nm range. The SPB maximum and bandwidth are indeed influenced by a number of factors, such as particle size, shape, solvent, dielectric properties and temperature, and also by aggregate morphology, surface functionalization and the refractive index of the surrounding medium (for a more detailed account on the photophysics of AuNPs see Daniel and Astruc [44]) [45, 46].

In the field of sensors and labels, interesting applications can be found based on SPB shift [47].

As schematized in Fig. 5, the binding of a target analyte can induce NPs aggregation. Since the plasmon-resonance spectrum of free single particles differs significantly from that of aggregated ones, it is possible to obtain quantitative measurements of the aggregating species present in solution by measuring the SPB shift caused by the recognition event [48, 49].

As far as luminescence is concerned, gold nanoparticles [50] generally quench the emission of fluorophores adsorbed or bound at their surface but it has to be said that both radiative and nonradiative rates critically depend on the size and shape of the AuNPs, the distance between the dye molecules on the surface, the orientation of the dipole with respect to the dye-nanoparticle axis and the overlap of the molecule's emission with the nanoparticles absorption spectrum [51]. It has also been observed that very small gold nanoparticles (with a diameter smaller than 1.5–2 nm) can present an intrinsic luminescence that is centred in the NIR spectral region [52, 53].

Finally, colloidal gold offers some unique advantages over other labelling agents, e.g. QDs or organic dyes. For instance, it does not undergo any photodecomposition,

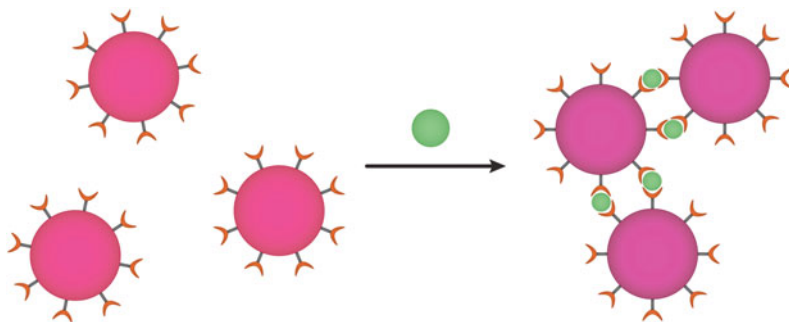


Fig. 5 Aggregation of gold nanoparticles induced by coordination leads to a red-shift of the surface plasmon resonance band

which is a common problem encountered while using fluorescent dyes. Second, it is not intrinsically toxic (gold, in fact, is one of the few metals that is not rejected by our body), it is reasonably stable and it can also be stored in a dry state.

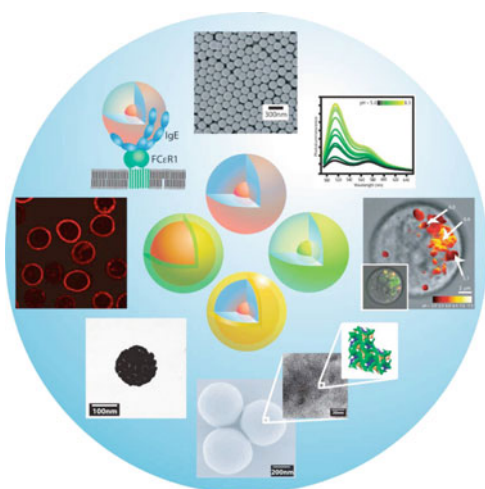
1.1.3 Luminescent Silica Nanoparticles

In the past few years, many reports have described the distinct advantages of luminescent silica nanoparticles over traditional dye molecules [54, 55]. These advantages allow their convenient use as fluorescent probes for applications ranging from biosensors [56, 57] to interfacial interaction studies such as immunoassays [58], multiplexed bio-analysis [59–61], nucleic acid analysis [62] and drug delivery [63] to name but a few (Fig. 6).

There are many different synthetic methods to prepare silica nanoparticles and in particular dye doped silica nanoparticles (DDSNs), all characterized by simplicity, low costs, versatility and great control over the architecture of the resulting materials. We will discuss in detail the most common procedures in the next section, with some emphasis on a new synthetic strategy that we have developed and patented [64, 65] that affords monodisperse silica nanoparticles with a particularly versatile and readily obtained core–shell architecture.

The ability to control the spatial organization of the molecular components of complex architectures, in fact, is an essential condition to design systems able to perform specific functions with high efficiency without losing excitation energy into parasite processes. Speaking more generally about efficient photochemical devices (that also include luminescent sensors), they are required to be (photo)chemically stable, to be compatible with the milieu of use and to present photo-physical properties that are not dependent on the environment, or only from a specific analyte. Moreover, ease of synthesis and low cost starting materials are

Fig. 6 An overview of the versatility of the fluorescent core–shell silica nanoparticle platform: illustrations of single and dual-emission particles as well as gold-nanoshell encapsulated core–shell particles are shown at the centre of the figure, while a variety of applications including bio-imaging, drug delivery, sensing and therapeutics are shown in the periphery. Reproduced with permission from [55]



also obviously desirable if the product is intended to be marketed. Finally, if the systems are prepared to be used for diagnosis or therapeutics (or both), they should be biocompatible and non-toxic, raising no concern about their disposal.

Luminescent silica nanoparticles are, in our opinion, the most promising and valuable of all the species presented till now in this brief introduction; they are potentially interesting for many applications like energy production and storage, catalysis and in particular sensing. After a description of the most common preparation methods in Sect. 2, we will present the state of the art for these particles as far as their application as chemosensors is concerned.

2 Synthesis of Fluorescent Silica Nanoparticles

The controlled preparation of monodispersed and stable colloidal silica was proposed for the first time by Stöber [66] and developed in the following years by many other scientists. They improved the method and increased the complexity of the resulting nanomaterial, with a consequential proliferation of possible applications, which proved once more the versatility of this kind of nanostructured scaffold. The concept of chemical functionalization was a crucial point in the design of new materials for practical applications. Van Blaaderen's idea of condensing fluorescent molecules with the monomeric tetraethoxysilane precursor (TEOS) during the growing step in the nanoparticles synthesis allowed the preparation of the first fluorescent silica nanoparticles containing an organic dye covalently linked to the silica matrix [67, 68]. Besides the methodology presented by Stöber and modified by van Blaaderen, other strategies have recently been developed, mainly based on the reverse microemulsion method [69, 70] or on the use of direct micelles as templates [71–72]. In addition to all these methods, our research group has recently developed a synthetic strategy that affords not only monodispersed but also ordered core-shell silica nanoparticles. We will discuss in detail in this section all these preparation approaches, in order to show the pros of each methodology as a function of the specific aim or application that the researcher has in mind.

2.1 *Stöber Method*

The chemical process at the basis of the silica formation is the controlled hydrolysis of tetraethoxysilane (TEOS) molecules and their ammonia catalysed condensation in ethanol/water/ammonia solution. This method allows the continuous and easy control of the nanoparticle dimensions by a suitable choice of the concentrations and ratios of the components of the reaction mixture (TEOS, water and ammonia). Several optimized synthetic protocols with well defined experimental conditions allow one to obtain nanoparticle samples in a dimensional range of about

15–200 nm (up to ca. 800 nm with one pot procedure), that useful for bio-analytical applications.

Although the colloidal silica suspensions obtained with this method are already strongly stabilized in water solutions by electrostatic repulsion, controlling the properties of NPs surface is fundamental to tune their solubility and adhesion properties and to avoid irreversible aggregation. Moreover, exterior functionalization is often essential for many applications. Triethoxysilane groups are suitable for surface modifications and properly silanized molecules can be grafted onto the silica surface to modify its functionalities. Such reagents anyway do not guarantee complete passivation: the residual undesirable reactivity due to the external Si-OH sites may require further treatment with end-capping reactants such as $(\text{CH}_3)_3\text{SiCl}$ or monoalkoxysilanes.

Such a covalent approach also allows one to obtain luminescent silica nanoparticles capping the surface with fluorophores. These emitting systems are usually indicated as dye coated silica nanoparticles (DCSNs) (Fig. 7).

The main synthetic procedures leading to alkoxy-functionalized fluorophores include the hydrosilylation reaction and especially the use of commercial alkoxy-silanes bearing a useful reactive functional group. Among these reagents we often find triethoxy(3-isocyanatopropyl)silane as one of the most useful. Belonging to the *click chemistry* family, its reaction with fluorophore derivatives bearing an amine group is fast and quantitative. Furthermore, the formation of the ureidic group in the adduct often increases the solubility of lipophilic organic dyes in polar solvent (ethanol, water) to concentrations useful for the nanoparticle preparation.

During the synthesis the condensation of trialkoxysilane derivative is almost quantitative, but sometimes the separation of the nanoparticles from the unreacted silane derivatives could be necessary and can be achieved by centrifugation, ultrafiltration or dialysis. Centrifugation/re-dispersion cycles are generally of use when nanoparticles are sufficiently heavy (in term of size, 100–200 nm of diameter and more) [73], and if their surfaces are tightly passivated/stabilized to prevent irreversible aggregation via condensation between the outer siloxanic groups. However, as nanoparticles re-dispersion is often obtained by sonication or vigorous stirring, this strategy is not generally applicable to delicate systems like nanoparticles/biomolecule conjugates. Ultrafiltration and dialysis are the best techniques to purify solutions of small nanoparticles; they in fact allow one to maintain the

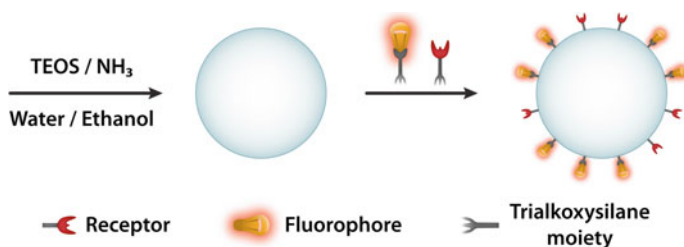


Fig. 7 Stöber synthesis of dye coated silica nanoparticles (DCSNs)

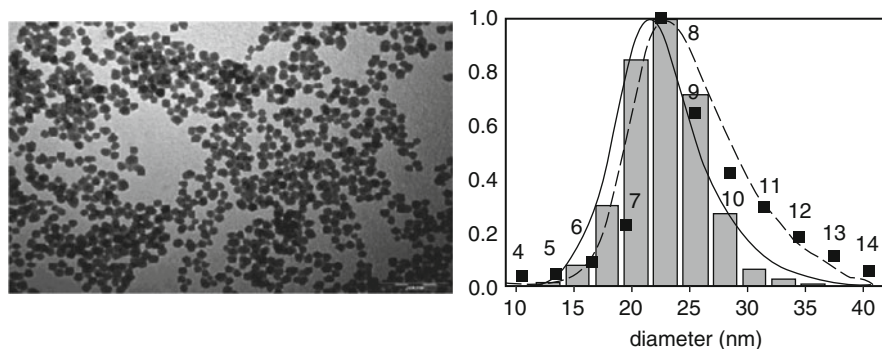


Fig. 8 *Left*: TEM picture of the fluorescent silica nanoparticles. *Right*: size distribution of the nanoparticles obtained from TEM images (*bars*); absorbance at 500 nm during the FIFFF elution of the nanoparticles (*dashed line*); numerical size distribution curve calculated from FIFFF (*continuous curve*); fluorescence intensities of the fraction n with a diameter between $3n - 1$ and $3n$ (*squares*). Adapted with permission from [74]

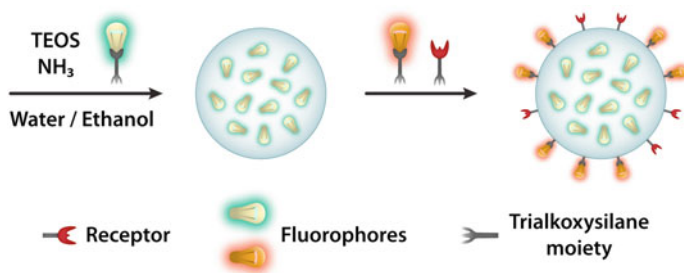


Fig. 9 Van Blaaderen modification of the Stober method for the synthesis of dye doped silica nanoparticles

monodispersity of the samples and, when required, to replace the alcoholic environment with aqueous solutions. We recently also showed that FIFFF (Flow Field Flow Fractionation) is a powerful technique to size sort and purify fluorescent colloids of nanometric dimension [74] (Fig. 8).

The Stober method was brilliantly modified by van Blaaderen who had the idea of co-condensing fluorescent molecules with the monomeric tetraethoxysilane (TEOS) precursor during the growing step in the nanoparticles synthesis, yielding systems in which organic dyes are covalently linked to the silica matrix [67, 68]. These architectures are commonly addressed as DDSN and present a high versatility since different species can be inserted inside the nanoparticles and, moreover, the surface is still available for further functionalization (Fig. 9).

The photophysical properties of dye molecule in DDSNs can also be tuned by exploiting plasmonic effects, that is by growing the silica nanoparticle around a metal core. Experimentally, such sophisticated structures are achieved by carrying out the Stober synthesis in the presence of preformed metal nanoparticles stabilized

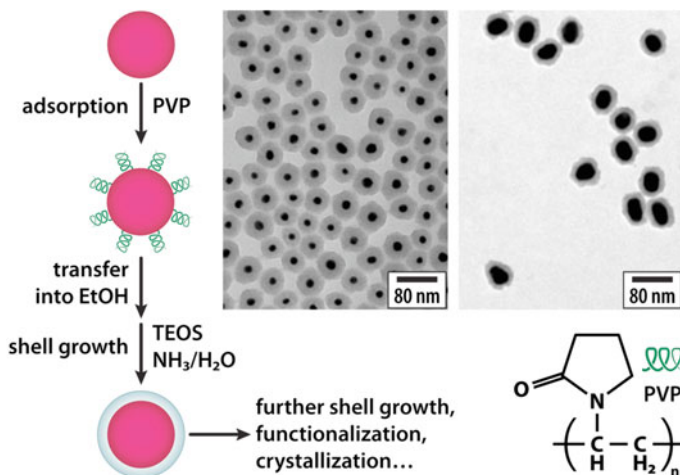


Fig. 10 Diagram of the general procedure for the coating of colloids with silica and TEM pictures of gold nanoparticles coated with silica (*left*: 7 nm Au NPs with 18 nm of silica shell; *right*: 20 nm Au NPs with 12 nm of silica shell). Adapted with permission from [75]

by polyvinylpyrrolidone (PVP) [75]. The reaction condition can be tuned to control the thickness of the resulting silica shell (Fig. 10).

2.2 Reverse Microemulsion Method

The reverse microemulsion method is based on the controlled hydrolysis of tetraethoxysilane (TEOS) molecules and their ammonia catalysed condensation like the Stöber method, but the reaction milieu is in this case a stable and macroscopically isotropic dispersion of a surfactant and water in a hydrocarbon. In this system the hydrolysis is confined inside the aqueous nuclei where precursors condense to form the nanoparticles. Optimized synthetic protocols and experimental conditions allow one to obtain nanoparticle samples in the dimensional range of about 15–200 nm [70, 76] (Fig. 11).

The main discriminating parameters to control the nanoparticle dimensions in the microemulsion method are the kind of surfactant and the surfactant to water molar ratio [77]. An advantage of this method is that it often does not require the functionalization of the fluorophores (when hydrophilic) that can be physically trapped inside the matrix or via non-covalent interactions. Derivatization of the dye molecules with a trialkoxysilane group is anyway preferable in order to avoid the leaching of the doping material, especially when small particles (with a diameter close to 20 nm) and a high level of doping (which usually varies between 0.1% and 1% but can be as high as 10% vs moles of TEOS) is required.

Also, in this case, the condensation of trialkoxysilane derivative is generally almost quantitative, but the separation of the nanoparticles from the unreacted

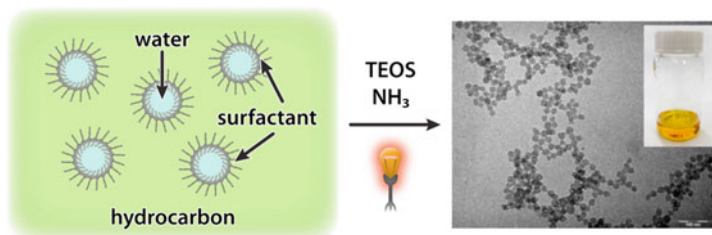


Fig. 11 Schematic representation of the reverse microemulsion method for the synthesis of dye doped silica nanoparticles

silane derivatives, and from the reaction media (surfactant, etc.) is necessary and can be obtained by precipitating the particles with an organic solvent. In this case the surface derivatization can be obtained through addition of silanized molecules before the purification step.

Microemulsion based methods can also allow one to prepare species that combine interesting optical and magnetic properties, thanks to the inclusion of an iron oxide magnetic nucleus (especially magnetite, Fe_3O_4). The resulting hybrid materials, if properly synthesized, can merge a high biocompatibility and hydrophilicity with a magnetic behaviour suitable for several medical and technological applications. Precursor magnetic nanoparticles with a narrow size distribution and with tuneable diameter (4–20 nm) are prepared by reverse microemulsion based methods [78, 79] or thermal decomposition of iron precursors in organic media [80–83]. Silica shell formation may be based either on modified Stöber methods (as seen for metal cores) or reverse microemulsion methods. Interestingly, the presence of a magnetic core, which is advantageous for dual imaging and for a specific positioning in a controlled magnetic field, can also be exploited for the recovery and hence for the purification of these hybrid materials.

2.3 Direct Micelles as Template

This approach is probably the most recent within those described so far. It is based on the use of a surfactant in water solution (sometimes together with a co-surfactant) in which the micellar aggregates (or co-aggregates) behave as templates, where the formation of the nanoparticle structure takes place. The strong point of the strategy is the use of cheap reagents in aqueous solution, for a reaction which provides extremely mono-disperse water soluble nanoparticles, with diameters within quite a narrow range (10–50 nm), these being the most desirable dimensions in most in vivo and in vitro bio-analytical applications.

Within the examples appearing in the literature, the synthetic strategy used by Prasad and coworkers to obtain the so-called ORMOSIL (ORGanic-MODified SILica) nanoparticles stands out for versatility and simplicity. It is based on an

oil in water method utilising a surfactant/1-butanol/DMSO and water mixture. The surfactants normally used are AOT [bis(2-ethylhexyl) sulfosuccinate sodium salt] or Tween 80, while the silica precursor is VTES (triethoxyvinylsilane). The organosilane condensation is promoted using APTES (3-aminopropyltriethoxysilane) or ammonia, and is followed by two purification steps, dialysis and ultrafiltration. The method provides highly monodisperse and stable aqueous suspensions of nanoparticles in the 20–30 nm range that exhibit some degree of mesoporosity. The multimodality of the nanoparticles, that is the ability to carry out multiple functions, is conferred mainly through surface functionalization and encapsulation. The introduction of functional groups on the nanoparticles surface ($-\text{NH}_2$, $-\text{COOH}$, $-\text{SH}$) together with PEG chains [84] allow for targeting through the coupling with bioactive molecules such as transferrin, monoclonal antibodies [85] or DNA [86, 87], while the encapsulation of imaging or therapeutic agents such as single and two photon fluorophores [88], PDT agents [89, 90], QDs and magnetic nanoparticles (Fe_3O_4) [91] address the ORMOSIL particles as imaging and therapeutic agents. Due to the porosity of the organo-silica matrix, in many cases the conjugation of the fluorophore and/or of the PDT agent with the silica matrix is required to avoid the possibilities of leakage [92] (Fig. 12).

Inspired by the work of Liu and co-workers who have described a new kind of core-shell (silica-PEG) nanoparticles as platform for drug-delivery [71], we have very recently proposed [93] a synthetic strategy that affords monodispersed and ordered core-shell silica nanoparticles. Such systems allow the irreversible inclusion of dye molecules in the silica core and present a stable biocompatible and water soluble polymeric protective shell. For these reasons these materials appear particularly promising in the development of luminescent probes for *in vitro* and, hopefully, *in vivo* medical and bio-analytical applications.

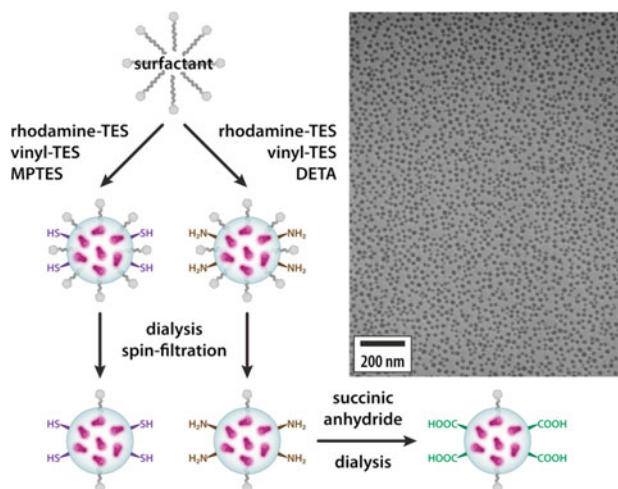


Fig. 12 Synthetic scheme for the preparation of functionalized ORMOSIL nanoparticles. Adapted with permission from [85]

This synthetic strategy is based on the formation of direct micelles of Pluronic® F127 in water. Pluronic F127® is a non-ionic triblock copolymer surfactant terminating in primary hydroxyl groups, and presenting a poly(ethylene glycol)-poly(propylene oxide)-poly(ethylene glycol) structure (PEG-PPO-PEG, MW 12600), that is relatively non-toxic.

The subsequent addition of tetralkoxysilane (TEOS) in acidic (or even neutral) conditions leads to the formation of a silica core, due to the fact that, especially before hydrolysis, alkoxy silane are rather apolar species and tend to migrate and accumulate in the central part of the polymeric micelles, the more hydrophobic area where the silicate condensation is promoted. This induces the formation of the silica nanoparticles only inside the micelles, as the condensation proceeds, leading to the entrapment of the surfactants molecules and to the final silica core-PEG shell architecture (Fig. 13).

As already mentioned for other synthetic strategies, the silicate condensation needs to be controlled in order to avoid the inclusion in the matrix of the whole PEG segments, or the aggregation through inter-particles polymerization. This can be achieved by adding to the reaction mixture, in due time, DEDMS (diethoxydimethylsilane) or TMSCl (trimethylsilylchloride) that are capping agents able to stop the silica condensation.

The addition of dyes in the initial reaction mixture affords dye-doped silica cores. According to their solubility, in fact, they partition between water and hydrophobic micelles, the latter fraction remaining physically entrapped in the silica network. Derivatizing the dye with a trialkoxysilane group leads to its co-condensation with TEOS, resulting in robust luminescent systems. Thus, this method allows the physical or covalent entrapment of dozens of molecules to a small silica core, providing very bright nanosystems.

Targeting moieties exposed on the surface of silica nanoparticles would account for bio-recognition and bio-specificity, opening up a number of possibilities in biomedical and analytical applications. We are currently exploring the possibility of linking such targeting moieties to the surface with a versatile procedure: through either standard conjugation protocols or more recent click chemistry strategies, we have substituted the terminal -OH groups of the triblock copolymers by proper functional groups (-COOH, -NH₂, -SH, -N₃, alkynes...). The co-micelles of

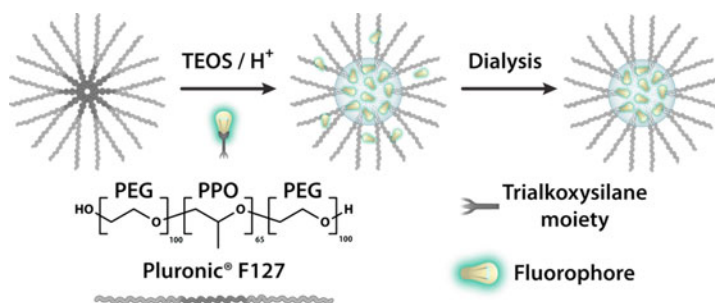


Fig. 13 Schematic representation of the Pluronic® assisted method for the synthesis of dye doped silica nanoparticles

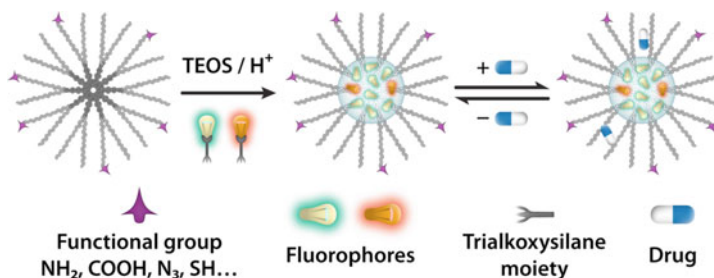


Fig. 14 Diagram showing some features of the silica core-PEG shell nanoparticles

original and modified Pluronic[®] F127 afford nanoparticles that, as prepared, exhibit functional groups on the surface that can subsequently link the particle to a variety of targeting moieties (Fig. 14).

Transmission electron microscopy (TEM) images show very uniform spherical particles $d = (10 \pm 1)$ nm. This is the image of the more dense silica cores, the polymeric shell being too soft to be observed with this technique. Light scattering measurements on the same samples provide a hydrodynamic diameter in the 20–30 nm range, very close to that measured for pure F127 surfactant solutions [94–96]. This larger hydrodynamic diameter also takes into account the contribution of the flexible PEG chains in solution.

These core-shell nanoparticles are extremely soluble and stable (up to several month) in water (or phosphate buffered saline solutions, PBS) in which they maintain an outstanding monodispersity. The strength of this strategy is mainly being a one-pot method, in which very cheap and basically non-toxic components are used even if the synthesis pertains to functionalized nanoparticles. Moreover, the PEG shell boosts the performances of the colloidal system looking at *in vivo* and *in vitro* bio-analytical applications. The PEG shell provides a stabilizing stealth layer [97] and as a matter of fact in simulated physiological or bio-analytical protocols work-up conditions (PBS 1x, bovine serum albumin up to 10 wt%) these colloidal systems retain their stability and mono-dispersion.

Another feature is the ability to host in the outer PEG shell water insoluble materials such as dyes [98] or chemosensors. In perspective these systems seem to be good candidates for the development in an easy and rapid fashion of chemosensors presenting valuable features like signal amplification due to light harvesting properties.

3 Luminescent Silica Nanoparticles as Chemosensors

3.1 Introduction

Introducing this chapter, we have demonstrated the advantages in passing from conventional luminophores to complex architectures, and in particular why in our opinion luminescent silica nanoparticles are the most interesting and promising

nanosystems to be exploited in many fields like energy production and storage, catalysis, and, in particular, sensing for medical or environmental applications.

To obtain sensitive luminescent chemosensors, many requirements must be met. In particular the material should be (photo)chemically stable, compatible with the milieu of use, should present photophysical properties that do not depend on the environment or on a specific analyte; for marketing in general it should be obtained with an easy synthesis and low cost starting materials, and for their use in the medical field they should be biocompatible, non toxic and environmental friendly as far as their disposal is concerned.

Hereafter we discuss in more detail how luminescent silica nanoparticles can potentially fulfil all of these crucial features:

1. Silica is photophysically inert, i.e. it is transparent to visible light and is not involved in energy- and electron-transfer processes. For this reason, all the photochemical properties of the luminescent silica nanoparticles are mainly conferred by the doping material and, when present, by the capping agents. Photoactive matrices, in contrast, can be involved in photodecomposition processes (titania) [99] or simply cause quenching of the luminescence (gold) [100].
2. Silica does not present intrinsic toxicity, and for this reason silica NPs are environmentally friendly and can be suitable for *in vivo* applications because they do not undergo microbial attack. Although a deeper investigation is still necessary in this context, preliminary experiments are in favour of the benign nature of silica nanoparticles, also supporting their use for *in vivo* diagnosis and therapy [101]. From this point of view, QDs suggest much bigger concerns about their use in clinical applications [102–104] and their disposal, because of their constituting elements such as cadmium and selenium.
3. Each silica nanoparticle can contain a large number of photochemically active species; for example, a nanoparticle with a diameter of 60 nm used for labelling purposes can contain as much as 10^4 – 10^5 fluorophores. Thanks to these large amounts of dyes incorporated in a small volume, the goal of obtaining a particle with brighter luminescence can easily be fulfilled [105] since its extinction coefficient is equal to the sum of those of the single chromophores.
4. The silica matrix has the capability to protect the active material segregated inside the nanoparticle from external chemicals. Large species cannot, in fact, permeate inside the nanoparticle, while small ones can but with a much reduced diffusion coefficient. This feature still allows, on one hand, the use of NPs as chemosensors for analytes of small dimensions (the dye interacts in its ground state), and on the other hand it decreases the possibility of undesired photoreactions (the excited state of the dye cannot undergo bimolecular reactions), thus increasing the photostability of the fluorophores inside the nanoparticle. The inclusion in this kind of matrix also helps to provide the active species with an almost constant environment in chemical terms.
5. There are many different methods to synthesize luminescent silica NPs, as reported in detail in Sect. 2, but they share valuable common features: they usually require inexpensive reagents and mild conditions, they are rather simple

and do not involve complicated separation procedures. Furthermore, the versatility of the synthesis allows one to design luminescent nanoparticles with chemical properties suitable for the desired applications, including *in vivo* ones. Surface modification with well known chemical procedures [76] allows one to optimize their already good compatibility with water, the solvent of choice for the largest part of purposes, and with the biological microenvironment (cellular membranes, biomolecules, etc.). A simple tuning of the diameter is also possible through the control of the condition of growth of the nanoparticles. A fine control of these two variables (size and functionalization) often has a synergic action to obtain long-life systems in which the nanoparticle head off by RES (Reticulo-Endothelial System) is delayed. RES is a mechanism by which foreign particles are removed from blood or lymph by macrophages in vertebrate organisms. In addition to this, the great versatility of the synthetic strategies opens also up the possibility to adapt these materials for very different applications without requiring each time the design of the synthesis from scratch. This is also facilitated by the ability to realize *onion-like* multilayer structures, i.e. formed by a core, as many layers as desired, and an external modifiable surface (in case one or more of these parts might be of a different material if the application should require it) (Fig. 15).

These five points make clear how luminescent silica nanoparticles are particularly suitable to be used to engineer efficient fluorescent chemosensors, due both to their intrinsic properties and to their versatility. It has to be underlined again, anyway, how all the photophysical properties of luminescent silica nanoparticles are conferred by the doping species, and therefore the photophysical properties of the dyes are the first determining point of the performance of these systems in sensing and imaging fields. This is not a trivial point since, besides their own characteristics, in the final objects their possible cross-interactions can also play a major role. Numerous works in literature highlight that FRET, steady-state and time-resolved fluorescence and fluorescence anisotropy measurements are powerful tools to provide information on the rotational mobility of the photoactive dyes, on the distance and communication between them and on signal amplification effects [106]. In DDSNs homo-energy transfer processes are very important, since they can, on the one hand, lead to undesired self-quenching phenomena, while, on the other hand, in more complex systems such as multilayered *onion-like* structures,

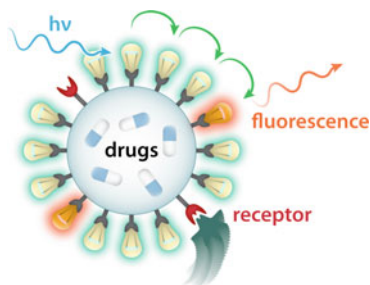


Fig. 15 Versatility of silica nanoparticles: receptor units on the surface recognize their analytes; fluorophores may undergo energy transfer processes; drug can be hosted inside

they are essential to convey all the energy gathered in a single shell to an adjacent one, favouring directional energy transfer from the core to the periphery or vice versa.

As far as hetero-energy transfer processes are concerned, when DDSNs are loaded with different dyes, they can be intentionally avoided with a structure design able to prevent all electronic interactions, thus yielding ratiometric systems for quantitative measurements [107, 108]. On the other hand, it is also possible to take great advantage from interchromophoric interactions in DDSNs to optimize internal FRET to yield high fluorescence intensity, large Stokes shift and wide absorption with multiple emission colours for applications in multiplex FRET bioassays [109]. Nowadays, numerous papers show appealing results in this field [61, 73], and have shown that, by precisely controlling and varying the concentrations of the dyes within the NP, excitation with a single wavelength can lead to different emission signals, permitting the simultaneous and sensitive detection of multiple targets.

To summarize, energy transfer processes can induce in luminescent silica nanoparticles very valuable collective properties, yielding species that can be gathered in three main classes:

1. *Antenna systems*, which present an enhanced light-sensitivity obtained by an increase in the overall cross-section for light absorption.
2. *Systems that present spectral sensitization*, very important when the light absorption properties of a potentially photoactive (generally, luminescent) species does not permit efficient excitation in the desired wavelength range. This kind of phenomenon is crucial for many applications in different fields, such as, for example, the spectral sensitization of semiconductor electrodes in solar energy conversion.
3. *Systems performing light-energy up-conversion*, that is to say showing anti-Stokes luminescence, a very particular and precious function [110].

Within this very wide panorama we will discuss in this section DDSNs designed to work as sensors and that can be included in one or more of these classes. Efficient nanosensors, in fact, can exploit the antenna effect to obtain signal amplification [111] that leads to a large increase of the sensitivity, and, as a consequence, to lower detection limits.

It is clear at this stage that, to obtain any of these photophysical devices able to perform valuable functions, it is of great importance to know how the different dyes are located and distributed inside the nanoparticle. Such information is not easy to obtain, and we have spent much research effort in recent years in this direction [112].

They can also take advantage of spectral sensitization to obtain remarkable Stokes shifts that typically allow a dramatic increase of the signal to noise ratio for more sensitive and precise photoluminescence measurements.

There are two main approaches possible for the design of these innovative nanostructured sensors, in which the receptor and luminescent units can – or can not – be covalently linked together to form a chemosensor. These groups should be

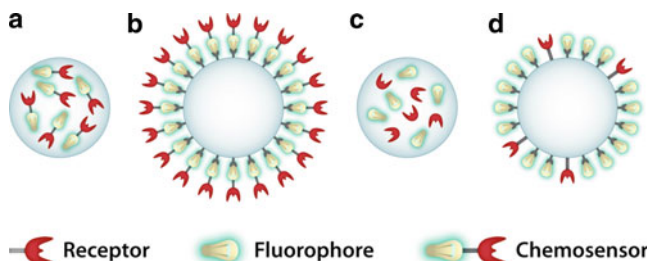


Fig. 16 Different approaches in the design of nanostructured sensors

successively derivatized with a triethoxysilane group, which permits their further condensation inside the nanoparticle (if this is porous or small enough to allow the interaction of the sensor with the target) [25] or on its surface (if the final solubility of the system results suitable for the analysis milieu) [113]. This will enable one to develop four different kinds of multichromophoric nanostructures, in which (1) the chemosensor is included in the core of the nanoparticle (Fig. 16a), (2) the chemosensor is linked to the surface of the nanoparticle (Fig. 16b), (3) the separate luminescent and receptor units are condensed in the core of the nanoparticle (Fig. 16c) and (4) the separate luminescent and receptor units are linked to the surface of the nanoparticle (Fig. 16d).

It is very important to note that all these structures do not show equivalent properties and performances. They present different pros and cons; for example when the active species are segregated inside, they are more stable and the water solubility of the matrix is maintained, but they can be much less accessible to the target. On the other hand, when the sensing species decorate the surface they are readily available for binding but this can also result in less stable and soluble systems. Moreover, from our recent studies, we have shown that the packing of the moieties on the surface of the nanoparticles is more efficient than that obtainable in the core. Therefore, on the surface the bound species are closer and their mobility is much higher, and this can cause an increase in electronic interactions that could, in some cases, yield the desired signal amplification effect [23, 114] and an increase of the complexation constants caused by synergic effects of more neighbouring receptors [115]. It is therefore very important to be able to optimize these structures in view of the application of interest, that is to say taking into account the environment, the mobility and steric hindrance of the target and the desired communication level between the various units. This does not sound like – and actually is not – an easy task.

We will discuss hereafter many recent examples of chemosensors based only on luminescent silica nanoparticles but, even if this can appear to be a narrow field, the scenario is instead very wide. Therefore, with the aim of clarity, we have divided them in two main sections, one dealing with systems presenting the signalling units on the surface (dye coated silica nanoparticles, DCSNs) and the other with systems presenting it segregated inside the silica matrix (DDSNs). Moreover, for both

architectures, as we have already mentioned, we have distinguished between species presenting the chemosensor directly bound to the matrix as such or self-assembled starting from separated receptor and luminescent signalling units.

3.1.1 Silica Nanoparticles with Chromophores on Their Surface

Directly Bound Sensing Subunits

With the aim of sensing applications, multichromophoric systems obtained by the organization of active units on the surface of silica nanoparticles sound more promising than those resulting from silica doping, since they allow a higher local density of molecules and hence a stronger electronic communication.

Following the synthetic strategy of the DCSNs, we have demonstrated the possibility to take advantage of the spatial organization and electronic communication between chromophoric units on the surface of silica nanoparticles for the development of a self-organized Zn(II) fluorescent chemosensor [116]. We used a triethoxysilane derivative of TSQ (6-methoxy-(8-*p*-toluenesulfonamido)quinoline) to realize a multichromophoric network on the surface of preformed silica nanoparticles. TSQ is a widely used fluorescent chemosensor able to bind Zn(II) ions with good selectivity. It is characterized by an off–on response due to an internal charge transfer (ICT) in the Zn(II)TSQ and Zn(II)(TSQ)₂ complexes (Fig. 17).

In our system the off–on fluorescence signal was amplified by the energy transfer process from the uncomplexed non-fluorescent TSQ units to the neighbouring luminescent Zn(II) complexes. In a low Zn(II) concentration regime, these self-organized chemosensors showed a 50% increase of the response with respect to the reference system TSQ in the same conditions. Even if the total sensitivity gain is quite

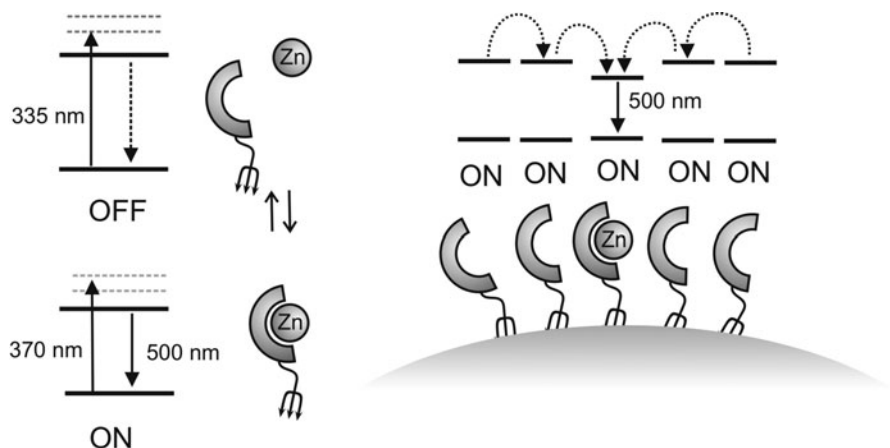


Fig. 17 *Left*: changes in the photophysical properties of TSQ upon complexation. *Right*: schematization of the processes occurring in silica nanoparticles coated with TSQ at low zinc concentration. Reproduced with permission from [24]

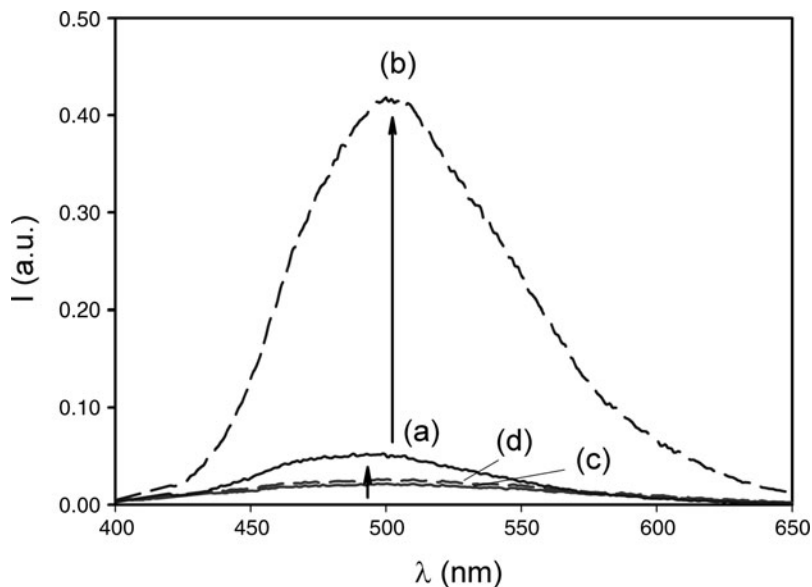


Fig. 18 Fluorescence spectra of a solution of nanoparticles coated with TSQ before (a) and after (b) the addition of zinc (1×10^{-6} M). The same addition to a solution of TSQ with the same concentration of dye cause very small changes (from c to d). Reproduced with permission from [24]

limited, this is, to our knowledge, the first example of an amplification effect in an off-on system (Fig. 18).

These phenomena, together with the enhanced affinity toward the substrate (the association constant increases of almost four orders of magnitude in the NPs), induced by the self-organized network on the surface of the nanoparticles, lead to a great increase in the sensitivity of the system, and provide interesting hints for the development of new fluorescent chemosensors. The same TSQ derivative was included in the silica matrix by Mancin and coworkers [25] that reported how its fluorescence was still sensitive to the presence of zinc ions but no amplification effect could be observed, as we will discuss more in detail in Sect. 3.1.2.

Another two nanosensors for copper ions proposed by Jong Hwa Jung and coworkers are based on the use of preformed silica nanoparticles 15 nm in diameter capped with silane derivatives of luminescent chemosensors. The first [117] presents a phenanthroline based sensing unit covalently bound to silica supporting structures of three different morphologies, including nanoparticles. They compared the fluorescent response and found that all the systems were very selective for copper, which was the only metal to induce a significant fluorescence quenching even in the presence of excess of other metal cations. The same group has recently published [118] a similarly selective but more efficient system to detect Cu^{2+} in living cells. They bound a fluorescein derivative bearing a trialkoxysilane moiety and two coordinating sites to the surface of commercial silica nanoparticles,

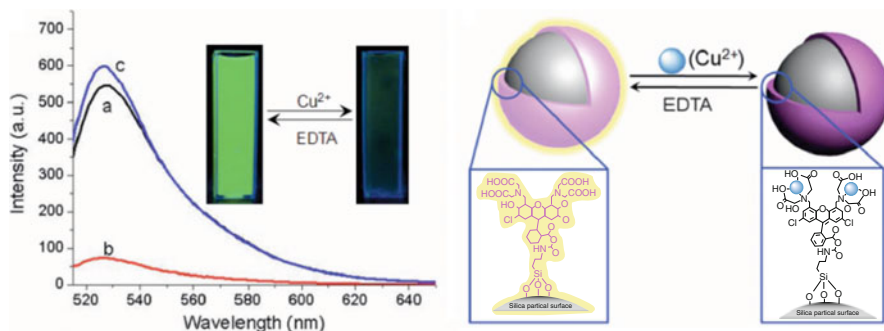


Fig. 19 *Left*: fluorescence spectra of 10- μ M silica nanoparticles without (a) and with (b) 100 eq. of Cu^{2+} and after treatment with EDTA in water (c). *Right*: proposed structure of Cu^{2+} -bound nanoparticles before and after treatment with EDTA. Adapted with permission from [118]

yielding a selective and reversible (upon addition of EDTA) nanosensor for copper in water at pH 7.4, with a detection limit of 0.5 μM . The incubation of human cancer cells (Hela cells) with the sensitive nanoparticles showed that they are cell permeable, and still able to signal the presence of Cu^{2+} (Fig. 19).

Besides selectivity, another very valuable characteristic of nanosensors is certainly the possibility of use to perform quantitative analysis, such as ratiometric measurements. Xi Chen and coworkers have reported a quite elaborate ratiometric fluorescent system for the detection of mercury ions in aqueous solution [119]. The nano-sensor architecture presents a silica core with a diameter of 100 nm surrounded by a shell of CdTe QDs embedded in silica, these nanospheres then being capped with a silane derivative of rhodamine 6G. This system presents a well-resolved dual fluorescence emission centred at 545 nm (rhodamine) and at 625 nm (QDs), but while the intensity of the second is unaffected by pH variations the first is pH dependent. In PBS buffered solution the rhodamine is present in the lactam form (cyclic amide) so that its fluorescence is quenched. Adding increasing amounts of Hg^{2+} a strong enhancement can be observed, since the interaction with mercury induces the same effect of protonation: ring opening of the lactam form of rhodamine. The high selectivity toward Hg^{2+} , together with the low detection limit (of the order of nanomolar), precision, reversibility and reproducibility, induced the author to envisage potential application to the monitoring and analysis of waters.

The same ratiometric approach is also the basis of another nanosensor proposed by Tristan Doussineau and coworkers [107]. In this case the rhodamine is segregated inside silica nanoparticles of diameter about 100 nm, prepared following the Stöber method, and then functionalized at the surface with a fluorescent naphthalimide derivative using bridges of different length. The two nanosensors do not show drastic differences in performance, but the one bearing the external fluorophore in close proximity of the surface was more dimensionally polydispersed, and slightly less stable towards aggregation. Both two-dye nanosystems revealed an interesting pH sensitivity in a physiologically relevant pH range. In particular, while the naphthalimide fluorescence intensity at 525–535 nm decreases with increasing pH, the

rhodamine emission at 585 nm remains unaffected, making these tools potentially non-invasive and selective systems for monitoring pH in biosamples, a field of general huge interest.

The great demand for suitable materials to be used in medical and biological analysis in the last few years has, unfortunately, been pained by the urge for sensors able to detect species relevant to security, such as spores and explosives.

Wenbin Lin and K. M. L. Taylor have proposed an interesting system for spore detection based again on a ratiometric approach. Dipicolinic acid (DPA) is a major component of endospores (for example *B anthracis* spores) [120]. It is already known that there is an affinity of this species for Tb(III) ions, extensively used in fluorescence methods to detect DPA: when the complex is formed the ligand gives rise to an efficient energy transfer to the metal excited states that results in an enhanced luminescence. The authors present here a system that gathers many terbium EDTA complexes on the surface of silica nanoparticles prepared via a well-established water-in-oil reverse microemulsion procedure, and doped with a ruthenium trisbipyridyl complex, yielding quite monodispersed spheres about 37 nm in diameter. The terbium complex was covalently bound on the surface via one or even two silane bridging chains, and the metal complex luminescence intensity was found to be linearly enhanced by the addition of increasing amounts of DPA in solution, while it did not change in the presence of even large excesses of potentially competing ligands. As expected, the luminescence of the ruthenium complex was totally unaffected by the DPA presence acting as an internal standard, also allowing for ratiometric detection at nanomolar concentrations of the analyte (Fig. 20).

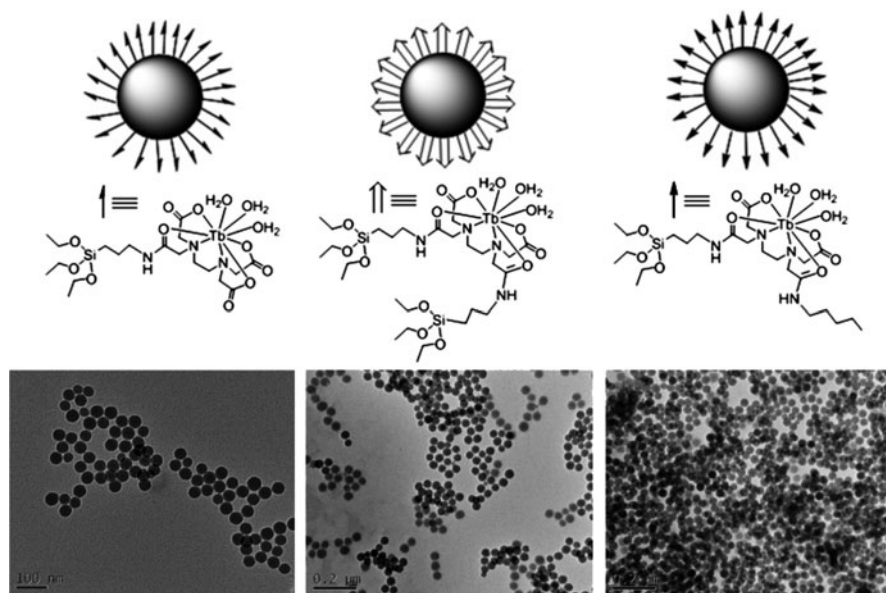


Fig. 20 Schematic representation and TEM images of silica nanoparticles coated with three different modified EDTA-Tb complexes. Adapted with permission from [120]

As mentioned above, the other important class that causes civil and military security concerns is that of explosives, and within them the nitroaromatics are particularly common. Conjugated polymers have been widely explored as chemosensors for the fluorescence detection of trinitrotoluene (TNT), as has their incorporation into organic-inorganic hybrid materials in order to tune their photophysical properties and to improve their stability. One very recent example in this direction is described by Yang Li and coworkers [121]. The binding of a conjugated polymer containing diethynylbenzene and diiodo-dipropylsulphonate benzene units (PPS) on silica nanoparticles has been brought to a stable system showing an intense fluorescence that is efficiently quenched in the presence of TNT. The authors found that the fluorescence of the material and its detection performance are strongly dependent on both the solvent and the nanoparticle dimensions, but in all cases it demonstrated a high sensitivity toward the analyte in solution.

Non-Directly Bound Sensing Subunits

As already stressed in the introduction, silica nanoparticles can be used for an uncommon approach to the preparation of chemosensors. As suggested by Tonellato et al. [122], they can act as a template for the self-organization of the key subunits of a sensor, the fluorescent moiety and the receptor. Even if the components are not previously mutually connected, and therefore they do not directly interact, the self-assembly itself induces their spatial closeness that consequently ensures the electronic communication between the bound substrate and the dye. The appropriate transduction mechanism must be envisaged in the sensor design in order to have a sufficient electronic communication to make possible energy- and/or electron-transfer processes converting the recognition event in a drastic change of the photophysical properties of the signalling dye.

The same authors proposed this strategy to prepare a selective copper chemosensor self-assembling the receptor, a picolinamide, and the signalling unit, a dansylamide, on the surface of preformed silica nanoparticles (20 nm in diameter) [115]. The grafting via the silanization of the sensor components ensured their spatial proximity and yielded a nanomaterial able to detect selectively Cu^{2+} ions down to micromolar concentrations via dansyl fluorescence quenching. Moreover, the affinity of the ligand for the target ions increased, and this was ascribed to the organization of the picolinamide moieties on the surface that can induce cooperative effects among the neighbouring binding sites (Fig. 21).

These authors successively proved the versatility of the new approach, preparing different nanoparticles by varying the signalling units and/or the ligands grafted onto the silica nanoparticles [113]. With careful choice of the components and of their ratio, they were able to obtain an amplified quenching response in which each single copper binding event was able to quench up to ten surrounding dyes, a particularly important demonstration of collective effects in nanomaterials (Fig. 22).

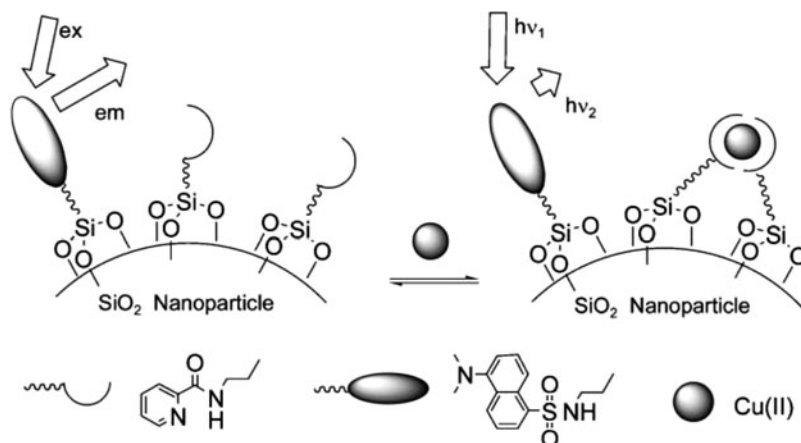


Fig. 21 Coated silica nanoparticles based self-organized fluorescence chemosensor. Adapted with permission from [113]

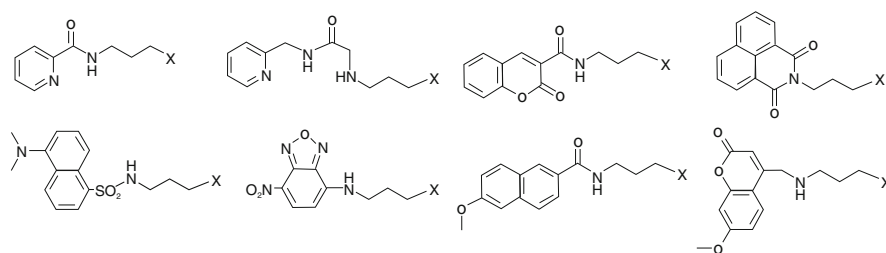


Fig. 22 Ligands and fluorescent dyes used for the coating of silica nanoparticles (where X can be $-\text{Si}(\text{OEt})_3$ or $-\text{H}$)

Ramón Martínez-Máñez et al. followed the identical approach to prepare anion sensors self-assembling anthracene and different thiourea silane derivatives on commercial silica nanoparticles (18 nm in diameter) [123]. Different methods of grafting were compared and particularly the consecutive and simultaneous grafting of the two sensing subunits. The authors prepared a batch of coated nanoparticles differing in the nature of the ligand and the ratio of the components and they carried out a systematic study on their fluorescence in solution in presence of organic (acetate, benzoate) and inorganic (phosphates, sulphates and halogenides) anions. All the materials were non-particularly selective and the fluorescence of the hybrid nanoparticles underwent only moderate changes, but the relatively low synthetic effort and the modular procedure were proved, opening up the possibility for great improvements of the performance.

They then focused their attention on polyanions and in particular on charged polysaccharides, proposing a new hybrid nanosensor for heparin [124]. In this case, the system presents only amine and thiol binding sites grafted onto the surface of

the commercial silica nanoparticles, and the mechanism of detection is based on the chemosensing ensemble strategy [17]. The signalling unit is now a squaraine free in solution that, in the absence of heparin, interacts with the thiols on the surface of the nanoparticles. This binding causes changes in the squaraine absorbance at 643 nm and quenching of its emission at 679 nm. The presence of heparin restores the typical values of the free dye in solution. The interactions of the polysaccharide with the amines on the surface of the nanoparticles in fact drives their wrapping by the heparin, making them no longer accessible to the signalling reporter that recovers its fluorescence. This system is therefore a sensitive (down to 2 μM) and selective chromo-fluorogenic hybrid nanosensor for heparin, even in the presence of large amounts of inorganic anions, monosaccharides, charged disaccharides and other charged polysaccharides.

The research group led by Zhongping Zhang is also extensively exploring the same modular approach, that is to say the silica nanoparticle template self-assembly, but in this case for the preparation of chemosensors for explosives (TNT) and herbicides (2,4-dichlorophenoxyacetic acid) [125]. They used nitrobenzoxadiazole (NBD) and organic amines as dye and receptor to decorate the surface of silica nanoparticles (150 nm in diameter) where they experience special proximity. Their reciprocal distance is short enough to allow photoinduced electron transfer (PET) from the amines to the NBD that causes the quenching of the dye fluorescence. Protonation of the amino ligands leads to fluorescence enhancement due to inhibition of PET, making this system a good, reversible and stable pH nanosensor. The herbicide 2,4-dichlorophenoxyacetic acid, being able to exchange protons, can be effectively detected by taking advantage of the same mechanism (Fig. 23).

This hybrid nanomaterial also proved to be sensitive to TNT, but in this case the recognition event causes a quenching of the fluorescence of the system. This can be explained since in the presence of this analyte FRET from the dye to the complex formed between the primary amine and TNT becomes predominant on PET. The authors have also assembled these nanoparticles in etched microwells on a silicon chips to prepare inexpensive solid state sensing materials for protons, herbicide and TNT that could be detected down to micromolar concentrations (Fig. 24).

They have also used the same approach to detect TNT using capping silica nanoparticles (200 nm in diameter) with primary amine receptors and fluorescein or rhodamine dyes [126]. The analyte brings about induced quenching of the fluorescence for both species again via a FRET mechanism. Nanoparticle assembled chips were able to detect TNT in solution down to nanomolar concentrations while when deposited as a thin film could sense nitroaromatic vapours down to 4 ppb in air.

There is another interesting system that exploits the same FRET mechanism, to obtain in this case fluorescence amplification, but based on the addition of a non-bound second fluorophore. Bin Liu and Yusong Wang [127] have immobilized a DNA strand on monodispersed silica nanoparticles (100 nm in diameter) and then hybridized it with a fluorescein labelled complementary DNA engineered to induce in the final double strand three pairs of T-T mismatches that are specific coordination sites for mercury ions. After incubation with metal ions and thermal washing, a cationic conjugated polymer was added. This last component was selected in order

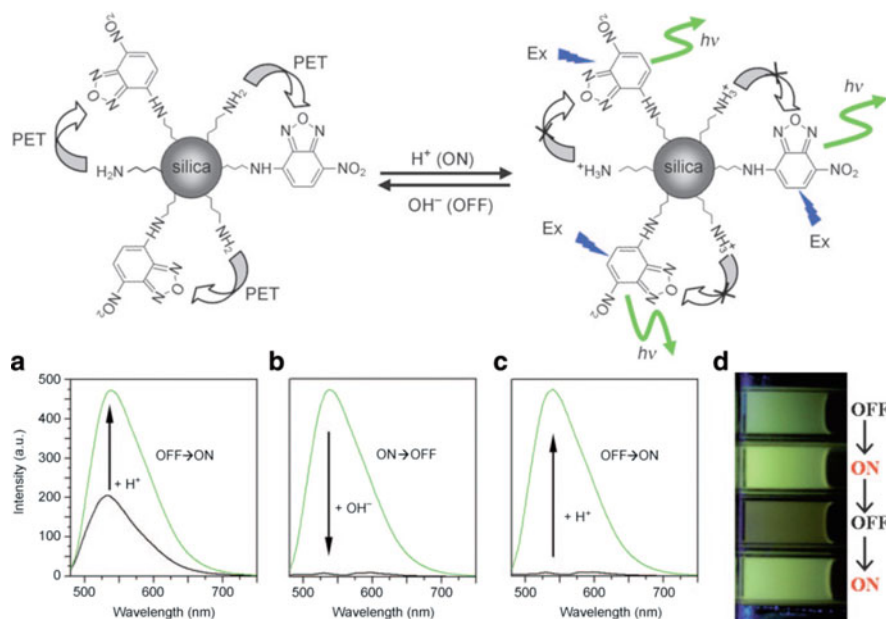


Fig. 23 Above: schematic diagram of the reversible fluorescence switch by sequential titration of HCl and NaOH into the suspension of NBD-(NH₂)-silica nanoparticles. Below: reversible fluorescence switch effect of NBD-(NH₂)-silica nanoparticles in ethanol with sequential addition of 1 mM HCl (a), NaOH (b), and HCl (c), with corresponding visual fluorescence changes, excited with a 365 nm UV lamp (d). Adapted with permission from [125]

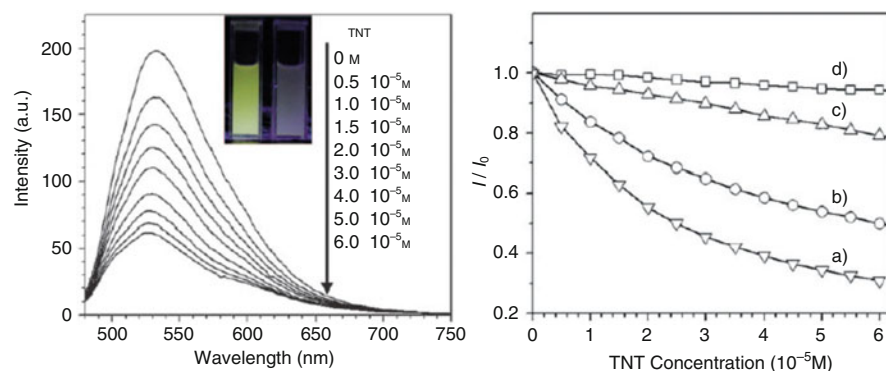


Fig. 24 Left: evolution of the fluorescence spectra of NBD-(NH₂)-silica nanoparticles with increasing TNT concentrations (the inset shows the fluorescence images before and after addition of TNT with excitation by a 365 nm UV lamp). Right: variation in fluorescence intensity with increasing TNT concentrations for NBD-(NH₂)-silica nanoparticles with different ratios of NBD to amino groups: 1:40 (a), 1:10 (b), 3:1 (c), and free NBD-APTES conjugates (d). Adapted with permission from [125]

to present good spectral overlap with fluorescein so that energy transfer could occur, and the initial low fluorescence intensity of the labelled complex system was enhanced via sensitization. The system becomes very selective for Hg^{2+} ions since the formation of this complex induces a significant increase in the melting temperature of the material. Therefore, with careful thermal washing, it was possible to denature all the double strands containing metal ions different from mercury. The photoluminescence enhancement is linear in low concentration regimes both of metal ions and nanoparticles.

3.1.2 Silica Nanoparticles Containing Chromophores

As we have already mentioned, the trapping or co-condensation of luminophores (or luminescent chemosensors) within the silica matrix yields dye doped nanoparticles (DDSNs) that contain the photoactive units and present an unreacted surface. This opens up two different strategies to exploit these systems as luminescent chemosensors. The signalling units and the receptors (as a whole or as separate moieties) can be inserted inside the particle and the target analyte must diffuse through the silica matrix in order to interact with the ligand and be detected. This is obviously possible only for small species such as protons or metal ions. For bigger analytes another architecture can assure better performance, a setting with the signalling units located inside the particle and the receptor components bound on the surface.

It is fundamental to highlight that, for both assemblies, the particle size is a very important parameter that influences the efficiency of the sensors. We have, in fact, shown experimentally that the particles are accessible to the solvent and the analyte only up to a certain depth [128]. When the particle is small, the solvent permeable layer is deep enough to make the whole body of the particle accessible to the analyte. On the other hand, the luminophores contained close enough to the surface are able to sense the state of the receptors so that all the fluorophores are effectively responding to the external signal. These two features are not guaranteed as the diameters of the colloid increases. It is therefore self-evident that many parameters have to be taken into account when designing a chemosensor and each architecture presents pros and cons. For example, we have already discussed the interesting results obtained binding TSQ [6-methoxy-(8-*p*-toluensulfonamide)quinoline] to the surface of silica nanoparticles: the proximity of the chemosensors induced and enhancement of the binding constant and a 50% increase in the response with respect to the reference system TSQ in the same conditions. These very positive results are unfortunately accompanied by a substantial change in the solubility of the system that, after TSQ grafting, could be efficiently dissolved only in DMSO.

An elegant way to overcome this solubility problem is to include the same TSQ derivative in the silica matrix, preserving the hydrophilicity typical of this material. Mancin and co-workers [25] reported the preparation of SiO_2 nanoparticles (15 nm in diameter) doped with covalently bound TSQ. This system is soluble in water/ethanol 1:1 and is also porous enough to allow the diffusion of zinc ions inside the

silica matrix. This was proved by the fact that the chemosensor fluorescence is still sensitive to the presence of zinc ions in solution. The drawback, in this case, is that the initial quantum yield of TSQ doped nanoparticles is higher than that of molecular TSQ in the same conditions, probably due to a partial protonation of the dyes by the acidic silanol groups. This has a negative consequence on the sensitivity of the material since the relative variation of the fluorescence caused by ion complexation is lower and the binding ability suffers a certain decrease. This could not be counterbalanced by the expected possible amplification effect due to chemosensors proximity, since no amplification could be observed in this case, probably because of the excessive distance between the receptor molecules. Mancin and coworkers have also prepared a totally similar system differing only in the addition of another dye in the particle. They used a coumarin derivative, indifferent to the analyte, that presents an emission band centred at 410 nm that remains constant in intensity and position during the whole titration with Zn^{2+} acting as an internal reference and validating the particles as ratiometric chemosensors.

The same authors had, shortly before, already proposed an even simpler and more versatile strategy to obtain silica nanosensors for metal cations [129]. They noticed that the silica itself provides a certain metal adsorption ability and they thought it could have been possible to exploit directly this feature to avoid the addition of a receptor moiety. They prepared silica particles doped with the dansylamide dye by co-polymerization of tetraethoxysilane (TEOS) and a dansyl triethoxysilane derivative by following the Stöber/van Blaaderen method. The resulting DDSNs showed a high sensitivity to the presence of Cu^{2+} ions that caused a strong fluorescence quenching, allowing the metal detection down to micromolar range. In this case, the silica itself or, better, the acidic silanol groups network on the particles surface are the receptor unit of the sensor. The small diameter of the spheres (about 15 nm) assures enough proximity of the Cu^{2+} ions bound on the particle and the fluorescent units segregated inside the core to quench their emission. Therefore the simple formation of the nanoparticles led to the straightforward conversion of fluorescent dyes into chemosensors. As mentioned above, the efficiency of sensors presenting architectures of this kind is greatly influenced by the particle size, and the authors have experimentally demonstrated this point, investigating the response to copper ions of analogous DDSNs with different diameters. Smaller particles show an almost complete quenching of the emission, while the larger ones present only a much smaller variation.

Even if the described system demonstrated an unexpected selectivity for Cu^{2+} ions, it is obvious that the modification of the outer shell of silica with other functional groups could increase the affinity of the system toward the desired metal ion, as the same authors have demonstrated for another self-organized fluorescent nanosensor able to detect Pb^{2+} ions [108]. Mancin et al. prepared in this case three different batches of DDSNs always following the Stöber/van Blaaderen procedure. The first ones (about 50 nm in diameter) presented dansyl units covalently bound inside and a surface coated with (mercaptopropyl)triethoxysilane (MPS). These particles are soluble in polar solvents (including water) and their photophysical properties are typical of the dansyl dye. The presence of thiols

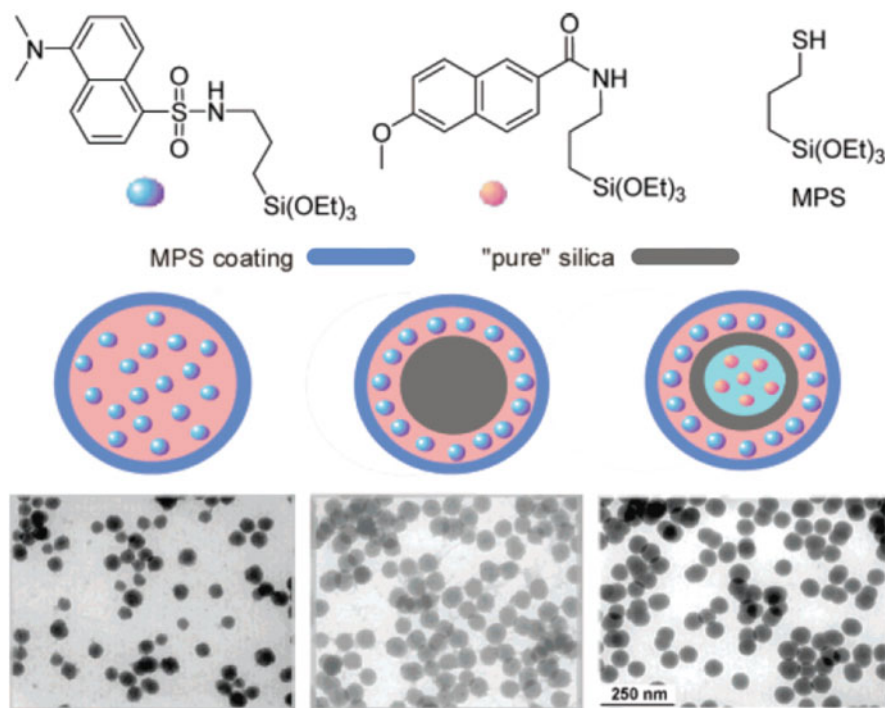


Fig. 25 Schematic representation of dye-doped silica nanoparticles with corresponding TEM images and structures of the dyes employed as sensors for Pb^{2+} ions. Adapted with permission from [108]

makes the system more selective for lead ions and their addition to a buffered (pH 7) solution of the nanoparticles causes a substantial quenching, even if in saturation conditions the system still presents a residual fluorescence of 60% with respect to the initial one (Fig. 25).

This can again be explained by the inaccessibility of the particle core: a second set of core-shell systems where a 50 nm diameter sphere of pure silica was coated with an approximately 5-nm dansyl doped silica shell capped with MPS showed in fact a remarkable sensitivity with only a 30% residual fluorescence. Mancin and coworkers have then designed a last batch of particles to obtain lead ratiometric detection. This was made by a multishell system with a silica core doped with a reference coumarin derivative surrounded by a 7-nm insulating pure silica layer and an outer 3-nm dansyl doped silica shell capped with MPS. The behaviour of this last system was analogous to the previous one but in this case ratiometric detection and calibration were possible thanks to the presence of the reference coumarin emission.

All the examples discussed till now make clear many advantages of using DDSNs to design sensors instead of dye capped silica nanoparticles or single dyes, but still no examples of signal amplification has been shown.

Our research group is indeed very interested in this phenomenon and, in order to demonstrate the possibility of amplifying the response of a fluorescence chemosensor by inclusion in SNPs, we synthesized a proof of principle system based on the dansylated 3-[2-(2-aminoethylamino)ethylamino]propyl-trimethoxysilane commercial receptor [23] (Fig. 26).

The nanoparticles were synthesized with the Stöber method, maximizing the density of the fluorophores with the aim of allowing the occurrence of multicomponent cooperative photophysical processes. Interestingly, the addition of copper, cobalt and nickel ions induced a strong quenching of the fluorescence intensity even at nanomolar concentrations (Fig. 27).

The ability of Cu^{2+} , Ni^{2+} and Co^{2+} to quench the fluorescence of this dye had already been reported for polyaminic dansylated systems and had been explained on the basis of energy transfer processes involving the dansyl excited state and the

Fig. 26 Fluorescence spectra of dansylated silica nanoparticles ($\lambda_{\text{em}} = 335 \text{ nm}$) for different concentrations of added copper ions. Reproduced with permission from [23]

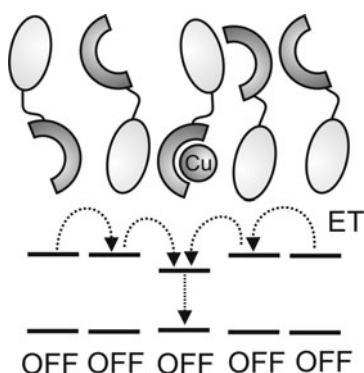
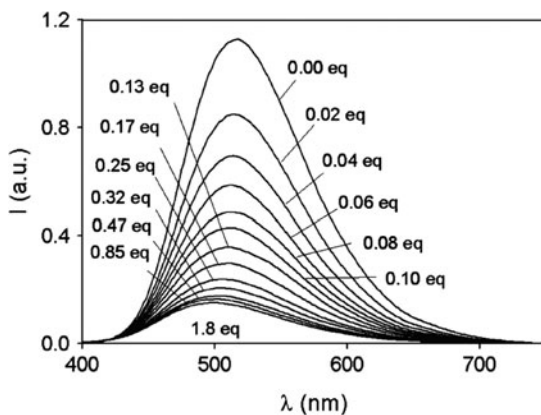


Fig. 27 Schematization of the energy transfer processes occurring in silica nanoparticles doped with 3-[2-(2-aminoethylamino)ethylamino]propyltrimethoxysilane. Complexation of a single Cu^{2+} ion causes the average quenching of 13 fluorophores (only five are reported in the picture for simplicity). Reproduced with permission from [24]

metal ion. The results obtained with our system, however, suggest that each copper ion, the species having the highest affinity, could quench up to 13 dansyl units, leading to strong signal amplification. This fluorescence response to complexation showed by the nanoparticles is in our opinion extremely interesting since, not only does it prove that they are porous enough to let in small cations, as already reported by other authors, but also that the proximity of the chemosensor units allows the communication of each receptor moiety with all the neighbouring fluorophores.

If silica matrices are permeable to small cations, they will be even more permeable to protons, and many authors have thought to take advantage of this property to design silica nanoparticles for pH sensing [130–132]. Most interestingly, Kemin Wang and coworkers [130] have described a ratiometric system able to sense pH variations in a range between 4 and 7 in murine macrophages and in living human cancer cells (Hela cells) during apoptosis. The authors have synthesized DDSNs (average 42 nm in diameter) containing both a silane fluorescein derivative, the luminescent sensing species, and the tris(2,2'-bipyridyl)ruthenium (II) as an internal standard reference. After investigating the stability and photostability of the system they incubated the nanosensors with murine macrophages and then monitored the changes in lysosomal pH in real time after exposure to chloroquine, an antimalarian drug. The comparison of the variations in the ratio between the fluorescein fluorescence intensity and the ruthenium complex luminescence intensity in time for reference samples and for different amounts of added drug showed how chloroquine stimulates lysosomal pH changes that can be revealed with high sensitivity using this method. The results obtained with Hela cells also demonstrated that intracellular acidification in apoptotic cancer cells, after treatment with dexametasone, a glucocorticoid commonly used in medicine, could be monitored in real time with a response of less than 1 s. The system also presented good reversibility, high stability and excellent quantification performance also thanks to its ratiometric nature.

The same fluorescein isothiocyanate (FITC) silanized via its reaction with (3-aminopropyl)triethoxysilane (APTES) was used in dye doped silica nanoparticles with a diameter of about 100 nm by Feng Gao and coworkers to prepare stable water soluble species for hydrogen peroxide indirect sensing [133]. The reverse microemulsion method was used to synthesize the doped nanospheres that had then been aminated at the surface. They used the same strategy to obtain analogous species for glucose detection but with a europium(III) complex as dye doping unit [134]. The authors also performed the analysis of blood glucose in human serum samples with this fluorescence-based approach, and the results were in good agreement with the data obtained via other common clinical methods.

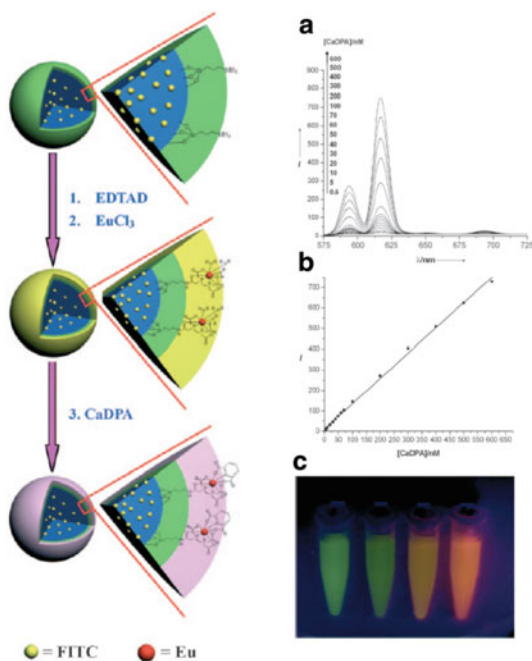
In general, lanthanide-based sensors have strongly attracted the attention of the scientific community worldwide for some decades due to their unique and outstanding photophysical characteristics such as long emission lifetimes, very narrow emission bands and large Stoke shifts. These spectroscopic features allow time resolved detection that is the most elegant way to clear measurements from background fluorescence with a consequent remarkable sensitivity enhancement. As already mentioned in Sect. 3.1.1.1 [120], DPA or better calcium dipicolinate

(CaDPA) has a high affinity for lanthanide ions and in particular terbium(III) complexes are considered the best probes for the detection of this species which is a unique biomarker for bacillus spores such as *B. anthracis*, known as a potential agent for biological terroristic attacks.

Lehui Lu and coworkers have recently published a very interesting study on a new nanosensor based on DDSNs for CaDPA that for the first time uses a europium complex as chemosensor [135]. The use of europium can offer some advantages over terbium such as a larger Stoke shift and a red emission. They have prepared fluorescein doped silica nanoparticles (65 nm in diameter) and then grafted onto their surface silanized ethylenediaminetetraacetic dianhydride (EDTAD) that was directly converted into its europium derivative via reaction with EuCl_3 . In this complex, three of the coordinating positions of the lanthanide are occupied by water molecules that enhance non-radiative quenching of the metal excited state, the system in fact being non-emitting (Fig 28).

On the other hand, these water molecules are only weakly bound to the metal centre and they are readily substituted by DPA when present in solution, resulting in a significant enhancement of the complex emission intensity. The authors showed a linear correlation between the maximum emission intensity of the nanosensor and the concentration of CaDPA in solution in the range 0.6–600 nM with a detection limit down to 0.2 nM. Therefore it was very sensitive but also very selective over other aromatic ligands. The rapid and ultrasensitive detection of *B. anthracis* spores in water was also helped by the ratiometric nature of the material since the

Fig. 28 *Left:* design strategy for Eu-based fluorescence nanoparticle sensor (EDTAD is ethylenediamine tetraacetic acid dianhydride). *Right:* (a) fluorescence response of the sensor (Eu^{II} content: 10 μM) upon addition of different concentrations of CaDPA at pH 6.5, (b) fluorescence intensity at 616 nm of the sensor as a function of CaDPA concentration. (c) visual fluorescence colour changes of the sensor (Eu^{II} content: 120 μM) upon addition of different concentrations of CaDPA (from left to right: 0, 25, 50, 100 μM). Adapted with permission from [135]



fluorescein emission of the nanoparticle core is totally unaffected by the presence of the CaDPA substrate.

3.1.3 Luminescent Silica Core–Shell Nanoparticles

In the previous section we have already described some multilayered systems [108] constituted by differently doped silica strata, but here we will report on a few examples of core–shell nanoparticles that combine the properties of different materials. Silica is a key component in this area since it offers unique characteristics of ease of synthesis, biocompatibility and a ductile chemistry able to merge many different substances including biomolecules, therefore opening up the possibility of using these new tools in the fields of biology and medicine [136, 137].

On the other hand, silica is often used as an insulating layer when direct *communication* between different components of a complex systems has to be avoided. For example, for a few years an unprecedented method has been proposed for increasing the efficiency of energy transfer exploiting the effect of plasmonic nanostructures [138–140]. In this systems *contact* of the fluorophores with the metal (usually silver) must be prevented since it would result in excitation energy dissipation and, most importantly, the increase in the efficiency of the energy transfer can be obtained only if the metal nanostructure is localized at a optimal distance.

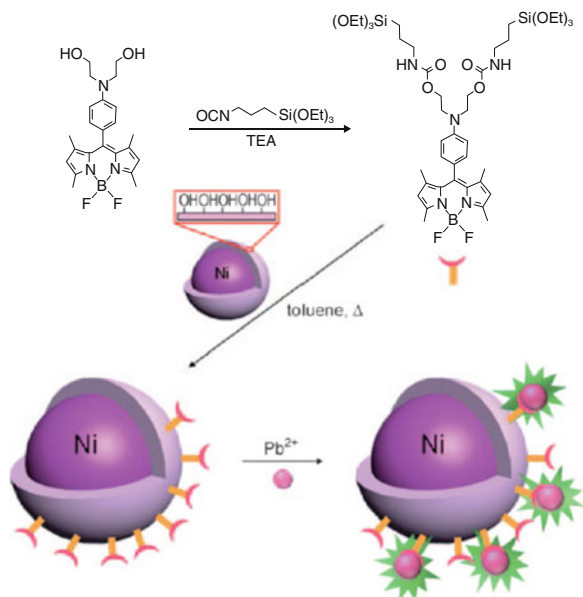
It is now clear how these hybrid core–shell materials present a very complex structure but also how, at the same time, they can assure the possibility of obtaining a great richness in functionalities, properties and performance [141].

In particular, magnetic silica nanoparticles are of great interest for research and applications in a variety of fields because they are stable and biocompatible. With the use of an external magnet they can be isolated, treated and repeatedly utilized. In biomedical and environmental applications they have been studied and used for bio-separation, enzyme immobilization, protein purification, as magnetic resonance imaging (MRI) contrast agents, and to remove toxins or pollutants different samples.

In this last area of sensing and separation, Weihong Tan and coworkers had proposed some years ago a very interesting *genomagnetic nanocapturer* for the collection of trace amounts of DNA/mRNA in cancer cells [142]. They prepared magnetic cores with a silica shell covalently functionalized at the surface with molecular beacons as a DNA probe for gene recognition and collection. These complex nano-objects presented a diameter of about 30 nm and some valuable features such as the possibility of monitoring the process in real-time, a very low limit of detection and collection (down to femtomolar) and an excellent specificity due to the use of molecular beacons.

The system was quite efficient and was probably an inspiration for Jong Hwa Jung et al. [143] who, more recently, have proposed a similarly engineered system for the sensing and separation of toxic species like lead and mercury in different matrices. They have synthesized nickel nanoparticles coated with a silica shell (30–40 nm in diameter), then grafted with a di-silanized 4,4-difluoro-4-bora-3a,-4a-diaza-*s*-indacene (BODIPY) derivative (Fig. 29). This dye, buffered at pH 7, is

Fig. 29 Synthesis of BOD-IPY-functionalized magnetic silica nanoparticles. Adapted from [143]



almost nonfluorescent due to an internal PET, but in the presence of lead ions it shows an about eightfold chelation-enhanced fluorescence CHEF at 510 nm, that is reversible with the addition of a strong base.

Titration experiments with Pb²⁺ revealed the formation of a 1:1 complex and a detection limit lower than 15 ppb that is the maximum limit allowed for the lead in drinking water. Moreover, the preorganization on the silica surface of the chemosensors led to a high selectivity for Pb²⁺ over the other possible interfering cations, and this suggested to the authors that it could have been a promising candidate for the separation of this toxic ion. They performed pilot experiments to remove lead cations, using a small external magnet, from water and human blood, where they could separate 96% of the total contain (100 ppb) selected as the lower unsafe limit of Pb²⁺ content in children blood (Fig. 30).

The analogous experiment in water allowed them to remove the 97% of the initial 15 ppb of Pb²⁺, validating the potentialities of this new type of magnetic biocompatible systems to detect and separate heavy metal toxins from different matrices.

The same authors, further developing this idea, prepared another core-shell nanosystem presenting an Fe₃O₄ nucleus with a silica coating superficially functionalized with aminonaphthalimide units [144]. In this case the material proved to be sensitive and selective for mercury and methylmercury ions in the pH range 4–11, and the experiments to test its ability to remove these toxic agents from drinking water containing 100 ppb of both of them showed 100% efficiency.

The sensing of mercury ions in water was also the aim of Enrique García-España, Javier Alarcón and coworkers [145] who have reported on a core-shell material modified with a fluorescent chemosensor based on anthracene and simple secondary

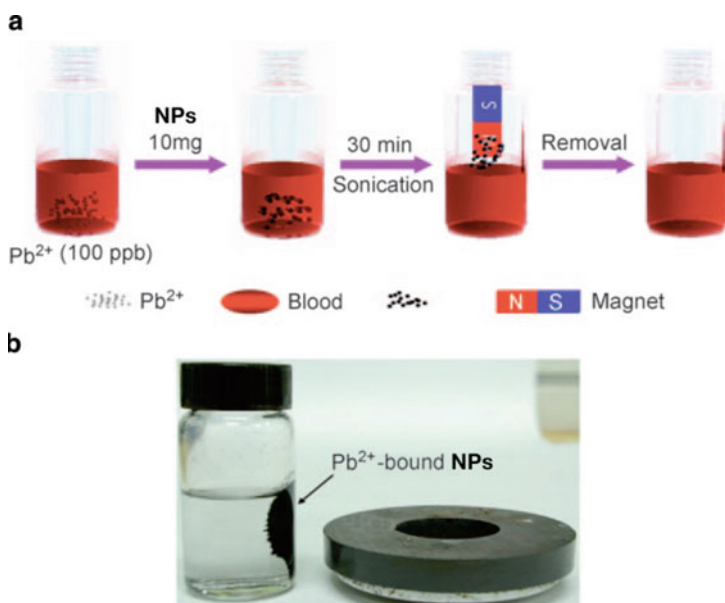


Fig. 30 (a) Illustration of the removal of Pb^{2+} from human blood. (b) Photograph of a magnet attracting Pb^{2+} -bound nanoparticles in water. Adapted from [143]

amines as receptors. The aluminosilicate nucleus is surrounded by a silica shell that allows the covalent bounding of the active units on the surface of the nanosystem (5–10 nm in diameter). In aqueous solutions with a pH in the range 3.5–5.5, the presence of Hg^{2+} caused a significant decrease of the luminescence of the nanosensor, allowing a detection limit in pure water of 0.2 ppb and very selective detection. A further advantage, in this case, is that the gelification at pH 11 of the material allows its recovery by simple centrifugation.

4 Some General Remarks

Nanofunctional materials in general, and nanoparticles in particular, are the basic constituents of the nanosciences, a field characterized by an unprecedented interdisciplinarity that merges chemistry with engineering, physics with material sciences and medicine. The importance of this topic is definitely substantial, as testified by the astonishing and increasing number of related publications. This lively research indicates not only that a certain degree of maturity in the know-how has been reached, but also that the development of nanotechnological products, even if more and more extensive, is only in its *infancy*.

The world of nanoparticles is amazingly many-sided and manifold with huge versatility in exploitation from industrial areas to bio-analysis and catalysis.

In particular, luminescent and magnetic nanoparticles attract the utmost attention in biology, medical diagnosis and therapy, where they already find many applications.

In this so fascinating and wide framework we have focused our attention particularly on luminescent silica nanoparticles able to act as sensing materials. After highlighting the first important aim to gain very precise knowledge and control of their structures, we have briefly presented the state of the art and progress in the synthetic protocols that allow one to prepare differently organized and precise architectures. This is of fundamental importance for the aim of sensing; in fact, the performance of a chemosensor is totally dependent on its design.

Among the different possible signalling methods, luminescence offers great advantages and is therefore the preferred one in many kinds of applications. In particular, fluorescent chemosensors grafted or self-assembled and self-organized on/in nanoparticles find wide applications in two major areas: (1) the detection of analytes in bulk biological or environmental solutions, and (2) the intracellular measurement of pH, oxygen, and reactive oxygen species, cations, etc. In this last case, silica nanoparticles are particularly suitable not only for their intrinsic low cytotoxicity but also because the gathering of the signalling molecules inside them, or on their surface, brings down their toxicity in comparison with the use of the same species as free indicators.

With the examples reported we have tried to show how luminescent silica based nanosensors can be seen as very promising systems offering many advantages such as solubility and stability in aqueous solvents and in physiological conditions, the possibility to insert targeting moieties for bio-conjugation and an intrinsic multichromophoric nature. This last point also allows, with a suitable choice of dyes and close control of the structure, signal amplification effects via collective energy and electron transfer processes.

All these features make luminescent silica nanosensors unique platforms. Their versatility, in fact, opens up the possibility to implement them in so many ways and different approaches that it is impossible to predict now the potentialities of the resulting final materials and of their applications.

We are convinced that the field of nanoscience will quickly make substantial steps forward and that, in this framework, silica nanoparticles will be one of the main characters with a fundamental role in the new ambitious applications, probably now difficult to envisage, that will surely have a great impact on the quality of our lives.

Acknowledgements The financial support of MIUR (LATEMAR FIRB and PRIN projects) and the Fondazione Cassa di Risparmio in Bologna is gratefully acknowledged.

References

1. Balzani V, Scandola F (1991) *Supramolecular photochemistry*. Ellis Horwood Ltd, Avon
2. Semeraro M, Silvi S, Credi A (2008) Artificial molecular machines driven by light. *Front Biosci* 13:1036–1049
3. Bassani DM (2006) From supramolecular photochemistry to self-assembled photoactive architectures: the emergence of photochemical nanosciences. *Chimia* 60:175–178

4. De Silva AP, Leydet Y, Lincheneau C, McClenaghan ND (2006) Chemical approaches to nanometer-scale logic gates. *J Phys Condens Matter* 18:S1847–S1872
5. Fukuzumi S, Kojima T (2008) Photofunctional nanomaterials composed of multiporphyrins and carbon-based π -electron acceptors. *J Mater Chem* 18:1427–1439
6. Lakowicz JR (2006) Principles of fluorescence spectroscopy, 3rd edn. Springer, New York
7. De Silva AP, Gunaratne HQN, Gunnlaugsson T, Huxley AJM, McCoy CP, Rademacher JP, Rice TE (1997) Signaling recognition events with fluorescent sensors and switches. *Chem Rev* 97:1515–1566
8. Haugland RP (2005) A guide to fluorescent probes and labeling technologies, 10th edn. Invitrogen Corporation, San Diego
9. Giepmans BNG, Adams SR, Ellisman MH, Tsien RY (2006) The fluorescent toolbox for assessing protein location and function. *Science* 312:217–224
10. Mancin F, Rampazzo E, Tecilla P, Tonellato U (2006) Self-assembled fluorescent chemosensors. *Chem Eur J* 12:1844–1854
11. Fabbri L (2000) Special issue on luminescent sensors. *Coord Chem Rev* 205:1–232
12. Ellis AB, Walt DR (2000) Special issue on chemical sensors. *Chem Rev* 100:2477–2738
13. Lee JY, Kim SH, Jung JH, Kim JS (2005) Bifunctional fluorescent calix[4]arene chemosensor for both a cation and an Anion. *J Org Chem* 70:1463–1466
14. Huston ME, Engleman C, Czarnik AW (1990) Chelatorselective fluorescence perturbation in anthranylazamacrocyclic conjugate probes. Electrophilic aromatic cadmiation. *J Am Chem Soc* 112:7054–7056
15. Czarnik AW (1993) Fluorescent chemosensors for ion and molecule recognition, vol 538. American Chemical Society, Washington DC
16. Wiskur SL, Ait-Haddou H, Lavigne JJ, Anslyn EV (2001) Teaching old indicators new tricks. *Acc Chem Res* 34:963–972
17. Fabbri L, Licchelli M, Taglietti A (2003) The design of fluorescent sensors for anions: taking profit from the metal-ligand interaction and exploiting two distinct paradigms. *Dalton Trans* 39:3471–3479
18. Buryak A, Severin K (2004) An organometallic chemosensor for the sequence-selective detection of histidine- and methionine-containing peptides in water at neutral pH. *Angew Chem Int Ed* 43:4771–4774
19. Borisov SM, Klimant I (2008) Optical nanosensors-smart tools in bioanalytics. *Analyst* 133:1302–1307
20. Mancin F, Scrimin P, Tecilla P, Tonellato U (2009) Amphiphilic metalloaggregates: catalysis, transport, and sensing. *Coord Chem Rev* 253:2150–2165
21. Doussineau T, Schulz A, Lapresta-Fernandez A, Moro A, Körsten S, Trupp S, Mohr GJ (2010) On the design of fluorescent ratiometric nanosensors. *Chem Eur J* 16:10290–10299
22. Goemann H, Feldmann C (2010) Nanoparticulate functional materials. *Angew Chem Int Ed* 49:1362–1395
23. Montalti M, Prodi L, Zaccheroni N (2005) Fluorescence quenching amplification in silica nanosensors for metal ions. *J Mater Chem* 15:2810–2814
24. Bonacchi S, Genovese D, Juris R, Marzocchi E, Montalti M, Prodi L, Rampazzo E, Zaccheroni N (2010). Energy transfer in silica nanoparticles: an essential tool for the amplification of the fluorescence signal. *Reviews in Fluorescence* 2008, vol 5. Springer, New York, pp 119–137
25. Teolato P, Rampazzo E, Arduini M, Mancin F, Tecilla P, Tonellato U (2007) Silica nanoparticles for fluorescence sensing of Zn(II): exploring the covalent strategy. *Chem Eur J* 13:2238–2245
26. Michalet X, Pinaud FF, Bentolila LA, Tsay JM, Doose S, Li JJ, Sundaresan G, Wu AM, Gambhir SS, Weiss S (2005) Quantum dots for live cells, in vivo imaging, and diagnostics. *Science* 307:538–544
27. Gill R, Zayats M, Willner I (2008) Semiconductor quantum dots for bioanalysis. *Angew Chem Int Ed* 47:7602–7625

28. Ferrari M (2005) Cancer nanotechnology: opportunity and challenges. *Nat Rev Cancer* 5:161–171
29. Medintz IL, Uyedo HT, Goldman ER, Mattoussi H (2005) Quantum dot bioconjugates for imaging labelling and sensing. *Nat Mater* 4:435–446
30. Scholes GD, Rumbles G (2006) Excitons in nanoscale systems. *Nat Mater* 5:683–696
31. Chen Y, Rosenzweig Z (2002) Luminescent CdS quantum dots as selective ion probes. *Anal Chem* 74:5132–5138
32. Medintz IL, Clapp AR, Mattoussi H, Goldman ER, Fisher B, Mauro JM (2003) Self-assembled nanoscale biosensors based on quantum dot FRET donors. *Nat Mater* 2:630–638
33. Sharma P, Brown S, Walter G, Santra S, Moudgil B (2006) Nanoparticles for bioimaging. *Adv Colloid Interface Sci* 123–126:471–485
34. Kirchner C, Liedl T, Kudera S, Pellegrino T, Javier AM, Gaud HE, Stolzle S, Fertig N, Parak WJ (2005) Cytotoxicity of colloidal CdSe and CdSe/ZnS nanoparticles. *Nano Lett* 5:331–338
35. Selvan ST, Tan TT, Ying JY (2005) Robust, non-cytotoxic, silica-coated CdSe quantum dots with efficient photoluminescence. *Adv Mater* 17:1620–1625
36. Kim S-W, Zimmer JP, Ohnishi S, Tracy JB, Frangioni JV, Bawendi MG (2005) Engineering InAs_xP_{1-x}/InP/ZnSe III–V alloyed core/shell quantum dots for the near-infrared. *J Am Chem Soc* 127:10526–10532
37. Xie R, Chen K, Chen X, Peng X (2008) InAs/InP/ZnSe core/shell/shell quantum dots as near-infrared emitters: bright, narrow-band, non-cadmium containing, and biocompatible. *Nano Res* 1:457–464
38. Kim S, Lim YT, Soltesz EG, De Grand AM, Lee J, Nakayama A, Parker JA, Mihaljevic T, Laurence RG, Dor DM, Cohn LH, Bawendi MG, Frangioni JV (2004) Near-infrared fluorescent type II quantum dots for sentinel lymph node mapping. *Nat Biotechnol* 22:93–97
39. Aharoni A, Mokari T, Popov I, Banin U (2006) Synthesis of InAs/CdSe/ZnSe core/shell1/shell2 structures with bright and stable near-infrared fluorescence. *J Am Chem Soc* 128:257–264
40. Medintz IL, Mattoussi H (2009) Quantum dot-based resonance energy transfer and its growing application in biology. *Phys Chem Chem Phys* 11:17–45
41. Bradley JS (1994) In: Schmid G (ed) *Clusters and colloids: from theory to applications*. VCH, Weinheim, pp 459–544, Chap. 6
42. Brust M, Walker M, Bethell D, Schiffrin DJ, Whyman R (1994) Synthesis of thiol-derivatized gold nanoparticles in a two-phase liquid-liquid system. *J Chem Soc Chem Commun* 801–802
43. Mie G (1908) Contributions to the optics of turbid media, especially colloidal metal solutions. *Annal Phys* 25:377–445
44. Daniel MC, Astruc D (2004) Gold nanoparticles: assembly, supramolecular chemistry, quantum-size-related properties, and applications towards biology, catalysis and nanotechnology. *Chem Rev* 104:293–346
45. Kamat PV (2002) Photophysical, photochemical and photocatalytic aspects of metal nanoparticles. *J Phys Chem B* 106:7729–7744
46. Thomas KG, Kamat PV (2003) Chromophore-functionalized gold nanoparticles. *Acc Chem Res* 36:888–898
47. Lai S, Grady NK, Kundu J, Levin CS, Lassiter JB, Halas NJ (2008) Tailoring plasmonic substrates for surface enhanced spectroscopies. *Chem Soc Rev* 37:898–911
48. Lin SY, Chen CH, Lin MC, Hsu HF (2005) A cooperative effect of bifunctionalized nanoparticles on recognition: sensing alkali ions by crown and carboxylates moieties in aqueous media. *Anal Chem* 77:4821–4828
49. Watanabe S, Sonobe M, Arai M, Tazume Y, Matsuo T, Nakamura T, Yoshida K (2002) Enhanced optical sensing of anions with amide-functionalized gold nanoparticles. *Chem Commun* 2866–2867

50. Prodi L, Battistini G, Dolci LS, Montalti M, Zaccheroni N (2007) In: Andrews DL, Gaburro Z (eds) *Frontiers in surface nanophotonics: principles and applications*, vol 133, Springer Series in Optical Sciences. Springer, New York, pp 99–128
51. Gu T, Whitesell JK, Fox MA (2003) Energy transfer from a surface-bound arene to the gold core in ω -fluorenyl-alkane-1-thiolate monolayer-protected gold clusters. *Chem Mater* 15:1358–1366
52. Montalti M, Zaccheroni N, Prodi L, O'Reilly N, James SL (2007) Enhanced sensitized NIR luminescence from gold nanoparticles via energy transfer from surface-bound fluorophores. *J Am Chem Soc* 129:2418–2419
53. Huang T, Murray RW (2001) Visible luminescence of water-soluble monolayer-protected gold clusters. *J Phys Chem B* 105:12498–12502
54. Wang L, Wang K, Santra S, Zhao X, Hilliard LR, Smith JE, Wu Y, Tan W (2006) Watching silica nanoparticles grow in biological world. *Anal Chem* 78:646–654
55. Burns A, Ow H, Wiesner U (2006) Fluorescent core-shell silica nanoparticles: towards “Lab on a particle” architectures for nanobiotechnology. *Chem Soc Rev* 35:1028–1042
56. Burns A, Sengupta P, Zedayko T, Baird B, Wiesner U (2006) Core/shell fluorescent silica nanoparticles for chemical sensing: towards single-particle laboratories. *Small* 2:723–726
57. Farruggia G, Iotti S, Prodi L, Montalti M, Zaccheroni N, Savage PB, Trapani V, Sale P, Wolf FI (2006) 8-Hydroxyquinoline derivatives as fluorescent sensors for magnesium in living cells. *J Am Chem Soc* 128:344–350
58. Tan M, Wang G, Hai X, Yuan J (2004) Development of functionalized fluorescent europium nanoparticles for biolabeling and time-resolving fluorometric applications. *J Mater Chem* 14:2896–2901
59. Yan J, Estevez MC, Smith JE, Xiaoxiao H, Wang L, Tan W (2007) Dye-doped nanoparticles for bioanalysis. *Nanotoday* 2:44–50
60. Niemeyer CM (2004) *Bioconjugation protocols: strategies and methods*. Humana Press, Totowa, NJ
61. Wang L, Tan W (2006) Multicolor FRET silica nanoparticles by single wavelength excitation. *Nano Lett* 6:84–88
62. Grifantini R, Bartolini E, Muzzi A, Draghi M, Frigimelica E, Berger J, Ratti G, Petracca R, Galli G, Agnisdei M, Giuliani MM, Santini L, Brunelli B, Rappuoli R, Randazzo F, Grandi G (2002) Previously unrecognized vaccine candidates against group B meningococcus identified by DNA microarrays. *Nat Biotechnol* 20:914–921
63. Barbé C, Bartlett J, Kong L, Finnie K, Lin HQ, Larkin M, Calleja S, Bush A, Calleja G (2004) Silica particles: a novel drug-delivery system. *Adv Mater* 16:1959–1966
64. Bonacchi S, Juris R, Montalti M, Prodi L, Rampazzo E, Zaccheroni N (2010) Active particles for bio-analytical applications and methods for the preparation of said particles. PCT/IB2009/006432 pp 122 Alma Mater Studiorum – Università di Bologna, Italy
65. Bonacchi S, Juris R, Montalti M, Prodi L, Rampazzo E, Zaccheroni N, Della Ciana L, Fabbroni S, Grilli S, Marzocchi E (2010) Active particles for bio-analytical applications and for imaging agents and methods for their preparation. PCT/IB2009/006435 pp 47 Alma Mater Studiorum – Università di Bologna, Italy; Cyanagen S.r.l.
66. Stober W, Fink A, Bohn E (1968) Controlled growth of monodisperse silica spheres in the micron size range. *J Colloid Interface Sci* 26:62–69
67. Van Blaaderen A, Imhof A, Hage W, Vrij A (1992) Three-dimensional imaging of sub-micrometer colloidal particles in concentrated suspensions using confocal scanning laser microscopy. *Langmuir* 8:1514–1517
68. Verhaegh NAM, van Blaaderen A (1994) Dispersion of rhodamine-labeled silica spheres: synthesis, characterization and fluorescence confocal scanner laser microscopy. *Langmuir* 10:1427–1438
69. Zanarini S, Rampazzo E, Della Ciana L, Marcaccio M, Marzocchi E, Montalti M, Paolucci F, Prodi L (2009) Ru(bpy)₃ covalently doped silica nanoparticles as multicenter tunable structures for electrochemiluminescence amplification. *J Am Chem Soc* 131:2260–2267

70. Bagwe RP, Yang C, Hilliard LR, Tan W (2004) Optimization of dye-doped silica nanoparticles using a reverse microemulsion method. *Langmuir* 20:8336–8342
71. Huo Q, Liu J, Wang L-Q, Jiang Y, Lambert TN, Fang E (2006) A new class of silica cross-linked micellar core-shell nanoparticles. *J Am Chem Soc* 128:6447–6453
72. Das S, Jain TK, Maitra A (2002) Inorganic-organic hybrid nanoparticles from *n*-octyl triethoxy silane. *J Colloid Interface Sci* 252:82–88
73. Wang L, Yang CY, Tan W (2005) Dual-lumiphore-doped silica nanoparticles for multiplexed signaling. *Nano Lett* 5:37–43
74. Montalti M, Prodi L, Zaccheroni N, Zattoni N, Reschiglian P, Falini G (2004) Energy transfer in fluorescent silica nanoparticles. *Langmuir* 20:2989–2991
75. Graf C, Vossen DLJ, Imhof A, van Blaaderen A (2003) A general method to coat colloidal particles with silica. *Langmuir* 19:6693–6700
76. Bagwe RP, Hilliard LR, Tan W (2006) Surface modification of silica nanoparticles to reduce aggregation and nonspecific binding. *Langmuir* 22:4357–4362
77. Arriagada FJ, Osseosare K (1995) Synthesis of nanosize silica in aerosol OT reverse microemulsion. *J Colloid Interface Sci* 170:8–17
78. Pileni M-P (2001) Magnetic fluids: fabrication, magnetic properties, and organization of nanocrystals. *Adv Funct Mater* 11:323–336
79. Pileni M-P (1997) Nanosized particles made in colloidal assemblies. *Langmuir* 13:3266–3276
80. Rockenberger J, Scher EC, Alivisatos AP (1999) A new nonhydrolytic single-precursor approach to surfactant-capped nanocrystals of transition metal oxides. *J Am Chem Soc* 121:11595–11596
81. Sun S, Zeng H, Robinson DB, Raoux S, Rice PM, Wang SX, Li G (2004) Monodisperse MFe_2O_4 ($M=Fe, Co, Mn$) nanoparticles. *J Am Chem Soc* 126:273–279
82. Pinna N, Grancharov S, Beato P, Bonville P, Antonietti M, Niederberger M (2005) Magnetite nanocrystals: nonaqueous synthesis, characterization, and solubility. *Chem Mater* 17:3044–3049
83. Li Z, Chen H, Bao H, Gao M (2004) One-pot reaction to synthesize water-soluble magnetite nanocrystals. *Chem Mater* 16:1391–1393
84. Kumar R, Roy I, Ohulchanskyy TY, Vathy LA, Bergey EJ, Sajjad M, Prasad PN (2010) In vivo biodistribution and clearance studies using multimodal organically modified silica nanoparticles. *ACS Nano* 4:699–708
85. Kumar R, Roy I, Ohulchanskyy TY, Goswami LN, Bonoiu AC, Bergey EJ, Trampusch KM, Maitra A, Prasad PN (2008) Covalently dye-linked, surface-controlled, and bioconjugated organically modified silica nanoparticles as targeted probes for optical imaging. *ACS Nano* 2:449–456
86. Roy I, Ohulchanskyy TY, Bharali DJ, Pudavar HE, Mistretta RA, Kaur N, Prasad PN (2005) Optical tracking of organically modified silica nanoparticles as DNA carriers: a nonviral, nanomedicine approach for gene delivery. *Proc Natl Acad Sci USA* 102:279–284
87. Bharali DJ, Klejbor I, Stachowiak EK, Dutta P, Roy I, Kaur N, Bergey EJ, Prasad PN, Stachowiak MK (2005) Organically modified silica nanoparticles: a nonviral vector for in vivo gene delivery and expression in the brain. *Proc Natl Acad Sci USA* 102:11539–11544
88. Kim S, Huang H, Pudavar HE, Cui Y, Prasad PN (2007) Intraparticle energy transfer and fluorescence photoconversion in nanoparticles: an optical highlighter nanoprobe for two-photon bioimaging. *Chem Mater* 19:5650–5656
89. Kim S, Ohulchanskyy TY, Pudavar HE, Pandey RK, Prasad PN (2007) Organically modified silica nanoparticles co-encapsulating photosensitizing drug and aggregation-enhanced two-photon absorbing fluorescent dyes aggregates for two-photon photodynamic therapy. *J Am Chem Soc* 129:2669–2675
90. Roy I, Ohulchanskyy TY, Pudavar HE, Bergey EJ, Oseroff AR, Morgan J, Dougherty TJ, Prasad PN (2003) Ceramic-based nanoparticles entrapping water-insoluble photosensitizing

- anticancer drugs: a novel drug-carrier system for photodynamic therapy. *J Am Chem Soc* 125:7860–7865
91. Law W-C, Yong K-T, Roy I, Xu G, Ding H, Bergey EJ, Zeng H, Prasad PN (2008) Optically and magnetically doped organically modified silica nanoparticles as efficient magnetically guided biomarkers for two-photon imaging of live cancer cells. *J Phys Chem C* 112:7972–7977
 92. Ohulchanskyy TY, Roy I, Goswami LN, Chen Y, Bergey EJ, Pandey RK, Oseroff AR, Prasad PN (2007) Organically modified silica nanoparticles with covalently incorporated photosensitizer for photodynamic therapy of cancer. *Nano Lett* 7:2835–2842
 93. Zanarini S, Rampazzo E, Bonacchi S, Juris R, Marcaccio M, Montalti M, Paolucci F, Prodi L (2009) Iridium doped silica-PEG nanoparticles: enabling electrochemiluminescence of neutral complexes in aqueous media. *J Am Chem Soc* 131:14208–14209
 94. Yang PD, Zhao DY, Margolese DI, Chmelka BF, Stucky GD (1998) Generalized synthesis of large-pore mesoporous metal oxides with semicrystalline frameworks. *Nature* 396:152–155
 95. Desai PR, Jain NJ, Sharma RK, Bahadur P (2001) Effect of additives on the micellization of PEO/PPO/PEO block copolymer F127 in aqueous solution. *Colloid Surf A* 178:57–69
 96. Chu B, Zhou Z (1996) In: Nace VM (ed) *Nonionic surfactants; surfactant science*, vol 60. Marcel Dekker, New York, p 67
 97. Knop K, Hoogenboom R, Fisher D, Shubert US (2010) Poly(ethylene glycol) in drug delivery: pros and cons as well as potential alternatives. *Angew Chem Int Ed* 49:6288–6308
 98. Rampazzo E, Bonacchi S, Juris R, Montalti M, Genovese D, Zaccheroni N, Prodi L, Rambaldi DC, Zatonni A, Reschiglian P (2010) Energy transfer from silica core-surfactant shell nanoparticles to hosted molecular fluorophores. *J Phys Chem B*. doi:10.1021/jp1023444
 99. Wu J-M, Zhang T-W (2005) Large-scale preparation of ordered titania nanorods with enhanced photocatalytic activity. *Langmuir* 21:6995–7002
 100. Jennings TL, Singh MP, Strouse GF (2006) Fluorescent lifetime quenching near $d = 1.5$ nm gold nanoparticles: probing NSET validity. *J Am Chem Soc* 128:5462–5467
 101. Jin YH, Kannan S, Wu M, Zhao JXJ (2007) Toxicity of luminescent silica nanoparticles to living cells. *Chem Res Toxicol* 20:1126–1133
 102. Shiohara A, Hoshino A, Hanaki K, Suzuki K, Yamamoto K (2004) On the cyto-toxicity caused by quantum dots. *Microbiol Immunol* 48:669–675
 103. Alivisatos AP, Gu W, Larabell C (2005) Quantum dots as cellular probes. *Annu Rev Biomed Eng* 7:55–76
 104. Choi J, Burns AA, Williams RM, Zhou Z, Flesken-Niktin A, Zipfel WR, Wiesner U, Niktin AY (2007) Core-shell silica nanoparticles as fluorescent labels for nanomedicine. *J Biomed Opt* 12:064007–064017
 105. Larson DR, Ow H, Vishwasrao HD, Heikal AA, Wiesner U, Webb WW (2008) Silica nanoparticle architecture determines radiative properties of encapsulated fluorophores. *Chem Mater* 20:2677–2684
 106. Lettinga MP, van Zandvoort MAMJ, van Kats CM, Philipse AP (2000) Phosphorescent colloidal silica spheres as tracers for rotational diffusion studies. *Langmuir* 16:6156–6165
 107. Doussineau T, Trupp S, Mohr GJ (2009) Ratiometric pH-nanosensors based on rhodamine-doped silica nanoparticles functionalized with a naphthalimide derivative. *J Colloid Interface Sci* 339:266–270
 108. Arduini M, Mancin F, Tecilla P, Tonellato U (2007) Self-organized fluorescent nanosensors for ratiometric Pb(II) detection. *Langmuir* 23:8632–8636
 109. Wang L, O'Donoghue MB, Tan W (2006) Nanoparticles for multiplex diagnostics and imaging. *Nanomed* 1:413–426
 110. Wolfbeis OS et al. (2010) Luminescent chemical sensing, biosensing, and screening using upconverting nanoparticles. *Top Curr Chem* 1–22

111. Rurack K et al. (2010) Luminescence amplification strategies integrated with micro- and nanoparticle platforms. *Top Curr Chem* 1–41
112. Rampazzo E, Bonacchi S, Montalti M, Prodi L, Zaccheroni N (2007) Self-organizing core-shell nanostructures: spontaneous accumulation of dye in the core of doped silica nanoparticles. *J Am Chem Soc* 129:14251–14256
113. Rampazzo E, Brasola E, Marcuz S, Mancin F, Tecilla P, Tonellato U (2005) Surface modification of silica nanoparticles. A new strategy for the realization of self-organized fluorescence chemosensors. *J Mater Chem* 15:2687–2696
114. Montalti M, Prodi L, Zaccheroni N, Falini G (2002) Solvent-induced modulation of collective photophysical processes in fluorescent silica nanoparticles. *J Am Chem Soc* 124:13540–13546
115. Brasola E, Mancin F, Rampazzo E, Tecilla P, Tonellato U (2003) A fluorescence nanosensor for Cu(II) on silica particles. *Chem Commun* 3026–3027
116. Bonacchi S, Rampazzo E, Montalti M, Prodi L, Zaccheroni N, Mancin F, Teolato P (2008) Amplified fluorescence response of chemosensors grafted onto silica nanoparticles. *Langmuir* 24:8387–8392
117. Lee JL, Bae DR, Han WS, Lee SS, Jung JH (2008) Different morphological organic-inorganic hybrid nanomaterials as fluorescent chemosensors and adsorbents for Cu(II) ions. *Eur J Inorg Chem* 1559–1564
118. Seo S, Lee HY, Park M, Lim JM, Kang D, Yoon J, Jung JH (2010) Fluorescein-functionalized silica nanoparticles as a selective fluorogenic chemosensor for Cu(II) in living cells. *Eur J Inorg Chem* 843–847
119. Liu H, Yu P, Du D, He C, Qiu B, Chen X, Chen G (2010) Rhodamine-based ratiometric fluorescence sensing for detection of mercury(II) in aqueous solution. *Talanta* 81:433–437
120. Taylor KML, Lin W (2009) Hybrid silica nanoparticles for luminescent spore detection. *J Mater Chem* 19:6418–6422
121. Feng J, Li Y, Yang M (2010) Conjugated polymer-grafted silica nanoparticles for sensitive detection of TNT. *Sens Actuator B Chem* 145:438–443
122. Arduini M, Rampazzo E, Mancin F, Tecilla P, Tonellato U (2007) Template assisted self-organized chemosensors. *Inorg Chim Acta* 360:721–727
123. Calero P, Martínez-Mañez R, Sancenón F, Soto J (2008) Synthesis, characterisation and optical properties of silica nanoparticles coated with anthracene fluorophore and thiourea hydrogen-bonding subunits. *Eur J Inorg Chem* 5649–5658
124. Climent E, Calero P, Marcos MD, Martínez-Mañez R, Sancenón F, Soto J (2009) Selective chromofluorogenic sensing of heparin by using functionalised silica nanoparticles containing binding sites and a signalling reporter. *Chem Eur J* 15:1816–1820
125. Geng J, Liu P, Liu B, Guan G, Zhang Z, Han M-Y (2010) A reversible dual-response fluorescence switch for the detection of multiple analytes. *Chem Eur J* 16:3720–3727
126. Gao D, Wang Z, Liu B, Ni L, Wu M, Zhang Z (2008) Resonance energy transfer-amplifying fluorescence quenching at the surface of silica nanoparticles toward ultrasensitive detection of TNT. *Anal Chem* 80:8545–8553
127. Wang Y, Liu B (2009) Amplified fluorescence turn-on assay for mercury(II) detection and quantification based on conjugated polymer and silica nanoparticles. *Macromol Rapid Commun* 30:498–503
128. Montalti M, Prodi L, Zaccheroni N, Battistini G, Marcuz S, Mancin F, Rampazzo E, Tonellato U (2006) Size effect on the fluorescence properties of dansyl-doped silica nanoparticles. *Langmuir* 22:5877–5881
129. Arduini M, Marcuz S, Montolli M, Rampazzo E, Mancin F, Gross S, Armelao L, Tecilla P, Tonellato U (2005) Turning fluorescent dyes into Cu(II) nanosensors. *Langmuir* 21:9314–9321
130. Peng J, He X, Wang K, Tan W, Wang Y, Liu Y (2007) Noninvasive monitoring of intracellular pH change induced by drug stimulation using silica nanoparticles sensors. *Anal Bioanal Chem* 388:645–654

131. Gao F, Tang L, Dai L, Wang L (2007) A fluorescence ratiometric nano-pH sensor based on dual-fluorophore-doped silica nanoparticles. *Spectrochim Acta Part A* 67:517–521
132. Gao F, Wang L, Tang L, Zhu C (2005) A novel nano-sensor based on rhodamine- β -isothiocyanate – doped silica nanoparticles for pH measurement. *Microchim Acta* 152: 131–135
133. Luo F, Yin J, Gao F, Wang L (2009) A non-enzyme hydrogen peroxide sensor based on core/shell silica nanoparticles using synchronous fluorescence spectroscopy. *Microchim Acta* 165:23–28
134. Gao F, Luo F, Chen X, Yao W, Yin J, Yao Z, Wang L (2009) A novel nonenzymatic fluorescent sensor for glucose based on silica nanoparticles doped with europium coordination compound. *Talanta* 80:202–206
135. Ai K, Zhang B, Lu L (2009) Europium-based fluorescence nanoparticles sensor for rapid and ultrasensitive detection of an anthrax biomarker. *Angew Chem Int Ed* 48:304–308
136. Thanh NTK, Green LAW (2010) Functionalisation of nanoparticles for biomedical applications. *Nano Today* 5:213–230
137. Salgueiriño-Maceira V, Correa-Duarte MA (2007) Increasing the complexity of magnetic core/shell structured nanocomposites for biological application. *Adv Mater* 19:4131–4144
138. Aslan K, Wu M, Lakowicz JR, Geddes CD (2007) Fluorescence core-shell Ag@SiO₂ nanocomposites for metal-enhanced fluorescence and single nanoparticles sensing platforms. *J Am Chem Soc* 129:1524–1525
139. Zhang J, Fu Y, Chowdhury MH, Lakowicz JR (2007) Enhanced Forster resonance energy transfer on single metal particles. 2. Dependence on donor-acceptor separation distance, particles size, and distance from metal surface. *J Phys Chem C* 111:11784–11792
140. Lessare-Viger M, Rioux M, Rainville L, Boudreau D (2009) FRET enhancement in multi-layer core –shell nanoparticles. *Nano Lett* 9:3066–3071
141. Schaertl W (2010) Current directions in core-shell nanoparticles design. *Nanoscale* 2: 829–843
142. Zhao X, Tapeç-Dytioco R, Wang K, Tan W (2003) Collection of trace amounts of DNA/mRNA molecules using genomagnetic nanocaptors. *Anal Chem* 75:3476–3483
143. Lee HY, Bae DR, Park JC, Song H, Han WS, Jung JH (2009) A selective fluoroionophore based on BODIPY-functionalized magnetic silica nanoparticles: removal of Pb(II) from human blood. *Angew Chem Int Ed* 48:1239–1243
144. Park M, Seo S, Lee IS, Jung JH (2010) Ultraefficient separation and sensing of mercury and methylmercury ions in drinking water by using aminonaphthalimide-functionalized Fe₃O₄@SiO₂ core/shell magnetic nanoparticles. *Chem Commun* 4478–4480
145. Delgado-Pinar E, Montoya N, Galiana M, Albelda MT, Frias JC, Jimenez HR, Garcia-España E, Alarcon J (2010) Preparation of Hg(II) selective fluorescent chemosensors based on surface modified core-shell aluminosilicate nanoparticles. *New J Chem* 34:567–570

Fluorescence Based Sensor Arrays

Roberto Paolesse, Donato Monti, Francesca Dini, and Corrado Di Natale

Abstract Fluorescence-based cross reactive sensor arrays have experienced significant development in the last decade because of the advantages that they can offer with respect to other transduction mechanisms, in terms of the usual performance parameters such as sensitivity, selectivity and so on. From this point of view, a great impulse to this development has been due to the realization of novel transduction platforms, which has also taken advantage of the development of consumer electronics such as digital scanners, cameras, and screens, allowing the realization of low cost sensing layers suitable for many practical applications. This possibility, combined with continuous optimization of sensing material properties, the possible preparation of arrays with a high number of individual sensing elements and pattern recognition data analysis, has led to novel opportunities for the creation of luminescence based sensor arrays with improved capabilities. Herein we report on the development of these devices witnessed in the last decade, dividing the developed devices according to their exploitation in gaseous or in solution phase.

Keywords Electronic nose, Fluorescence, Ion sensors, Optical sensors, Sensor arrays

Contents

1	Introduction	140
2	Fluorescence Based Sensor Arrays for Gas Detection	141
	2.1 Fibre Optics Sensor Arrays	141
	2.2 Micro Arrays	147

R. Paolesse (✉) and D. Monti

Dipartimento di Scienze e Tecnologie Chimiche, University of Rome “Tor Vergata”, via della Ricerca Scientifica 1, 00133, Rome, Italy

e-mail: roberto.paolesse@uniroma2.it

F. Dini and C. Di Natale

Dipartimento di Ingegneria Elettronica, University of Rome “Tor Vergata”, via della Ricerca Scientifica 1, 00133, Rome, Italy

2.3	Computer Screen Photoassisted Technique	148
3	Fluorescence Arrays for Analytes in Solution	153
3.1	Cation Sensing	153
3.2	Anion Sensing	163
3.3	Other Analytes	164
4	Conclusions	170
	References	170

1 Introduction

Chemical sensors have assumed an important role in life nowadays because these devices can supplement analytical instrumentation for the detection of target analytes, an urgent requirement for security and safety reasons. The instruments exploited in analytical chemistry protocols can in fact guarantee the highest level of sensitivity and accuracy necessary for the control of different matrices, but their inherent drawbacks are usually long response times and cost, which preclude a continuous control of the target matrix. Chemical sensors are the solutions of choice that can also satisfy these requirements in remote mode. The sensor performances necessary to fulfil their tasks are mostly guaranteed by the sensing materials, the sensor component that interacts with the target analyte modifies some physico-chemical property as a consequence of such an interaction. This in turn will be transduced into a readable signal by the transducer, the second component of the device [1]. From this point of view, optical transducers represent one of the most widely used mechanisms and, among them, luminescence is probably the most useful in terms of sensitivity and selectivity properties [2]. Furthermore, there are several ways to measure fluorescence variation, so increasing the transduction mechanism versatility.

For this reason much effort has been devoted to the preparation of highly selective receptors, which can signal the target analytes upon selective binding through luminescence variation [3]. From this point of view the supramolecular chemistry concepts have revolutionized the synthesis of such a species, giving a rational approach to the preparation of receptors inspired by the “key-lock” mechanism that drives the selectivity of biological systems [4]. Several elegant examples of the rational preparation of such a species, usually called chemosensors, have been reported in the literature [5], although it is important to note that realization of a sensor needs a further step, the coupling of these receptors with a transducer. The binding interaction observed in solution should be matched with the transducer mechanism and the deposition of the chemosensor in a solid film should also preserve the selectivity observed in solution. This step is of paramount importance for device realization and it should be noted that the high selectivity observed in solution has rarely been reflected in the development of highly selective chemical sensors.

This feature has been considered for long time the most serious drawback of these devices that has hampered their exploitation in real applications. On the other hand, their low selectivity, which was initially considered a drawback, later became

one of the useful characteristics of chemical sensors for several application fields [6]. In the case of complex chemical environments, where the analytes characterizing the target matrix are numerous, the exploitation of highly selective sensors could be on one hand complicated and on the other detrimental to the analysis. The complication is derived from the fact that it is difficult, and sometimes a tantalising task, to develop highly selective chemical sensors for a large number of analytes, while the inherent drawback is due to the fact that the exploitation of a limited set of sensors could drastically reduce the chemical information contained in the measured environments. However, in this case, nature is a wonderful teacher, because the olfaction and taste receptors, the sensor analogues in these “chemical” perception senses, are not highly selective but are able to interact with almost all the chemical compounds present in the sample matrix, although with different intensities [7]. The attempt to mimic such an approach has led to the development of sensing platforms, based on an array of chemical sensors coupled with a suitable data analysis system, which have been called electronic noses or tongues to underline the attempt to imitate their biological counterparts [8].

While a variety of different transduction mechanisms have been used to develop these arrays, those based on fluorescence have been exploited more recently, although their potentials in terms of sensitivity and selectivity are particularly appealing for these applications.

The field has advanced a lot in the last decade and now several examples of luminescence based cross-reactive sensor arrays have been reported in the literature, for the analysis of both gaseous and liquid phases. Furthermore, the development of consumer electronics has allowed the possibility of using these devices, originally conceived for different applications, to develop optical based sensor arrays. In this chapter we will review the progress of the luminescence based cross reactive sensor arrays reported in this first decade of the new century.

2 Fluorescence Based Sensor Arrays for Gas Detection

2.1 Fibre Optics Sensor Arrays

Walt and coworkers reported the first example of an optical sensor array based on the fluorescence change of a single chromophore, the commercially available Nile Red dye [9, 10]. This fluorophore shows significant shifts in the emission peak depending on the chemical environment wherein the dye is dissolved. Different sensing materials can be obtained by dispersing the Nile Red in polymeric matrices selected in order to modulate the polarity media, so inducing different fluorescence responses of the dye. The good solubility and stability of the Nile Red resulted in a series of sensing materials, which were deposited onto the fibre optic tips. The deposition of the polymeric matrix was performed by photopolymerization or by simple dip coating, depending on the polymer type. The functionalized fibre optics

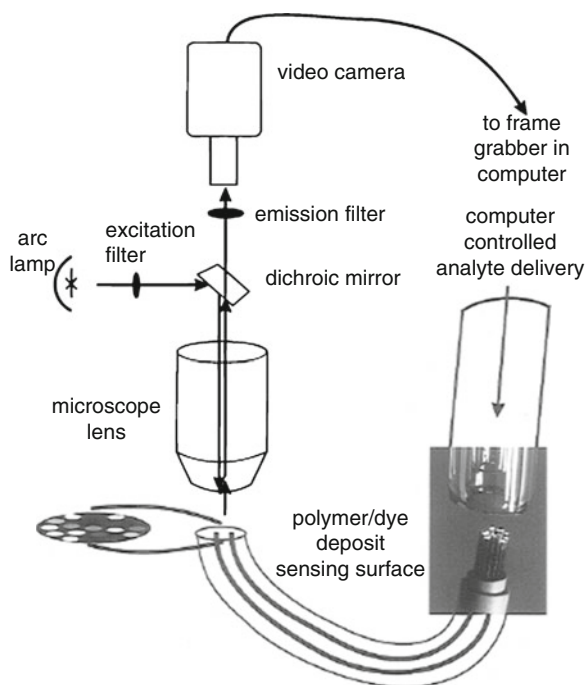


Fig. 1 Set-up of the fibre optic sensor array. Reprinted with permission from [10]

were bundled together and then exposed to the volatile organic compound (VOC) vapours by the sensing apparatus described in Fig. 1. The fluorescence changes were recorded by a CCD video camera; the responses of the individual fibres upon exposure to VOCs showed different shapes in both amplitude and temporal behaviours, depending on both the analyte and the related concentration. The response patterns also depended on other parameters, such as dye concentration, polymer thickness and so on, opening the combinatorial fabrication of a wide range of sensors based on the same dyes. The individual sensors are obviously broadly selective towards chemical species detection, but the complexity of the response patterns contains the information for analyte recognition, achieved by pattern recognition analysis.

Other than the selectivity, the sensors developed showed a sensitivity in the range of hundreds of ppm for the tested analytes, with a variable lifetime, which depended on the polymer composition. Another important problem was the reproducibility of the sensor preparation, which was very low, as expected, in consideration of the various parameters affecting the sensor preparation.

Some important modifications to this sensor array offered a solution to these initial drawbacks. The first was the exploitation of polymer or porous silica microspheres as support for the deposition of the Nile Red fluorescent dye [11, 12]; in the case of polymeric beads, the adsorption of VOCs induced a swelling of the

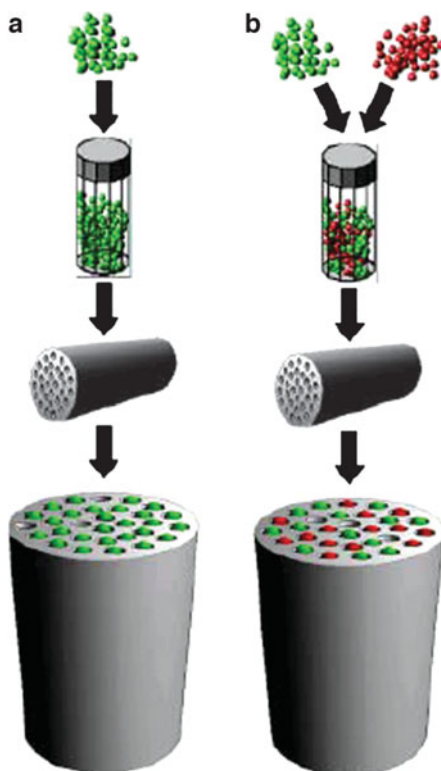


Fig. 2 Preparation of (a) homogeneous and (b) randomized sensor array. Reprinted with permission from [15]

polymeric structure, with a change of the dye chemical environment and a consequent fluorescence variation; the silica microspheres were removed from HPLC columns and they differed with regard to the surface substituents, which resulted in environment of different polarities. These microspheres were stained with Nile Red dyes and their different surface polarity induced different photophysical properties of the chromophore, as observed in the case of polymers. These silica nanoparticles were later chosen for the development of the sensor array, because of the several advantages that allowed significant improvements in sensor performances. The first advantage is related to the high number of individual sensor units obtained using such an approach: each single silica microsphere is in fact a sensor element and in this way it is possible to overcome the reproducible production of sensor units.

These microspheres could be deposited into etched microwells positioned at the distal tip of fibre optics, so allowing the simultaneous imaging of a large number of individual sensing units, also obtaining reproducible responses for those functionalized in the same way (Fig. 2a).

This feature also offered the advantage of obtaining an averaged sensor response, which increases the signal to noise ratio, with a dramatic improvement

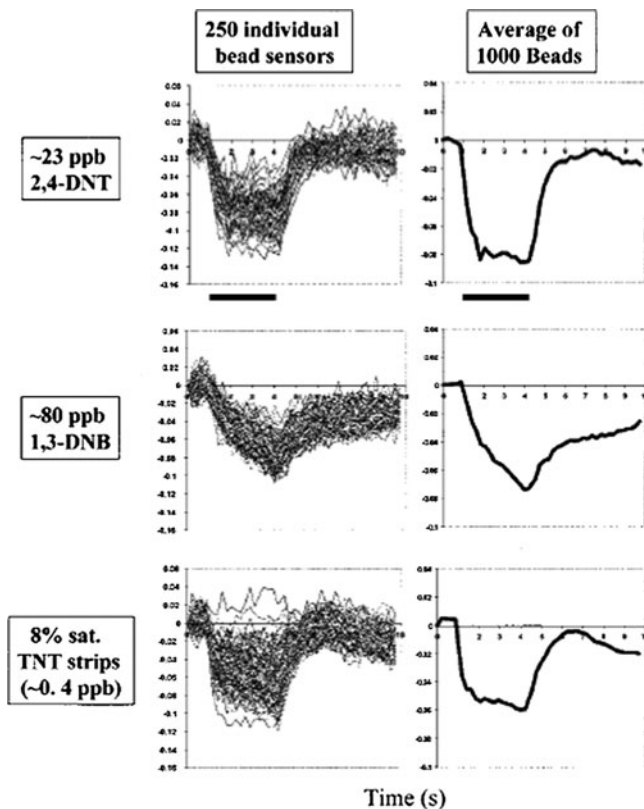


Fig. 3 Comparison of individual and averaged responses for microbead fibre optic sensor array. Reprinted with permission from [12]

of the related sensor detection limits [11, 12]. The functionalities of the developed array were tested in the case of fluorescence detection of analytes simulating explosives, such as dinitrobenzene or even TNT vapours (see Fig. 3) [12]. These compounds are known to be fluorescence quenchers and this property was exploited for the detection of wide ranges of nitroaromatics, as a simulation of explosives. The luminescence sensor array showed promising features for explosive-like vapour detection because of the short response time, the high sensitivities and the reproducible responses obtained.

The reproducible preparation of a large number of sensing elements also opened up their possible exploitation as disposable units, so solving the lifetime problems due to photobleaching of the dye upon illumination [12]. In this case, however, it is necessary to ensure the possible transfer of the training data from the initial array to the new ones; this possibility was proven to be viable by using the discrimination of nitroaromatic compounds in the presence of high concentration of other VOCs as a study case [13]. The training was performed on one array and the data set obtained was then used for two subsequent arrays prepared up to 6 months after the first training. In this case a

correct classification higher than 93% was obtained, giving evidence of the possibility of transferring the training data from one array to others freshly prepared.

The fibre optic sensor array was also tested in a classic electronic nose application, showing the ability to discriminate between pure analytes and more complex odours, such as those of coffee beans [14].

Another important characteristic of these fibre optic luminescent sensor arrays that has been investigated is related to their preparation. The simplest route for the fabrication of fibre optic arrays is related to depositing each fibre with the same kind of functionalized silica microspheres. The sensor array is then obtained with the different fibre optics bundled together and coupled with the microscope imaging system, a CCD detector and the vapour delivery system. Although simple, this approach has inherent complications when the number of different sensing elements increases, due to the decrease in resolution. An interesting alternative is the random deposition of different functionalized silica microspheres onto the same fibre optic (Fig. 2b) [15]. These randomized arrays are of simple preparation, although it is obviously necessary to recognize the different sensors in categories to obtain valuable results for their applications. The optical decoding procedure of course requires that identical sensors should behave in a reproducible way, a requirement that was already demonstrated for silica microspheres. Two different optical decoding methods were possible, supervised or unsupervised, both of them demonstrating that these luminescence based sensor arrays can be positionally registered simply by using the sensor response profiles.

However, the optical decoding of the sensor array was a costly procedure in terms of resources for data analysis. A second procedure explored was related to the exploitation of the collective sensor responses upon VOC exposure, where all the sensor responses were combined to give one signal for analyte [16]. While this approach resulted in a drastic reduction of response data, it did not significantly affect the array discriminant performances, showing that the chemical information was preserved even with the data reduction. Although the decoded sensor array worked better, this simplified data collection showed the possibility of saving time and resources without compromising the array performances.

A common problem of optical sensor arrays is related to the photobleaching of the dyes over time. To investigate the possibility of extending the lifetime of luminescent microsphere sensor arrays, Walt and coworkers followed two different approaches [17]; on the one hand they modulated the excitation light power, with a gradual increase aimed to compensate the dye photobleaching and on the other they illuminated only a section of the array area. The huge number of individual sensing elements and their reproducible properties allowed the exploitation of a limited area of the sensor array without decrease of array performances. This strategy optimized the lifetime of the sensor array, enabling a continuous light exposure for over 160 h. Under operative conditions, the longevity of the sensor array could be predicted to be in the order of the years, by optimizing the array light exposure.

The developed sensing platform was also modified to be exploited for the detection of organophosphate simulant of chemical warfare agents [18]. In this

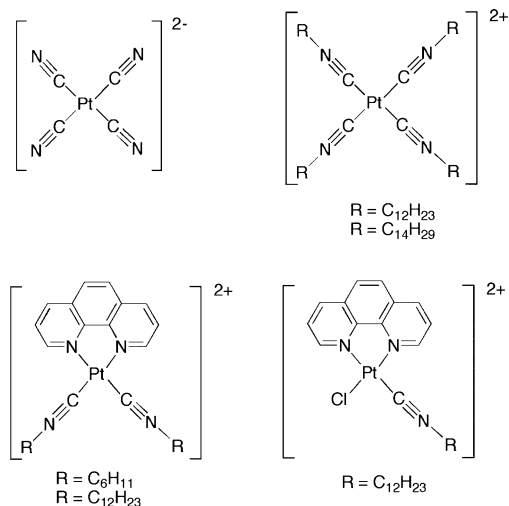


Fig. 4 Molecular structures of vapoluminescent Pt salts

case a different dye was used to obtain the sensitivity towards diethyl chlorophosphate, chosen as reactive simulant of nerve agents such as Sarin or Soman. The same group had already demonstrated that fluoresceinamine, a commercial dye, shows fluorescence turn-on behaviour upon interaction with acyl and phosphoryl halides. Although in this case the interaction is not reversible, this is not a serious drawback for the particular application, where it is important to have a detector signalling the alert for nerve agent detection.

Metal complexes have also been exploited as sensing materials in fluorescence based sensor arrays. Vapoluminescent platinum complexes have been reported in the literature [19]. In these complexes the vapour inclusion induces changes in their optical properties derived from a combination of dielectric constant, hydrogen bonds and expansion or contraction of the crystal lattice variations, which can be exploited in the solid state. Vapoluminescent Pt(II) salts (Fig. 4) were exploited in a three-channel array for the recognition of organic solvent vapours. The device was constructed by using blue-light emitting diodes as a light source, bifurcated fibre optics for transmission and a CCD spectrophotometer as detector; the sensing layers were deposited onto a measurement cell connected to a gas delivering system, where saturated vapours were diluted by mass flow controllers using nitrogen as carrier gas. Ten solvents have been tested and the luminescence spectra obtained upon exposure of diluted vapours to the sensor array were analyzed by PCA, showing good discrimination between the different solvents. Although the array suffered low reversibility and reproducibility responses after solvent vapour exposures, thermal treatment, consisting in a cycle of heating and cooling of the array elements in nitrogen atmosphere, significantly improved the array sensing performances. Significant interference was due to humidity, as expected, due to the salt nature of the Pt(II) complexes.

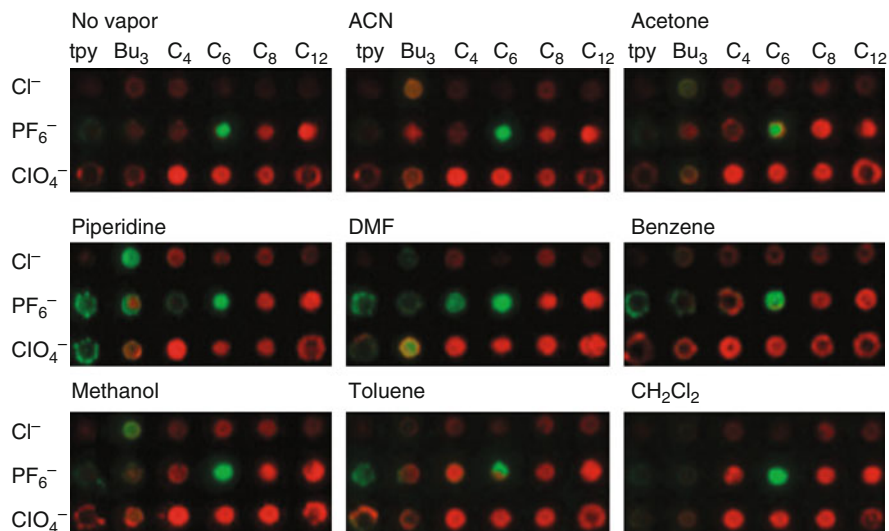


Fig. 5 Response of the Pt(II) terpyridyl complexes sensor array to different VOCs. Reprinted with permission from [20]

2.2 *Micro Arrays*

Pt(II) terpyridyl complexes have been used as sensing materials in cross-reactive sensor arrays and tested for the discrimination of VOCs [20]. In this case Pt(II) complexes were deposited onto microplates and they were imaged before and after VOC exposure by a flatbed scanner. Data analysis of the digitalized images afforded red, green and blue (RGB) pictures, showing the array responses to the different VOCs (Fig. 5). A different pattern related to the particular VOC was clearly evident. The interaction was reversible, although freshly prepared microplates were used for each solvent test. Both colorimetric and luminometric variations were used for the analyte discrimination. The luminescence properties strongly depended on the Pt(II) terpyridyl counter ion, with the chloride salts the least emissive of the compounds tested.

The combinatorial possibility to synthesize a large number of different receptors based on DNA structure has been exploited for the development of luminescent-based sensor arrays [21]. In this case DNA is particularly attractive, because it offers the stability and the versatility as a biopolymer to allow the preparation of a wide range of different structures, which can also be tailored to the particular application. The DNA structure should be functionalized with a fluorescent dye, which acts as the unit signalling the interaction with the analyte. Initially both single and double stranded DNAs have been tested for sensing application, but only the single-stranded DNAs showed different responses to the VOCs tested, which can be related to the DNA sequences exploited. In these preliminary studies DNA oligomers were first stained in solution with two different dyes, both of them

commercially available, before spotting and drying the receptor onto a solid substrate. To investigate better the sensing performances of DNA based receptors, labelled oligonucleotides were synthesized with the fluorescent dye Cy3 covalently attached to the 5' end. These Cy3-labelled oligonucleotides were spotted onto cover slips and inserted into a measurement chamber to be exposed to VOCs. Filtered LEDs were used as light sources and photodiodes as detectors of the developed sensor arrays: VOC vapours were injected into the measurement chamber by a syringe and the fluorescence changes of the different DNA spots were recorded. The result obtained showed that, in the solid state, DNA sequences were able to interact with the different analytes in different ways, confirming their suitability for sensor array applications. It is interesting to note that a wide library of cross-reactive receptors can be obtained with these DNA based sensors, which differ from other nucleotide based sensing materials, such as aptamers. Aptamers, in fact, are selected to optimize highly selective interaction with target analytes, while these DNA sensing materials are broadly selective, as requested for electronic nose applications.

A chemical nose dedicated to the detection of alkylating agents has been reported in the literature [22]. These compounds are interesting for practical applications because they are used as chemical warfare agents and the detection mechanism exploited is based on the fluorescence changes that π -conjugated oligomers (or polymers) undergo upon interaction with alkylating agent vapours. The recognition of the different analytes was based on the response pattern of an array of fluorophores, although in this case we should talk in terms of detectors and not of sensors, because the interaction is not reversible. A simple seven spot chemical nose was able to discriminate between a series of different alkylating agents, showing saturation at very low concentrations, lower than 50 ppb.

2.3 Computer Screen Photoassisted Technique

The advantages of optical sensor arrays may be badly balanced by the fact that standard image sensors of high quality are usually bulky and expensive. On the other hand, in the last decade we have seen a fast growth of performance in fields such as consumer electronics, giving rise to a range of low-cost advanced optical equipment such as digital scanners, cameras and screens whose characteristics largely fit the requirements necessary to capture changes in optical properties of sensitive layers in many practical applications.

Digital cameras and flatbed scanners are devices for colour measurement. Colour is the human visual perception of a narrow bandwidth of the electromagnetic radiation spectrum, approximately between 400 and 700 nm. Human sight is founded on three wide-band detectors whose action provides a synthesis of the incoming radiation spectrum into three colour channels corresponding to the primary colours red, green and blue. The spectral sensitivity of human sight detectors can be technically reproduced and devices able to provide a digital measure of colour are available and, besides the obvious use in photography, they

are found as embedded in a number of worldwide diffused devices such as portable computers and mobile phones.

The measuring of colour, if compared with the spectra measured by a spectrophotometer, is expected to be highly ambiguous, in the sense that different spectra can give rise to the same triplet of primary colour (metamerism). Nonetheless, Suslick and his coworkers demonstrated that simple and inexpensive devices, such as digital scanners, can capture the subtle changes occurring in dye indicators when they are exposed to guest molecules either in air or in liquid. The application of conventional image processing tools (such as Adobe Photoshop[®]) amplifies these colour changes and their differences are made visible in an appealing colour code [23–25]. The analytical properties of digital flatbed scanners were also demonstrated for biological investigation such as the detection of DNA hybridization in a DNA array replacing the fluorophore with gold nanoparticles colour indicators [26]. Besides scanners, the optical properties of DVD or CD drives have also been investigated, considering that a CD drive is based on a laser diode and a photodetector scanning the CD-ROM surface with high spatial resolution [27].

In contrast to traditional instrumentation approaches, regular consumer optoelectronic devices transformed into measuring platforms are affordable alternatives that are being increasingly explored. A non-negligible added value behind this approach is that successful sensing applications can be as pervasive as the devices supporting them.

All the systems described so far are characterized by a fixed light source, for instance in a digital scanner a fluorescence light source produces the “white” light that is used to illuminate the sample.

The trivial observation that computer monitors can be programmed to display millions of different colours has led to the development of an experimental technique based on the simultaneous use of a standard computer screen as a controlled light source, and a digital camera, such as a web camera, as an imaging detector for the evaluation of diverse optical properties of chemically sensitive substances. The first demonstration of this concept was published back in 2003 [28], and the technique was nicknamed as Computer Screen Photo-assisted Technique (CSPT).

Currently most computer screens are liquid crystal displays (LCD). The screen illumination unit controlled by the computer is a pixel, and in an LCD screen each cell of the screen contains a liquid crystal between two crossed linear polarizers. If a voltage is applied to the cell the liquid crystals rotate the direction of polarization of the light, allowing the regulation of the intensity escaping from the second polarizer. A large area white backlight completes the screen. Colour screens are produced by the repetition of groups of cells with RGB filters. These filters are band limited emitters of visible light corresponding to the perception of RGB colours ($R(\lambda)$, $G(\lambda)$ and $B(\lambda)$). Since the size of the three emitting regions is smaller than the eye’s spatial resolution, the emitted radiance is perceived as the sum of the primaries [29]. Any other colour can be composed by the weighted combination of these screen primary spectral radiances according to

$$c_i(\lambda) = r_i R(\lambda) + g_i G(\lambda) + b_i B(\lambda),$$

where $c_i(\lambda)$ is the spectral radiance of any particular colour i , defined by the triplet of weights $\{r_i, g_i, b_i\}$. Conventional true colour displays, have a resolution of 8 bits (0–255 values) for each colour channel.

With respect to conventional illumination sources, computer screens can be used as large area light sources [30], illuminating entire assays at the same time, such as in the case of microtiterplates [31]. Furthermore, one of the most useful features of the screens, regarding CSPT determinations, is the possibility of modulating the spectral composition of the illumination, highlighting spectral features of tested substances. In particular, if fluorescence is excited at wavelengths greater than 400 nm, the computer screen can be used as a light source in fluorescence measurement. More interestingly, it has been demonstrated that a polychromatic light source, such as a computer screen, can efficiently replace the usual monochromator in excitation emission matrix (EEM) spectroscopy [32]. EEM is a valuable method providing highly distinctive signatures of fluorescent substances and it is also a powerful method for the analysis of complex mixtures [33].

Computer screens as light sources are naturally complemented by image detectors. Web cameras are perhaps the most affordable colour-imaging devices, and are still representative of a number of other digital imaging recorders. They use imaging detectors that can be either based in CMOS sensors or charge-coupled devices (CCD sensors) [34]. Typical spatial resolutions are 640 pixels \times 480 pixels but also allowing different sub-resolutions, and 8 bits intensity levels. Then 24 bits colour resolutions are obtained by filtering the light that reaches the detector in three partially overlapped bands, corresponding to the perception of RGB colours.

The implementation of these filters consists of a checker pattern where some image elements have a red filter, others green and others blue. They are arranged in a repetitive pattern (Bayer filter) with 50% of the elements covered by green filters and the other 50% equally covered by red and blue areas. Accordingly, the spatial resolution in colour mode is lower than that of the image detector, and the reported result of each pixel is the average of neighbours (demosaicing algorithms) [35].

In CSPT spectral fingerprinting experiments, part of the computer screen is used as a light source displaying a sequence of colours that illuminate a target substance, while the web camera captures the image of the substance under these particular illuminations.

One of the most interesting features of CSPT is the separation of absorption and emission phenomena. This capability is based on the wavelength profile of the three filters defining the red, green and blue colours. Indeed, these are partially overlapped, and red and blue channels are completely separated in wavelength by a band gap of about 50 nm centred approximately at 550 nm [36]. Intuitively, excitations occurring at wavelengths between 400 nm and 500 nm and emissions at wavelengths between 600 nm and 700 nm can be easily detected illuminating the sample with the screen showing a full a blue colour and reading the signal of the camera red channel.

A proper modulation of the screen colour can capture the fluorescence even in more subtle cases when excitation and emission do not fall in separate colour channels. A thorough calculation of the relationship between Excitation Emission

Matrix and CSPT fingerprint is available, providing the means to evaluate the applicability of CSPT to measure fluorescence of spectrally characterized compounds [37].

A first example of the sensing capabilities of CSPT was provided considering an array of sensing spots on a glass slide. The sensing materials in this example were two metalloporphyrins complexes (zinc and iron), and biladiene. They were blended with PVC and spotted on a glass slide placed in between the optical path connecting the computer screen with the web camera [38].

Upon exposure to controlled concentrations in gas nitrogen of NH_3 , NO_x , CO and triethylamine (TEA), distinctive optical changes in the absorption and emission spectra of these substances can be captured and identified using CSPT. In these experiments, part of the screen displays a sequence of 50 colours, from violet to red, at a rate of 1 colour/s with the web camera in synchronism with the illumination. In order to illustrate the principle of measurement the case of a layer of biladiene exposed to 750 ppm of triethylamine is discussed here. Biladienes are linear tetrapyrroles usually met in the synthetic pathway to porphyrinoids. The interest in using these molecules as a chemical indicator is their colour signature that is related to the degree of protonation from red (dication), to orange (monocation) and finally to green (neutral free base) [39]. The molecular structure of the biladiene used is shown in Fig. 6a, this particular compound having been previously synthesised as an intermediate step for corrole preparation [40]. Figure 6b shows the indicator spots on the glass substrate; in the same figure, two regions of interests (ROI) are indicated. They are centred on the biladiene spot and on a nearby free glass region used as a reference background. The average intensities of all pixels within each ROI (~ 150 pixels), are collected along the different illumination sequences, resulting in an intensity profile in the RGB camera channels for each ROI and measuring condition. The intensity profiles of the ROIs are composed by concatenating the RGB signals. Finally, the fingerprint for the indicator is calculated by subtracting the intensity profile of the background (ROI 2) and the indicator (ROI 1).

Figure 6c shows the fingerprints of the biladiene spot measured during the exposure to pure nitrogen gas and after the addition of 750 ppm of vapours of triethylamine. It is worth observing that, during the exposure to pure nitrogen gas, two negative peaks are visible in the red channel. A negative value of the fingerprint indicates that in correspondence of that illumination the red component of the light collected through the indicator is larger than the red component emitted by the computer screen. This phenomenon is attributed to the biladiene fluorescence excited by the blue component of the screen light. This feature disappears during the exposure to triethylamine as a result of the quenching effect of triethylamine on biladiene, as observed with a standard spectrofluorimeter.

A comparison of fingerprints illustrates the colour change with an increase of absorbance in correspondence of the red channel and a decrease of absorbance in green and blue channels. This behaviour reveals the colour transition of biladiene due to the change of protonation state as previously discussed.

Finally, in Fig. 6d the difference between the fingerprints recorded during the exposure to reference and reference plus triethylamine is shown.

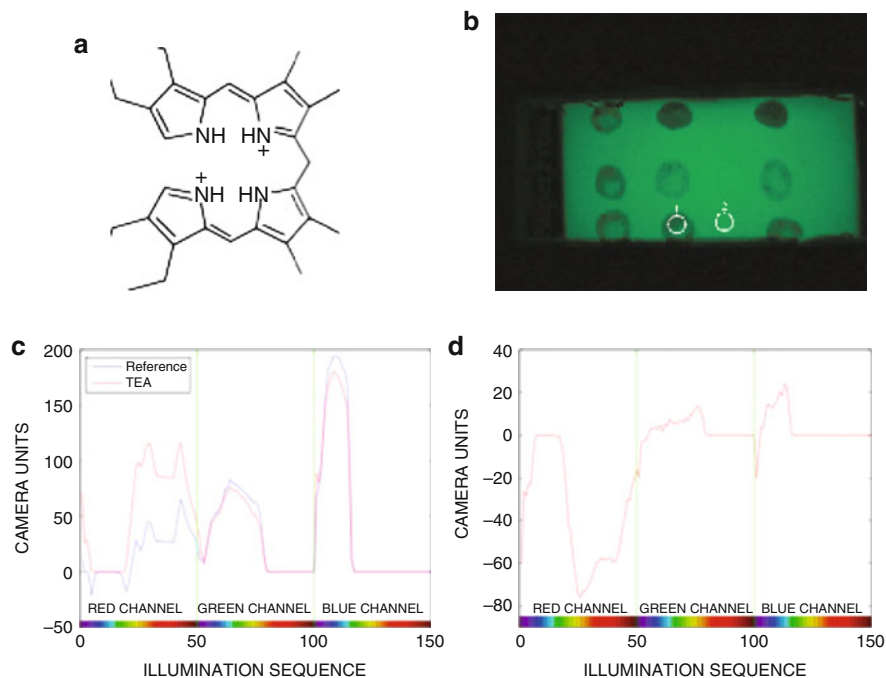


Fig. 6 Example of application of CSPT as a transducer for chemical sensor. **(a)** Sensing molecule: 1,19-dideoxy-2,3,17,18-tetraethyl-7,8,12,13-tetramethyl-*a,c*-biladiene. **(b)** Image of the sensing molecules spotted on a glass slide. *Circles* indicate the region of interest (ROI) considered in this example. ROI 1 is the biladiene spot and ROI 2 is a bare glass region used as reference. **(c)** Biladiene CSPT fingerprint measured in a reference internal gas (nitrogen) and after the addition of 750 ppm of triethylamine (TEA). Noteworthy, the negative portion of the fingerprint captures the fluorescence of biladiene; this feature, present in the reference fingerprint, disappears during the exposure to TEA as a consequence of the quenching effect of this molecule on biladiene. **(d)** The difference between the fingerprints of Fig. 6c puts in evidence the colours at which the largest response can be observed. This information may be used to optimize the illumination sequence

The nature of CSPT arrangement to measure simultaneously the optical properties of a number of indicators makes this system particularly suitable for the development of artificial olfaction and an indicator arrangement similar to that shown in Fig. 6b was used, for instance, to study the freshness decay of fish [41]. More interestingly, CSPT offers the opportunity to reconsider the work of Walt and Kauer that used optical imaging as a mean to obtain arrays of hundreds of sensors. On this basis, an artificial olfaction system based on the imaging of a continuous layer of chemical indicators was recently introduced [42]. In this situation, an image sensor provides a segmentation of the whole sensing layer in a number of elementary units corresponding to the pixels of the image. Eventually, since it is possible to evaluate the optical properties of every single pixel, each pixel of the image may correspond to an individual sensor. In this regard, even low-resolution images may easily result in thousands of independent sensing units.

In this system, a collection of arbitrarily shaped regions of colour indicators is illuminated by a controlled source; the optical characteristics of each pixel of the image are measured by a camera providing the intensity of light in the three channels: red, green and blue. The combination of illumination sequence and camera read-out results in a fingerprint encoding the optical properties of the sensing layer portioned in image pixels. A simple classification of these fingerprints assigns each pixel to a class, and each class contains pixels carrying the same colour indicator. This arrangement resembles the association between olfactory receptor neurons carrying the same chemical receptor into the same glomerulus [43]. On the basis of this analogy it is straightforward to describe the layer of indicators as an artificial epithelium, pixels of the image as artificial olfactory neurons and the classes provided by the classifier as an abstract representation of artificial glomeruli.

Furthermore, in this system it is also possible to follow the dynamic diffusion of airborne molecules through the sensing layer, giving rise to spatio-temporal response patterns resembling those observed in the olfaction of animal models. This feature can be adequately exploited to develop a sort of artificial olfactory mucosa [44].

Finally, the surprising sensitivity of CSPT based sensors when compared with the performance of the most common transducers used as chemical sensors must be commented upon. For instance, with a standard CSPT set up, the minimum detectable amount of triethylamine absorbed in a layer of Zn-TPP is 33 femtomoles per pixel; the correspondent value for the same sensing layer on a 20-MHz Quartz Microbalance is about 5 picomoles [45]. In this regard, a caveat is necessary to indicate that these figures are the resolution in terms of absorbed mass and not in terms of the concentration in air and that this also turns out to depend on the active sensor area.

3 Fluorescence Arrays for Analytes in Solution

3.1 Cation Sensing

The rational design of fluorescent sensor arrays for the detection of ions in aqueous solution relies on the addressed utilisation of conjugated chromophores (fluorophores), linked to a recognition site (selective receptor). The binding step results in a change of the fluorescence state (ON or OFF, or variation of the intensity) of the fluorophore reporter, so signalling the detection event [46, 47].

These systems are of striking importance for the detection of water contaminants, either from natural or anthropogenic sources, such as heavy metal ions and likes. This approach has been successfully exploited for the detection of anions, a difficult task to be accomplished in water, with a high degree of selectivity.

In this section, some fluorescent systems based on sensor arrays, particularly addressed to the detection of these ions, will be presented.

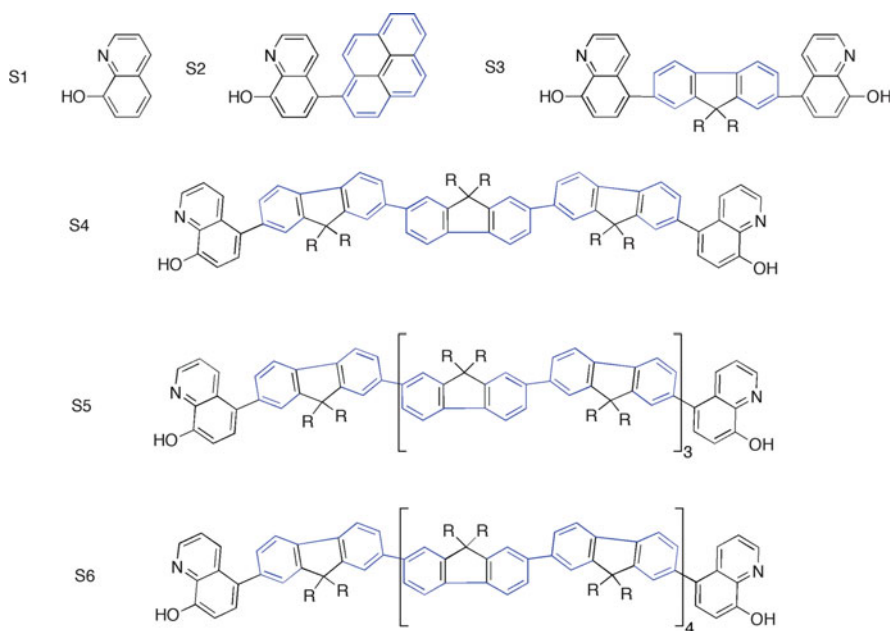


Fig. 7 Structures of the sensing materials based on 8HQs. R = *rac*-2-ethylhexyl, R' = *n*-hexyl. The extended conjugated chromophores are shown in blue

In this regard, Anzenbacher and coworkers reported on the realization of a simple system constituted by an 8-hydroxyquinoline receptor (8HQ, Fig. 7) coupled to a conjugated fluorophore, a pyrene or a fluorene derivative, emitting in the blue region [48].

The 8HQ unit does not show appreciable emission above 300 nm. Its emission can be turned on by cation coordination of the quinolinolate form. Importantly, the relative contribution of the two “emitters” to the fluorescence output (quantum yield, intensity and wavelength maximum) is dependent on the type of interacting ion, in terms of electropositivity, spin–orbit coupling and excitation wavelength, as indicated in Fig. 8. This allows for discrimination with high accuracy between complex mixtures, constituted by up to ten species, namely Ca^{2+} , Mg^{2+} , Cd^{2+} , Hg^{2+} , Co^{2+} , Zn^{2+} , Cu^{2+} , Ni^{2+} , Al^{3+} and Ga^{3+} , by the usual principal component and linear discriminating analysis (PCA, and LDA).

The same approach has been extended to the successful identification of commercial soft drinks. The selectivity toward different ions can be modulated by changing the nature of the “turning-on” chromophores, so realizing a system for useful application for discriminating between different mineral water brands [49].

Recently, David Reinhoudt and coworkers prepared a sensor array, based on the deposition of fluorescent self-assembled monolayers (SAMs) on glass, for the detection of several ions [50]. The ease of preparation, due to the preorganisation of the receptor molecules induced by the surface, allowed for a combinatorial

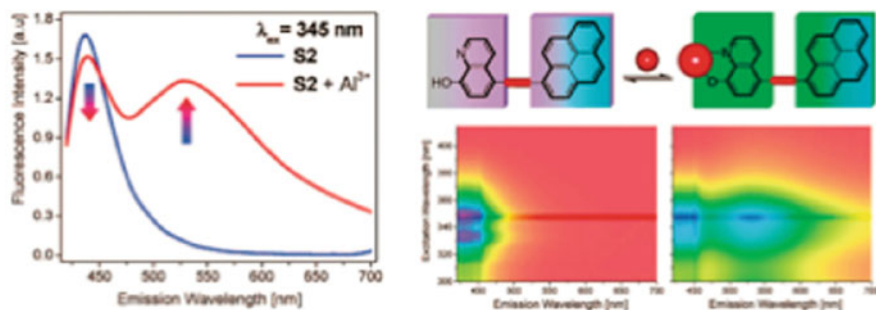


Fig. 8 Fluorescence spectra (*left*) and fluorescence ratiometric response of Al³⁺-S2 quinolinate complex (*right*). Reprinted with permission from [48]

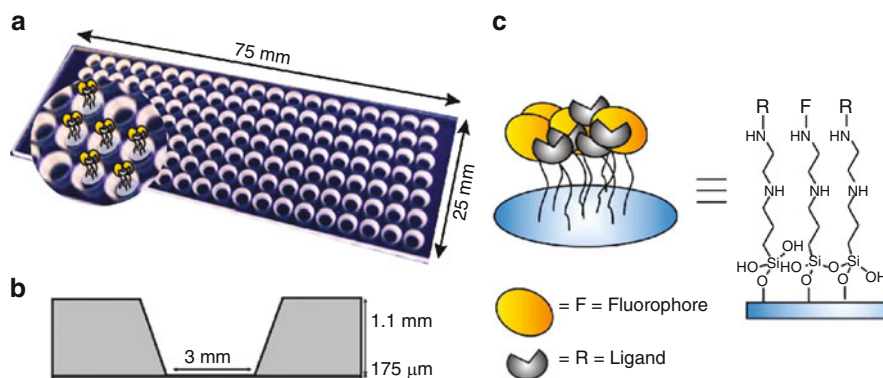


Fig. 9 (a) Picture of the 140 well glass microtiter plate (MTP) with a schematic representation of the well substitution (enlargement). Schematic representation of (b) single MTP well and (c) SAM formed in each well of MTP. Reprinted with permission from [50]

approach to sensing systems. This technique relies on the random sequential attachment of different fluorophores and ligands on a SAM on glass. This results in a close proximity of these effectors, for an efficient receptor (ligand) to signalling unit (fluorophore) communication (i.e. modulation of the emission intensity). The intrinsic feasibility of SAM's preparation, jointly with their high response rates, renders their use preferable to, for example, that of polymer-based optical sensors, which, although featuring a higher degree of sensitivity, are often characterised by a low physical and chemical permeability, and slow response time.

The sensing arrays were prepared by parallel synthesis of aminoterminated SAMs on glass, functionalised by different fluorophores, rhodamine derivatives (Fig. 9).

The library was confined to a microtiter plate, and was exploited for the detection of various metal ions such as Cu²⁺, Co²⁺, Ca²⁺, Pb²⁺ and Zn²⁺.

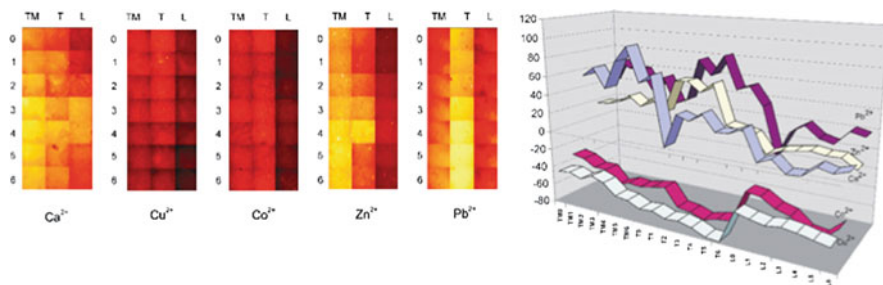


Fig. 10 *Left*: Fluorescence microscopy images of MTP walls after incubation with selected ions (10^{-4} M, MeCN). Each *square* represents an individual signal of the whole response pattern arrays. *Right*: Plot of the normalised fluorescence emission intensity changes in each sensing system of the arrays upon metal ion complexation. Negative values indicate a quenching of fluorescence, while positive values indicate increase of fluorescence intensity. Reprinted with permission from [50]

The microarrays produced a fingerprint type response, characteristic for each investigated analyte (Fig. 10).

A related microarray system, based on a microtiter plate containing proper fluorescent indicators, was formerly reported [51, 52]. With this simple system an efficient analysis of mixtures of ions (e.g. Ca^{2+} , Na^+ , Mg^{2+} , Hg^{2+} , SO_4^{2-} and Cl^-) has been carried out. The procedure followed entailed the excitation of the fluorophores (indicator) by an LED source ($\lambda_{\text{max}} \approx 470$ nm). The presence of ions varied the emission responses with respect to those of the reference solutions. The analyses were accomplished by quantitative imaging of the emission patterns by using a Charge Coupled Device (CCD) camera. The unselective responses of the indicators have been analysed by chemometric tools, based on their time-dependent decays (dual lifetime referencing process). The CCD has been widely used in analytical chemistry as it represents a useful tool for simultaneous detection, with fast image capturing, along with stable background, and consequent high S/N ratio and good linearity (for a recent example see [53]).

Ruiz-Molina and Maspoch reported on the construction of pH responsive fluorescent nanoarrays by Dip-Pen nanolithography (DPN) [54]. This technique has emerged among other related techniques owing to the capacity of direct structuring of a wide range of highly ordered arrays of substances on surfaces, on a nanometric scale and with excellent resolution [55]. The authors chose fluorescein as a pH-dependent probe, as it presents negligible quantum yield under acidic condition ($\phi^f \approx 0$, $\text{pH} < 4$), but it features high fluorescence intensities under alkaline conditions ($\phi^f \approx 1$, $\text{pH} > 8$). Fluorescein-based nanoarrays were fabricated by direct-write DPN, and the obtained systems were exploited as pH-sensors, upon exposition to environments of different acidity. The direct-write procedure consisted of the patterning of a surface by commercially available nano-pen array, with the aid of Atomic Force Microscopy (AFM) devices, by traversing the tips over the chosen surface, and by tuning the contact time, to form the desired pattern. The optical imaging was subsequently acquired, by using a confocal scanning fluorescence microscope.

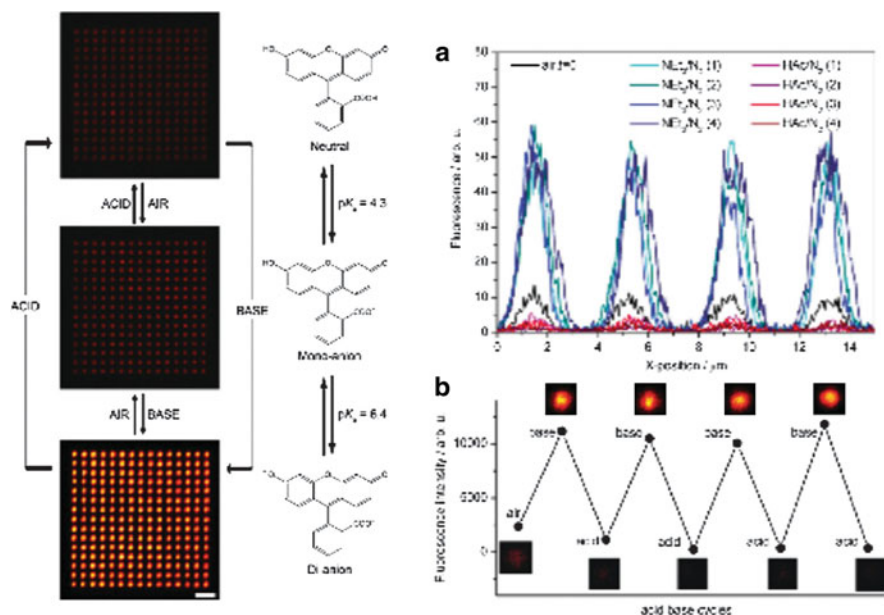


Fig. 11 *Left*: Confocal fluorescence microscopy images of fluorescein dot array (15×15 dots, $30 \mu\text{m} \times 30 \mu\text{m}$, *scale bar* = $4 \mu\text{m}$) showing emission changes (λ_{exc} 532 nm; $I_{\text{min}} = 0$ kilocounts s^{-1} ; $I_{\text{max}} = 600$ kilocounts s^{-1}) upon pH variation (pH ≈ 4 , *top*; pH ≈ 6 , *middle*; pH ≈ 12 , *bottom*). Chemical structures indicate predominant molecular forms at corresponding pH range. *Right*: Mean intensity cross-section of the fluorescence images (λ_{exc} 532 nm) exposed to four consecutive acid-base cycles (a). Reversible averaged emission profiles upon pH variation (b). Reprinted with permission from [54]

The protonated-deprotonated form of fluorescein was generated by exposing the samples to acid/ N_2 or amine/ N_2 gas flows. Figure 11 depicts the most important topics of the system.

Capitán-Vallvey and coworkers reported on a multisensor system based on ionophore-chromionophore for optical monitoring of potassium, magnesium ions and hardness of waters [56]. The analytical procedure relies on the use of a black and white CCD camera. In optimised experimental conditions the procedure applied gave a large linear concentration range, up to six orders of magnitude, and good detection limits. Moreover, the protocol has been successfully applied to real systems, such as natural water and beverages of different origins.

Crego-Calama et al. reported on the construction of a new type of sensor array based on a microfluidic chip (Fig. 12) [57]. This technique has recently been developed and exploited in broad analytical applications [58] and clinical diagnostics [59], as it provides convenient small platforms, and usually requires small sample volumes, in a continuous flow, for real-time measurements. In particular the authors developed a microfluidic chip, with the microchannel walls combinatorial-based functionalised by SAMs of five fluorescence-responsive receptors, as schematically depicted in Fig. 7. The detection of analytes, namely Ca^{2+} and Cu^{2+} , has

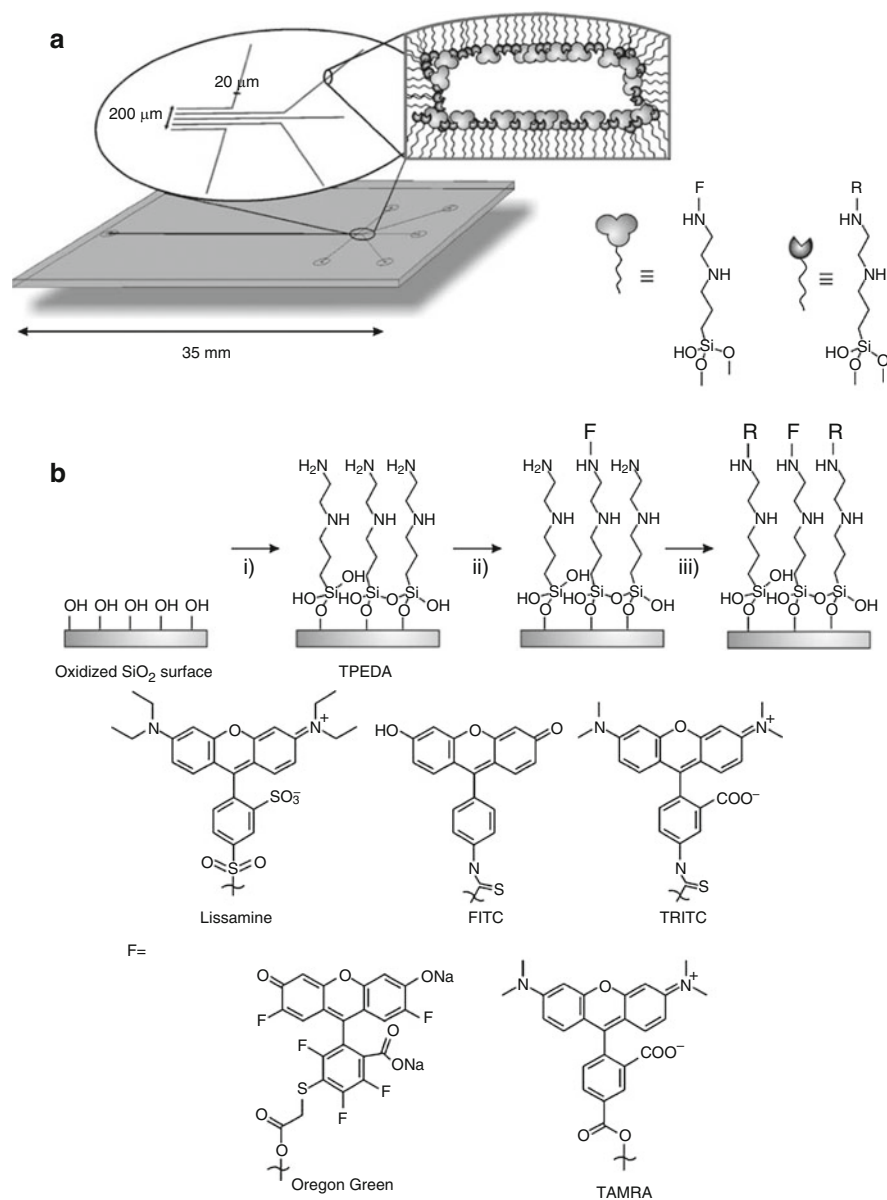


Fig. 12 (a) Schematic representation of five-channel chip and the channel walls functionalised with fluorescence SAM. (b) Schematic procedure applied for the functionalisation of the walls of the microchannels, and chemical structures of the fluorophores employed (F) in the studies. Reprinted with permission from [57]

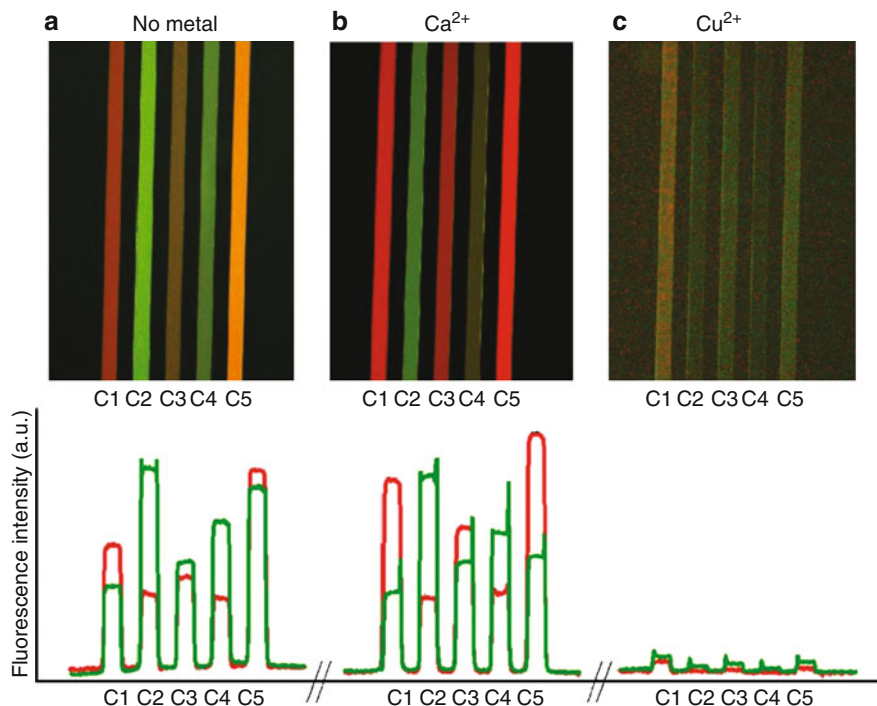


Fig. 13 *Top*: Overlay image of the multichannel chip with an array of five different sensing fluorescent sensing reporters filled with: (a) MeCN, (b) Ca²⁺ (perchlorate salt 10⁻⁴ M in MeCN), (c) Cu²⁺ (perchlorate salt 10⁻⁴ M in MeCN). *Bottom*: Corresponding fluorescence intensity profiles. *Red and green traces* correspond to the above imaged *red and green channel*, respectively. Reprinted with permission from [57]

been performed by fluorescence microscopy based apparatus, equipped with a CCD camera. The characteristic fluorescence responses have been reported in Fig. 13.

Mesoporous silicas have been widely employed as supporting material for optical sensors due to their high porosity, large surface area, robustness and facile preparation and functionalisation [60, 61]. A fluorescent sensor array, based on ion-imprinted mesoporous silica, has been developed by Yan and coworkers [62].

The imprinted materials were prepared via a co-condensation method with aminopropyltriethoxysilane (TEOS), and monomers containing 8-hydroxyquinoline (8-HQ) moieties, in the presence of proper metal ion (Zn²⁺ or Cd²⁺).

The presence of the ions is necessary to freeze the embedded fluorophores in a favourable “frozen” proximal arrangement. The system was assayed as reporter fluorophores for the above cations in water, and compared to those prepared in the absence of metal ions, which present a random (non-templated) fluorophore distribution.

The binding of cations caused an increase of the emission of the fluorophores, as reported in Fig. 14.

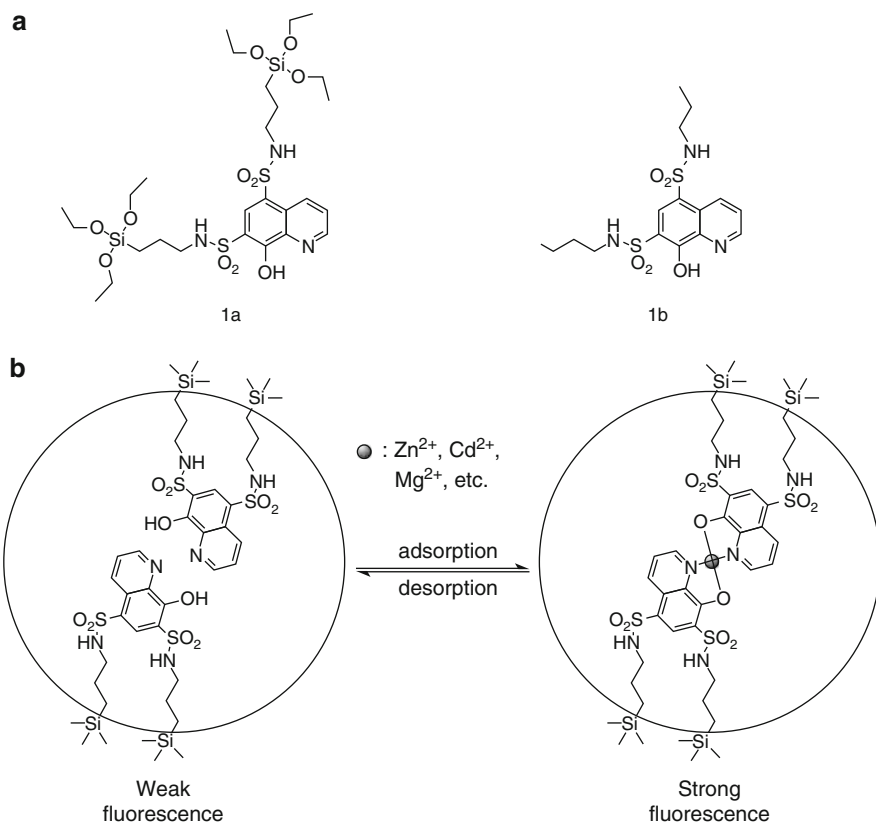


Fig. 14 (a) Molecular structures of receptors employed in the work. (b) Schematic representation of fluorescent ion-imprinted mesoporous silica. Reprinted with permission from [62]

A sensor array was composed by assembling three different sensors consisting of Zn-, Cd- and non-imprinted materials, and it allowed for discrimination of the title ions, within the range of 10–100 μM concentration, against non-templated ions such as Mg²⁺, Ca²⁺ and Al³⁺. The principal component analysis (PCA) showed a clear discriminative and reproducible pattern (Fig. 15).

A prototype device based on concomitant photo- and ion-sensing was realised by Sawada and coworkers [63]. In this system a photo-sensor is fused with an ion-sensor allowing simultaneous detection of photo-signals and ion density in the same chosen area. The sensing region is composed by layers of Si₃N₄ and SiO₂, on a p-type Si substrate. The photo-sensing is based on a fluorescence sensitive detector. The system offers attractive features for possible application in bio-imaging.

A sensor array, in which a single entity acts as both host and indicator for several metal ions, has been produced by Anslyn and coworkers [64]. The system, a chemodosimeter, is based on a squaraine derivative as a signalling unit. Squaraines (SQ) are a class of zwitterionic dyes, in which a central squaric acid ring is

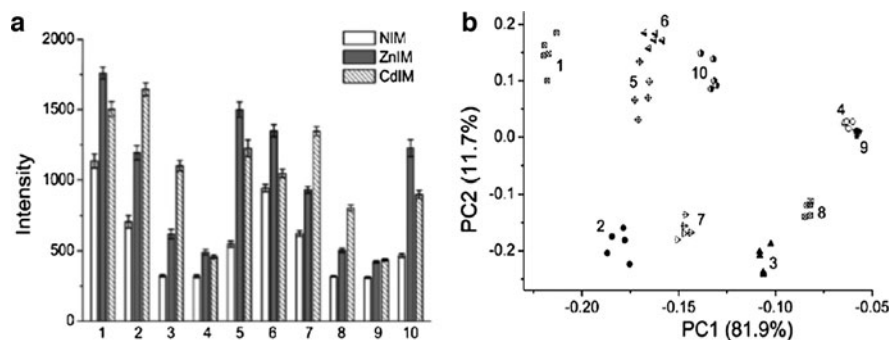


Fig. 15 (a) Plot of fluorescence intensity responses ($\lambda_{\text{exc}} = 340 \text{ nm}$) of an array composed of NIM, ZnIM and CdIM to five metal ions at two different concentrations, tested in five replicates. (b) Corresponding two-dimensional PCA plot of the above array. Metal ions: (1) $\text{Zn}^{2+} 10^{-4} \text{ M}$; (2) $\text{Cd}^{2+} 10^{-4} \text{ M}$; (3) $\text{Mg}^{2+} 10^{-4} \text{ M}$; (4) $\text{Ca}^{2+} 10^{-4} \text{ M}$; (5) $\text{Al}^{3+} 10^{-4} \text{ M}$; (6) $\text{Zn}^{2+} 5 \times 10^{-5} \text{ M}$; (7) $\text{Cd}^{2+} 5 \times 10^{-5} \text{ M}$; (8) $\text{Mg}^{2+} 5 \times 10^{-5} \text{ M}$; (9) $\text{Ca}^{2+} 5 \times 10^{-5} \text{ M}$; (10) $\text{Al}^{3+} 5 \times 10^{-5} \text{ M}$. Reprinted with permission from [62]

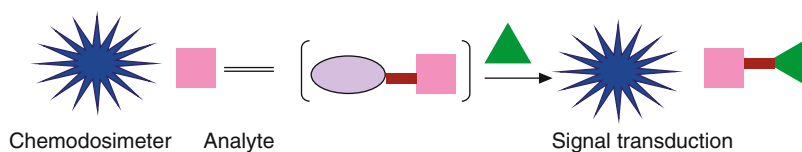


Fig. 16 Schematic representation of the chemodosimeter function. *Blue star*: receptor with *blue colour*; *pink square*: thiol; *green triangle*: metal ion. Reprinted with permission from [64]

stabilised by resonance with two aniline units in a donor-acceptor-donor arrangement (D-A-D). These molecules are strongly fluorescent, and the intensities can be effectively chemically changed. In the specific case, the emission of the moiety is quenched upon covalent linking to a thiol group (a pink box showed in the Fig. 16). The interaction with a metal ion (green triangle) restores the initial fluorescence emission, restoring the “unthiolated” SQ form, according to the scheme reported in Fig. 17.

Palladium, mercury, copper and iron were chosen in the construction of an array, differing in degree of thiophilicity. An array system consisting in SQ, the five different thiols, and the title ions in DMSO, was arranged in a 96-well plate, and the change of emission intensity was recorded and analysed by PCA. A good differentiation between the ions investigated was achieved with ACM group, as shown in Fig. 18.

A related thiol- functionalised rhodamine-based chemodosimeter selective for Cu^{2+} ions, and with promising exploitation in microarray devices, has been recently proposed by Kim and coworkers [65].

The Cu-sensing mechanism is based on structural changes of the rhodamine derivative, i.e. spirolactam (OFF) to open ring (ON) form, upon ion coordination (Fig. 19).

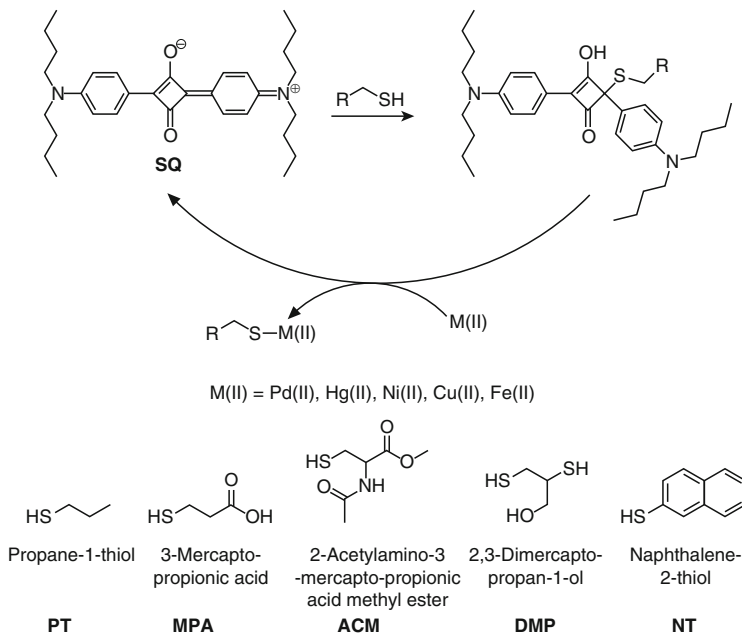


Fig. 17 Molecular structures of the detected thiols. Reprinted with permission from [64]

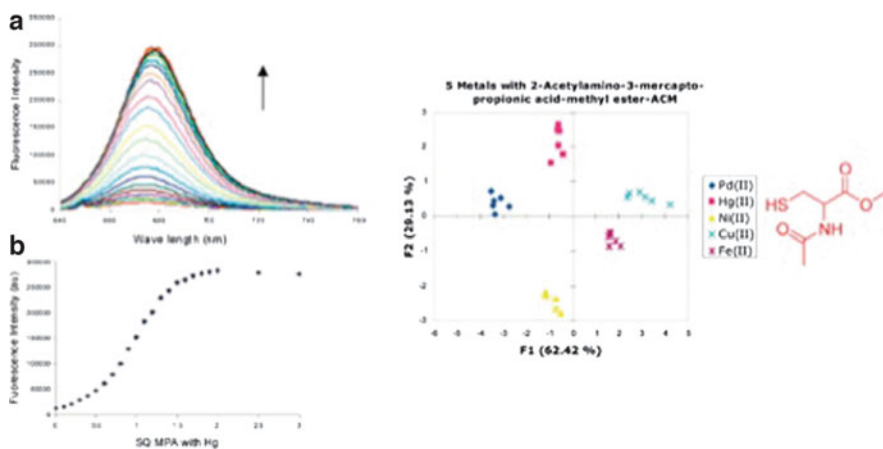


Fig. 18 *Left*: Fluorescence spectral pattern changes (a), and corresponding binding isotherm (b) of titration of a solution of $Hg(OAc)_2$ 4×10^{-5} M in DMSO into a solution of SQ/MPA complex 2×10^{-6} M in DMSO. *Right*: Pattern-based recognition of five metals with 2-acetylamino-3-mercapto-propionic acid methyl ester. Reprinted with permission from [64]

The sensing material consists of a SAM immobilised on platinum by simple dipping the solid substrate into a proper solution of receptors. The use of platinum circumvents the problem arising from the use of other metal surfaces, such as Au,

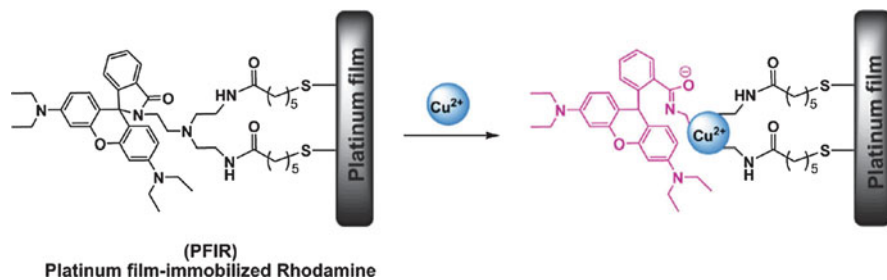


Fig. 19 Pt film-immobilised rhodamine system for Cu^{2+} -induced ring-opening of spirolactam. Reprinted with permission from [65]

which usually act as quenchers, hampering the efficiency of the systems. The ultrathin Pt layer (10 nm thickness) was prepared by argon sputtering on glass slides as solid inert supports. Fluorescence images (emission wavelength at 573 nm) were obtained via confocal laser-scanning microscopy, at an excitation wavelength of 488 nm.

3.2 Anion Sensing

The quest for sensor devices for selective detection of anions is a more challenging task, with respect to the recognition of cations, due to their peculiar physico-chemical properties [66]. For example, anions are in general coordinatively saturated species, and bind to designed hosts only by weak and aspecific interactions. Many anions exist only in a relatively narrow pH window, are generally large and with higher free energy of solvation, with respect to cations with similar size. Moreover, they differ widely in shape, being spherical (halides), linear (CN^- , N_3^-), planar (CO_3^{2-} , NO_3^-), tetrahedral (SO_4^{2-} , PO_4^{3-}), octahedral (PF_6^-) and so on. For these reasons reliable sensing of anions in water is a very intriguing problem, and analytical means, including sensor devices, for selective sensing of multiple anions are still very rare.

Some recent advancement in this field, based on sensor arrays, is reported. An early report by Reinhoudt and Crego-Calama entailed the construction of a self-assembled library of addressed anion receptors on glass, which could be of potential use in the development of microarray systems [67].

More recently, Anzenbacher et al. developed a supramolecular-based sensor array for detection of complex matrices of anions [68]. The arrays were prepared by implementing colorimetric sensors in polyurethane hydrogel. The sensor elements are reported in Fig. 20, based on calyxpyrrole, and anthraquinone moieties.

These structures have been chosen on the basis of their affinity toward investigating anions, by independently measured binding affinities.

The synergy between these two systems would mimic the cooperative mechanisms operating in biological machineries (apoenzyme and cofactors). The role of the host hydrogel, besides that of supporting the molecular receptor, is to extract the

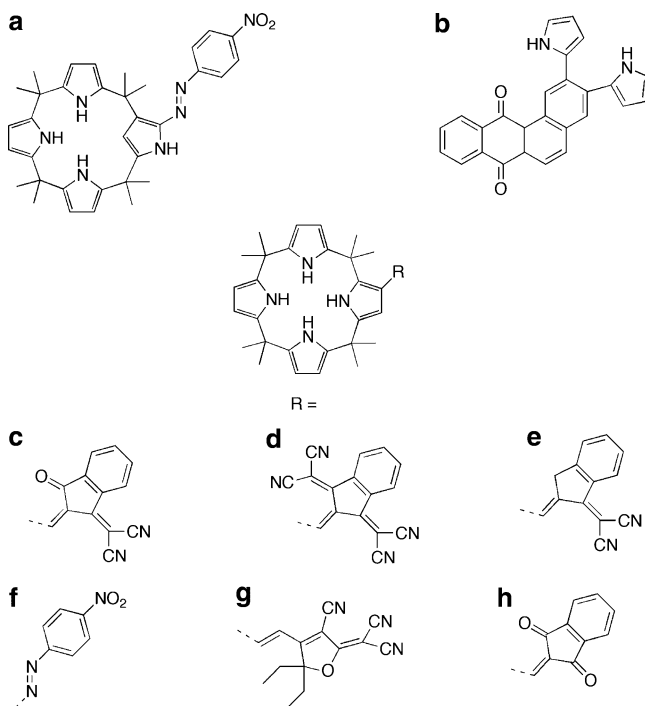


Fig. 20 Molecular structures of the sensing materials exploited in [68]

ion from the bulk solution stripping the solvating water. The sensible material was prepared by simply casting a proper THF solution of polyurethane hydrogel and receptor in microwell array. The colour responses were recorded by RGB scanner, and the images deconvoluted into RGB channels, and referenced against the images taken before anion exposures (blank).

An eight sensor-array was produced, showing selectivity for fluoride and pyrophosphate ions, and concomitant cross-reactivity for carboxylate, phosphate, and chloride. This was used to differentiate between 10 anions (Fig. 21).

The statistical evaluation of the array response to aqueous solutions of ions was determined by PCA and by Hierarchical Clustering Analysis, as reported in Fig. 22.

This protocol was effectively exploited in the analysis of very complex real matrices, such as toothpaste brands.

3.3 Other Analytes

One of the first examples of a sensing platform operating in solution and devoted to the pattern recognition of different analytes, is the “electronic tongue” developed at the University of Texas, Austin [69]. In this system, a Si/SiN wafer was

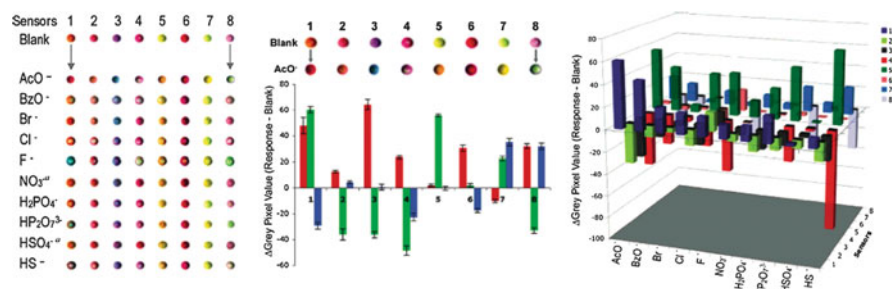


Fig. 21 *Left*: Typical eight-sensor array response to anion aqueous solution (200 nL, 5 mM; NO₃⁻ and HSO₄⁻ concentration was 20 mM). *Centre*: Net response profile of sensors 1–8 to the addition of aqueous AcO⁻ (200 nL). *Right*: Pattern generated by the array in the *green* channel in the presence in the same conditions used in the *left* panel. Reprinted with permission from [68]

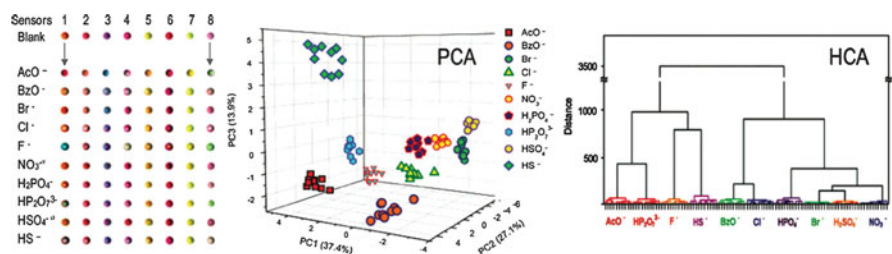


Fig. 22 *Left*: Typical array responses to aqueous anion solutions. *Centre*: PCA score plot of the first three PCs for 100 samples (10 anions each) showing clear clustering of the trials. *Right*: Corresponding HCA dendrogram, showing Euclidean distance between the trials. Reprinted with permission from [68]

micromachined to create cavities holding polymeric beads, functionalized with different broadly selective colorimetric or fluorescent dyes. The device was tested for the recognition of analytes, such ATP, pH and more recently small peptides, although colorimetric variations were mostly exploited in these applications [70].

The pattern recognition of peptides and proteins has received increasing attention, due to the potential applications in the fields of proteomic, diagnostic or bioclinical analyses, of paramount importance in biological and medical research [71].

Hamilton and coworkers took advantage of the interaction of functionalized tetraphenylporphyrins with the protein surfaces [72, 73].

The hydrophobic core of the porphyrin is the most important in driving the binding to the proteins, while the peripheral functionalization can orient the selectivity towards different proteins (Fig. 23). The detection of metal ion containing proteins was based on the fluorescence quenching of porphyrin upon protein binding; porphyrins are highly fluorescent compounds, ensuring the necessary sensitivity, and furthermore this feature avoids the functionalization of the protein

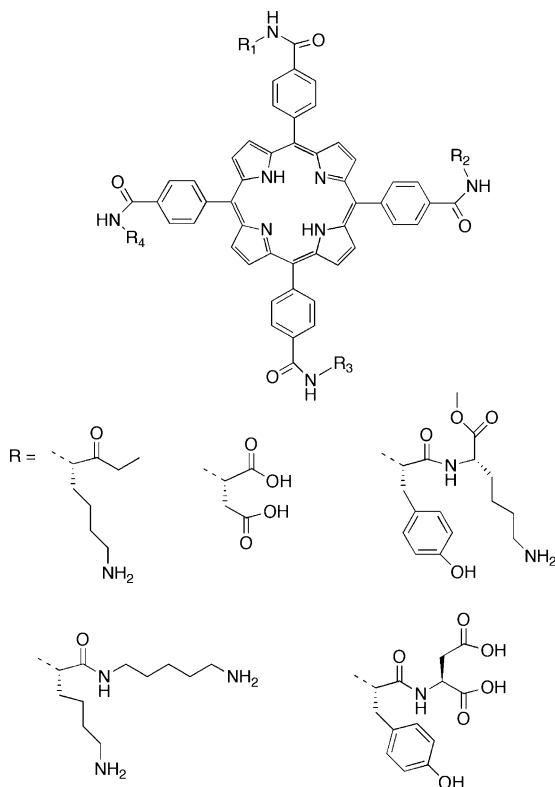


Fig. 23 Molecular structures of the functionalised porphyrins exploited for protein recognition

backbone. The recognition could also be performed in the case of proteins not bearing metal ions; while the much smaller responses did not allow naked eye recognition, the exploitation of simple data analysis, such as PCA, afforded clear discrimination between the proteins studied.

A cross-reactive sensor array based on luminescence changes has been reported by Severin and coworkers [74]. In this case no synthetic modifications were operated, but the sensing elements were created by mixing some metal complexes with fluorescent dyes. The complex formation between metal ions, such as Rh, Ru or Pd, quenches the dye fluorescence; the peptide competes with the dye for metal ion complexation, removing it from the complex. The fluorescence turn on is the signal of the peptide interaction. The activation of fluorescence is also an indication of the equilibrium reported in Fig. 24 and it is the basis of the peptides discrimination. The sensor array was able to differentiate between several dipeptides at $20\text{--}50 \times 10^{-6}$ M concentration; higher oligopeptides, such as bradykinin and kallidin were also discriminated and the system was also able to differentiate between two dipeptides, carnosine and homocarnosine, in a more complex environment such as human serum.

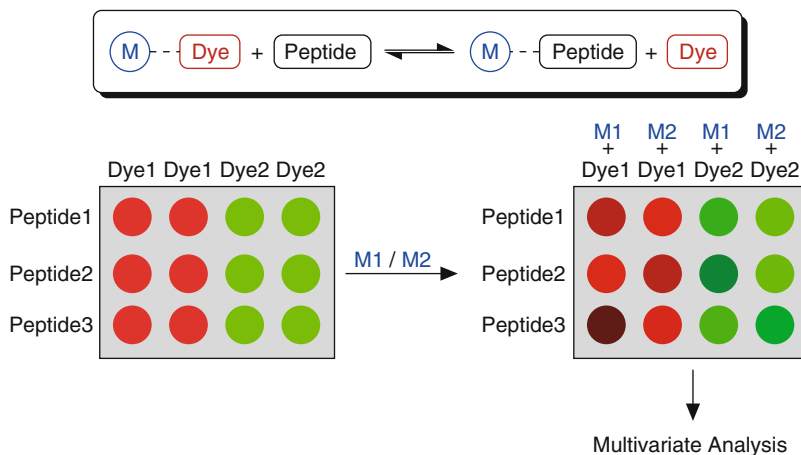


Fig. 24 Sensing mechanism of the metal-dye array for peptide recognition. Reprinted with permission from [74]

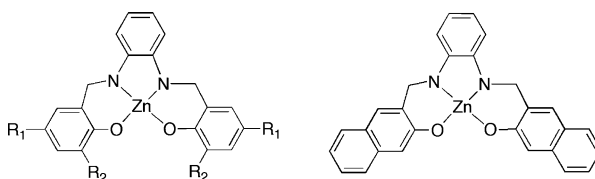


Fig. 25 Molecular structures of the Zn(salicylaldimine) complexes

As observed for the gaseous phase, one of the most pursued applications of luminescence based sensor arrays is related to the security field, in particular for the detection of nitroaromatics as mimics of explosives. Also, in this case, the sensing mechanism takes advantage of the characteristics of fluorescence quenchers of the nitro groups. For example, Germain and Knapp used different Zn(salicylaldimine) complexes for the detection of nitroaromatics and explosive mimics in acetonitrile solution (Fig. 25) [75]. Samples were measured in polypropylene microplates, with λ_{exc} at 400 nm and λ_{em} at 520 nm. The array was able to differentiate between different nitroaromatics, showing better discrimination performances than those of semiconducting polymers. In the case of Zn (salicylaldimine) complexes, the quenching mechanism is both static and dynamic and for this reason the luminescence quenching depends on the nature of the nitroaromatic and also on the steric requirements of the complex, so improving the discriminative properties among structurally similar compounds.

Molecular imprinting technique was exploited to prepare a sensor array based on phenylboronic acid functionalized mesoporous silica [76]. The phenylboronic acid, chosen as the saccharide receptor, was used to functionalize triethoxysilane, which was then used to prepare the mesoporous silica by the sol gel technique.

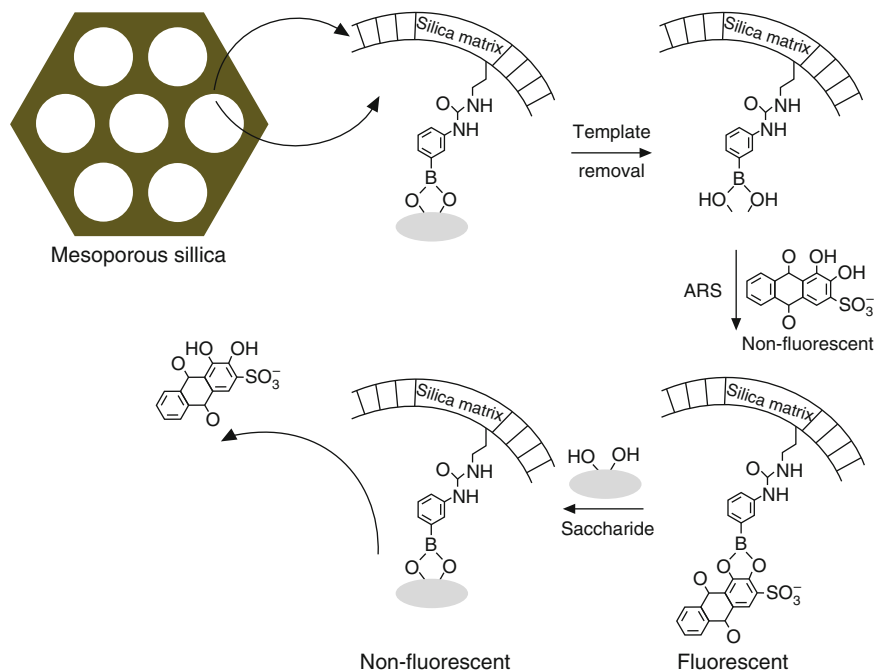


Fig. 26 Sensing mechanism of the molecularly imprinted sensor array. Reprinted with permission from [76]

The molecular imprinting was done during this step, which was carried out in the presence of D-fructose or D-xylose. The saccharides were removed after the sol gel process to furnish two different imprinted silica powders. The molecular imprinting was coupled with the indicator-displacement strategy, using a commercially available fluorescent dye, Alizarin Red S. The sensing mechanism of these materials is represented in Fig. 26.

Although only two saccharides were used for the imprinting technique, the imprinted silica obtained was exploited to develop a sensor array devoted to the discrimination between several saccharides; the concept is that the imprinting is done with D-fructose and D-xylose, two saccharides having very different molecular size and binding affinity with phenylboronic acid, so the templating process could allow different responses toward saccharides and creating a series of cross reactive sensors. The discriminative properties of the system were studied towards a series of saccharides and also successfully tested to discriminate between real samples, such as orange juice beverages.

Moczko and coworkers followed a different approach to develop a sensing platform for the determination of some analytes of physical parameters, such as pH, temperature, ionic strength and dissolved oxygen [77]. Instead of the exploitation of different spatially distributed sensing elements, they used a mixture of dyes, whose fluorescence was sensitive to the target parameters, dissolved in solution.

different depending on the particular type of cells analyzed. The different patterns in the fluorescence responses were analyzed by Linear Discrimination Analysis, which showed the ability of the sensor array to discriminate between different cell types and, more interesting, between normal, cancerous and metastatic cells of two different kind of tumour (human breast and murin epithelial cell lines).

A sensor array based on chemiluminescence has been reported by Zhang and coworkers [79]; in this case, catalytic nanomaterials of different types are the sensing elements of the array. When a gaseous analyte interacted with the sensing elements, the chemiluminescence produced by a catalytic reaction was the signal used as the sensor response. The nanomaterials were cross reactive and different response patterns were obtained by the analytes studied. The clear advantage of such an array is related to the long-term stability of the sensing elements, because the emission was due to a catalytic reaction, so excluding the photobleaching that usually affects luminescent dyes. Furthermore, because the sensing mechanism depends on a catalytic reaction, the responses depended on the working temperature and this information enriched the discrimination power of the array, making this system promising for sample recognition. The sensing platform was tested for the discrimination of real samples, such as cigarettes of different brands.

4 Conclusions

Fluorescence based cross reactive sensor arrays nowadays represent a versatile and powerful tool for applications in the real field. The high sensitivity, characteristic of fluorescence transduction, coupled with the possibility of measuring simultaneously the fluorescence of a large number of indicators, is the basis of the development of these devices witnessed in the last decade.

The increasing sophistication of consumer electronic devices has further enhanced the application opportunities of these arrays; this strategy co-opts the technical and optical capabilities of devices originally conceived for different purposes, turning them into chemical sensing platforms, by adding functional sensing materials. The rationale behind this approach is that successful sensing applications can be as ubiquitous as the devices supporting them, which in some cases means a globally disseminated (and interconnected) infrastructure at a scale not available just for chemical sensing purposes.

References

1. Gründler P (2007) Chemical sensors. Springer, Berlin
2. Wolfbeis OS (2008) Sensor paints. *Adv Mater* 20:3759–3763
3. Prodi L (2005) Luminescent chemosensors: from molecules to nanoparticles. *New J Chem* 29:20–31

4. Anslyn EV (2007) Supramolecular analytical chemistry. *J Org Chem* 72:687–699
5. Czarnik AW, Yoon J (2007) Chemosensors: synthetic receptors in analytical sensing applications. In: Reinhoudt DN (ed) *Perspectives in supramolecular chemistry: supramolecular materials and technologies*, vol 4. Chichester, Wiley
6. Persaud K, Dodd G (1982) Analysis of discrimination mechanisms in the mammalian olfactory system using a model nose. *Nature* 299:352–355
7. Schiffman SS, Pearce TC (2002) Introduction to olfaction: perception, anatomy, physiology, and molecular biology. In: Pearce TC, Schiffman SS, Nagle HT, Gardner JW (eds) *Handbook of machine olfaction*. Weinheim, Wiley-VCH
8. Röck F, Barsan N, Weimar U (2008) Electronic nose: current status and future trends. *Chem Rev* 108:705–725
9. Dickinson TA, White J, Kauer JS, Walt DR (1996) A chemical-detecting system based on a cross-reactive optical sensor array. *Nature* 382:697–700
10. White J, Kauer JS, Dickinson TA, Walt DR (1996) Rapid analyte recognition in a device based on optical sensors and the olfactory system. *Anal Chem* 68:2191–2202
11. Dickinson TA, Michael KL, Kauer JS, Walt DR (1999) Convergent, self-encoded bead sensor arrays in the design of an artificial nose. *Anal Chem* 71:2192–2198
12. Albert KJ, Walt DR (2000) High-speed fluorescence detection of explosive-like vapors. *Anal Chem* 72:1947–1955
13. Stitzel SE, Cowen LJ, Albert KJ, Walt DR (2001) Array-to-array transfer of an artificial nose classifier. *Anal Chem* 73:5266–5271
14. Albert KJ, Walt DR, Gill DS, Pearce TC (2001) Optical multibead arrays for simple and complex odor discrimination. *Anal Chem* 73:2501–2508
15. Albert KJ, Walt DR, Gill DS, Pearce TC (2002) Automatic decoding of sensor types within randomly ordered, high-density optical sensor arrays. *Anal Bioanal Chem* 373:792–802
16. Albert KJ, Walt DR (2003) Information coding in artificial olfaction multisensor arrays. *Anal Chem* 75:4161–4167
17. Bencic-Nagale S, Walt DR (2005) Extending the longevity of fluorescence-based sensor arrays using adaptive exposure. *Anal Chem* 77:6155–6162
18. Bencic-Nagale S, Sternfeld T, Walt DR (2006) Microbead chemical switches: an approach to detection of reactive organophosphate chemical warfare agent vapors. *J Am Chem Soc* 128:5041–5048
19. Drew SM, Janzen DE, Mann KR (2002) Characterization of a cross-reactive electronic nose with vapoluminescent array elements. *Anal Chem* 74:2547–2555
20. Muro ML, Daws CA, Castellano FN (2008) Microarray pattern recognition based on Pt^{II} terpyridyl chloride complexes: vapochromic and vapoluminescent response. *Chem Commun* 6134–6136
21. White J, Truesdell K, Williams LB, AtKisson MS, Kauer JS (2008) Solid-state, dye-labeled DNA detects volatile compounds in the vapor phase. *PLoS Biol* 6:e9
22. Hertzog-Ronen C, Borzin E, Gerchikov Y, Tessler N, Eichen Y (2009) Detection and identification of alkylating agents by using a bioinspired “Chemical Nose”. *Chem Eur J* 15:10380–10386
23. Rakow N, Suslick K (2000) A colorimetric sensor array for odour visualization. *Nature* 406:710–713
24. Rakow N, Sen A, Janzen M, Ponder J, Suslick K (2005) Molecular recognition and discrimination of amines with a colorimetric array. *Angew Chem Int Ed* 44:4528–4532
25. Lim S, Feng L, Kemling J, Musto C, Suslick K (2009) An optoelectronic nose for the detection of toxic gases. *Nat Chem* 1:562–567
26. Taton T, Mirkin C, Letsinger R (2000) Scanometric DNA array detection with nanoparticle probes. *Science* 289:1757–1760
27. Potyrailo R, Morris W, Leach A, Sivavec T, Wisnudel M, Boyette S (2006) Analog signal acquisition from computer optical disk drives for quantitative chemical sensing. *Anal Chem* 78:5893–5899

28. Filippini D, Lundström I (2003) Computer screen as a programmable light source for visible absorption characterization of (bio)chemical assays. *Chem Commun* 2:240–241
29. Westland S, Ripamonti C (2004) Computational colour science. Wiley, Chichester
30. Filippini D, Lundström I (2003) Chemical images generated by large area homogeneous illumination of metal–insulator–semiconductor structures. *Appl Phys Lett* 82:3791–3793
31. Filippini D, Andersson T, Svensson S, Lundström I (2003) Microplate based biosensing with a computer screen aided technique. *Biosens Bioelectron* 19:35–41
32. Gatto E, Malik M, Di Natale C, Paolesse R, D'Amico A, Lundström I, Filippini D (2008) Polychromatic fingerprinting of excitation emission matrices. *Chem Eur J* 14:6057–6060
33. Hershberger L, Callis J, Christian G (1981) Liquid chromatography with real-time video fluorometric monitoring of effluents. *Anal Chem* 53:971–975
34. Ng K (1995) Complete guide to semiconductor devices. McGraw-Hill, New York
35. Sharma G (ed) (2003) Digital color imaging handbook. CRC Press, Boca Raton
36. Filippini D, Di Natale C, Paolesse R, D'Amico A, Lundström I (2007) Computer screen photo-assisted techniques for global monitoring of environmental and sanitary parameters. *Sens Actuators B* 121:93–102
37. Malik M, Gatto E, Macken S, Di Natale C, Paolesse R, D'Amico A, Lundström I, Filippini D (2009) Imaging fingerprinting of excitation emission matrices. *Anal Chim Acta* 635:196–201
38. Filippini D, Alimelli A, Di Natale C, Paolesse R, D'Amico A, Lundström I (2006) Chemical sensing with familiar devices. *Angew Chem Int Ed* 45:3800–3803
39. Paolesse R, Alimelli A, D'Amico A, Venanzi M, Battistini G, Montalti M, Filippini D, Lundström I, Di Natale C (2008) Insights on the chemistry of a, c-biladienes from a CSPT investigation. *New J Chem* 32:1162–1166
40. Paolesse R (2000) Syntheses of corroles. In: Kadish KM, Smith KM, Guillard R (eds) *The porphyrin handbook*, vol 2. Academic Press, New York
41. Alimelli A, Pennazza G, Santonico M, Paolesse R, Filippini D, D'Amico A, Lundström I, Di Natale C (2007) Fish freshness detection by a computer screen photoassisted based gas sensor array. *Anal Chim Acta* 582:320–328
42. Di Natale C, Martinelli E, Paolesse R, D'Amico A, Filippini D, Lundström I (2008) An experimental biomimetic platform for artificial olfaction. *PLoS ONE* 3:e3139
43. Mombaerts P (1999) Molecular biology of odorant receptors in vertebrates. *Annu Rev Neurosci* 22:487–509
44. Dini F, Filippini D, Paolesse R, D'Amico A, Lundström I, Di Natale C (2010) Polymers with embedded chemical indicators as an artificial olfactory mucosa. *Analyst* 135:1245–1252
45. Di Natale C, Santonico M, Paolesse R, Filippini D, D'Amico A, Lundström I (2010) Evaluation of the performance of sensors based on optical imaging of a chemically sensitive layer. *Anal Bioanal Chem* 397:613–621
46. Fabbri L (ed) (2000) Special issue on luminescent sensors. *Coord Chem Rev* 205:1–232
47. Ellis AB, Walt DR (eds) (2000) Special issue on chemical sensors. *Chem Rev* 100:2477–2738
48. Palacios MA, Wang Z, Montes VA, Zyryanov GV, Anzenbacher P (2008) Rational design of a minimal size sensor array for metal ion detection. *J Am Chem Soc* 130:10307–10314
49. Wang Z, Palacios MA, Anzenbacher P (2008) Fluorescence sensor array for metal ion detection based on various coordination chemistries: general performance and potential application. *Anal Chem* 80:7451–7459
50. Basabe-Desmonts L, van der Baan F, Zimmerman RS, Reinhoudt DM, Crego-Calama M (2007) Cross-reactive sensor array for metal ion sensing based on fluorescent SAMs. *Sensors* 7:1731–1746
51. Mayr T, Igel C, Liebsch G, Klimant I, Wolfbeis OS (2003) Cross-reactive metal ion sensor array in a micro titer plate format. *Anal Chem* 75:4389–4396
52. Mayr T, Liebsch G, Klimant I, Wolfbeis OS (2002) Multi-ion imaging using fluorescent sensors in a microtiter plate array format. *Analyst* 127:201–203

53. Jolling K, Vandeven M, van Den EJ, Ameloot M, van Kerkhove E (2007) A high reliable and budget-friendly Peltier-cooled camera for biological fluorescence imaging. *J Microsc* 228:264–271
54. Martínez-Otero A, Hernando J, Ruiz-Molina D, Maspoch D (2008) pH-responsive fluorescent nanoarrays fabricated by direct-write parallel dip-pen nanolithography. *Small* 4:2131–2135
55. Salaita K, Wang Y, Mirkin CA (2007) Applications of dip-pen nanolithography. *Nat Nanotechnol* 2:145–155
56. Lapresta-Fernández A, Huertas R, Melgosa M, Capitán-Vallvey LF (2009) Multianalyte imaging in one-shot format sensors for natural water. *Anal Chim Acta* 636:210–217
57. Basabe-Desmots L, Benito-López F, Gardeniers HJGE, Duwel R, van den Berg A, Reinhoudt DN, Crego-Calama M (2008) Fluorescent sensor array in microfluidic chip. *Anal Bioanal Chem* 390:307–315
58. Vilkner T, Janasek J, Manz A (2004) Micro total analysis systems. Recent developments. *Anal Chem* 76:3373–3385
59. Yager P, Edwards T, Fu E, Helton K, Nelson K, Tam MR, Weigl BH (2006) Microfluidic diagnostic technologies for global public health. *Nature* 442:412–418
60. Descalzo AB, Marcos MD, Monte C, Martínez-Mañez R, Rurack K (2007) Mesoporous silica materials with covalently anchored phenoxazinone dyes as fluorescent hybrid materials for vapour sensing. *J Mater Chem* 17:4716–4723
61. Chandra D, Yokoi T, Tatsumi T, Bhaumik A (2007) Highly luminescent organic-inorganic hybrid mesoporous silica's containing tunable chemosensor inside the pore wall. *Chem Mater* 19:5347–5354
62. Tan J, Wang H-F, Yan X-P (2009) A fluorescent sensor array based on ion imprinted mesoporous silica. *Biosens Bioelectron* 24:3316–3321
63. Sawada K, Oshima T, Hizawa T, Takao H, Ishida M (2005) A novel fused sensor for photo- and ion-sensing. *Sens Actuators B* 106:614–618
64. Hewege H, Anslyn EV (2009) Pattern-based recognition of thiols and metals using a single squaraine indicator. *J Am Chem Soc* 131:13099–13106
65. Kim Y-R, Kim HY, Kim JS, Kim H (2008) Rhodamine-based “turn-on” fluorescent chemodosimeter for Cu(II) on ultrathin platinum films as molecular switches. *Adv Mater* 20:4428–4432
66. Steed JW, Atwood JL (2001) *Supramolecular chemistry*. Wiley, Chichester (UK)
67. Basabe-Desmots L, Beld J, Zimmerman R, Hernando J, Mela P, García Parajó MF, van Hulst NF, van den Berg A, Reinhoudt DN, Crego-Calama M (2004) A simple approach to sensor discovery and fabrication on self-assembled monolayers on glass. *J Am Chem Soc* 126:7293–7299
68. Palacios MA, Nishiyabu R, Marquez M, Anzenbacher P Jr (2007) Supramolecular approach to the design of a high-resolution sensor array for multianion detection in water. *J Am Chem Soc* 129:7538–7544
69. Goodey A, Lavigne JJ, Savoy SM, Rodriguez MD, Currey T, Tsao A, Simmons G, Wright J, Yoo S-J, Sogn Y, Anslyn EV, Shear JB, Neikirk DP, McDevitt JT (2001) Development of multianalyte sensor arrays composed of chemically derivatized polymeric microspheres localized in micromachined cavities. *J Am Chem Soc* 123:2559–2570
70. Yoo S-J, Goodey A, Anslyn EV, McDevitt JT, Shear JB, Neikirk DP (2005) A microbead array chemical sensor using capillary-based sample introduction: toward the development of an “electronic tongue”. *Biosens Bioelectron* 21:303–312
71. Collins BE, Anslyn EV (2007) Pattern-based peptide recognition. *Chem Eur J* 13:4700–4708
72. Baldini L, Wilson AJ, Hong J, Hamilton AD (2004) Pattern-based detection of different proteins using an array of fluorescent protein surface receptors. *J Am Chem Soc* 126:5656–5657
73. Zhou H, Baldini L, Hong J, Wilson AJ, Hamilton AD (2006) Pattern recognition of proteins based on an array of functionalized porphyrins. *J Am Chem Soc* 128:2421–2425

74. Rochat S, Gao J, Qian X, Zaubitzer F, Severin K (2010) Cross-reactive sensor arrays for the detection of peptides in aqueous solution by fluorescence spectroscopy. *Chem Eur J* 16:104–113
75. Germain ME, Knapp MJ (2008) Discrimination of nitroaromatics and explosives mimics by a fluorescent Zn(salicylaldimine) sensor array. *J Am Chem Soc* 130:5422–5423
76. Tan J, Wang H-F, Yan X-P (2009) Discrimination of saccharides with a fluorescent molecular imprinting sensor array based on phenylboronic acid functionalized mesoporous silica. *Anal Chem* 81:5273–5280
77. Moczko E, Meglinski IV, Bessant C, Piletsky SA (2009) Dyes assay for measuring physico-chemical parameters. *Anal Chem* 81:2311–2316
78. Bajaj A, Miranda OR, Kim I-B, Phillips RL, Jerry DJ, Bunz UHF, Rotello VM (2009) Detection and differentiation of normal, cancerous, and metastatic cells using nanoparticle-polymer sensor arrays. *PNAS* 106:10912–10916
79. Wu Y, Na N, Zhang S, Wang X, Liu D, Zhang X (2009) Discrimination and identification of flavors with catalytic nanomaterial-based optical chemosensor array. *Anal Chem* 81:961–966

Enantioselective Sensing by Luminescence

Alessandro Accetta, Roberto Corradini, and Rosangela Marchelli

Abstract Enantiomeric analysis is one of the crucial points for the sensor technology, due to the increasing importance that enantiomerically pure compounds and drugs have in pharmaceutical and agrochemical applications. Enantiomeric luminescent sensors give different responses by interaction or reaction with chiral molecules, allowing one to assess their optical purity by spectroscopic measurements. Moreover, chemosensors have been developed to perform enantiomeric analysis of both luminescent and non-luminescent organic compounds. In the present chapter we focus on the recent advances in the sensing of chiral molecules by luminescent sensory systems, with the aim of outlining different mechanisms: fluorescence quenching by metal complexes, photoinduced electron transfer (PET) quenching, fluorescence enhancement by PET inhibition, analyte induced sensor conformational changes, modulation of excimer and exciplex formation, and aggregation induced emission enhancement (AIEE). Recent advances in the use of more elaborate techniques such as anisotropy measurements, gated detection, circularly polarized luminescence (CPL) and perspectives in the field are also discussed. Emphasis is given to the methods which have provided high enantioselectivity and which are amenable to fast screening procedures.

Keywords Chiral analysis · Enantiomeric recognition · Fluorescent sensors · Luminescence

A. Accetta, R. Corradini (✉), and R. Marchelli
Dipartimento di Chimica Organica e Industriale, Università di Parma, Parco Area delle Scienze 17/A, 43124 Parma, Italy
e-mail: alessandro.accetta@unipr.it, roberto.corradini@unipr.it, rosangela.marchelli@unipr.it

Contents

1	Introduction	177
2	Enantio-Discriminating Effects in Luminescence	177
3	Fluorescent Chemosensors	180
3.1	Enantioselective Fluorescence Quenching	184
3.2	Sensing by Collisional Fluorescence Quenching	185
3.3	Enantioselective Quenching Involving Metal Complexes	185
3.4	Enantioselective Quenching by PET and Related Mechanisms	189
3.5	Fluorescence Enhancement by PET Inhibition	193
3.6	Fluorescence Response Due to Changes in the Sensor Structure	196
3.7	Modulation of Excimer or Exciplex Formation	200
4	Enantioselectivity in Aggregation/Precipitation Induced Fluorescence Emission	203
5	Displacement and Non-Covalent Sensory Systems	205
6	Advanced Luminescence Techniques	207
7	Conclusions and Perspectives	209
	References	210

List of Abbreviations

AIEE	Aggregation induced emission enhancement
BINOL	1,1-Binaphthol
Boc	<i>tert</i> -Butoxycarbonyl
BODIPY	Boron dipyrromethene
BSA	Bovine serum albumin
CD	Cyclodextrin
CPL	Circularly polarized luminescence
DFT	Density functional theory
ECL	Electrochemiluminescence
ET	Energy transfer
Glu	Glutamic acid
HSA	Human serum albumin
LEC	Ligand exchange chromatography
LUMO	Lowest unoccupied molecular orbital
Lys	Lysine
MIP	Molecularly imprinted polymers
PA	Phenylalaninol
PET	Photoinduced electron transfer
QD	Quantum dot
TICT	Twisted intramolecular charge transfer
TRF	Time-resolved “gated” fluorescence

1 Introduction

Enantioselectivity remains a very important long-standing goal for sensor science [1, 2], since biological activity is strictly correlated with stereochemistry. Enantiomers of drugs can have different effects [3] and are subjected to specific regulations [4]. Very efficient enantioselective reaction schemes and catalysts are needed to produce enantiomerically pure compounds, since the market for single-enantiomer drugs is increasing in importance (in 2009, estimates suggest \$15 billion in revenue) [5]. Enantiomeric characterization is also increasingly important in the agrochemical area [6, 7] and in food analysis [8, 9]. Therefore, fast and easily performed tests for the assessment of the enantiomeric composition are needed in both process development and quality control.

Application of chemosensors as components of an “artificial tongue” to the parallel detection of organic molecules in solution has also been proposed [10–12]. Analogs of natural sensory systems should have the ability to discriminate between enantiomers [13, 14], such as L-amino acids, which are mostly bitter, from D-amino acids which are generally sweet.

Optical sensing methods, which have been successfully used for ions and organic compounds, have been demonstrated to be efficient tools for fast analytical procedures [15–17], and fluorescence sensors are particularly good performers, due to the high sensitivity and selectivity of the detection methods [18].

Enantioselectivity of fluorescent organic molecules were reviewed several years ago by Pu [19]; therefore this review will mainly discuss recent developments and applications of enantioselective luminescence sensing.

The development of a combinatorial approach to chemical synthesis [20] and catalysis [21] has created new needs for fast, reliable, and time-effective high-throughput enantiomeric analytical methods allowing one to screen the properties of the enormous number of new structures developed [22, 23]. Thus, new enantioselective catalysts have been developed using a combinatorial approach combined with fast screening of the enantiomeric excess generated [24, 25]. In the last few years, research has focused on the quest for high enantioselectivity of the fluorescence response, and on the application of luminescent sensors to the actual determination of enantiomeric excess (ee) with fast, parallel and high-throughput techniques. Important features for the successful development of enantioselective sensors, and some examples recently described, will be highlighted.

2 Enantio-Discriminating Effects in Luminescence

Although many optical techniques can be used for the discrimination of enantiomers in a simple read-out format like UV-measurements, colorimetric, or even “naked eye” detection [26], the use of luminescence (mostly fluorimetric) detection has several advantages in terms of sensitivity and selectivity of the

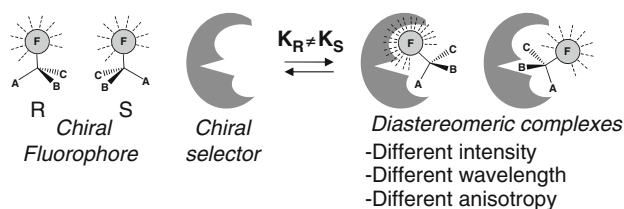
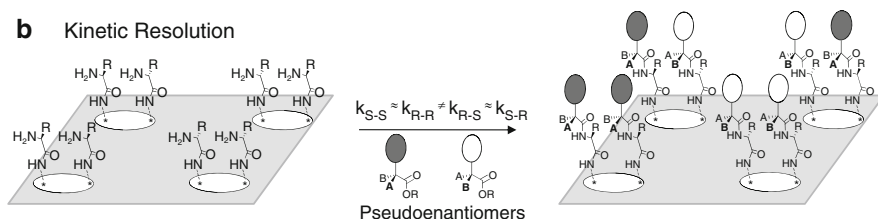
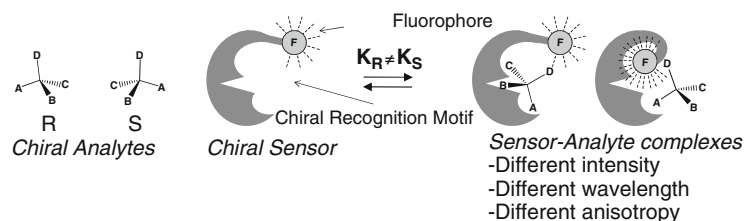
a Enantioselectivity of fluorescent analytes interactions**b** Kinetic Resolution**c** Enantioselective fluorescent sensors

Fig. 1 Different schemes for inducing an enantioselective fluorescence response: (a) interaction of a chiral fluorescent molecule with a chiral receptor; (b) kinetic resolution using fluorescent pseudoenantiomers; (c) discrimination of non-fluorescent molecules by fluorescent sensors

signal, due to the lower background. Thus, micromolar concentrations of the sensor and very little amounts of the analyte can be used. Common modern instrumentations allow very fast and parallel analysis of fluorescence and fluorescence lifetimes.

Luminescence can be used in different contexts to evaluate enantioselectivity (Fig. 1). Chiral analytes containing a luminescent group can interact with one enantiomer of a given chiral selector, thus forming diastereomeric complexes of different stability and structure. If the luminophore experiences a different environment in the complex, a change in the luminescence is observed (Fig. 1a).

Some remarkable examples are given by inclusion of a variety of fluorescent guests into toroidal-shaped hosts such as cyclodextrins [27, 28]. The inclusion process protects the fluorophore from collisional quenching by the solvent and changes the polarity of the microenvironment, thus inducing both enhancement and

wavelength changes. An interesting example of this approach is the enantioselective fluorescence response of the drug Zolmitriptan, for which small impurities of the (R)-enantiomer can significantly alter the clinical profile of the (S)-enantiomer active drug [29]. Phosphorescence can also be observed in inclusion complexes of compounds which in solution are non-phosphorescent, and this process can also be enantioselective, as reported in several examples from the literature [30–32]. Differences in fluorescence anisotropy and anisotropy decay can also be observed [33, 34].

Another example is given by the interaction of chiral metal complexes with fluorescent chiral analyte bearing metal binding sites. Enantioselective quenching of fluorescence can be observed in such cases as a result of coordination or ligand exchange processes [35–37].

Interaction of fluorophores with natural biopolymers such as proteins, polysaccharides, or DNA is also an enantioselective process and can be used to discriminate between two enantiomers of a specific compound. A remarkable example is the differential interaction of Λ and Δ isomers of luminescent octahedral metal complexes with DNA (metallointercalators), which generate a fluorescent signal and was shown to be dependent on the DNA helicity, as was reversed for right-handed B-DNA and left-handed Z-DNA [38]. However, in most studies, the main interest has usually been to probe the biopolymer conformation and not to generate an enantioselective fluorescence response of the probe.

Adsorption of fluorescent molecules on chirally modified surfaces and sol-gel films can also generate enantioselective effects [39].

A second strategy which is reported in the literature is that of using kinetic diastereoselectivity by fluorescently labeled pseudoenantiomeric reactants (Fig. 1b), in combination with automated instrumentation and microarray technology derived from genomic research [40]. In this approach, two enantiomers of a reactant (D- or L-proline) were labeled differently using either cyanine Cy3 or Cy5 fluorophores, (pseudoenantiomers or quasi-enantiomers) [41]. These molecules were then reacted and the analyte (another amino acid) linked to a microarray surface to form a covalent amide bond; due to the diastereoselectivity of the reaction, the prevalence of the Cy3 or Cy5 fluorophore (opportunistically calibrated) indicated the enantiomeric composition of the specific sample. In this way, a very high number of samples per day could be analyzed by fluorescence read-out of the microarray in both Cy3 and Cy5 channels. Pseudoenantiomers can also be used as substrates for enzymatic reactions, thus leading to a direct read-out of enantioselectivity [42].

Though the above reported selected examples show that enantioselectivity in fluorescence response can be achieved, and can be used for the detection of enantiomeric excess, they do not strictly belong to the field of luminescent sensor molecules and therefore will not be discussed in detail here. We will for the rest of this review focus on the use of fluorescent molecules as general sensors (Fig. 1c) able to produce enantioselective response in the presence of both fluorescent and non-fluorescent analytes.

3 Fluorescent Chemosensors

The generation of an enantioselective signal by a sensor molecule in the presence of enantiomers can be obtained according to several schemes, which are depicted in Figs. 2 and 11. A molecular (in particular enantio-discriminating) recognition event should occur, either dynamically (by collision or chemical reaction) or statically (by formation of a sensor–analyte complex at equilibrium). Using only one enantiomer of the chiral sensor will lead to the formation of transient or permanent diastereomers, with different chemical or physical properties. Obtaining enantioselectivity in this event is the first difficulty when designing enantioselective fluorescence sensors, since the two enantiomers differ only in the spatial distribution of functional groups, but can in principle give rise to the same type of interactions. Supramolecular chemistry can now provide a variety of models for obtaining strong binding and strongly discriminating interactions.

The parameters which are mostly used for describing the enantioselectivity of this process are the chiral recognition factor $\alpha = K_R/K_S$ where K_R and K_S are the stability constants of the fluorophore–analyte complex containing the R- or the S-enantiomer respectively, and the enantiomeric fluorescence difference ratio $ef = \Delta F_R/\Delta F_S = (F_R - F_0)/(F_S - F_0)$, where F_0 , F_R , and F_S represent the fluorescence intensity displayed by the sensors under certain conditions alone or in the presence of the R- or S-enantiomer respectively. The order in which R and S are placed in the definitions above can be reversed in some cases, depending on the enantioselectivity observed. An enantioselective response can be generated by differences in the α value for two diastereomeric complexes having the same emission properties, although cases are also reported of complexes showing $\alpha \approx 1$, but still with good ef value, due to specific local conformational properties.

In principle, the luminescent (mainly fluorescent) sensor can be any luminescent chiral molecule which can interact with the analyte. It is a generally accepted rule

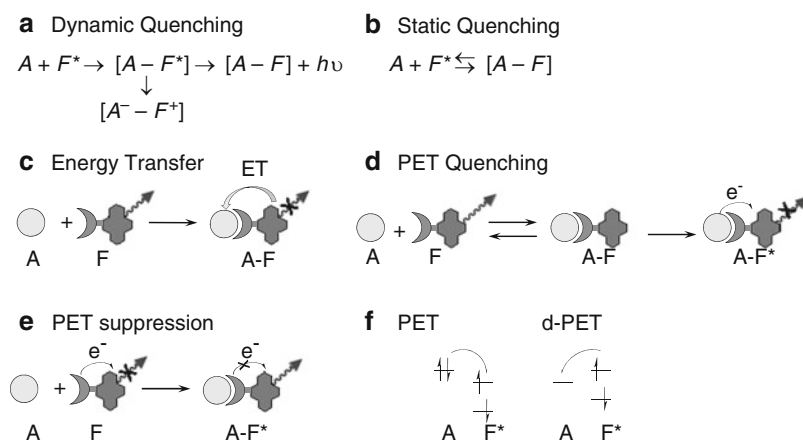


Fig. 2 Principal mechanisms of enantioselective sensing involving quenching processes

that rigid moieties can enhance enantioselectivity by imposing a stereochemical constraint to the interacting counterpart. Therefore, cyclic or rigid scaffolds are often used as components of enantioselective sensors; the chiral moiety can either be fluorescent itself or can be covalently linked to a fluorescent group. The binaphthyl unit, which has shown good discriminating properties in the development of enantioselective catalysts [43] and transport [44], and in particular the 1,1'-bi-2-naphthol (BINOL) group, has been the most widely used [19]. Other chiral inherently fluorescent molecules such as helicenes or 1,8-diacridylnaphthalene moiety (see Sects. 3.3 and 3.6) have been used. Non-fluorescent rigid scaffolds such as cyclodextrins or calixarenes have been opportunely equipped with functional groups and fluorophores in order to produce enantioselective sensors. These molecules have the advantage of presenting a well defined cavity as a recognition element, which can be used in order to bind aromatic groups by inclusion. Cyclodextrins, cyclic glucose oligomers with α -glycosidic linkages, able to discriminate between the two enantiomers of analytes in separation science [45], are particularly interesting since they can perform enantiomeric recognition in water, unlike most of the sensors based on organic molecules described in the literature. Other molecules from the chiral pool have been reported as scaffolds for the synthesis of enantioselective sensors, such as cholic acid, substituted cyclohexanes, amino acids, and peptides. Chiral polymers and molecularly imprinted polymers (MIP) can also be used as enantioselective elements in sensor technology [46, 47].

The presence of suitable binding groups able to form very stable bonds with the analyte is necessary in order to obtain strong complexation and enantioselectivity. Among these, ion-pair forming moieties has been used for acids and bases, while the boronic acid group has been widely used in order to bind diols, and in particular proximal hydroxylic groups in sugars [48]. Transition metal or lanthanide complexes have also been used as strong binding elements to which donor atoms can be bound, thus enforcing the analyte-sensor interaction. Hydrogen bonding has been used extensively as a binding element, in particular for anions (and thus for anionic organic molecules, including chiral ones) using the thiourea group, which undergo modification of their electronic properties and their ability to interact with neighboring groups upon hydrogen bonding formation. Hydrophobic effects (in water), and other specific interactions such as $\pi - \pi$ (stacking), or CH- π can be used to bind apolar groups.

The other key point is that the recognition event should then produce differences in the fluorescence properties of the sensor molecule in the presence of the two enantiomers of the analyte. Several mechanisms can be used to generate the fluorescence response (Figs. 2 and 11) by changing the electronic properties and the conformation of the sensor. Aggregation induced emission enhancement (AIEE) [49] was recently shown to be able to generate an enantioselective fluorescence response. Special optical techniques such as circularly polarized luminescence (CPL) are now available to detect enantioselective interactions occurring in the excited state or in the second coordination-sphere interactions [49].

In order to help the readers who are interested in the detection of enantiomeric excess of a specific class of analytes, an overview of the classes of molecules which have been reported in the recent literature is reported in Table 1. In the following

Table 1 Enantioselective luminescent sensing methods listed by analyte

Analytes	Mechanism	Sensors
Amines	Dynamic quenching PET Conformational change	(<i>R</i>)-Binaphthyl [50] BINOL derivatives [19], Helicene-diol (19) [51], binaphthofuran-yl-crown ether (20) [52] Bi(oxazolonyl)phenols 41 [53], 1,8-diacridylinaphthalene <i>N,N</i> -dioxide (11) [54, 55], HSA and BSA [56]
Alcohols	Conformational change	HSA and BSA [56]
Amino alcohols	Metal-mediated PET	Polymer 14 [57] Calixarenes (15) [58–61], BINOL derivatives (16–18, 22) [19, 62, 63] 1,8-Diacridylinaphthalene <i>N,N</i> -dioxide (11)-Sc(III) [64]
α -Hydroxy acids	Quenching by metal scavenging Excimer formation Exciplex and ET inhibition AIEE Metal-mediated quenching PET PET inhibition Aggregation AIEE	Calixarene (49) [65], Helicene-diol (19) [51] Ferrocenyl macrocycle (51) [66] Derivative (53) [67] Dianthryl ligand (12) [68] BINOL derivatives (22) [62], boronic acids (28) [69] BINOL amine derivatives (33, 34) [70–79], cleft-like (36) [80] Schiff base (52) [81] BINOL-based (55) [82] Xanthene-based (26) [83]
α -Hydroxy acids derivatives		
Carboxylic acids		
α -Amino acids	Metal-mediated quenching PET Conformational change Displacement CPL ECL	1,8-Biacridylinaphthalene (42) [84, 85], 1,8-diacridylinaphthalene <i>N,N</i> -dioxide (11) [86] Fluorescent cyclodextrins (1–4) [87–92], zinc complex (13) [93] Calixarene (15) [61], cholic acid derivatives (24) [94] BINOL macrocycles (39) [95] Poly-Lys TiO ₂ film [96], quantum dots (57) [97] Tb(dpa) ₃ ³⁻ [98] Ru(bipy) ₃ ²⁺ [99]
α -Amino acids amides	Metal-mediated quenching	Fluorescent cyclodextrins (1–3) [92]
<i>N</i> -Protected α -amino acids	PET PET inhibition Conformational change Exciplex inhibition	Calyx[4]arenes (15) [59, 61], anthracene clefts (25) [100], BINOL derivative (22) [62] BINOL-amino ligands (34, 36) [71, 74, 75], amino acid-thiourea 37 [101] 1,8-Diacridylinaphthalene <i>N,N</i> -dioxide (11) [54] Macrocyclic (50) [102–104]

α -Amino acids esters		Binaphthofuranyl-crown ether (20) [52], antibody 43 [105, 106]
Dicarboxylic acids	PET	Calixarenes (15) [60, 61], BINOL-based-AA derivatives (21) [107]
	Excimer formation	Cholic acid-pyrene (47) [108, 109], cyclohexane-naphthalene (48) [110, 111]
	PET inhibition	Bis-boronic acid (29) [112]
	AIEE	Derivative 54 [113]
	Time-resolved fluorescence	Eu(tetracycline) [114]
Tartaric acid derivatives	PET inhibition	Tetraamidic 35 [115]
Monosaccharides	PET inhibition	Bis-boronic acid (27 , 30) [48, 116, 117]
Apolar organic molecules	Conformational change	Fluorescent cyclodextrins [118–121]
	Exciplex disruption	Cyclodextrin 45 [122]
	Induced Phosphorescence	Cyclodextrin: 1-bromonaphthalene (58) [123]
Nucleosides	Conformational change	DNA aptamer 44 [124]
	Anisotropy	DNA aptamer [125]

parts of this review, we will present the fundamentals and recent specific examples of different type of mechanisms used for obtaining enantioselective sensing, with particular emphasis on the effects suitable for enantiomeric excess determination and high-throughput screening.

3.1 Enantioselective Fluorescence Quenching

Fluorescence quenching is due to non-radiative loss of energy from the excited state as a consequence of either collision with a quencher ion (or molecule) in solution or by formation of a non-fluorescent or poorly fluorescent fluorophore–quencher complex. In both cases the quenching process follows the Stern–Volmer equation:

$$F_0/F = 1 + K_{SV}[Q], \quad (1)$$

where F_0 and F are the fluorescence in the absence and in the presence of the quencher, respectively, $[Q]$ is the concentration of quencher, and K_{SV} is the Stern–Volmer constant, which is a measure of the efficiency of quenching and can be obtained by a simple linear regression. In the case of collisional (dynamic) quenching (Fig. 2a), the quantity $[Q]$ corresponds to the actual total concentration of the quencher, while in the case of static quenching, the equilibrium described in Fig. 2b should be considered. Therefore, the quantity $[Q]$ in this case represents the concentration of the *free* quencher, and K_{SV} corresponds to the stability constant of the FQ complex. Deviation from linearity of the Stern–Volmer plot (F_0/F vs $[Q]$) indicates the presence of both static and collisional quenching or can be the result of a different stoichiometry of the fluorophore–quencher complex. It should be noted that the equilibrium in Fig. 2b for certain quencher–fluorophore combinations might involve protonation or deprotonation of one of the two components; thus the K_{SV} in this case can be considered to be a *conditional stability constant* at a given pH, but it would change with the pH of the solution. If enantioselective fluorescence quenching is present, the Stern–Volmer equation for a mixture of a given analyte can be used in the following form [13]:

$$F_0/F = 1 + K_S[Q_S] + K_R[Q_R] = 1 + [K_S + (K_S - K_R)x_S][Q], \quad (2)$$

where F_0 is the fluorescence intensity of the fluorophore without quencher, F is the fluorescence observed after addition of the quencher molecule, x_S and x_R are the molar fraction of the two enantiomers of the quencher molecule Q_S and Q_R , $[Q]$ is the total quencher concentration, and K_R and K_S are the Stern–Volmer constants. If the total quencher concentration is kept constant in a series of measurements, F_0/F varies linearly with the enantiomer molar fraction x_S . This approach can be useful when the pure compounds are present, since a mixture of different compounds would give rise to a combination of effects. However, if this system is used for the measurement of the enantioselectivity of the reactions producing only one chiral

compound able to bind to the sensors, it can allow rapid screening of best performing reaction conditions. It should be noted that, according to this model, only the quantity F_0/F is linearly dependent on the enantiomeric composition.

3.2 Sensing by Collisional Fluorescence Quenching

Chiral amines have been shown to be able to quench the fluorescence of several fluorophores. The first cases were reported by Irie and coworkers, who described that the collisional quenching of (*R*)-binaphthyl by *N,N*-dimethyl-1-phenylethylamine was dependent on the stereochemistry of the latter [50]. The mechanism of this process corresponds to a series of subsequent events: formation of an encounter complex between the excited fluorophore and the quencher, which can then give rise to a tight exciplex ($[A-F^*]$ in Fig. 2a) or to an electron transfer ion pair $[A^-F^+]$ (Fig. 2a). This can explain the strong dependence of both quenching and enantioselectivity upon the polarity of the solvent observed in these studies [126].

The low fluorescence in the FQ complex can be derived from non-radiative decay due to the occurrence of either energy or electron transfer. These processes are difficult to demonstrate, and even more difficult to design. Therefore in the recent literature this approach has not been extensively used for the design of enantioselective sensors, though combination of static and dynamic quenching has been documented in some cases.

3.3 Enantioselective Quenching Involving Metal Complexes

Chiral fluorescent molecule bearing binding sites for metal ions are commonly used to obtain metal ion sensors [127], but can also be an efficient tool to induce enantiomeric recognition, since the ion can behave as a strong binding site for very polar analytes containing donor atoms. Furthermore, several metal ions, such as copper(II) or nickel(II) quench the fluorescence of many fluorophores, thus providing the signaling process needed for sensing. Copper(II) is a very efficient quencher, as it is able to quench the fluorescence of groups not directly linked in its proximity [128]. If the fluorescent sensor is a copper(II) complex of a chiral ligand, metal binding molecules, such as amino acids or hydroxy acids, can undergo chiral discrimination since they form ternary diastereomeric complexes with the ligand, with different stabilities and different physical properties, as in the case of ligand exchange chromatography (LEC) [129]. Cyclodextrins bearing a metal binding site can be used in this context as ditopic receptors able to combine the coordination properties of a metal ion and inclusion of apolar moieties in the cyclodextrin cavity [130, 131], thus obtaining high enantioselectivity [36, 37].

Cyclodextrins modified with dansyl (5-dimethylamino-1-naphthalenesulfonyl) fluorophore were used by us for generating enantioselective fluorescence response

using copper(II) quenching. The modified cyclodextrins bearing the fluorophore linked to the upper rim (C6 atom of one glucose unit), reported in Fig. 3, are highly fluorescent, if compared to the free fluorophore in solution, due to the self inclusion of the dansyl moiety within the cyclodextrin cavity [132].

Since donor atoms are present in the linking moiety connecting the cyclodextrin to the dansyl group, they are able to interact with copper(II) ions giving rise to a non-fluorescent binary complex. The fluorescence of the cyclodextrin is recovered enantioselectively by addition of enantiomers of amino acids (Fig. 3b) [87]. Cyclodextrins bearing an L-amino acid derivatives as linker (**S**)-**1-4** gave the best enantioselectivity. If the quenching experiment is carried out using the copper(II) complex of the analyte (instead of the analyte itself) on the free cyclodextrin (Fig. 3c), ternary diastereomeric complexes of different stabilities can be obtained [88]:

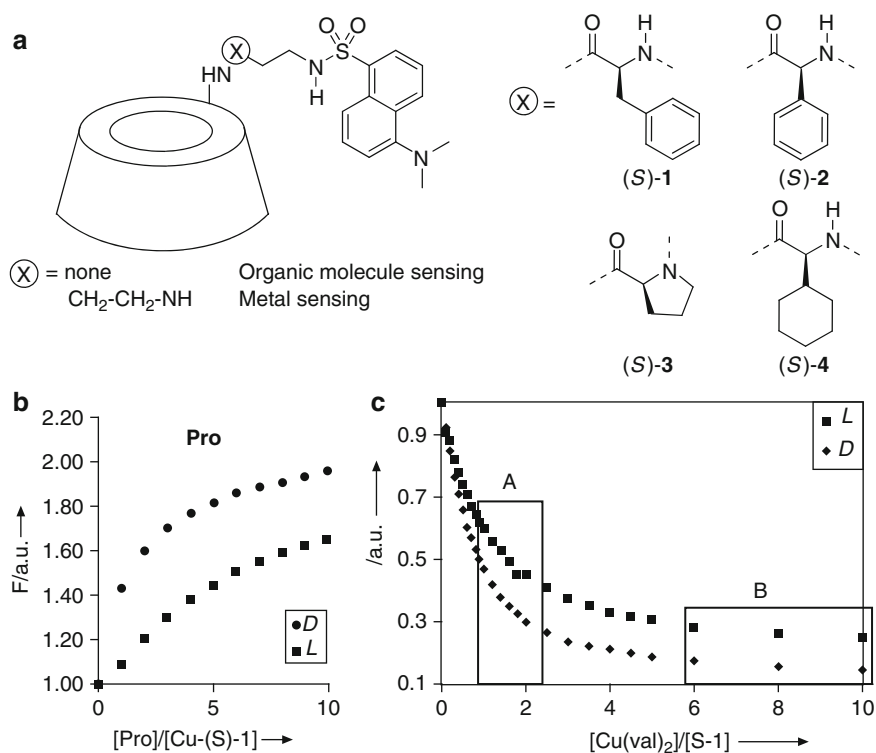
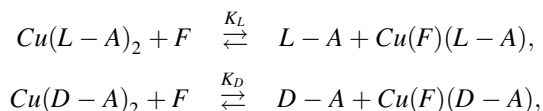


Fig. 3 (a) Fluorescent cyclodextrins used for enantioselective sensing of amino acids; (b) enhancement of fluorescence by addition of proline to Cu(**S**)-**1** (reprinted with permission from Elsevier from [87]); (c) quenching of fluorescence by addition of Cu(AA)₂ to the free cyclodextrin (**S**)-**1**; in box **A** the signal is strongly dependent on the concentration of Cu(AA)₂ and in box **B** it is mainly dependent on the stereochemistry of the analyte. (reprinted from [90] with permission by the Royal Society of Chemistry)



where L-A and D-A are the D- and L-amino acid (in the anionic form), F is the fluorescent sensor, and Cu(L-A)₂ or Cu(D-A)₂ are the binary copper(II) complexes and Cu(F)(L-A) and Cu(F)(D-A) are the ternary copper(II)/sensor/amino acid. Since the two constants for the formation of the diastereomeric ternary complexes K_L and K_D are different, the amount of the free sensor is different when the two enantiomers of the same amino acid are used. Mechanistic studies showed that chiral discrimination is indeed due to the formation of diastereomeric non-fluorescent ternary complexes. The enantioselective effect was carefully evaluated, from the point of view of analytical applications, by performing statistical analysis and *t*-test for the significance of the differences observed [89]. We strongly recommend this approach in the evaluation of enantioselectivity, especially in the case of very small differences [89].

These chiral sensors were used for the determination of enantiomeric excess using a fast, simple, and low cost technique, such as fluorescence on microplate readers (Fig. 4a). It was possible to perform calibration experiments at low sensor concentration (60 μM) using cyclodextrin (S)-1-3 and adding Cu(A)₂ complexes of proline and valine. The fluorescence measured was a function of the enantiomeric composition of each sample, as reported in Fig. 4a, for cyclodextrin S-2 and valine [90].

Quantitative data were obtained with a 6% accuracy. The entire process (duplicate calibration curves and five samples in triplicate) was performed in 2 min, thus showing that a large number of samples can be analyzed in 1 day using this approach. This was one of the first examples in which the enantiomeric composition was evaluated by very rapid techniques using appropriate calibration curves. The cyclodextrin (S)-4 was also found to be very enantioselective, allowing one to perform calibration of the enantiomeric excess of valine and proline by fluorimetry at a very low (1 μM) sensor concentration [91]. Amino acids were found to be best recognized in terms of both response and enantioselectivity. Good enantioselectivity was observed for *N*-alkyl amino acids and for amino acid amides [92]. The enantiomers of 2-aminocaprolactam 10 (Fig. 4c), which is an important amide intermediate for the synthesis of lysine and can be processed by very enantiospecific enzymes, were analyzed in a similar way using cyclodextrin (S)-2 [91].

This approach is particularly interesting because it requires very low concentrations of the sensor, and it allows one to perform enantioselective sensing in water on very low quantity of unmodified amino acids, which are insoluble in most organic solvents used in the vast majority of sensory systems described in the literature.

A conceptually similar approach was reported recently by Wolf and coworkers. 1,8-Diacridylnaphthalene *N,N'*-dioxide derivative 11, described in Fig. 5a, was found to bind selectively scandium(III) ions, giving rise to fluorescence enhancement [64]. The addition of amino alcohols induced a quenching of the fluorescence of this complex, which was found to be due to ternary scandium–ligand–analyte complex formation, followed by scandium(III) scavenging by the analyte, thus

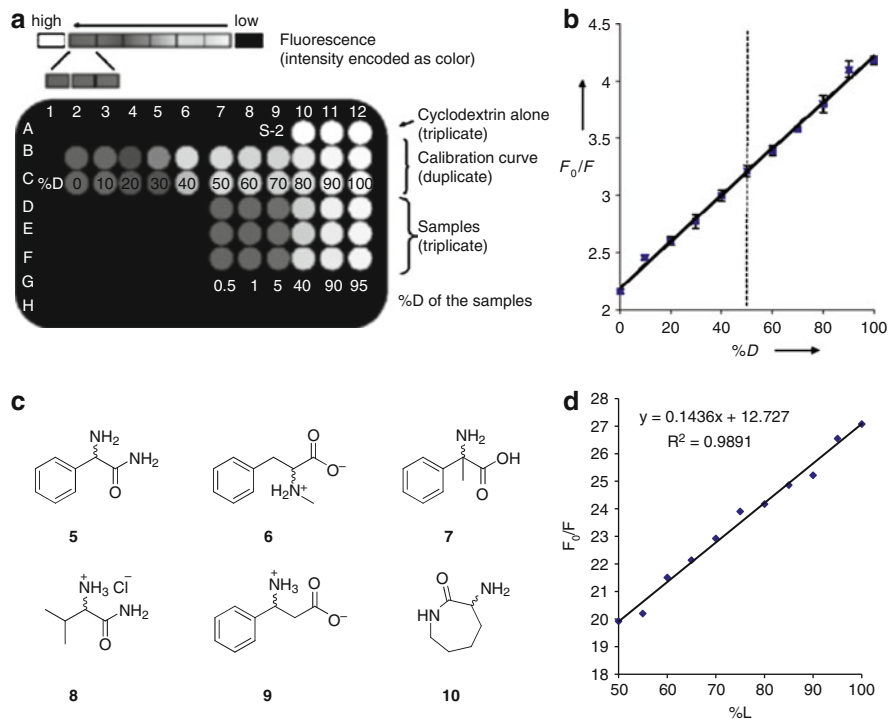


Fig. 4 (a) Enantioselective analysis of valine performed using (S)-2 in 2 min time in a microplate reader; (b) calibration curve of enantiomeric composition obtained for valine using cyclodextrin (S)-2 (a,b: [90]. Reproduced by permission of The Royal Society of Chemistry); (c) analytes (5–10) enantiomerically discriminated using fluorescent cyclodextrins in this type of analysis; (d) calibration curve obtained for the 2-aminocapro lactam using cyclodextrin (S)-2 (from [91] with kind permission from Springer Science + Business)

producing quenching. Using the optically pure scandium complex, high enantioselectivity of the quenching process was observed (e.g., reported in Fig. 5b). Thus using the racemic sensor, the total amino alcohol concentration could be calculated, while by using the optically pure form of the sensor the actual enantiomeric excess was evaluated with about 5% maximum deviation from real values.

Copper(II) complexes of a glutamic acid derived diamido-diamino ligands **12** (Fig. 5c) containing anthracene units were also used as enantioselective sensors for α -hydroxy acids (in particular mandelate) and amino acids [68]. The ligand fluorescence was quenched by copper(II) and recovered by addition of the analytes. A mechanism involving photoinduced electron transfer (PET) was proposed, and the conditional stability constants of the ternary complexes was found to be different for the two mandelate enantiomers (with $K_L/K_D = 15.2$) in this study.

A chiral zinc(II) complex containing a terpyridine fluorophore with C2 symmetry **13** (Fig. 5c) and a crown ether residue was recently reported as fluorescent sensor for amino acids, using the metal ion and the crown ether unit as binding sites

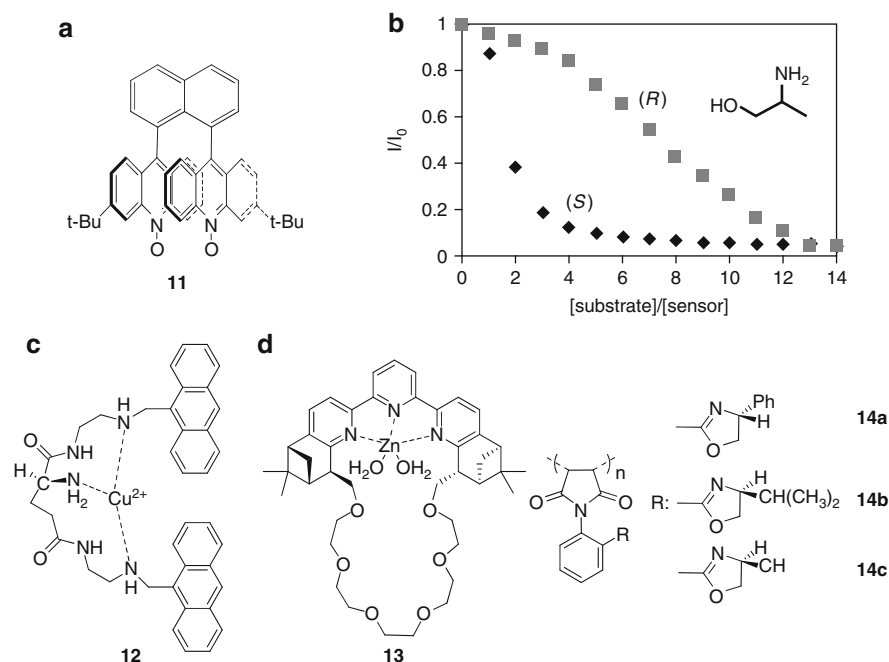


Fig. 5 Examples of quenching enantioselective sensors involving metal ions: (a) *N,N'*-dioxide of the 1,8-diacridylnaphthalene units which can form a scandium(III) complex; (b) high enantioselective quenching obtained by the scandium complex of **11** for 2-aminopropanol (reprinted with permission from [64]. Copyright 2008 American Chemical Society); (c) triamino-diamido copper (II) complex (**12**); (d) Zn (II) complex with terpyridine based chiral ligand (**13**); (e) chiral oxazoline containing maleimido polymers (**14**)

for the carboxylate and the ammonium ion, respectively. This compound was quenched by addition of phenylglycine, but not of other amino acids, in an enantioselective manner, [93].

Recently, poly(*N*-phenylmaleimides) **14a–c** (Fig. 5d) bearing a chiral oxazolinyll pendant were shown to bind zinc(II) and copper(II) ions with moderate and intense quenching respectively. The zinc ion could be used as a coordinating groups for enhancing the interactions with analyte molecules. The addition of enantiomers of BINOL or of 2-amino-1-propanol was shown to modulate the fluorescence intensity with quenching for the former and enhancement of the latter [57].

3.4 Enantioselective Quenching by PET and Related Mechanisms

The interactions of luminescent sensors with analytes can generate or inhibit PET (Fig. 2d). If there is a suitably positioned occupied state at higher energy, the electronic hole generated by the excitation process can be filled by transfer of

one electron to the ground state of the fluorophore, thus inhibiting the radiative decay. This process is strongly dependent on the electron donor–fluorophore distance and, unlike energy transfer (ET), can be slowed down by lowering the temperature. Amino groups are particularly suited as electron donors in PET, although other groups such as amides and thiourea have been reported to be responsible for PET.

Enantioselective quenching of *p*-*tert*-butyl-calix[4]arenes linked to a chiral residue containing a fluorophore by chiral amines (phenylethylamine and norephedrine) was reported earlier; in particular the (*S*)-di-2-naphthylprolinol-containing receptor **15a** (Fig. 6) was found to give rise to enantioselectivity in fluorescence, though differences between the two enantiomers were rather low, but still sufficient to allow one to obtain calibration curves of the enantiomeric composition [58]. Host–guest interactions were found to be responsible for quenching, with a possible PET effect. More recently, a 1,4-disubstituted calyx[4]arene containing aminoacylhydrazide and dansyl groups **15b** (Fig. 6) has been shown to undergo enantioselective quenching by

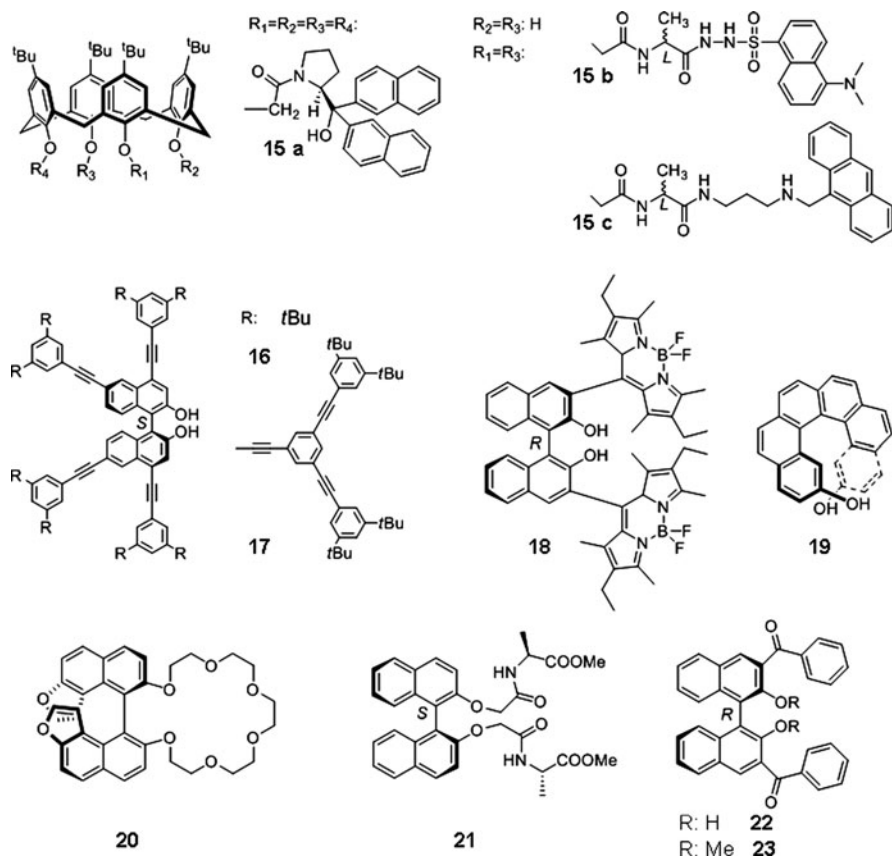


Fig. 6 Examples of sensors based on PET-mediated quenching

N-protected alanine or phenylalanine anions in chloroform; the interaction occurred through hydrogen bonding, as demonstrated by NMR. The quenching effect was attributed to facilitated receptor–fluorophore PET [59]. A similar design was used with the anthracene fluorophore **15c** (Fig. 6), showing enantioselective sensory properties towards malate anions in CDCl_3 , with selectivity K_D/K_L up to 10.41 [60]. Using tryptophan as fluorophore, fluorescent sensors showing enantioselectivity for a wide range of biologically relevant molecules, including free and N-Boc-protected amino acids, amino alcohols, and tartaric and malic acid, were reported in DMSO, with selectivity (K_D/K_L) up to 7.2 [61].

Binding of a molecule containing an amino group held in a position vicinal to a binaphthyl fluorophore is the basic mechanism of a series of studies carried out by Pu and coworkers for enantioselective sensing of compounds containing an amino group [19]. These authors showed that BINOL derivatives are particularly suited for the enantioselective sensing of amino alcohols in organic solvents, due to hydrogen bond formation between the naphthol hydroxyl group and the hydroxyl group of the analyte. This approach was extended to highly conjugated binaphthyl fluorophores with aromatic groups linked through alkyne spacers **16** (Fig. 6) with an enhancement of the fluorescence intensity through intramolecular energy transfer; these molecules were also more sterically demanding sensors for achieving enantioselectivity. An extension of this approach led to the use of binaphthol-based dendrimers **17** (Fig. 6), which showed high fluorescence intensity, increasing with the number of external chromophores. More recently, tetrahydroxy 1,1'-binaphthyl compounds were proposed within the same scheme, though with weak enantioselectivity for amino alcohols and diamines [133]. A binaphthyl core conjugated with other aromatic moieties and fluorophores, such as boron-dipyrromethene (BODIPY) **18** (Fig. 6) was shown to exhibit an enantioselective response [134]. Helicene-diol based sensors **19** (Fig. 6) also showed enantioselectivity in quenching by chiral amines and amino alcohols [51].

More recently, binaphthyl fused with a furane ring ((*R*)-(–)[9,9']-bi[naphtho(2,1-*b*)furanyl]-8,8'-diol) linked to a crown ether residue **20** was shown to be able to discriminate between enantiomers of phenylethylamine and valine ethyl ester by quenching, allowing calibration of the quenching effect as a function of enantiomeric composition [52].

BINOL derivatives substituted at the phenolic oxygen by a carboxymethyl group linked to amino acids methyl esters **21** (Fig. 6) performed as dicarboxylic acid-responsive sensors, showing enantiodiscrimination for dibenzoyl tartrate (as tetrabutylammonium salt) in DMSO solutions. A facilitated PET process from the amide to the BINOL moiety was proposed to be occurring also in this case, leading to fluorescence quenching, with a $K_D/K_L = 17.35$ for the alanine containing sensor [107].

Simple sensors such as 3,3'-dibenzoyl-BINOL **22** and its dimethylated analog (Fig. 6) were recently reported to give enantioselective quenching by a variety of molecules, namely Boc-protected amino acids, hydroxy acids, and amino alcohols, with a maximum selectivity K_R/K_S of 7.72 for Boc-Phe [62]. A PET process was also proposed in this case, in analogy with previous studies on anion binding.

BINOL derivatives containing two thiourea residues (binding site for anions) have recently been used to obtain PET enantioselective quenching with α -hydroxy as well as α -amino acids [63].

Cholic acid amidothiourea derivatives containing an anthracene unit were shown to be selective fluorescent sensors for different anions (Br^- , F^- , acetate, benzoate, and phosphate) due to the modulation of PET from the sulfur atom to the anthracene moiety [135]. The presence of a chiral cholic acid residue suggested that enantiomeric sensing could also be achieved. Therefore, two receptors of this type, **24**, containing an additional chiral diaminocyclohexane group were used for enantioselective sensing of tetrabutylammonium salts of amino acids in acetonitrile by quenching. Since these molecules are ditopic receptors, best results were obtained with amino acids containing polar groups, such as Ser, Thr, Lys, Tyr, with a reversed selectivity as a function of the diaminocyclohexane stereochemistry. Structural studies carried out by NMR provided evidence for the interaction of the analyte with both the thiourea and the diaminocyclohexane groups. Calibration of the fluorescence intensity vs D-Ser percentage (using 50 equivalent excess) was shown to be linear [94].

The thiourea units were also used by Hyun and coworkers for the design of an anthracene containing chiral cleft molecule **25** including two glucopyranosyl groups (Fig. 7). These compounds were shown to undergo enantioselective quenching in the presence of Boc- and dinitrobenzoyl (DNB)-protected amino acids in acetonitrile, with α values up to 10.4. Both quenching efficiency and stereoselectivity were found to be dependent on the type of linker between anthracene and the thiourea units [100].

The combination of enantioselective selectors with fluorophore residues allowed one to use other preorganized scaffolds for enantioselective sensing. For example, using diamine-9,9-dimethylxanthenes modified with dansyl-leucine (**26** Fig. 7) it was possible to obtain the enantioselective quenching of carbamoyl lactic acid, which was attributed to a PET mechanism [83].

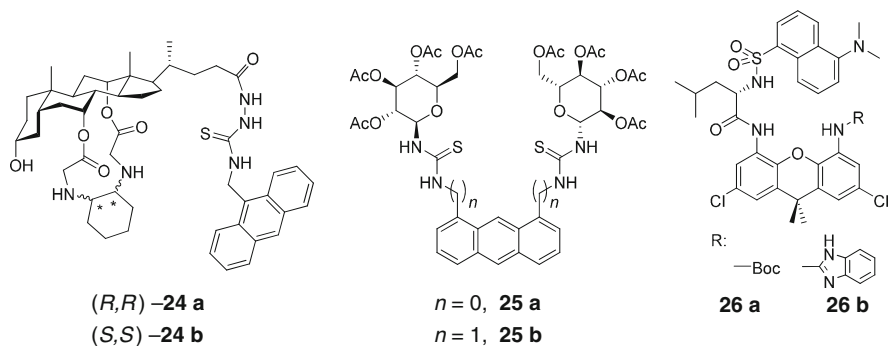


Fig. 7 Cleft-like molecules showing PET enantioselective quenching

3.5 Fluorescence Enhancement by PET Inhibition

Intramolecular PET processes can also be exploited for inducing a fluorescence enhancement in the presence of the analyte, which is a highly desirable effect in sensor technology. The proximity of a suitable fluorophore to an unprotonated amino group can generate low fluorescence of the sensor in its unbound state, due to the PET from the nitrogen lone pair to the excited state of the fluorophore. This effect was extensively utilized by several groups to generate metal ion sensors, since coordination of the lone pair prevents PET, thus “switching on” the fluorescence signal [136]. Organic molecules can produce a similar effect by protonation of the amino group with formation of an ion pair [137].

One of the most important classes of “switching on” fluorescent sensors was proposed by James and Shinkai several years ago and is based on the combination of the binaphthyl unit with boronic acid binding sites **27** (Fig. 8), which were shown to undergo fluorescence enhancement upon addition of sugars, giving an enantioselective response with D- or L-glucose [48]. The mechanism for carbohydrate sensing has been shown to be due to the substitution reaction of the OH groups of the boronic acid with the hydroxyl groups of the sugar. This substitution enhances the Lewis acidity of boron, and enforces its interaction with the nitrogen lone pair (Fig. 8b), thus suppressing the PET process to the fluorophore, and allowing the fluorescence to switch on. Enantioselective “to be switched on” was observed for the enantiomers of fructose, glucose, and galactose, with the D-enantiomer being more effectively bound [116].

Other bifunctional molecules such as hydroxy acids can bind to the boronic acid residue; following this model, an anthracene derived chiral monoboronic acid sensor **28** was recently described by James [69] (Fig. 8) and fluorescence enhancement due to PET suppression was observed, with enantioselectivity for lactic, mandelic, and tartaric acids. In a more recent study, a 3,6-disubstituted carbazole-derived bis-boronic acid **29** (Fig. 8) was described [112], showing very interesting fluorescent properties. A reversed PET mechanism, i.e., quenching of fluorescence due to transfer of one electron from the fluorophore excited state (d-PET), has been proposed for these molecules. Calculation of the frontier molecular orbitals by density functional theory (DFT) indicated that this mechanism is likely to occur and can be rationally designed [138]. When a positively charged ammonium group is generated in the proximity of carbazole, fluorescence quenching is observed due to transfer of one electron from the fluorophore to the ammonium group (as evaluated by electron density in the LUMO). Thus these molecules exhibit a fluorescence which is a function of both pH and of the presence of guests, which might stabilize the positive charge by ion-pair formation. By opportunely tuning the pH at which the analyte is added, an enhancement or a quenching can be obtained. (Fig. 8b, c). At pH 7.4 a high fluorescence enhancement was observed for L-tartaric acid and a very weak one for D-tartaric acid, whereas at pH 5.4 the L-enantiomer induced enhancement, while the D- was found to produce quenching. Cyclic peptides containing two boronic acid units **30** (Fig. 8) were also employed for sensing of

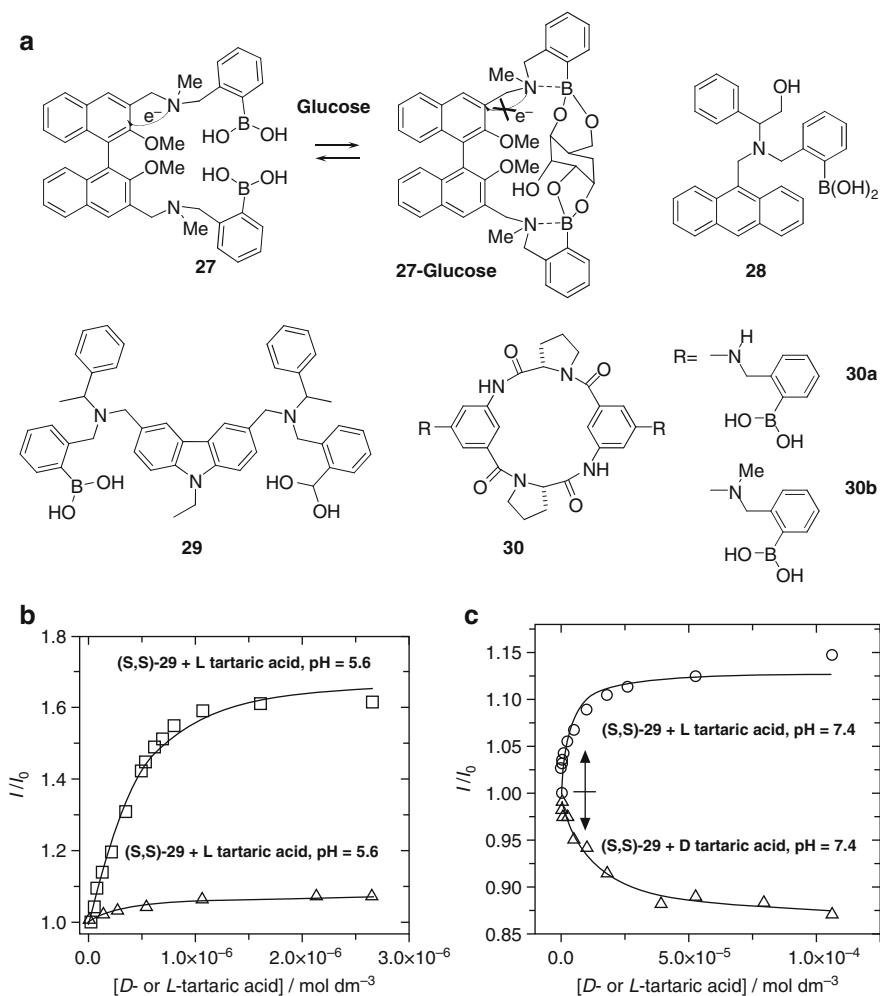


Fig. 8 (a) Enantioselective sensors based on boronic acid units for PET suppression. (b,c) Fluorescence response of the sensor **29** in the presence of either D- or L-tartaric acid at pH 5.6 (b) and 7.4 (c) (reprinted with permission from [112]. Copyright 2008 American Chemical Society)

carbohydrates, with enantioselectivity demonstrated for D- and L-glucose, attributed to enhanced PET [117].

The incorporation of amines into binaphthyl-based sensors can also be used in order to induce intramolecular PET on the sensor, which is then inhibited by binding to acidic compounds, thus enabling one to discriminate between enantiomers of organic acids. Additional binding sites and hydrogen bonding groups can enhance both binding and enantioselectivity (Fig. 9).

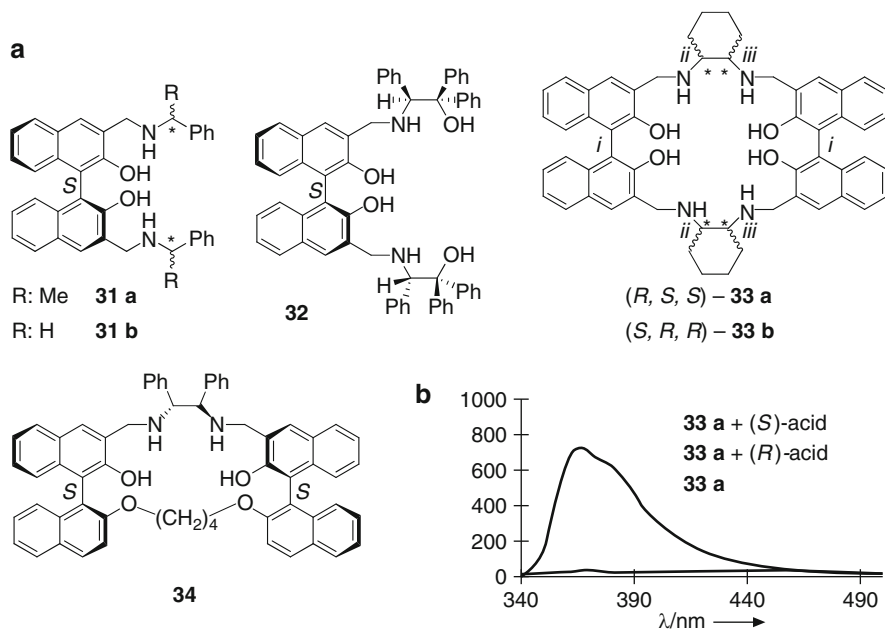


Fig. 9 (a) BINOL-based enantioselective sensors showing PET inhibition; (b) fluorescence response of (*S*)-**33** for (*R*)- and (*S*)-mandelic acid, an example of efficient “yes or no” response (reproduced with permission from [77]. Copyright Wiley-VCH Verlag GmbH & Co. KGaA)

Coupling of the chiral BINOL unit with two chiral arms containing an amino group was found to give rise to enantioselective fluorescence “switch on” in the presence of organic acids. α -Hydroxy acids and benzyloxycarbonyl (*Z*)-protected amino acid derivatives were shown to produce enantioselective “switch on” in binaphthyl-derived sensors containing an *N*-alkylaminomethyl moiety, with good enantioselectivity [70]. Similar compounds were subsequently found to have good enantioselectivity in the fluorescence enhancement for Boc-amino acids, with $\Delta F_R/\Delta F_S$ of 10.4 for the proline derivative [71].

The use of a disubstituted amino alcohol in cleft-like derivatives **32** (Fig. 9) was recently described as an efficient strategy for obtaining very high enantioselectivity ($ef = 11.2$ for mandelic acid enantiomers) [72]. This system was shown to act with different mechanisms according to its stereochemistry, since one of the two enantiomers induced recovery of fluorescence of the binaphthyl group, while the other was shown to induce exciplex formation, quenching the fluorescence of the monomeric fluorophore.

BINOL derivatives with pendant thiourea residues were also described, with some enantioselectivity for mandelic acid enantiomers [73].

Chiral constrained amines, such as 1,2-diaminocyclohexane, were used to induce higher enantioselectivity. 1,2-Diphenylethylenediamine was initially used by Pu and coworkers, showing that a macrocyclic structure could produce enantioselective response for amino acid derivatives and hydroxy acids [74, 75]. In a recent

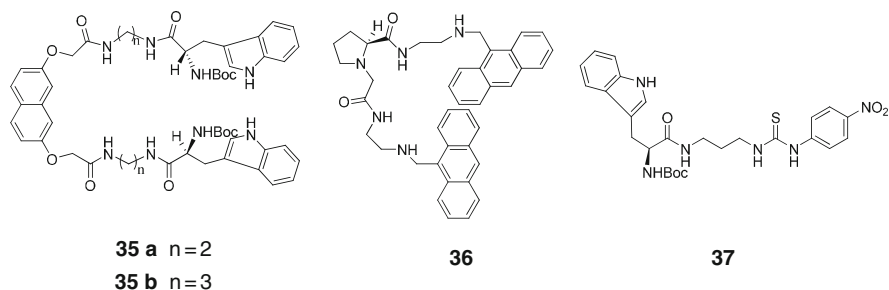


Fig. 10 Enantioselective cleft-like sensors showing fluorescence enhancement due to PET suppression

and very efficient example, hydroxy acids were shown to be sensed in a “yes or no” fashion using the cyclic derivative **33** (Fig. 9) containing two 1,2-diaminocyclohexane units: an *ee* of up to 46 was achieved in these studies (Fig. 9b) [76, 77]. On account of the good enantioselectivity shown by these systems, it was possible to use fluorescence measurements to monitor the enantioselectivity of formation of *para*-substituted mandelic acids from benzaldehyde in the presence of chiral catalysts, with results comparable to those obtained with a chiral HPLC method [78].

A similar cyclic system with an achiral flexible spacer **34** was also described (Fig. 9), but the enantioselectivity in this case was not as high as that observed for the more rigid sensors [79].

Naphthalene based chiral cleft-like molecules were also used, such as the tetraamidic compounds **35** (Fig. 10) which were shown to be able to discriminate between enantiomers of dibenzoyl tartrate. Inhibition of the PET from neighboring amide groups was proposed as a possible sensing mechanism, with an observed binding enantioselectivity of $K_D/K_L \approx 6.2$ [115]. Cleft-like molecules containing a proline linker and two anthryl moieties **36** (Fig. 10) were described by He with enantioselective fluorescence enhancement demonstrated for mandelic acid in DMSO [80]. Enhancement of the fluorescence intensity was also reported for a tryptophan derivative **37** (Fig. 10) bearing a linking amide group and a thiourea moiety: this compound was shown to undergo fluorescence enhancement upon addition of Boc-amino acids in DMSO, with some enantioselectivity for Ala and Glu derivatives. A suppression of a PET induced effect was suggested in the case of Ala, while a new excimer emission appeared for Glu [101].

3.6 Fluorescence Response Due to Changes in the Sensor Structure

The formation of the sensor–analyte complex can lead to changes in the structure of the emitting species such as change of conformation, excimer formation, and

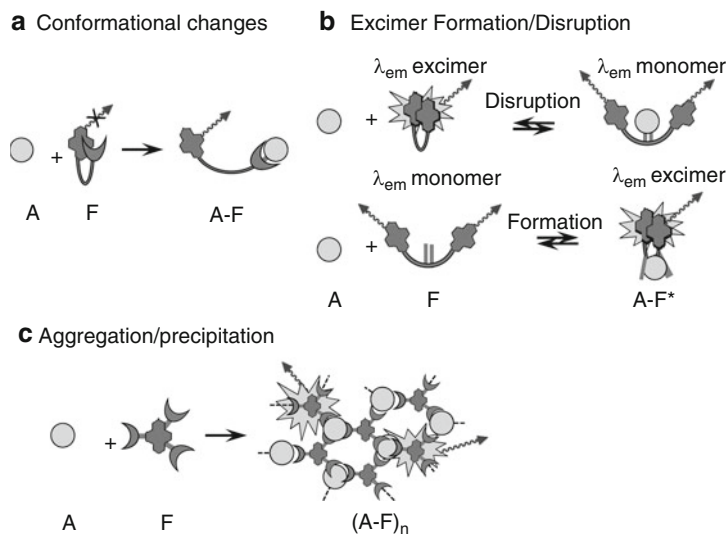


Fig. 11 Mechanism of sensing due to changes in the conformation/aggregation of emitting species

aggregation. If these changes are able to affect the fluorescence emission properties, changes in intensity and in wavelength can be observed (Fig. 11).

One model which has been largely used in sensory systems is the change of conformation in modified cyclodextrins (CD) containing a lipophilic fluorescent group. The self inclusion process is dependent on the size of the cavity (therefore it depends upon the use of α , β , or γ -cyclodextrins) and for larger cavities inclusion of two fluorophores with excimer formation was observed. The mechanism of sensing is reported in Fig. 12a. The inclusion of a chiral guest can displace the fluorophore from the cavity, thus inducing different fluorescent properties. For example, the *p*-dimethylaminobenzoyl unit showed a twisted intramolecular charge transfer (TICT) when included in the β -cyclodextrin cavity, whereas an emission typical of a planar excited state was observed upon addition of organic guests, with enantioselectivity for D- and L-menthol [118]. In general, cyclodextrins have been shown to give rise to good chemoselectivity and usually weak enantioselectivity [119, 120] due to their relatively symmetric cavity, which allows inclusion of both enantiomers of lipophilic guests. In order to increase enantioselectivity, a successful strategy was that of inserting binding sites (such as for metal ions as discussed before) or additional chiral residues on the cyclodextrin rim, as demonstrated for a series of dansylamino acid derived β -cyclodextrins, which were able to discriminate between a series of organic molecules by enantioselective inclusion [121].

Macrocyclic receptors containing two binaphthol groups with imidazolium-based linkers **38**, **39** (Fig. 12) were shown to undergo enantioselective fluorescence enhancement in the presence of D- and L-Trp in water, due to a rearrangement of the receptor conformation upon complexation [95].

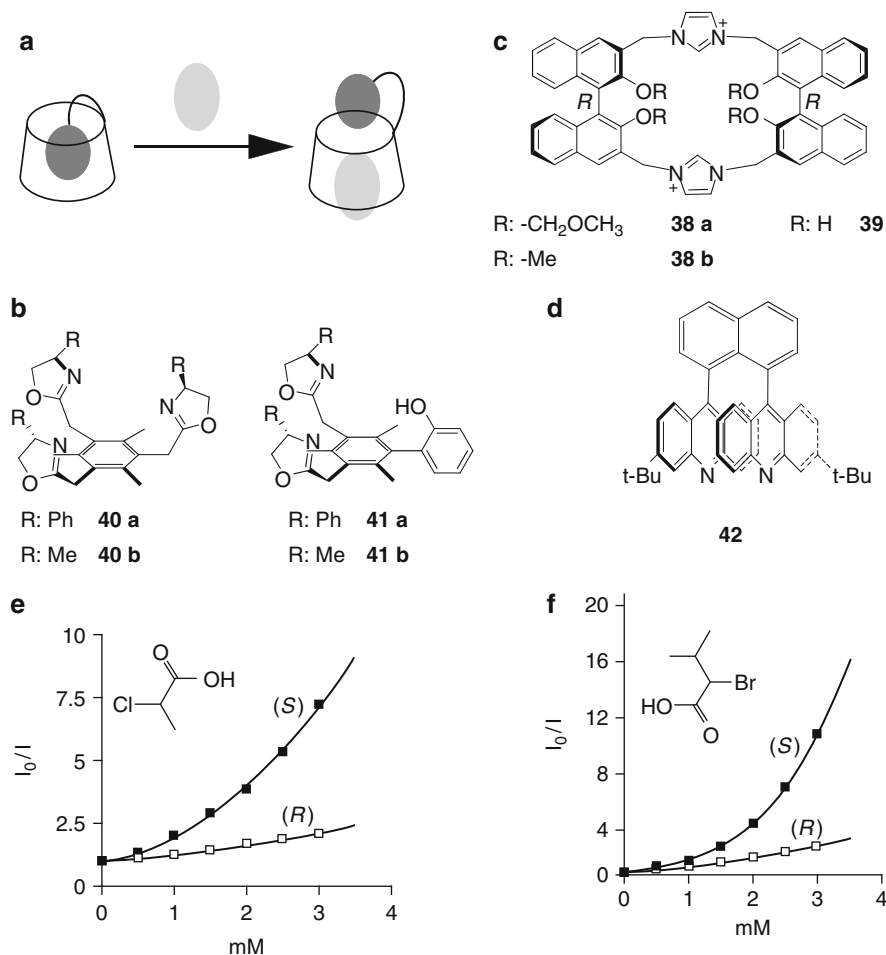


Fig. 12 Enantioselective sensing by conformational changes in the sensors. **(a)** Mechanism of sensing in fluorophore-bearing cyclodextrins by interaction with a guest; **(b)** water soluble imidazolium containing BINOL macrocycles **38**, **39**; **(c)** tris- and bis(oxazolonyl)phenols (**40**, **41**); **(d)** 1,8-bis(9,9'-diacridyl)naphthalene derivative **42**; **(e)** Stern–Volmer plot of **42** upon interaction with enantiomers of α -halo acids (*left* 2-chloropropanoic acid, *right* 2-bromo-3-methylbutanoic acid), showing nonlinear response (from [85]; reproduced by permission of The Royal Society of Chemistry)

Tripodal cleft-like molecules such as **40** were shown to act as fluorescence sensors for ammonium ions; starting from this model bis(oxazolonyl)phenols (**41**) were developed and were shown to undergo conformational changes, due to the interaction with amine guests, leading in some cases to fluorescence enhancement and in others to fluorescence sensing. Enantioselective fluorescence sensing of phenylethylamine was observed. The steric interactions between the oxazolonyl

phenyl substituents and the guest's α -substituents were thought to be responsible for the observed differential binding [53].

Even more selective molecular clefts are those based on the 1,8-biarylnaphthalene scaffold developed by Wolf and coworkers. The 1,8-diarylnaphthalene unit has a high rotational energy barrier, which allowed these authors to obtain stable enantiomeric atropoisomers and create a very narrow lipophilic pocket [139]. Using monosubstituted acridine residues, this barrier is very high, and stable enantiomers are obtained which can be separated by chiral HPLC. For example, 1,8-bis(3,3'-(3,5-dimethylphenyl)-9,9'-diacridyl)naphthalene enantiomers were resolved. This molecule has a C₂ symmetric cleft and was used as a fluorescent sensor for a broad variety of carboxylic acids, including protected amino acids, aliphatic acids, arylalkanoic acids, and α -halogenated carboxylic acids, all giving rise to enantioselectivity due to complex formation (static quenching), with K_R/K_S up to 4.5 for the most sterically hindered acid, for which an enantiomeric purity was calculated by fluorescence measurements with $\pm 3\%$ accuracy [84]. A similar sensor with *tert*-butyl substituents on the acridine rings **42** was shown to be able to discriminate between enantiomers of carboxylic acids and protected amino acids. A method for the analysis of α -chloropropionic acid was thus developed, enabling these authors to calculate both the total analyte concentration, using the racemic mixture of the sensor (with 3% maximum deviation) and the enantiomeric excess using a single-enantiomer (with 2% maximum deviation) [85]. Nonlinearity of the Stern–Volmer plot was observed (Fig. 12e), attributed to the presence of both static and dynamic quenching, as demonstrated by fluorescence lifetime measurements [140]. Due to this nonlinear effect, enantioselectivity in fluorescence response increased as the concentration of the analyte increased.

The *N,N*-dioxide of this compound **11** (Fig. 5) showed changes in fluorescence upon addition of guest molecules, with opposite effects for *N*-protected amino acids (showing quenching) and diamines (showing fluorescence enhancement), both effects being the result of the formation of a complex [54]. The enantiomeric discrimination of *trans*-1,2-diaminocyclohexane by this type of sensor was used as a screening method for the evaluation of enantioselectivity in *Candida antarctica* lipase catalyzed acylation reactions: results, compared with HPLC chiral analysis, gave 8% maximum deviation [55]. The fluorescent sensor offered the advantage of direct read-out without laborious sample treatment. Subsequent work involving chiral carboxylic acids showed that the total analyte concentration and the enantiomeric excess (both with about 10% maximum deviation) could be calculated [86].

Differences in the fluorescent intensities upon induction of conformational changes are observed in the case of fluorescently labeled biopolymers such as protein or DNA, though these scaffolds have not been extensively used so far for the synthesis of enantioselective luminescent sensors. An advantage of using these natural scaffolds is that high enantiomeric recognition is one of their intrinsic properties [141].

In a study aimed at obtaining enantioselective quartz crystal microbalance (QCM) sensors, it was found that bovine serum albumin (BSA) and human serum albumin (HSA) bind enantioselectively amines, alcohols, and esters with a decrease

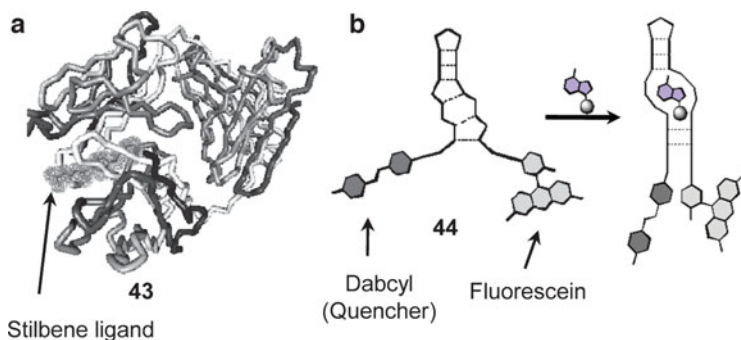


Fig. 13 Biomolecules used as enantioselective fluorescence sensors. (a) Blue fluorescent antibody **43** interacting with stilbene derivatives (structure from protein data bank, entry:1FL3 [124]; (b) sensing of adenosine enantiomers by the DNA aptamer **44**

in fluorescence, attributed to static quenching [56]. A blue fluorescent antibody **43** (19G2), which emits blue fluorescence upon binding to stilbene tags (Fig. 13), was developed as fluorescent sensor by Matsushita, Janda and coworkers. It was found that each of the chiral *trans*-stilbene amino acid esters (R) and (S) could bind to 19G2, but that only the (S)-19G2 complex gave a blue fluorescent emission (λ_{exc} 327 and 410 nm) [105]. This property was used to screen enantioselectivity in a chiral phase transfer catalyst library and with Jacobsen's chiral catalysts in the asymmetric epoxide opening reaction by azide in stilbene-linked substrates [106].

Aptamers are functional oligonucleotides which are obtained by a feedback driven selection scheme in order to be able to give strong and selective interactions for a given target molecule. Fluorescence labeling of aptamers can lead to sensory systems of remarkable specificity. The use of this strategy for enantioselective sensing has, however, been explored only recently. One of the possible designs is of the "molecular beacon" type, in which a fluorophore and a quencher are linked to the opposite ends of an oligonucleotide. The interaction between these two residues by energy transfer (ET) causes quenching of the fluorophore. If a conformational change occurs, the two residues can either be separated, giving rise to a recovery of the fluorescence signal, or be enforced in a close position, causing a more efficient quenching. DNA aptamers **44** targeted against ATP were synthesized with a beacon design (Fig. 13b) and were shown to undergo a quenching process in the presence of adenosine, while they were not affected by other nucleosides. D- and L-adenosine were found to give different quenching, but with a weak difference between them [124].

3.7 Modulation of Excimer or Exciplex Formation

Since excimers and exciplexes give rise to distinct emission bands from monomeric fluorophores, the conformational changes of a given sensor bearing two identical

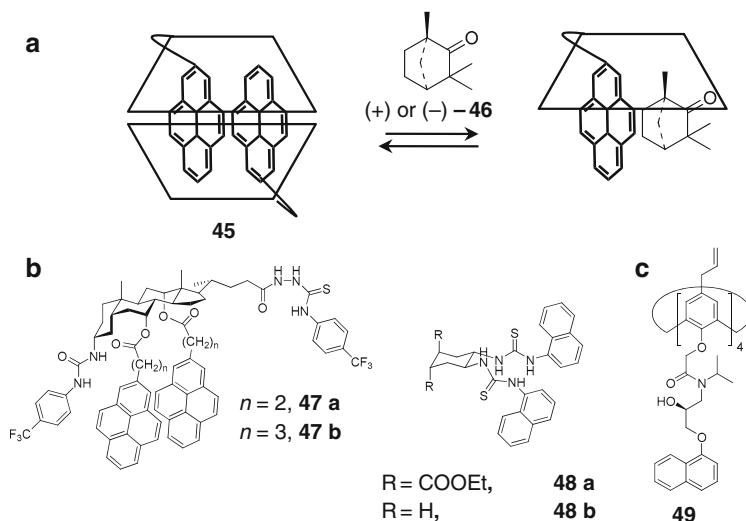


Fig. 14 Examples of enantioselective sensors based on excimer formation. **(a)** Dimeric pyrene-containing γ -cyclodextrins and their mechanism of enantioselective sensing upon interaction with a guest molecule; **(b)** cleft-like sensors based on excimer modulation; **(c)** naphthol containing calixarene derivative **49**

fluorophores can in some cases be easily detected by the appearance or disappearance of the exciton band at longer wavelength (Fig. 11b).

The disruption of a dimeric form of cyclodextrins containing an appended pyrene unit (Fig. 14a) as a result of the inclusion of a guest compound was the rationale of the observed quenching of the pyrene excimer band observed by Ueno and coworkers [122]. Small differences in the inclusion of the two fenchone enantiomers (+)- and (-)-**46** were reported.

The cholic acid derived sensors containing two pyrene units **47** (Fig. 14) showed excimer emission. The presence of two thiourea units allowed one to form stable complexes with dicarboxylic acids (with K_{ass} in the range of 10^5 – 10^7 M^{-1} in acetonitrile), with a decrease of the fluorescence of the excimer band. This interaction was attributed to the enhancement of the PET effect and to a decrease of the π - π stacking interaction of the two pyrene units, which was found to be different for the two tetrabutylammonium salts of D- and L-glutamic acid [108]. Similarly, enantioselective quenching of bands due to both the monomeric fluorophore and the excimer emission was observed for the mandelate anion in a related sensor containing only one thiourea unit [109].

In an interesting case, the naphthalene containing sensors **48** were reported to have little or no enantioselectivity as far as the formation constants were concerned, although significant differences in both absorbance and fluorescence spectra were observed upon addition of D- and L-aspartate, glutamate, and tartrate [110], arising from enhanced preferential boat-like conformation of the selector, which induced excimer formation. When the ethoxycarbonyl units were removed (**48b**), this

conformational preference changed and a 2:1 complex was observed by addition of the enantiomer of dicarboxylic acids such as Asp, Glu, and camphoric acid in a DMSO solutions, leading to weaker differences in the fluorescence spectra [111].

Enhancement of the excimer band was observed for the interaction of the (R)-enantiomer of phenylalaninol (PA) with the substituted calyx[4]arene **49**, which was demonstrated to be due to a change in the calixarene conformation induced by complexation of the guest molecule. The monomeric band was instead quenched by both enantiomers, suggesting that complexation occurred also in the case of the (S)-enantiomer. The enantioselectivity was found to be solvent dependent, being present in the case of chloroform but absent in methanol [65].

The appearance of a new fluorescence band was also observed in the case of the macrocyclic receptors containing naphthalene and valine **50** (Fig. 15), as a consequence of an unusual intramolecular exciplex with the amino groups [102]. Binding of protected amino acids in dichloromethane led to a quenching of the exciplex band (390 nm) and enhancement of the monomer band (340 nm). This process was found to be enantioselective and dependent on the size of the macrocycle. Measurement of the ratio between the monomer and exciplex emission allowed one to measure differences in fluorescence with a higher precision [103]. A detailed study based on ESI-MS and NMR allowed these authors to propose a proton transfer mechanism from the acidic moiety of the amino acid to the amino group of the receptor, followed by the formation of an intimate ion pair stabilized by aromatic–aromatic interactions. This process competes with the exciplex formation, thus leading to enhancement of the naphthalene emission [104].

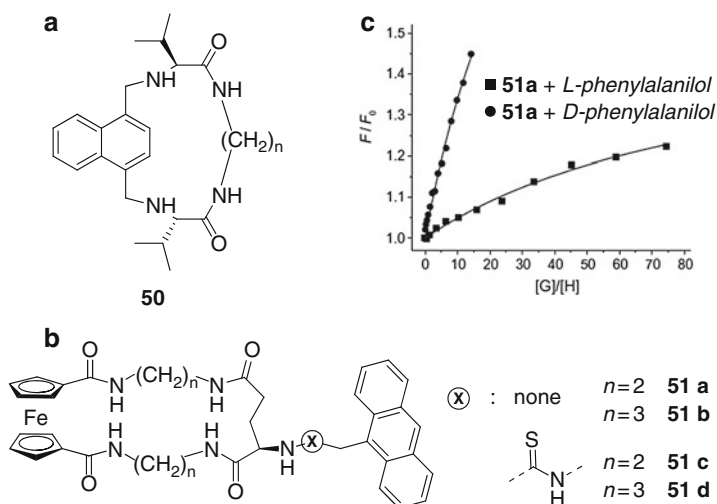


Fig. 15 Examples of macrocyclic receptors showing exciplex formation. (a) Valine derived macrocyclic sensor; (b) complex sensors bearing ferrocene and anthracene units; (c) fluorescence enhancement at 414 nm of the sensor **51a** upon addition of phenylalaninol, showing a high enantioselective response (reprinted from [66]. Copyright (2009) with permission from Elsevier)

Ferrocenyl containing macrocycles **51** (Fig. 15), using as chiral source a D-glutamic acid residue, showed specific complexation for phenylglycinol and phenylalaninol, due to favorable π - π stacking interactions, and was accompanied by an increase of the fluorescent intensity, which was different for the different emission bands with high enantioselectivity (Fig. 15c). This was interpreted as the occurrence of an exciplex between the selector and the analyte, and a corresponding inhibition of energy transfer between the anthracene residue and the ferrocenyl quencher [66].

4 Enantioselectivity in Aggregation/Precipitation Induced Fluorescence Emission

Aggregation of molecules into homo- and hetero-oligomeric supramolecular entities is a process which can modulate electronic properties of the monomeric units, including fluorescence. This effect has been also exploited in several recent applications in the field of enantioselective sensing. Some selectors designed to perform simple host-guest interactions with a specific analyte turned out to have peculiar properties due to the formation of high molecular weight aggregates.

The Schiff bases obtained by reaction of 4-methyl-2,6-diformylphenol with L- or D-phenylglycinol **52** (Fig. 16) were found to interact enantioselectively with the two enantiomers of mandelic acid on account of the appearance of a fluorescent component with a longer lifetime. A job plot of the complex formation, however, revealed a 2:3 guest: host stoichiometry of the complex formed, thus suggesting an oligomeric form of the type reported in Fig. 16b. The good enantioselectivity observed ($K_S/K_R = 4$ for the (R,R)-sensor) also allowed these authors to calibrate the fluorescence response vs the enantiomeric compositions of mandelic acid in benzene solutions containing 10^{-4} M of the sensor [81].

Aggregation induced emission enhancement (AIEE) is a property displayed by organic compounds which are non- or poorly fluorescent in solution, but that form highly fluorescent solids and/or suspensions. By combining moieties of organic compounds able to produce AIEE with chiral units, it is possible to modulate the aggregation process by enantioselective interactions. Zheng and coworkers linked a dibenzoyl tartrate residue to the AIEE moiety 2-phenyl-3-(*p*-aminophenyl)acrylonitrile: the acidic sensor **53** obtained (Fig. 16c) was found to undergo AIEE upon interaction with chiral amines; the precipitation process turned out to be nonlinearly dependent on the enantiomeric composition of the analyte and of the receptor. 2-Amino-1,2-diphenylethanol enantiomers were found to produce a remarkably high difference, with the (1R,2S)-enantiomer producing an enhancement 262 times higher than its (1S,2R) enantiomer when using the L-tartrate derivative. Very high ratios were also observed for other amino alcohols and amines [67].

The same moiety was linked to the (1R,2S)- and (1S,2R)-enantiomers of 2-amino-1,2-diphenylethanol through a carboxymethyl spacer, obtaining the chiral

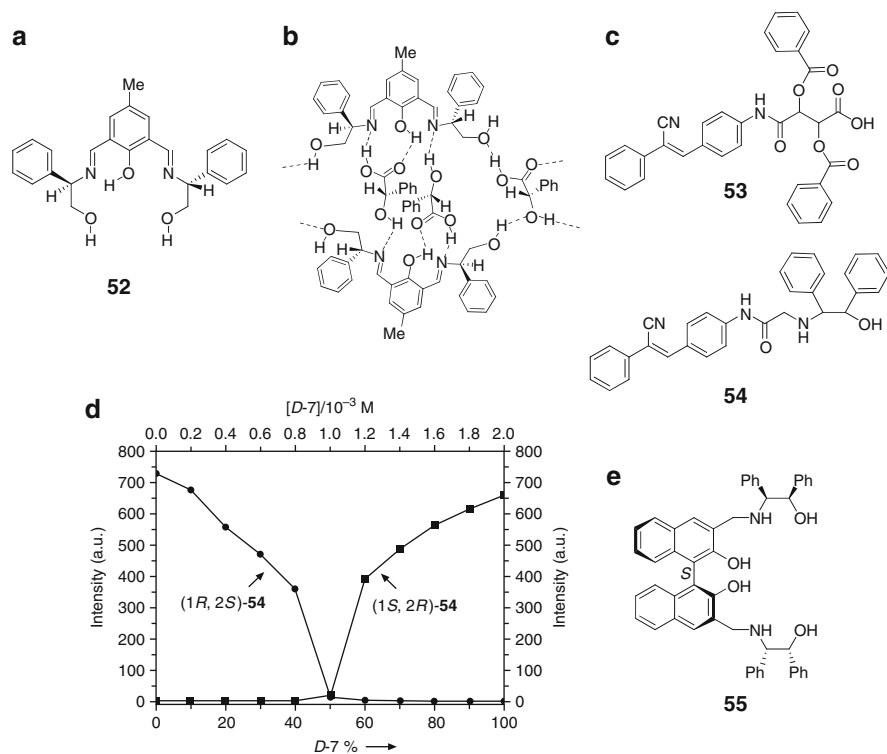


Fig. 16 Sensors used in enantioselective aggregation induced enhancement. **(a)** Phenylglycinol-derived Schiff base **52**; **(b)** proposed mechanism of oligomeric interaction of **52** with mandelic acid enantiomers; **(c)** chiral derivatives of 2-phenyl-3-(*p*-aminophenyl)acrylonitrile **53**, **54** showing an AIEE effect in the presence of bases and acids respectively; **(d)** fluorescence response as a function of enantiomeric excess of dibenzoyl tartrate observed using the amine **54** (adapted from [113]. Copyright (2010) with permission from Elsevier); **(e)** AIEE sensor **55**, based on BINOL

compound **54** (Fig. 16). Precipitation of this compound was observed in 10 mM solutions of the (1*S*,2*R*)-sensor and *D*-dibenzoyl tartrate (equimolar amounts) 30 min after mixing, while it did not occur under the same conditions for the *L*-enantiomer. The fluorescence intensity ratio was also very high in this case with $F_D/F_L = 196$. The dependence of the fluorescence intensity upon the enantiomeric composition changed abruptly after 50% *D* was reached (Fig. 16e), suggesting the presence of a large cooperative effect. The same held true for the *L*-enantiomer using the opposite chirality of the AIEE sensor. Thus this system seems to be particularly suited to detecting very small enantiomeric excesses [113].

Pu and coworkers described the same type of effect on the BINOL derivative containing enantiomers of the 2-amino-1,2-diphenylethanol unit **55** upon interaction with enantiomers of mandelic acid in benzene. By using the (*S*)-sensor, (*S*)-mandelic acid induced precipitation and formation of a highly fluorescent suspension with an enhanced fluorescence intensity of 950 times. In contrast, (*R*)-mandelic acid did not

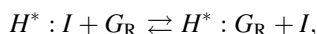
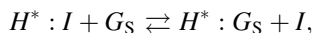
induce precipitation and the fluorescence remained almost unchanged [82]. Thus, the differences in fluorescent intensity observed with this strategy are among the highest observed in enantioselective sensing.

5 Displacement and Non-Covalent Sensory Systems

Sensory systems can also be produced using supramolecular (i.e., non-covalent) assemblies. Using this idea, a fluorophore can be non-covalently associated with a chiral molecule and be displaced by interaction of the latter with the chiral analyte. The advantage of this approach is that complicated synthesis can be avoided and a large variety of existing chiral molecules and fluorophores, including biopolymers, can in principle be used.

A poly-L-lysine coating of a TiO₂ gel film, was used to bind anionic fluorophores (sulforhodamine-B or carboxyfluorescein) by electrostatic interactions. Enantioselective anion exchange was observed when this solid material was exposed to a solution containing D- or L-glutamic acid (10 μM), with a fluorescence increase, due to the release of the fluorophore in the solution, which was found to be higher when using D-Glu [96].

A series of work exploiting the concept of non-covalent assembly has been reported by Anslyn and coworkers for the development of the colorimetric detection of enantiomers [142, 143] according to the following indicator-displacement equilibria:



where H* is a chiral receptor, I is an indicator, and G_R and G_S are the two enantiomers of the guest analyte. This method is based on the different absorbance and fluorescence properties of the free indicator and of its H:I complex.

The same concept was used for sensing α-hydroxycarboxylic acids and diols using chiral boronate **56** (Fig. 17a) containing a displaceable fluorescent group [144]. Formation of the boronate resulted in an increased fluorescence of a coumarin derived fluorophore, while displacement by the hydroxy acid restored the weaker emission of the free fluorophore. The enantioselective fluorescent response was sufficient for the determination of the enantiomeric excess of phenyllactic acid with a 0.13 (13%) maximum deviation from the actual values. A mathematical algorithm has recently been proposed for the calculation of both stability constants and enantiomeric excess in these indicator-displacement assays [145].

In a more elaborate non-covalent scheme, a β-cyclodextrin unit was recently linked to a CdSe/ZnS quantum dot (QD) surface via formation of a boronate with the glucose secondary hydroxyls, bearing a fluorophore included in the cyclodextrin

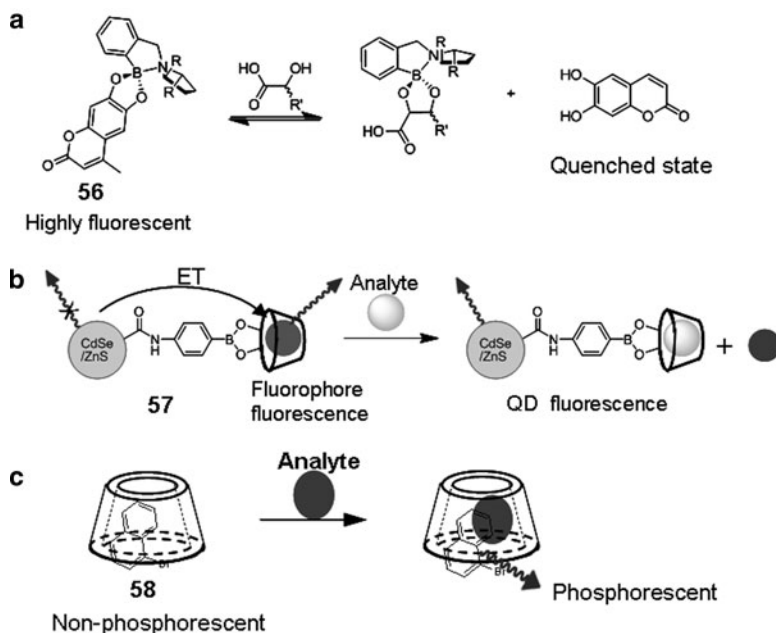


Fig. 17 Fluorescent sensors based on displacement of fluorophores. (a) Chiral boronate **56** containing a fluorophore which is quenched upon displacement; (b) CdSe/ZnS quantum dot (QD) modified with a spacer and a boronic acid unit bound to a fluorophore-containing β -cyclodextrin **57**, which, upon interaction with the analyte, releases the fluorophore, thus preventing energy transfer (ET) from QD; (c) guest-induced phosphorescence of CD-1-bromonaphthalene complex

cavity (**57**) (Fig. 17b); an energy transfer process can occur and excitation of the quantum dot results in the emission of the fluorophore included. Thus, the displacement of these groups by a guest can bring about changes in the fluorescence observed. This was demonstrated using a rhodamine B as the fluorophore included, which was displaced by guests able to interact with the cyclodextrin cavity such as adamantane carboxylic acid, a process which restored the QD fluorescence at around 530 nm and quenched the longer wavelength (ca. 580 nm) emission due to energy transfer. This process was found to be enantioselective for phenylalanine and tyrosine as guests [97].

A non-covalent sensory system based on phosphorescence was also described recently. The inclusion complex of 1-bromonaphthalene with β -cyclodextrin (**58**) shows room temperature phosphorescence in the presence of menthol enantiomers, due to the formation of ternary complexes with both menthol and 1-bromonaphthalene included. The phosphorescence lifetime was found to be different for the two enantiomers (4.28 ± 0.06 and 3.71 ± 0.06 ms for (–)-menthol and (+)-menthol, respectively) due to the higher exposure to dissolved oxygen of the latter complex [123].

6 Advanced Luminescence Techniques

It is worth mentioning that other techniques can show even more subtle differences in the luminescence properties of the sensor generated by enantioselective interactions, thus providing more potent tools for this type of analysis.

Fluorescence anisotropy is one of the properties which can be used in the study of biomolecules and their association. Fluorescence anisotropy (r) which can be measured on normal spectrofluorimeters and microplate readers using a polarizing filter in the excitation and another in the emission beam is defined as

$$r = \frac{I_{\parallel} - I_{\perp}}{I_{\parallel} + 2I_{\perp}},$$

in which I_{\parallel} and I_{\perp} are the fluorescence intensity observed when the two polarizing filters are parallel and perpendicular, respectively. Diastereomeric fluorophore/analyte complexes can in principle have different anisotropies due to the differences in the molecular structure. However, since anisotropy is higher for compounds which tumble slowly in solution, differences readily observed with this technique are those produced for rapidly tumbling small fluorophores upon association with a large biomolecule (proteins, DNA or polysaccharides), while tiny differences in the structure of two diastereomeric complexes of small molecules are more difficult to observe. Therefore, small enantioselectivity in anisotropy change (increase) was reported only for the interaction of a DNA aptamer with the enantiomers of adenosine, due to opening of the biomolecule by binding to the analyte [125].

For chiral complexes of luminescent lanthanide ions, significantly different distribution of excited state lifetimes (usually in the range of microseconds or more) can be detected upon interaction with two enantiomers of a molecule bearing donor groups. For example, the complex of europium with tetracycline has an emission at 618–619 nm which is strongly enhanced by formation of a ternary complex with L-malate, and not with the D-enantiomer. The presence of three different components for the two diastereomeric complexes was demonstrated using single photon counting measurements, with average decay times of 84 and 48 μ s for L- and D-malate, respectively. This effect could be exploited using time-resolved (“gated”) fluorescence (TRF). In this technique, the fluorophore is excited with a pulsed lamp and the emitted light is detected only after a delay. Since one of the two enantiomers shows a faster decay, by using a 120 μ s delay, the ratio between the intensities of the two enantiomers could be maximized [114]. This technique can be performed by common multi-well benchtop spectrofluorimeters, thus allowing one to detect enantiomeric excess in a parallel way. Time-resolved imaging is also possible using these measurements [114].

The peculiar properties of lanthanide luminescence also make these ions attractive in the generation of CPL. In this technique, a pulse of light is used for excitation and circular polarization of the emitted light is measured using a photomodulator, allowing one to select alternatively left- and right-handed circularly polarized light.

Therefore, this technique is able to report differences in the chirality of the excited state.

It is common to report the degree of CPL in terms of emission dissymmetry factor g

$$g_{\text{lum}}(\lambda) = 2 \frac{\Delta I}{I} = 2 \frac{(I_{\text{L}} - I_{\text{R}})}{I_{\text{L}} + I_{\text{R}}},$$

where I_{L} and I_{R} indicate, respectively, the intensity of left and right circularly polarized emissions. A value of 0 for g_{lum} corresponds to no circular polarization, while the absolute maximum value is 2. Complexes of lanthanide(III) ions have been extensively studied in connection with CPL, since their electronic structures allow circularly polarized electronic transitions involving f orbitals. These ions can give rise to large g_{lum} values (up to 1.38), while for most organic molecules this value is less than 1×10^{-2} .

A large variety of chiral molecules was found to discriminate between the two enantiomers of lanthanide chelates when acting as acceptor, thus creating non-zero CPL signals [146]. Enantioselectivity in the quenching (with different rates for the Δ and Λ enantiomer) of excited states of racemic pyridine-2,6-dicarboxylate (dpa) complexes $\text{Eu}(\text{dpa})_3^{3-}$ and $\text{Tb}(\text{dpa})_3^{3-}$ were observed using this technique and cyanocobalamin or related compounds as quenchers, though in the ground state no interaction could be detected by circular dichroism. Thus, using CPL, both coordination and outer-sphere interactions involving chiral species can be detected using racemic sensors. Interaction with either a chiral biological molecule or with enantiomeric analytes would give rise to CPL signals at specific wavelengths depending on the molecular environment, without disturbance of the free probe luminescence. This offers the possibility of probes able to report signatures of multiple interactions at the same time. Therefore, great effort for the characterization of luminescent lanthanide complexes as bioprobes has been made in the last decade [147–149] and dedicated instrumentation has been developed to exploit this type of measurements in biological systems [98].

The addition of chiral amino acids to a racemic mixture of lanthanide(III) complexes may lead to a perturbation of the ground state equilibrium without changing the local structure of the complexes involved (Pfeiffer effect), thus generating an enantiomeric excess in the ground state. It should be noted that, if enantioselective excited state quenching is not present, the enantiomeric excesses in the excited and ground states are equal. Muller and coworkers used this effect to show that by addition of D- and L-serine to the $\text{Tb}(\text{dpa})_3^{3-}$ complex, the CPL intensity observed varied linearly going from negative to positive values as a function of the enantiomeric excess [98].

Chemiluminescent reactions have been used for signal generation both in flow injection systems and in separation techniques such as HPLC or CE, often in combination with chiral analysis. Detection by chemiluminescence of enantioselective capture of fluorescent analytes such as dansyl-phenylalanine by molecularly imprinted polymers was also reported [150]. Electrochemiluminescence (ECL) is

one of the techniques which can be used for combining electrochemical stimuli with sensitive optical read-out in biochip technology. Tris(2,2'-bipyridine)ruthenium(II), $\text{Ru}(\text{bipy})_3^{2+}$, is one of the best ECL species as it gives strong emission and can be used repeatedly. Using this complex, an enantioselective electrochemical reaction was reported to be enantioselective both in intensity and in applied potential, and the determination of the D-proline concentration in synthetic samples was performed [99].

7 Conclusions and Perspectives

The occurrence of enantioselectivity in fluorescence and other luminescence-based techniques has undergone rapid development using advances from sensor technology and other fast developing areas, such as DNA and genomic technology, supramolecular chemistry, and polymer science. In recent years this has been enriched with new tools and fluorescent antibodies, aptamers, and molecularly imprinted polymers have been included in the list of potential enantioselective scaffolds. Thus the aim of most studies has now become to develop and optimize systems for enantioselective sensing which are applicable to the analysis of a large number of samples in support of chemical synthesis of enantiomeric compound and in asymmetric reaction optimization procedures. Several works have shown very high enantioselectivity in fluorescence responses, which makes them suitable for precise analytical performances. Sensors showing broad applicability to several classes of chiral molecules have been described in the last few years. Fluorescence sensing is now one very efficient, time-effective, and economic method for assessing the enantiomeric composition of samples to be screened in large scale studies. Several examples have been mentioned in this review of fast parallel read-out of enantiomeric composition using fluorescent methods. However, several challenges are still ahead, even with the present performances of sensors.

The use of combinatorial chemistry, which has proved to be effective for the design of very specific beacon-like sensors [151], has not been fully exploited for enantioselective sensors.

The combination of molecular sensors with devices able to perform repetitive measurements of enantiomeric analysis is also another challenge for the present technology. Studies on the development of sensor technologies allowing reuse of the sensing molecules, such as immobilized or surface-supported fluorescent sensors, are needed to accomplish such a goal.

Finally, a series of enantioselective methods based on advanced instrumentation (such as CPL or ECL) has become increasingly important. Integration of these technologies within the enantioselective tool-kit would allow even faster and more selective devices to be obtained. In this way, a fast, careful, and easy to perform control of the enantiomeric composition can become available in all steps of drug development and of quality control, as well as for the study of the role of enantiomers in biological systems.

References

1. Vogtle F, Knops P (1991) Dyes for visual distinction between enantiomers – crown ethers as optical sensors for chiral compounds. *Angew Chem Int Ed Engl* 30:958–960
2. Kasper M, Busche S, Gauglitz G (2005) Optical sensing of enantiomers. In: Orellana G, Moreno-Bondi MC (eds) *Frontiers in chemical sensors*, vol. 3. Springer, Berlin
3. Smith SW (2009) Chiral toxicology: it's the same thing. . . only different. *Toxicol Sci* 110:4–30
4. US FDA (1992) Development of new stereoisomeric drugs. Food and Drug Administration (FDA) Guidelines. <http://www.fda.gov/Drugs/GuidanceComplianceRegulatoryInformation/GuidanceG/ucm122883.htm>. Accessed 25 Mar 2010
5. Rouhi AM (2004) Chiral chemistry. *Chem Eng News* 82:47–62
6. Liu WP, Gan JY, Schlenk D, Jury WA (2005) Enantioselectivity in environmental safety of current chiral insecticides. *Proc Natl Acad Sci USA* 102:701–706
7. Liu W, Ye J, Jin M (2009) Enantioselective phytoeffects of chiral pesticides. *J Agric Food Chem* 57:2087–2095
8. Marchelli R, Dossena A, Palla G (1996) The potential of enantioselective analysis as a quality control tool. *Trends Food Sci Technol* 7:113–119
9. Gandolfi I, Palla G, Delprato L et al (1992) D-Amino acids in milk as related to heat-treatments and bacterial-activity. *J Food Sci* 57:377–379
10. Lavigne JJ, Savoy S, Clevenger MB, Ritchie JE, McDoniel B, Yoo S-J, Anslyn EV, McDevitt JT, Shear JB, Neikirk D (1998) Solution-based analysis of multiple analytes by a sensor array: toward the development of an “electronic tongue”. *J Am Chem Soc* 120:6429–6430
11. Zhong Z, Anslyn EV (2002) A colorimetric sensing ensemble for heparin. *J Am Chem Soc* 124:9014–9015
12. Prodi L, Bolletta F, Zaccheroni N et al (1998) A new family of luminescent sensors for alkaline earth metal ions. *Chem Eur J* 4:1090–1094
13. Prodi L, Bolletta F, Montalti M et al (2000) Luminescence signalled enantiomeric recognition of chiral organic ammonium ions by an enantiomerically pure dimethylacridino-18-crown-6 ligand. *New J Chem* 24:781–785
14. Lin J, Hu Q-S, Hua M-H et al (2002) A practical enantioselective fluorescent sensor for mandelic acid. *J Am Chem Soc* 124:2088–2089
15. Bell TW, Hext NM (2004) Supramolecular optical chemosensors for organic analytes. *Chem Soc Rev* 33:589–598
16. Czarnik AW (ed) (1992) *Fluorescent chemosensors for ion and molecule recognition*. ACS Symposium Series 538. American Chemical Society, Washington, DC
17. de Silva AP, Gunaratne HQN, Gunnaugsson T et al (1997) Signaling recognition events with fluorescent sensors and switches. *Chem Rev* 97:1515–1566
18. Callan JF, de Silva AP, Magri DC (2005) Luminescent sensors and switches in the early 21st century. *Tetrahedron* 61:8551–8588
19. Pu L (2004) Fluorescence of organic molecules in chiral recognition. *Chem Rev* 104:1687–1716
20. Szostak JW (1997) Introduction: Combinatorial Chemistry. *Chem. Rev.* 97:347–348, and all papers in the same issue
21. Reetz MT (2008) Combinatorial transition-metal catalysis: mixing monodentate ligands to control enantio-, diastereo-, and regioselectivity. *Angew Chem Int Ed Engl* 47:2556–2588
22. Tsukamoto M, Kagan HB (2002) Recent advances in the measurement of enantiomeric excesses. *Adv Synth Catal* 344:453–463
23. Revell JD, Wennemers H (2007) Identification of catalysts in combinatorial libraries. *Top Curr Chem* 277:251–266

24. Reetz MT, Sell T, Meiswinkel A, Mehler G (2003) A new principle in combinatorial asymmetric transition-metal catalysis: mixtures of chiral monodentate P ligands. *Angew Chem Int Ed Engl* 42:790–793
25. Yao S, Meng J-C, Siuzdak G, Finn MG (2003) New catalysts for the asymmetric hydro-silylation of ketones discovered by mass spectrometry screening. *J Org Chem* 68:2540–2546
26. Kubo Y, Maeda S, Tokita S et al (1996) Colorimetric chiral recognition by a molecular sensor. *Nature* 382:522–524
27. Frankewich RP, Thimmaiah KN, Hinze WL (1991) Evaluation of the relative effectiveness of different water-soluble beta-cyclodextrin media to function as fluorescence enhancement agents. *Anal Chem* 63:2924–2933
28. Galaverna G, Dall'Asta C, Corradini R et al (2008) Cyclodextrins as selectors for mycotoxin recognition. *World Mycotoxin J* 1:397–406
29. Kumar VP, Kumar PA, Suryanarayana I et al (2007) Chiral recognition of zolmitriptan by modified cyclodextrins. *Helv Chim Acta* 90:1697–1704
30. Lammers I, Buijs J, van der Zwan G et al (2009) Phosphorescence for sensitive enantioselective detection in chiral capillary electrophoresis. *Anal Chem* 81:6226–6233
31. Garcia-Ruiz C, Scholtes MJ, Ariese F et al (2005) Enantioselective room temperature phosphorescence detection of non-phosphorescent analytes based on interaction with β -cyclodextrin/1-bromonaphthalene complexes. *Talanta* 66:641–645
32. Zhang XH, Wang Y, Jin WJ (2008) Enantiomeric discrimination of 1,1'-binaphthol by room temperature phosphorimetry using γ -cyclodextrin as chiral selector. *Anal Chim Acta* 622:157–162
33. Xu Y, McCarroll ME (2004) Determination of enantiomeric composition by fluorescence anisotropy. *J Phys Chem A* 108:6929–6932
34. Kimaru IW, Xu Y, McCarroll ME (2006) Characterization of chiral interactions using fluorescence anisotropy. *Anal Chem* 78:8485–8490
35. Corradini R, Sartor G, Dossena A et al (1992) Enantioselective fluorescence quenching by a chiral copper(II) complex in ligand exchange equilibria. *J Chem Soc Perkin Trans II*:1979–1983
36. Impellizzeri G, Maccarrone G, Rizzarelli E et al (1991) 6-Deoxy-6-N-histamino β cyclodextrin copper(II) complex, a new enantioselective receptor for aromatic amino acids. *Angew Chem Int Ed Engl* 30(1348):1349
37. Corradini R, Dossena A, Impellizzeri G et al (1994) Chiral recognition and separation of amino acids by means of a copper(II) complex of histamine monofunctionalized β -cyclodextrin. *J Am Chem Soc* 116:10267–10274
38. Erkkila KE, Odom DT, Barton JK (1999) Recognition of metalointercalators with DNA. *Chem Rev* 99:2777–2795
39. Fireman-Shoresh S, Popov I, Avnir D et al (2005) Enantioselective, chirally templated sol-gel thin films. *J Am Chem Soc* 127:2650–2655
40. Korbel GA, Lalic G, Shair MD (2001) Reaction microarrays: a method for rapidly determining the enantiomeric excess of thousands of samples. *J Am Chem Soc* 123:361–362
41. Diaz DD, Yao S, Finn MG (2001) Measurement of enantiomeric excess of amines by mass spectrometry following kinetic resolution with solid-phase chiral acylating agents. *Tetrahedron Lett* 42:2617–2619
42. Knüttel T, Meyer H, Scheper T (2005) Synthesis, test and application of chiral fluorescence substrates to evaluate enzymatic processes in different reaction media. *Enzyme Microb Technol* 37:673–686
43. Noyori R, Takaya H (1990) Binap – an efficient chiral element for asymmetric catalysis. *Acc Chem Res* 23:345–350
44. Newcomb M, Helgeson RC, Cram DJ (1974) Enantiomer differentiation in transport through bulk liquid membranes. *J Am Chem Soc* 96:7367–7369
45. Chankvetadze B (2004) Combined approach using capillary electrophoresis and NMR spectroscopy for an understanding of enantioselective recognition mechanisms by cyclodextrins. *Chem Soc Rev* 33:337–347

46. Hembury GA, Borovkov VV, Inoue Y (2008) Chirality-sensing supramolecular systems. *Chem Rev* 108:1–73
47. Maier NM, Lindner W (2007) Chiral recognition applications of molecularly imprinted polymers: a critical review. *Anal Bioanal Chem* 389:377–397
48. James TD, Sandanayake KRAS, Shinkai S (1995) Chiral discrimination of monosaccharides using a fluorescent molecular sensor. *Nature* 374:345–347
49. Riehl J, Richardson FS (1986) Circularly polarized luminescence spectroscopy. *Chem Rev* 86:1–16
50. Irie M, Yorozu T, Hayashi K (1978) Steric effect on fluorescence quenching of 1,1'-binaphthyl by chiral amines. *J Am Chem Soc* 100:2236–2237
51. Reetz MT, Sostmann S (2001) 2,15-Dihydroxy-hexahelicene (HELIXOL): synthesis and use as an enantioselective fluorescent sensor. *Tetrahedron* 57:2515–2520
52. Upadhyay SP, Pissurlenkar RRS, Coutinho EC et al (2007) Furo-fused BINOL based crown as a fluorescent chiral sensor for enantioselective recognition of phenylethylamine and ethyl ester of valine. *J Org Chem* 72:5709–5714
53. Chung YM, Raman B, Ahn KH (2006) Phenol-containing bis(oxazolines): synthesis and fluorescence sensing of amines. *Tetrahedron* 62:11645–11651
54. Mei X, Wolf C (2004) A highly congested *N,N'*-dioxide fluorosensor for enantioselective recognition of chiral hydrogen bond donors. *Chem Commun* 2078–2079
55. Tumambac GE, Wolf C (2005) Enantioselective analysis of an asymmetric reaction using a chiral fluorosensor. *Org Lett* 7:4045–4048
56. Su WC, Zhang WG, Zhang S et al (2009) A novel strategy for rapid real-time chiral discrimination of enantiomers using serum albumin functionalized QCM biosensor. *Biosens Bioelectron* 25:488–492
57. Xi X, Lou L, Jiang L et al (2008) Poly(*N*-phenylmaleimides) bearing chiral oxazoliny pendant: supramolecular aggregation and enantioselectivity in fluorescence response. *Polymer* 49:2065–2070
58. Grady T, Harris SJ, Smyth MR et al (1996) Determination of the enantiomeric composition of chiral amines based on the quenching of the fluorescence of a chiral calixarene. *Anal Chem* 68:3775–3782
59. Liu SY, He YB, Qing GY et al (2005) Fluorescent sensors for amino acid anions based on calix[4]arenes bearing two dansyl groups. *Tetrahedron Asymmetry* 16:1527–1534
60. Qing GY, He YB, Chen ZH et al (2006) Sensitive fluorescent sensors for malate based on calix[4]arene bearing anthracene. *Tetrahedron Asymmetry* 17:3144–3151
61. Qing GY, He YB, Wang F et al (2007) Enantioselective fluorescent sensors for chiral carboxylates based on calix[4]arenes bearing an L-tryptophan unit. *Eur J Org Chem* 11:1768–1778
62. Xu KX, Qiu Z, Zhao JJ et al (2009) Enantioselective fluorescent sensors for amino acid derivatives based on BINOL bearing benzoyl unit. *Tetrahedron Asymmetry* 20:1690–1696
63. Hu C, He Y, Chen Z et al (2009) Synthesis and enantioselective recognition of an (S)-BINOL-based colorimetric chemosensor for mandelate anions. *Tetrahedron Asymmetry* 20:104–110
64. Liu S, Pestano JPC, Wolf C (2008) Enantioselective fluorescence sensing of chiral alpha-amino alcohols. *J Org Chem* 73:4267–4270
65. Lynam C, Diamond D (2005) Varying solvent polarity to tune the enantioselective quenching of a calixarene host. *J Mater Chem* 15:307–314
66. Qing GY, Sun TL, He YB et al (2009) Highly selective fluorescent recognition of phenyl amino alcohol based on ferrocenyl macrocyclic derivatives. *Tetrahedron Asymmetry* 20: 575–583
67. Zheng Y-S, Hu YJ (2009) Chiral recognition based on enantioselectively aggregation-induced emission. *J Org Chem* 74:5660–5663
68. Chen Z-H, He Y-B, Hu C-G et al (2008) Preparation of a metal–ligand fluorescent chemosensor and enantioselective recognition of carboxylate anions in aqueous solution. *Tetrahedron Asymmetry* 19:2051–2057

69. Chi L, Zhao J, James TD (2008) Chiral mono boronic acid as fluorescent enantioselective sensor for mono α -hydroxyl carboxylic acids. *J Org Chem* 73:4684–4687
70. Lin J, Rajaram AR, Pu L (2004) Enantioselective fluorescent recognition of chiral acids by 3- and 3,3'-aminomethyl substituted BINOLs. *Tetrahedron* 60:11277–11281
71. He X, Cui X, Li M et al (2009) Highly enantioselective fluorescent sensor for chiral recognition of amino acid derivatives. *Tetrahedron Lett* 50:5853–5856
72. Liu HL, Peng Q, Wu YD et al (2010) Highly enantioselective recognition of structurally diverse α -hydroxycarboxylic acids using a fluorescent sensor. *Angew Chem Int Ed* 49:602–606
73. Wei LH, He YB, Xu KX et al (2005) Chiral fluorescent receptors based on (*R*)-1,1'-binaphthylene-2,2'-bisthiourea: synthesis and chiral recognition. *Chin J Chem* 23:757–761
74. Lin J, Li ZB, Zhang HC et al (2004) Highly enantioselective fluorescent recognition of α -amino acid derivatives. *Tetrahedron Lett* 45:103–106
75. Li ZB, Lin J, Zhang HC et al (2004) Macrocyclic bisbinaphthyl fluorophores and their acyclic analogues: signal amplification and chiral recognition. *J Org Chem* 69:6284–6293
76. Li ZB, Lin J, Sabat M et al (2007) Enantioselective fluorescent recognition of chiral acids by cyclohexane-1,2-diamine-based bisbinaphthyl molecules. *J Org Chem* 72:4905–4916
77. Li ZB, Lin J, Pu L (2005) A cyclohexyl-1,2-diamine-derived bis(binaphthyl) macrocycle: enhanced sensitivity and enantioselectivity in the fluorescent recognition of mandelic acid. *Angew Chem Int Ed* 44:1690–1693
78. Li ZB, Lin J, Qin YC, Pu L (2005) Enantioselective fluorescent recognition of a soluble “supported” chiral acid: toward a new method for chiral catalyst screening. *Org Lett* 7:3441–3444
79. Li ZB, Pu L (2005) Synthesis of a new bisbinaphthyl macrocycle for enantioselective fluorescent recognition. *J Mater Chem* 15:2860–2864
80. Xu KX, Wu X-J, He Y-B et al (2005) Synthesis and chiral recognition of novel chiral fluorescence receptors bearing 9-anthryl moieties. *Tetrahedron Asymmetry* 16:833–839
81. Dhara K, Sarkar K, Roy P et al (2008) A highly enantioselective chiral Schiff-base fluorescent sensor for mandelic acid. *Tetrahedron* 64:3153–3159
82. Liu HL, Hou XL, Pu L (2009) Enantioselective precipitation and solid-state fluorescence enhancement in the recognition of α -hydroxycarboxylic acids. *Angew Chem Int Ed* 48:382–385
83. Muñiz FM, Simón L, Alcázar V et al (2009) A highly enantioselective receptor for carbamoyl lactic acid. *Eur J Org Chem* 31:5350–5354
84. Mei X, Wolf C (2004) Enantioselective sensing of chiral carboxylic acids. *J Am Chem Soc* 126:14736–14737
85. Wolf C, Liu S, Reinhardt BC (2006) An enantioselective fluorescence sensing assay for quantitative analysis of chiral carboxylic acids and amino acid derivatives. *Chem Commun* 4242–4244
86. Mei X, Wolf C (2006) Determination of enantiomeric excess and concentration of chiral compounds using a 1,8-diheteroarylnaphthalene-derived fluorosensor. *Tetrahedron Lett* 47:7901–7904
87. Pagliari S, Corradini R, Galaverna G et al (2000) Enantioselective sensing of amino acids by copper(II) complexes of phenylalanine-based fluorescent β -cyclodextrins. *Tetrahedron Lett* 41:3691–3695
88. Marchelli R, Corradini R, Galaverna G et al (2006) Enantioselective separation of amino acids and hydroxy acids by ligand exchange with copper(II) complexes in HPLC (chiral eluent) and fast sensing systems. In: Subramanian G (ed) *Chiral separation techniques*. Wiley-VCH, Weinheim
89. Pagliari S, Corradini R, Galaverna G et al (2004) Enantioselective fluorescence sensing of amino acids by modified cyclodextrins: role of the cavity and sensing mechanism. *Chem Eur J* 10:2749–2758
90. Corradini R, Paganuzzi C, Marchelli R et al (2005) Fast parallel enantiomeric analysis of unmodified amino acids with fluorescent β -cyclodextrins. *J Mater Chem* 15:2741–2746

91. Corradini R, Paganuzzi C, Marchelli R et al (2007) Fluorescent cyclodextrins bearing metal binding sites and their use for chemo- and enantioselective sensing of amino acid derivatives. *J Incl Phenom Macrocycl Chem* 57:625–630
92. Corradini R, Paganuzzi C, Marchelli R et al (2003) Design and synthesis of fluorescent β -cyclodextrins for the enantioselective sensing of α -amino acids. *Chirality* 15:S30–S39
93. Kwong HL, Wong WL, Lee CS et al (2009) Zinc(II) complex of terpyridine-crown macrocycle: a new motif in fluorescence sensing of zwitterionic amino acids. *Inorg Chem Commun* 12:815–818
94. Wang H, Chan WH, Lee AWM (2008) Cholic acid-based fluorescent probes for enantioselective recognition of trifunctional amino acids. *Org Biomol Chem* 6:929–934
95. Yang L, Qin S, Su X et al (2010) 1,1'-Binaphthyl-based imidazolium chemosensors for highly selective recognition of tryptophan in aqueous solutions. *Org Biomol Chem* 8:339–348
96. Paul S, Huang J, Ichinose I (2005) Enantioselective anion exchange on a positively charged poly(L-lysine) layer assembled on thin TiO₂-gel films. *New J Chem* 29:1058–1063
97. Freeman R, Finder T, Bahshi LL et al (2009) β -Cyclodextrin-modified CdSe/ZnS quantum dots for sensing and chiroselective analysis. *Nano Lett* 9:2073–2076
98. Muller G (2009) Luminescent chiral lanthanide(III) complexes as potential molecular probes. *Dalton Trans* 9692–9707
99. Zhao C, Xu S, Su Y et al (2002) Chiral discrimination for enantiomers of amino acids using an electrochemiluminescence method. *Analyst* 127:889–891
100. Kim YK, Lee HN, Singh NJ et al (2008) Anthracene derivatives bearing thiourea and glucopyranosyl groups for the highly selective chiral recognition of amino acids: opposite chiral selectivities from similar binding units. *J Org Chem* 73:301–304
101. Qing G, Sun T, Chen Z et al (2009) 'Naked-eye' enantioselective chemosensors for N-protected amino acid anions bearing thiourea units. *Chirality* 21:363–373
102. Galindo F, Burguete MI, Luis SV (2004) Photophysical study of a cyclophane displaying intramolecular exciplex emission. *Chem Phys* 302:287–294
103. Burguete M, Galindo F, Luis SV et al (2010) Ratiometric fluorescence sensing of phenylalanine derivatives by synthetic macrocyclic receptors. *J Photochem Photobiol A Chem* 209: 61–67
104. Alfonso I, Burguete MI, Galindo F et al (2009) Unraveling the molecular recognition of amino acid derivatives by a pseudopeptidic macrocycle: ESI-MS, NMR, fluorescence, and modeling studies. *J Org Chem* 74:6130–6142
105. Matsushita M, Yoshida K, Yamamoto N et al (2003) High-throughput screening by using a blue-fluorescent antibody sensor. *Angew Chem Int Ed* 42:5984–5987
106. Matsushita H, Yamamoto N, Meijler MM et al (2005) Chiral sensing using a blue fluorescent antibody. *Mol Biosyst* 1:303–306
107. Qin H, He Y, Hu C et al (2007) Enantioselective fluorescent sensor for dibenzoyl tartrate anion based on chiral binaphthyl derivatives bearing an amino acid unit. *Tetrahedron Asymmetry* 18:1769–1774
108. Liu S-Y, He YB, Chan WH et al (2006) Cholic acid-based high sensitivity fluorescent sensor for α,ω -dicarboxylate: an intramolecular excimer emission quenched by complexation. *Tetrahedron* 62:11687–11696
109. Liu SY, Law KY, Hea YB et al (2006) Fluorescent enantioselective receptor for S-mandelate anion based on cholic acid. *Tetrahedron Lett* 47:7857–7860
110. Costero AM, Llaosa U, Gil S et al (2009) Enantioselective sensing of dicarboxylates. Influence of the stoichiometry of the complexes on the sensing mechanism. *Tetrahedron Asymmetry* 20:1468–1471
111. Costero AM, Colera M, Gaviña P et al (2008) Chiral cyclohexane based fluorescent chemosensors for enantiomeric discrimination of aspartate. *Tetrahedron* 64:3217–3224
112. Han F, Chi L, Liang X et al (2009) 3,6-Disubstituted carbazole-based bisboronic acids with unusual fluorescence transduction as enantioselective fluorescent chemosensors for tartaric acid. *J Org Chem* 74:1333–1336

113. Zheng YS, Hu YJ, Li DM et al (2010) Enantiomer analysis of chiral carboxylic acids by AIE molecules bearing optically pure aminol groups. *Talanta* 80:1470–1474
114. Lin Z, Wu M, Wolfbeis OS (2005) Time-resolved fluorescent chirality sensing and imaging of malate in aqueous solution. *Chirality* 17:464–469
115. Xu KX, He YB, Qin HJ et al (2005) Enantioselective recognition by optically active chiral fluorescence sensors bearing amino acid units. *Tetrahedron Asymmetry* 16:3042–3048
116. James TD, Shinkai S (2002) Artificial receptors as chemosensors for carbohydrates. *Top Curr Chem* 218:159–200
117. Heinrichs G, Schellenträger M, Kubik S (2006) An enantioselective fluorescence sensor for glucose based on a cyclic tetrapeptide containing two boronic acid binding sites. *Eur J Org Chem* 18:4177–4186
118. Hamasaki K, Ikeda H, Nakamura A et al (1993) Fluorescent sensors of molecular recognition – modified cyclodextrins capable of exhibiting guest-responsive twisted intramolecular charge-transfer fluorescence. *J Am Chem Soc* 115:5035–5040
119. Tanabe T, Touma K, Hamasaki K et al (2001) Immobilized fluorescent cyclodextrin on a cellulose membrane as a chemosensor for molecule detection. *Anal Chem* 73:3126–3130
120. Ikeda H, Murayama T, Ueno A (2005) Skeleton-selective fluorescent chemosensor based on cyclodextrin bearing a 4-amino-7-nitrobenz-2-oxa-1,3-diazole moiety. *Org Biomol Chem* 3:4262–4267
121. Ikeda H, Li Q, Ueno A (2006) Chiral recognition by fluorescent chemosensors based on *N*-dansyl-amino acid-modified cyclodextrins. *Bioorg Med Chem Lett* 16:5420–5423
122. Ueno A, Suzuki I, Osa T (1990) Host guest sensory systems for detecting organic-compounds by pyrene excimer fluorescence. *Anal Chem* 62:2461–2466
123. García-Ruiz C, Hu XS, Ariese F et al (2005) Enantioselective room temperature phosphorescence detection of non-phosphorescent analytes based on interaction with β -cyclodextrin/1-bromonaphthalene complexes. *Talanta* 66:634–640
124. Urata H, Nomura K, Wada SI et al (2007) Fluorescent-labeled single-strand ATP aptamer DNA: chemo- and enantio-selectivity in sensing adenosine. *Biochem Biophys Res Commun* 360:459–463
125. Perrier S, Ravelet C, Guieu V et al (2010) Rationally designed aptamer-based fluorescence polarization sensor dedicated to the small target analysis. *Biosens Bioelectron* 25:1652–1657
126. Yorozu T, Hayashi K, Irie M (1981) Chiral discrimination in fluorescence quenching. *J Am Chem Soc* 103:5480–5484
127. Prodi L, Bolletta F, Montalti M et al (2000) Luminescent chemosensors for transition metal ions. *Coord Chem Rev* 205:59–83
128. Prodi L, Montalti M, Zaccheroni N et al (2001) Dansylated polyamines as fluorescent sensors for metal ions: photophysical properties and stability of copper(II) complexes in solution. *Helv Chim Acta* 84:690–706
129. Davankov VA, Navratil JD, Walton HF (1988) Ligand exchange chromatography. CRC, Boca Raton
130. Haider JM, Pikramenou Z (2005) Photoactive metallocyclodextrins: sophisticated supramolecular arrays for the construction of light activated miniature devices. *Chem Soc Rev* 34:120–132
131. Bellia F, La Mendola D, Pedone C et al (2009) Selectively functionalized cyclodextrins and their metal complexes. *Chem Soc Rev* 38:2756–2781
132. Corradini R, Dossena A, Marchelli R et al (1996) A modified cyclodextrin with a fully encapsulated dansyl group: self inclusion in the solid state and in solution. *Chem Eur J* 2:373–381
133. Wang Q, Chen X, Tao L et al (2007) Enantioselective fluorescent recognition of amino alcohols by a chiral tetrahydroxyl 1,1'-binaphthyl compound. *J Org Chem* 72:97–101
134. Beer G, Rurack K, Daub J (2001) Chiral discrimination with a fluorescent boron-dipyromethene dye. *Chem Commun* 1138–1139

135. Fang L, Chan WH, He YB et al (2005) Fluorescent anion sensor derived from cholic acid: the use of flexible side chain. *J Org Chem* 70:7640–7646
136. Czarnik AW (1994) Chemical communication in water using fluorescent chemosensors. *Acc Chem Res* 27:302–308
137. de Silva AP, Moody TS, Wright GD (2009) Fluorescent PET (photoinduced electron transfer) sensors as potent analytical tools. *Analyst* 134:2385–2393
138. Zhang X, Chi L, Ji S et al (2009) Rational design of d-PeT phenylethynylated-carbazole monoboronic acid fluorescent sensors for the selective detection of α -hydroxyl carboxylic acids and monosaccharides. *J Am Chem Soc* 131:17452–17463
139. Tumambac GE, Mei X, Wolf C (2004) Stereoselective sensing by substrate-controlled syn/anti interconversion of a stereodynamic fluorosensor. *Eur J Org Chem* 2004:3850–3856
140. Mei X, Martin RM, Wolf C (2006) Synthesis of a sterically crowded atropisomeric 1,8-diacridylnaphthalene for dual-mode enantioselective fluorosensing. *J Org Chem* 71:2854–2861
141. Corradini R, Sforza S, Tedeschi T et al (2007) Chirality as a tool in nucleic acid recognition: principles and relevance in biotechnology and in medicinal chemistry. *Chirality* 19:269–294
142. Folmer-Andersen JF, Lynch VM, Anslyn EV (2005) Colorimetric enantiodiscrimination of α -amino acids in protic media. *J Am Chem Soc* 127:7986–7987
143. Leung D, Folmer-Andersen JF, Lynch VM et al (2008) Using enantioselective indicator displacement assays to determine the enantiomeric excess of α -amino acids. *J Am Chem Soc* 130:12318–12327
144. Zhu L, Zhong Z, Anslyn EV (2005) Guidelines in implementing enantioselective indicator-displacement assays for α -hydroxycarboxylates and diols. *J Am Chem Soc* 127:4260–4269
145. Hargrove AE, Zhong Z, Sessler JL et al (2010) Algorithms for the determination of binding constants and enantiomeric excess in host:guest equilibria using optical measurements. *New J Chem* 34:348–354
146. Meskers SCJ, Dekkers HPJM (2001) Enantioselective quenching of luminescence: molecular recognition of chiral lanthanide complexes by biomolecules in solution. *J Phys Chem A* 105:4589–4599
147. Tsukube H, Shinoda S (2002) Lanthanide complexes in molecular recognition and chirality sensing of biological substrates. *Chem Rev* 102:2389–2403
148. Montgomery CP, New EJ, Parker D et al. (2008) Enantioselective regulation of a metal complex in reversible binding to serum albumin: dynamic helicity inversion signalled by circularly polarised luminescence. *Chem Commun* 4261–4263
149. Petoud S, Muller G, Moore EG et al (2007) Brilliant Sm, Eu, Tb, and Dy chiral lanthanide complexes with strong circularly polarized luminescence. *J Am Chem Soc* 129:77–83
150. Wang L, Zhang Z, Huang L (2008) Molecularly imprinted polymer based on chemiluminescence imaging for the chiral recognition of dansyl-phenylalanine. *Anal Bioanal Chem* 390:1431–1436
151. Chen C, Wagner H, Still WC (1998) Fluorescent, sequence-selective peptide detection by synthetic small molecules. *Science* 279:851–853

Index

A

Activators, 33
Activity enhancers, nanoparticles, 73
Adenosine enantiomers, 200
Aggregation induced emission enhancement (AIEE), 175, 181, 203
Aggregation/precipitation, enantioselectivity, 203
Alizarin Red S, 168
All-photon inputs, 13
Alzheimer's disease, 5
Amino acids, 177, 187, 208
2-Amino-1,2-diphenylethanol, 203
3-[2-(2-Aminoethylamino)ethylamino]propyltrimethoxysilane, 125
4-Amino-1,8-naphthalimide, 13
Aminomethylphenylboronic acid, 12
2-Aminophthalic acid, 75
Ammonia, 38, 102, 107
AND, 8
Anion inputs, 6
Anion sensing, 163
Antenna systems, 57, 68, 78, 112
Anthracenamide fluorophore, 8
Anthracene fluorophore, 7, 11, 16, 202
Antibodies, 29, 36, 59, 64, 69, 107, 200
 anti-BSA, 62
 anti-TNT, 61
Aptamers, 60, 148, 200
APTES (3-aminopropyltriethoxysilane), 107, 126

Artificial tongue, 177
Atomic force microscopy (AFM), 156
ATP, 165
Avidin, 44, 64, 70

B

Bacillus anthracis, 38, 117, 127
Benzo-15-crown-5 ether, 10
Benzonase endonuclease, 45
Biarylnaphthalene, 199
Biladienes, 151
BINOL, 68, 181, 191
Bioluminescence resonance energy transfer (BRET), 54, 62
Biosensors, 29, 42
 ligand-receptor interactions, 44
 proteins, 44
 proteins/enzymes, 44
Biotin, 44, 70
Bis(aminomethyl)pyridine receptor, 5
Bis(4-dialkylaminophenyl)-3-hydroxy-4-alkylsulfanylcyclobut-2-enone (APC), 72
Bis(oxazoliny)phenols, 198
BODIPY (boron dipyrromethene) fluorophore, 4, 128, 191
Bovine serum albumin (BSA), 199
Bradykinin, 166
Bromonaphthalene phosphor, 18
Bromothymol blue, 39
p-tert-Butyl-calix[4]arenes, 190

C

Calcium dipicolinate (CaDPA), 126
Calixarenes, 181, 190
Calixcrown, 18
Camphoric acid, 202
Candida antarctica, 199
Carbon dioxide, 38
Carboxyfluorescein, 205
Cardiac troponin T (cTnT), 59
Cation inputs, 3
Cation sensing, 153
Cell discrimination, cancer, 169
Charge-coupled devices (CCD sensors), 150
Chemiluminescence, 73
 gold nanoparticles, catalysts, 74
Chemiluminescence RET (CRET), 54, 62
Chemosensors, 29, 93
 fluorescent, 180
 luminescent silica nanoparticles, 109
 upconverting nanophosphors, 38
Chiral analysis, 175
Chloropropionic acid, 199
Chloroquine, 126
Cholic acid amidothiourea derivatives, 192
Circularly polarized luminescence (CPL),
 175, 181
Click chemistry, 103
Cocaine, QD-based sensing, 61
Collisional fluorescence quenching, 185
Computer screen photoassisted technique
 (CSPT), 148
Concanavalin A (ConA), 62
Connected inputs, 12
Copper, 115, 125, 161, 188
Copper(II), 185, 189
 quenching, 185
Cy3, 52, 179
Cy5, 35, 80, 83, 179
Cyclodextrins, 18, 62, 178, 197, 201
Cyclophanediene photochrome, 21
Cytokines, 36

D

Dansyl (5-dimethylamino-1-naphthalenesulfonyl) fluorophore, 185
Dansyl-phenylalanine, 208

DAPI (diamidino-2-phenylindole), 83
DEDMS (diethoxydimethylsilane), 108
Dendrimers, 67
1,8-Diacridylnaphthalene-*N*,
 N'-dioxide, 187
Diamido-diamino ligands, 188
Diamine-9,9-dimethylxanthenes, 192
Diaminocyclohexane, 195
Diazacrown, 5
Dibenzoyl tartrate, 196
2,4-Dichlorophenoxyacetic acid, 120
Diethyl chlorophosphate, 146
Diphenylethylenediamine, 195
Dipicolinic acid (DPA), 117
Dip-Pen nanolithography (DPN), 156
Displacement, 205
DNA, 80, 120, 128, 147
 aptamers, 183, 200
 helicity, 179
 microarrays, upconversion phosphor
 technology reporters, 35
Dopants, 30
Drug delivery, 71
Dye nanocrystals, encapsulated, 69
Dye-coated silica nanoparticles (DCSNs),
 93, 103
Dye-doped silica nanoparticles (DDSNs),
 101, 122
Dye-loaded mesoporous particles, 70
Dyes, enzyme-mediated release, 71
 photobleaching, 145

E

Electrochemiluminescence, 208
 particle-mediated enhancement, 76
Electronic nose, 139
Enantiomeric recognition, 175
Enantioselective quenching, metal
 complexes, 185
 PET, 189
Energy migration, 65, 68
Energy transfer (ET), 32, 112, 128, 190, 200
Energy transfer upconversion (ETU), 32
Enzymes, biosensors, 44
 gold nanoparticles, activity
 enhancers, 75
Erbium oxysulfide, 37

Erwinia herbicola, 38
Ethylenediaminetetraacetic dianhydride (EDTAD), 127
Excimer, 200
Exciplex, 185, 200
Excitation emission matrix (EEM) spectroscopy, 150
Excited state absorption (ESA), 32

F
Fenchone, 201
Ferrocenyl quenchers, 203
Ferrocyanide, 74
Fibre optics sensor arrays, 141
FITC (fluorescein isothiocyanate), 52, 70, 126
FIFFF (Flow field flow fractionation), 104
Flow cytometry, upconversion phosphor technology, 38
Fluorescein diacetate (FDA), 69
Fluoresceinamine, 146
Fluorescence, 93, 139
 anti-Stokes, 30
Fluorescence arrays, analytes in solution, 153
Fluorescence-based sensor arrays, gas detection, 141
Fluorescence enhancement, 2
 PET inhibition, 193
Fluorescence quenching, enantioselective, 184
Fluorescent molecular sensors, 1
Fluorescent “off-on” sensors, 2
Fluorescent sensors, 175
Fluoride ions, 164
Fluorophore-spacer-receptor, 3
Förster distance, 54
Förster-resonance energy transfer (FRET), 55, 61, 84, 99

G
GABA, 13
Gas detection, 141
Gated mesoporous particles, 70
Glucose detection, 126

Glucose oxidase (GOD), 75
Gold nanoparticles (AuNPs), 58, 74, 99

H

Half-adder, 20
Half-subtractor, 23
Helicenes, 181
Heparin, 119
Hepatitis C, 37
Horseradish peroxidase (HRP), 62
Human chorionic gonadotropin (hCG), 37
Human papilloma virus, 36
Human serum albumin (HSA), 182, 199
Hydroxy acids, 188, 195
Hydroxycarboxylic acids, 205
Hydroxyquinolines, 5
8-Hydroxyquinoline receptor (8HQ), 154

I

IgG 38, 44
Immunoassay, 69
INHIBIT, 18
Interferon, 37
Ion sensors, 139

K

Kallidin, 166

L

Lanthanides, 30, 64, 126, 181, 207
Lateral flow assays, upconversion phosphor technology, 36
Layer-by-layer (LbL) techniques, 69
Lead, 128
Ligand exchange chromatography (LEC), 185
Ligand-receptor interactions, 44
Light-energy upconversion, 112
Liposomes, 65
 functionalized, 70
Liquid crystal displays (LCD), 149
Logic gates, 1
Luciferase, 62

Luminescence, 29, 51, 93, 175
 amplification, plasmonic strategies, 76
 enantio-discriminating effects, 177
Luminescence resonance energy transfer
 (LRET), 42
Luminol, 62

M

Malate, 207
Mandelic acid, 68, 204
MEF-based signalling, 80
Menthol, 206
(Mercaptopropyl)triethoxysilane
 (MPS), 123
Mercury, 128
Metal nanoparticle-enhanced RET, 83
Metal surface, fluorescence
 enhancement, 77
Metal-enhanced fluorescence
 (MEF), 58, 79
Metal-enhanced phosphorescence, 82
4-Methyl-2,6-diformylphenol, 203
Methylmercury, 72, 129
Micelles, 106
Microarrays, 147
Microemulsion, reverse, 105
Molecular beacon, 200
Molecular computation, 1
Molecular logic, 1
Molecularly imprinted polymers
 (MIP), 181
MS2 coliphage, 38
Multi-chromophore systems, 51
Multiphoton excitation, 81
Myobacterium tuberculosis, 37

N

NAND, 17
Nanocapturer, genomagnetic, 128
Nanoparticles, 29, 51
 bioimaging/sensing, 97
Nanophosphors, upconverting, 33
Nanoplates/nanorods, 30
Nanotubes, 30
Naphthalenediimide, 13

Near infrared (NIR), 30
Nerve agents, 146
Nile Red, 141
Nitroaromatics, 144, 167
Nitrobenzoxadiazole (NBD), 120
Nitrocellulose membrane, 36
NOR, 16
NOT, cation/anion inputs, 6
Nucleic acids, 98, 101
 microarrays, 35

O

Olfaction, 153
Oligofluorene substituted POSS
 (OPF), 67
Oligonucleotides, biosensors, 42
Optical sensors, 139
OR, 15
ORMOSIL (organic-modified silica), 106
Ovalbumin, 38
Oxygen sensors, 41

P

Paraquat, 66
PEG-PPO-PEG, 108
Peptides, 11, 165, 181
 cyclic, 193
 phosphorylation, 11
Perylene bisimide (PBI), 59
Perylene tetracarboxydiimide, 14
pH, 3, 38
Phenanthroline fluorophore, 7
Phenolate-tris(bipyridyl)Ru(II), 7
Phenylalaninol (PA), 202
2-Phenyl-3-(*p*-aminophenyl)
 acrylonitrile, 203
Phenylethylamine, 198
Phenylglycinol, 203
Phosphor technology, upconversion, 33
Phosphoryl halides, 146
Photoinduced electron transfer (PET), 1,
 120, 175, 188
Photoluminescence quantum yield
 (PLQY), 52
Photon avalanche (PA), 32

Photon inputs, 7
Platinum salts, vapoluminescent, 146
Platinum(II) terpyridyl complexes, 147
Poly(allylamine hydrochloride), 69
Poly[9,9-bis(3'-(*N,N*-dimethyl)-*N*-ethylammonium)propyl)-2,7-fluorene-*alt*-1,4-phenylene] dibromide (PDFD), 62
Poly(*N*-phenylmaleimides), 189
Poly(propylene amine) dendrimer, 68
Poly(propylene ethynylene), 66
Poly(sodium, 4-styrene sulphonate), 69
Polyhedral oligomeric silsesquioxane (POSS), 67
Polylysin dendrimer, 68
Polymers, conjugated, 66
Porcine liver esterase, 72
Porphyrins, 165
Porphyrin-Zn(II), 17
Proteins, 38, 60, 75, 83, 97, 165, 199, 207
 purification, 128
Pseudoenantiomers, 178
Pseudorotaxane, 20
Pyridine-2,6-dicarboxylate, 208
Pyrophosphate ions, 164

Q

Quantum dots, 58, 60, 98, 205
Quartz crystal microbalance (QCM) sensors, 199

R

Radiative decay engineering (RDE), 76, 79
Rare earth doped solids, 31
Renilla reniformis luciferase, 62
Resonance energy transfer, 51, 53, 83
Rhodamine B, 71
Rotaxane, 19

S

Saccharides, 168
Safranin O, 72

Sarin, 146
Scandium(III), 189
Sensitizer, 32
Sensor arrays, 139
Sensory systems, noncovalent, 205
Separate inputs, 8
Signal amplification, 51, 93
Silica core-shell nanoparticles, luminescent, 128
Silica nanoparticles, 93
 fluorescent, 102
 luminescent, 101
Silver island films (SIFs), 80
Silver nanoparticles (AgNPs), 80
Soman, 146
Squaraines, 72, 160
Stern-Volmer equation, 184
Stöber method, 102
Streptococcus pneumoniae, 37
Sulforhodamine-B, 205
Surface plasmon resonance (SPR), 58, 77

T

Tartaric acid, 193
Terbium, 117, 127
Tetracycline, 207
Tetraethoxysilane (TEOS), 102, 123
Tetraphenylporphyrins, 165
Tetrathia-13-azacyclopentadecane, 4
Tetrathiafulvalene (TTF), 10
Thiols, 162
Time-resolved (“gated”) fluorescence (TRF), 207
TMSCl (trimethylsilylchloride), 108
TNT, 61, 68, 118, 120, 144
 QD-based FRET competition assay, 61
Triethoxyvinylsilane, 107, 159
Tris(bipyridyl)ruthenium, 6, 126, 209
TSQ (6-methoxy-(8-*p*-toluenesulfonamido)quinoline), 114, 122
Tunability, 99
Twisted intramolecular charge transfer (TICT), 197

U

Upconversion, 29
nanoparticles (UCNPs), 30, 58, 64
phosphor technology, 33
photonic, 32

V

Vibrio cholerae, 36
Viruses, 36, 38
Volatile organic compounds (VOC), 142

W

Web camera, 150

X

XOR, 20

Y

YES, 2
Yttrium oxysulfides, 34

Z

Zinc(II), 114, 122, 189
Zn(salicylaldimine), 167
Zolmitriptan, 179